Protein Quality Control in the Mammalian Endoplasmic Reticulum

by

Elizabeth J. Klemm

B.A. Molecular and Cell Biology
University of California, Berkeley, 2003

SUBMITTED TO THE DEPARTMENT OF BIOLOGY IN PARTIAL FULFILLMENT OF THE REQUIREMENTS FOR THE DEGREE OF

DOCTOR OF PHILOSOPHY IN BIOLOGY

AT THE
MASSACHUSETTS INSTITUTE OF TECHNOLOGY

FEBRUARY 2011

Signature of author: _____

Elizabeth J. Klemm
January 28, 2011

Certified by: _____

Hidde L. Ploegh
Professor of Biology
Thesis supervisor

Accepted by: _____

Robert Sauer
Co-chair of the Biology Graduate Committee

Protein Quality Control in the Mammalian Endoplasmic Reticulum

by

Elizabeth J. Klemm

**Submitted to the Department of Biology
on January 28, 2011 in Partial Fulfillment of the
Requirements for the Degree of Doctor of Philosophy in
Biology**

Abstract

Quality control is an important part of protein biogenesis. Aberrant proteins must be destroyed before they aggregate and cause deleterious effects. Failure to do so can result in cell death or malfunction and, ultimately, disease. Quality control involves the recognition of misfolded proteins and their degradation. For secretory and membrane proteins, folding occurs in the endoplasmic reticulum (ER), but degradation is performed by the cytosolic proteasome. Thus, quality control in the secretory system includes the dislocation of misfolded proteins from the ER to the cytoplasm. ER proteins that fail to fold correctly are identified and directed to the membrane-associated ER quality control machinery. They are then moved across the ER membrane, tagged with ubiquitin, and extracted from the membrane and complex. Finally, the dislocation substrate is taken to the proteasome where it is degraded.

Many proteins constituting the mammalian quality control machinery have been identified. Several different dislocation complexes work in parallel to clear misfolded proteins from the ER and they are distinguished by their E3 ubiquitin ligase. This thesis describes the identification and characterization of several previously unknown members of the HRD1-associated ER quality control complex. The newly-identified proteins are osteosarcoma amplified-9 (OS9), UBX domain containing-8 (UBXD8), Ubiquitin-conjugating enzyme-6e (UBC6e), and ancient ubiquitous protein-1 (AUP1).

Each of these proteins participates in different steps of ER quality control. OS9 directs misfolded soluble glycoproteins to the dislocation complex. The mannose-6-phosphate homology domain of OS9 is involved in the recognition of glycans on the misfolded protein. UBXD8 recruits p97, the AAA+ ATPase responsible for membrane extraction of dislocated proteins, to the ER using its UBX domain. UBC6e is a membrane-anchored E2 ubiquitin conjugating enzyme. AUP1 recruits a second E2, soluble UBE2G2. Additionally, AUP1 regulates substrate mono- and poly-ubiquitylation.

AUP1 is also necessary for lipid droplet formation. Lipid droplets are cytoplasmic organelles that store neutral lipids. Based on the data that AUP1 depletion affects both ER quality control and lipid droplet formation and that pharmacological inhibition of lipid droplet formation perturbs dislocation, we propose that lipid droplet formation may also play a role in ER protein quality control.

Thesis Supervisor: Hidde Ploegh
Title: Professor of Biology

Acknowledgements

Many people have contributed to making my graduate studies an educational and enjoyable experience. I would like to acknowledge my advisor, Hidde Ploegh for giving me the tools and encouragement to explore the scientific questions that interested me. It was a stimulating experience to work with someone who views research as an exciting endeavor with limitless possibilities.

I would like to thank all of the members of the Ploegh lab for creating an energizing and motivating environment. In particular, I thank Britta Mueller for sharing her project with me. The countless people with whom I was able to discuss experiments or share a laugh will not be forgotten.

I dedicate my thesis to my family.

Table of Contents

Chapter 1: Introduction

QUALITY CONTROL IN THE ENDOPLASMIC RETICULUM

Cells have evolved mechanisms to complete their tasks efficiently. Sometimes this involves giving up accuracy to gain speed. Therefore, a system must be in place to correct or remove mistakes. Such is the case for secretory protein synthesis. Aberrant secretory proteins that cannot fold may arise from genomic errors, as in certain inherited diseases, or from errors in transcription (estimated at 1×10^{-4} per codon in prokaryotes) or translation (estimated between 1×10^{-3} and 1×10^{-4} in prokaryotes)[1]. Protein folding also presents an error-prone process, especially in the crowded conditions of the endoplasmic reticulum (ER) lumen, where protein concentration reaches approximately 300mg/mL[2]. Protein folding times range from 50ms for simple proteins to hours for complex proteins[2] and the protein folding pathway may include several different intermediate conformations. Fortunately, the cell has an effective system to help secretory proteins fold as well as an ER quality control (ERQC) system in place to remove those proteins that are unable to achieve their correct three-dimensional structure. However, if the amount of misfolded protein exceeds the capacity of the ERQC system, the unfolded protein response (UPR) and, in some cases, autophagy are activated. If the cell is still not able to return to homeostasis, apoptosis is triggered. The numerous back-up systems underscore the importance of destroying misfolded proteins before they cause damage to the cell in the form of toxic aggregates.

History

Degradation of ER proteins was first observed for the human T-cell Receptor subunit α (TCRα)[3-4]. Experiments showed that the protein is degraded before trafficking

to the Golgi and its degradation is independent of the lysosome. The working hypothesis was that they are degraded in an unknown compartment or by an unidentified ER resident protease. Data later emerged that disruption of an E2 ubiquitin conjugating enzyme in yeast, Ubc6p, prevents the removal of a mutant version of an ER protein, Sec61p, and pharmacological inhibition of the proteasome stabilizes many ERQC substrates in both yeast and human cells[5-6]. At this point, it was understood that ER proteins are removed (dislocated) from the ER and degraded in the cytoplasm.

Dislocation substrates

What types of proteins are subjected to dislocation? As mentioned above, misfolded proteins are degraded for quality control reasons. Correctly folded proteins can also be removed from the ER as part of regulatory schemes. The common theme for all dislocated proteins is that they are transported from the ER to the cytoplasm, where they are degraded by the proteasome. The specific route that each substrate takes may vary slightly, but all follow the same general path.

What causes proteins to misfold? Several inherited diseases are marked by the absence of a specific secretory protein. These proteins are made, but due to a mutation are unable to fold and are degraded. For example, several disease-causing mutations in the secreted elastase inhibitor alpha-1 anti-trypsin (AAT) have been identified; the Null Hong Kong (NHK) variant has a premature stop codon[7] and the Z-variant has an amino acid substitution (E342K). Both mutations prevent proper folding and result in degradation. Mutations in the Cystic fibrosis transmembrane conductance regulator (CFTR) protein result in disease. The most common mutation is a single amino acid deletion, ΔF508. Although this mutant is actually a functional chloride channel, it is

recognized as misfolded by the cellular quality control machinery and never reaches the cell surface[8], causing disease pathology. An engineered truncated form of Ribophorin I (RI_{332}), consisting of the first 332 amino acids of the protein, is also subject to degradation[9]. Thus genomic mutations, including point mutations, frame-shifts and premature stop codons, often result in misfolding followed by dislocation.

Do wildtype cells also produce misfolded ER proteins? By comparing total nascent ER protein levels in control cells to cells treated with a proteasome inhibitor, it was estimated that up to 30% of proteins that enter the ER are degraded[10]. Very large or complex proteins show an even higher percentage of degradation, probably because they are more prone to be trapped in non-native folding intermediates. This information indicates that the reason ER proteins fail to fold is also due to errors in transcription, translation or folding.

Components of multi-subunit complexes are often dislocated if the partner subunit(s) are not present in a stoichiometric ratio. Examples of dislocated subunits include immunoglobulin chains, NMDA receptor subunits, and the T-cell Receptor (TCR) subunits TCRα and CD3δ[11-14]. This shows that even properly-folded proteins can be subject to dislocation if they are part of a complex and unable to associate with their binding partners.

Several proteins involved in lipid biosynthesis are dislocated based on intracellular lipid levels. When cholesterol or lipid levels are low, ApoB is dislocated instead of being incorporated into Very-Low Density Lipoprotein particles[15]. When intracellular sterol levels are high, 3-hydroxy-3-methyl-glutaryl-CoA reductase (HMGCoA reductase), the rate-limiting enzyme of cholesterol biosynthesis, is

degraded[16]. The calcium channel opening Inositol triphosphate (IP_3) receptor[17] is also regulated by dislocation. Thus the cell uses dislocation to remove folded ER proteins in order to regulate their activity.

Viral immune evasion using dislocation

During virus infections, the host cell normally loads virus-derived peptide antigens onto major histocompatibility complex (MHC) class I complexes in the ER. The MHC class I-antigen complexes traffic to the cell surface where they are recognized by cytotoxic T-cell lymphocytes that stimulate killing of the virus-infected cell. It was observed that Human Cytomegalovirus (HCMV)-infected cells do not have MHC class I molecules on the cell surface, and thus the host's immune system is unable to effectively fight the infection (Fig. 1.1). It was found that several viral genes in the Unique Short (US) region of the HCMV genome are responsible for the surface down-regulation of MHC class I[18] and that MHC class I heavy chain (HC) is rapidly degraded during HCMV infection[19], but the question remained of what was responsible for this degradation. It was found that if the proteasome is pharmacologically inhibited in cells expressing the immunoevasin US11, MHC class I HC is not degraded and found in the cytoplasm[6]. Later, US11 was found to interact with known components of the ERQC complex[6,20]. It was concluded that US11 is co-opting the host's ERQC machinery in order to dislocate MHC class I. Two other HCMV proteins, US2 and US10, were also found to hi-jack the dislocation machinery, but they have different MHC class I allele specificity, use

Figure 1.1

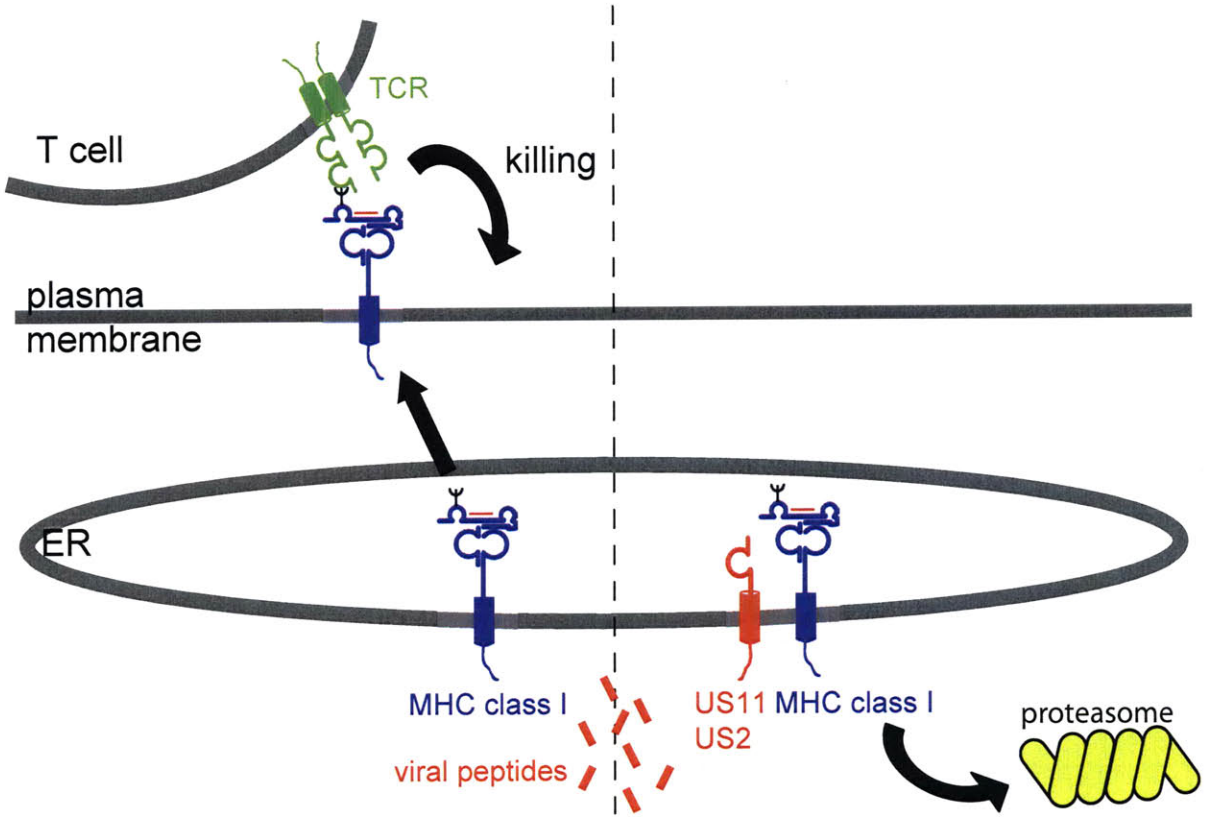

HCMV evades the host immune system by US2- and US11-mediated degradation of MHC class I
During viral infections (left side), intracellular viral peptides are loaded onto MHC class I molecules in the ER. MHC class I-peptide complexes traffic to the cell surface where they alert the host's immune system to viral infection. Cytotoxic T-lymphocytes with T-cell receptors that recognize the MHC class I-peptide complex kills the infected cell.
In cells expressing HCMV US2 or US11 (right side), the MHC class I is removed from the ER and degraded by the proteasome.

different host complexes, and carry out dislocation at different rates. US2 and US11 both mediate the rapid dislocation (half-life of 2-5 minutes) of MHC class I[6], but use different host ERQC complexes. US2 uses a complex that includes Signal Peptide Peptidase and TRC8[21-22]. US11 uses the better-understood HRD1/SEl1L complex[20,23]. US10 specifically targets HLA-G MHC class I alleles for degradation, but with significantly slower kinetics[24]. These HCMV proteins have proved to be valuable tools for probing the mechanism of dislocation.

Protein insertion into the ER

Proteins destined for secretion or residence in the plasma membrane, Golgi apparatus, lysosomes, or ER are first translocated into the ER. The ER is a membrane-bound compartment contiguous with the nuclear envelope. How do secretory proteins enter the ER? Translocation of most polypeptides into the ER lumen occurs co-translationally through the Sec61 protein channel[25]. Targeting of soluble ER proteins and Type I membrane proteins is achieved by an N-terminal signal sequence[26-27]. This hydrophobic stretch of amino acids is recognized by the Signal Recognition Particle (SRP) and ferried to the Sec61 translocon where it is inserted into the ER and the signal sequence is cleaved by Signal Peptidase[28]. Membrane proteins may also be targeted to the membrane independent of a signal sequence or post-translationally, as with tail-anchored proteins that are inserted into the membrane by the GET-pathway[29].

Folding: Chaperones

The observation that polypeptides enter the ER lumen co-translationally in an extended conformation and must fold in the luminal environment raised the following question: how are nascent ER proteins with exposed hydrophobic residues kept from

aggregating? Immunoglobulin (Ig) heavy chains, a protein expressed in high amounts by pre-B cells, were found to associate with binding immunoglobulin protein (BiP)[30]. BiP binds the Ig heavy chains in the absence of Ig light chain, and it was found that BiP acts as a chaperone to Ig heavy chains and all ER proteins. How does BiP act as a chaperone? BiP is a member of the Hsp70 family of proteins and the major ER lumenal chaperone. Like cytoplasmic chaperones, BiP maintains the polypeptides in a folding-competent conformation and prevents their aggregation. How does BiP bind its substrates? Using affinity panning of a peptide library, it was found that BiP preferentially binds amino acid sequences with alternating aromatic and hydrophobic residues[31]. Because this type of sequence is common in proteins, BiP can serve as a chaperone to most proteins and virtually coat the entire length of the polypeptide. Structural data showed that BiP engages polypeptides with its C-terminal substrate binding domain and the affinity of BiP for the polypeptide is determined by a conformational change resulting from nucleotide binding at the N-terminal domain. ERdj3, an Hsp40-family co-factor promotes ATP hydrolysis and peptide binding[32-33], and GrpE-like proteins promote nucleotide exchange and peptide release[34,35]. BiP is one of the first proteins that meets nascent polypeptides entering the ER along with other chaperones that are pre-assembled into a complex that is poised to interact with the incoming polypeptide[36] (Fig 1.2). The processive binding of BiP ensures uni-directional movement of polypeptides into the ER by preventing the nascent chain from slipping backward into the cytoplasm[37].

Folding: Glycosylation

Proteins containing the N-linked glycosylation consensus sequence (asparagine-X-serine/ threonine, where X is any amino acid except proline), are recognized by the

Figure 1.2
ER protein insertion, chaperone binding, and glycosylation

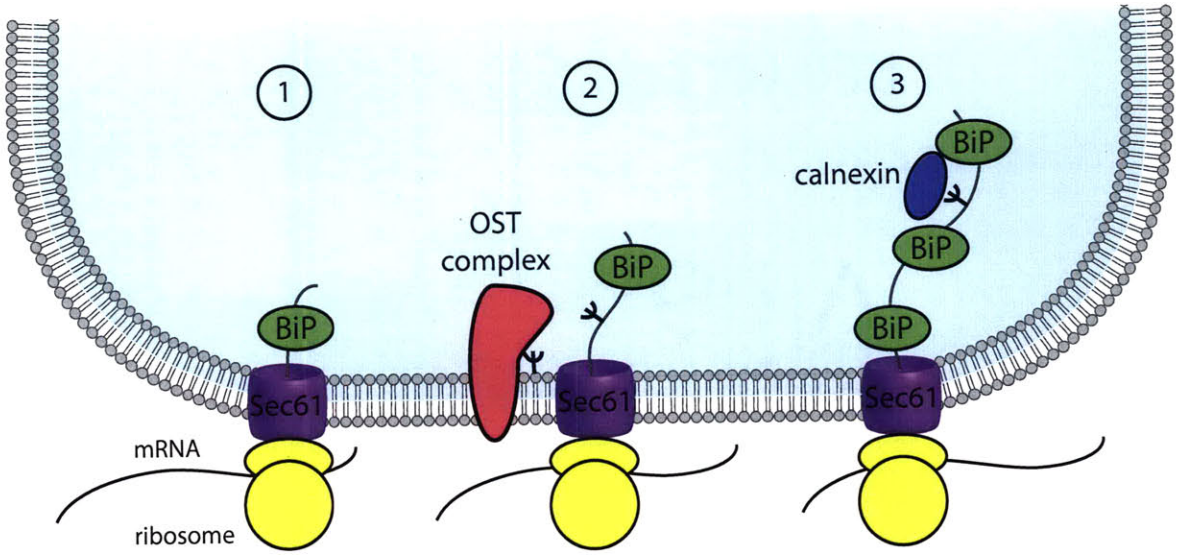

1 Polypeptide is inserted into the ER through Sec61 and bound by the Hsp70 chaperone, BiP
2 The Oligosaccharide Transferase (OST) complex transfers glycans from dolichyl pyroshosphate to the polypeptide
3 Calnexin binds the glycans and BiP binding and glycosylation continue as polypeptide elongates

Oligosaccharide Transferase (OST) complex as the polypeptide exits the translocon on the luminal side. If the glycosylation site occurs at the very N-terminus of the nascent chain, glycosylation will precede BiP binding[38]. Glycosylation increases the protein's solubility, aids in folding, and increases the stability of the folded protein, and may be involved in protein-protein interactions[39]. The OST complex is made up of Ribophorin I and II, OST48, OST4, DAD1, IAP/N33, and the catalytic subunits STT3A or STT3B[40]. The OST complex catalyzes the transfer of pre-assembled $Glc_3Man_9GlcNAc_2$ ($Glucose_3$, $Mannose_9$, $N\text{-}acetylglucosamine_2$) from Dolichyl pyroshosphate lipids onto the asparagine residue of the glycan acceptor site of the polypeptide[41]. This process largely occurs co-translationally, however, in some instances, it appears to happen post-translationally on poorly folded polypeptides by the STT3B isoform of the catalytic subunit[42].

Folding: Calnexin/ Calreticulin Cycle

Almost immediately after glycans are covalently attached to polypeptides, the two outermost glucose residues are removed by Glucosidase I and II[43-44]. This produces a $Glc_1Man_9GlcNAc_2$ glycan structure which is preferentially bound by the lectin chaperones calnexin and calreticulin[45](Fig. 1.3). Calnexin and calreticulin recruit ERp57, an enzyme that catalyzes one of the rate-limiting steps of protein folding, disulfide bond formation[46]. The binding of calnexin and calreticulin to polypeptide chains also provides time for the polypeptide to fold and serves as an ER-retention mechanism[47].

When calnexin releases the glycan, glucosidase II removes the third and final glucose moiety. If the glycoprotein is correctly folded by this time, it is allowed to continue its progression through the secretory pathway. If, however, the polypeptide has

Figure 1.3

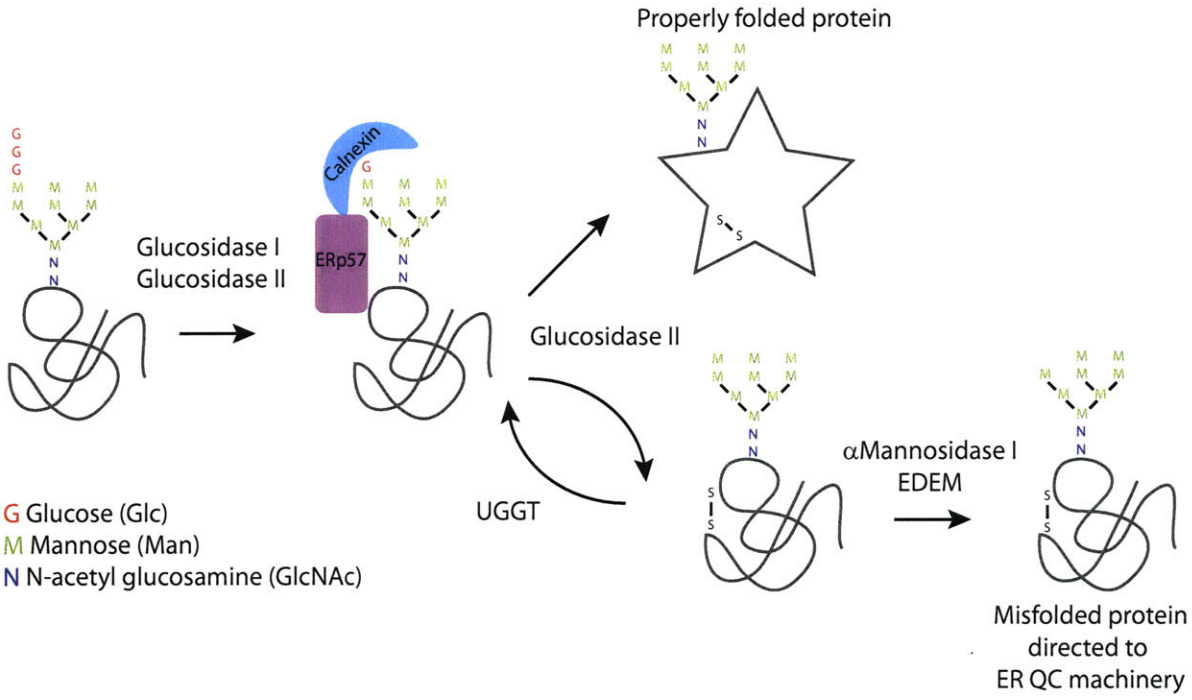

Calnexin folding cycle
Nascent proteins are modified with $Glc_3Man_9GlcNAc_2$ glycans. Glucosidases I and II remove the first and second terminal glucoses, respectively. $Glc_2Man_9GlcNAc_2$ is recognized by by the lectin chaperone calnexin.The glycoprotein attempts to fold and ERp57 mediates disulfide bond formation. Glucosidase II removes the last glucose. If the glycoprotein has attained the correct formation, it is allowed to progress through the secretory pathway. If the protein is not correctly folded, either the glycan is reglucosylated by UGGT and re-enters the calnexin cycle or a mannose is removed by αMannosidase I and/or EDEM proteins. The mannose removal serves as a signal to direct the protein to the ER quality control complex for degradation.

failed to fold correctly, it will be either given another chance to attempt folding or will be marked for removal from the ER[48]. Re-entry into the calnexin/calreticulin cycle is achieved by re-glucosylation of the glycan by UDP-glucose:glycoprotein glucosyltransferase (UGGT)[49].

Selecting misfolded ER proteins for dislocation

It is important that proteins are given ample chance to fold, but removed if they are terminally misfolded. Infinite cycling through the calnexin/calreticulin cycle would cause a deleterious back-log in the system. It was found that terminally misfolded proteins had glycans with $Man_8GlcNAc_2$ structures, lacking the mannose where UGGT re-attaches the glucose. ER α-mannosidase I, EDEM1, EDEM2, and EDEM3 are likely the mannosidases responsible for mannose trimming in mammalian cells[50-52]. Trimming mannoses off of the glycans before UGGT can replace the glucose precludes the possibility of the protein returning to the calnexin/calreticulin folding cycle. Thus the removal of the terminal mannose serves as the signal that consigns proteins to removal from the ER and degradation.

How does the cell distinguish on-pathway folding intermediates from hopelessly misfolded species and subject only the latter to mannose trimming? ER α-mannosidase I is active *in vitro* only under non-physiological concentrations[53]. If ER α-mannosidase I is concentrated at specialized subdomains of the ER, it may reach levels required for activity[54]. EDEM1 has also been observed in small vesicles called EDEMosomes that are cleared upon delivery to endo/lysosomes[55-56]. EDEM is also highly upregulated during the UPR in response to XBP-1 splicing[50,57-58]. Thus physical separation of the actively folding proteins from the mannosidases or adjustment of mannosidase levels may allow

the cell to tune the stringency of ER protein selection for degradation[59]. This hypothesis is termed ER tuning.

Directing misfolded ER proteins to the dislocation machinery

After mannose trimming, how are the misfolded glycoproteins directed to the dislocation machinery[60-61]? OS9, XTP3-B and SEL1L are required for the dislocation of soluble ER luminal glycoproteins[62-63], but not for membrane-bound proteins with misfolded luminal lesions[13]. Both XTP3-B and OS9 contain mannose-6-phosphate receptor homology domains that are important for their role in dislocation and act as glycan-binding sites. XTP3-B and OS9 may bind glycans on the misfolded proteins, but are also known to bind to glycans of downstream ER quality control factors, including SEL1L[63-64]. It was concluded that OS9, XTP3-B, and SEL1L act as adaptor proteins to direct soluble proteins to the site of dislocation (Fig. 1.4). Lateral diffusion of membrane-anchored dislocation substrates may be sufficient to target them to the dislocation machinery.

After multiple folding attempts, the dislocation substrate is no longer an extended polypeptide- it may contain disulfide bonds and glycans as well as partially-folded domains and regions with exposed hydrophobic residues. Does the protein unfold again before being dislocated? Mannose trimming is thought to serve to reduce physical bulkiness as well as signal for removal. Some disulfide bonds are also observed to be reduced prior to dislocation and three proteins are implicated in this process: ERdj5[65], BiP, and EDEM. In contrast, it has been shown that tightly folded domains (green fluorescent protein or dihydrofolate reductase) fused to dislocation substrates are not

Figure 1.4
HRD1 complex in mammalian cells

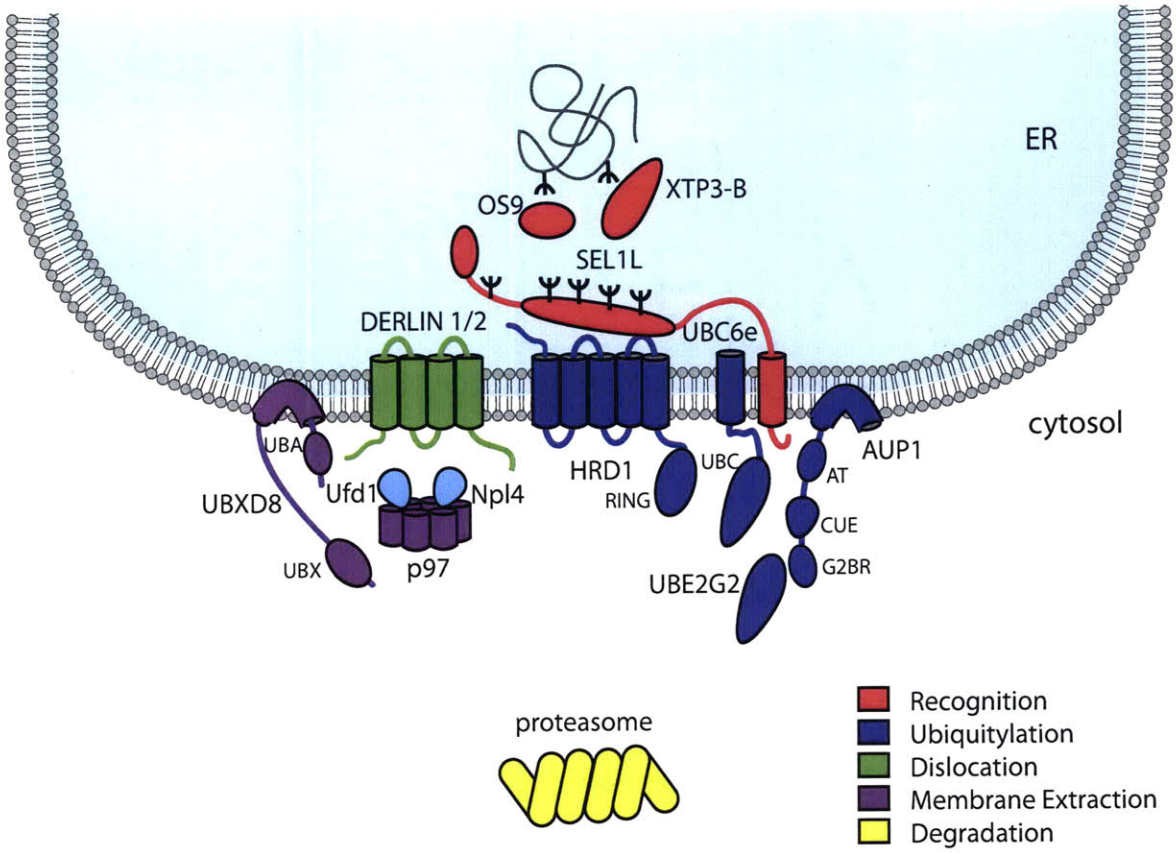

The HRD1 complex mediates the removal of proteins from the ER.
OS9 and XTP3-B are two glycan-binding proteins that direct misfolded soluble ER luminal proteins to the dislocation complex. SEL1L is also involved in the recognition of misfolded proteins. Dislocation substrates may be removed from the ER through a proteinaceous channel composed of DERLIN1/2 or HRD1. Ubiquitylation of misfolded ER proteins is performed by the HRD1 E3 ubiquitin ligase along with one of the associated E2 ubiquitin conjugating enzymes, tail-anchored UBC6e or soluble UBE2G2 which is recruited by AUP1. The dislocation substrate is extracted from the membrane and dislocon by the AAA+ ATPase p97 and its co-factors Ufd1 and Npl4. UBXD8 recruits p97 with its UBX domain. The misfolded proteins is then shuttled to the proteasome where it is degraded.

unfolded, but rather get dislocated in their native state[66]. Therefore the exact 3-dimensional requirements for the dislocated protein are not yet understood.

Dislocation

How do terminally misfolded proteins traverse the hydrophobic lipid bilayer? The dominant theory is that they exit through a proteinaceous channel, yet the identity of the protein(s) that serve as the channel is highly debated. The first candidate was the Sec61 translocon[67], which implied that proteins exited the ER through the same pore through which they entered. This was supported by data showing Sec61 physically associates with dislocation substrates. Crystal structures of archeal SecY show that the interior cyclinder is only wide enough to accommodate polypeptides in their extended conformation[68], and thus might not be consistent with data showing fusion proteins being dislocated while still partially folded. A second protein that might serve as a proteinaceous channel is Derlin1[20,69]. Derlin1 has four transmembrane segments and self-oligomerizes, typical structural features of membrane channels. Recently, Hrd1p, a yeast E3 ubiquitin ligase involved in ubiquitylating misfolded ER proteins, was also suggested to be the dislocon[70]. Dislocation substrates were cross-linked to Hrd1p mid-dislocation. Hrd1p encodes five to six transmembrane segments. An alternative model is that proteins instead exit in association with lipid droplets emerging from the ER[71]. This model eliminates size limitations imposed by proteinaceous channels and would account for how proteins can exit in a partially folded state and why a dislocation substrate has been found associated with cytoplasmic lipid droplets. This model will be discussed in more detail in a later section.

Ubiquitylation overview

Targeting to the proteasome is executed by the attachment of poly-ubiquitin tags. Ubiquitylation involves three enzymes, an E1 ubiquitin-activating enzyme, an E2 ubiquitin ligase, and an E3 ubiquitin conjugating enzyme (Fig. 1.5). In an ATP-dependent reaction, a single ubiquitin is attached to the E1 active site cysteine by a thioester bond. The ubiquitin is then transferred to an E2 enzyme. E3s provide the substrate specificity by recognizing the target to be ubiquitylated. The ubiquitin is usually attached to a lysine residue on the ERQC substrate, but has also been shown to be attached to the N-terminus and to serines and threonines[14,72]. E3s come in two flavors: HECT (Homologous to the E6-AP Carboxyl Terminus) or RING (Really Interesting New Gene) domain-containing. In the case of HECT domain E3s, the ubiquitin is transferred from the E2 to the E3 to the substrate. For RING domain E3s, the ubiquitin is transferred from the E2 directly to the substrate with the help of the E3. Mammalian cells encode two different E1s[73], approximately 40 E2s, and over 600 E3s[74]. Of those, four E2s and eleven E3s have been implicated in ubiquitylation of misfolded ER proteins in mammalian systems. All of the currently known ER quality control E3s contain RING domains.

E2 ubiquitin conjugating enzymes involved in ER protein quality control

The four E2s known to play a role in the ubiquitylation of dislocation substrates are UBE2G2 (UBC7), UBE2J1 (UBC6e), UBE2J2 (UBC6) and UBCH5. UBC6e and UBC6 are homologues of yeast Ubc6p[75]. UBC6e and UBC6 are both tail-anchored proteins with hydrophobic C-terminal membrane-anchor domains that are inserted post-translationally. UBE2G2 is a soluble cytoplasmic protein. It is recruited to the

Figure 1.5
Ubiquitylation

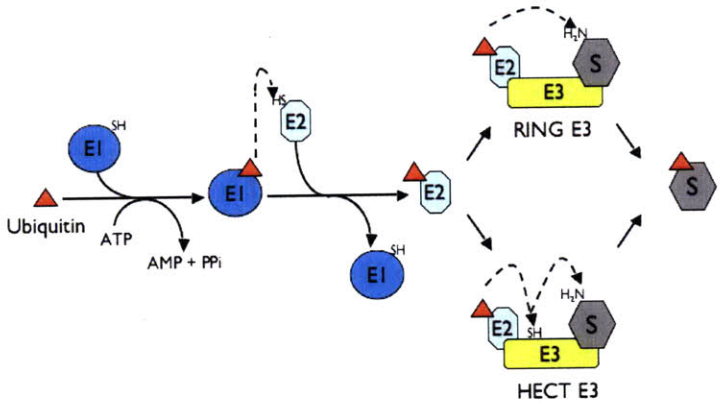

Ubiquitin is activated by the E1 enzyme in an ATP-dependent reaction. The ubiquitin is transferred to an E2 conjugating enzyme. The E3 ubiquitin ligase transfers the ubiquitin from the E2 to the substrate directly (for RING-domain E3s) or first to itself and then to the substrate (for HECT-domain E3s).
Illustration from B. Mueller

membrane by ancient ubiquitous protein-1 (AUP1) via its G2 binding region. UBE2G2 assembles K48-linked poly-ubiquitin chains which are transferred to the substrate by an E3 *en bloc*[76-77]. UBE2G2 binds the distal ubiquitin (with the free K48 residue) with higher affinity than the rest of the ubiquitin chain[78]. A fifth protein, E2-25K can serve as an E2 to dislocated MHC class I HC in a permeabilized cell system, but its relevance in intact cells remains to be shown[79].

E3 ubiquitin ligases involved in ER protein quality control

In yeast there is a clear distinction between which of the two ERQC E3s are used for substrate ubiquitylation, based on the location of the misfolded lesion. Doa10 specializes in the ubiquitylation of substrates with aberrant cytoplasmic regions and Hrd1p processes substrates with lesions in the membrane or ER luminal region[80-81]. For mammalian cells the distinction is not as clear, although there still appear to be differences in the substrate specificity of each E3. HRD1 specializes in the disposal of soluble ER luminal proteins[13]. Membrane-anchored dislocation substrates with misfolded luminal domains are less dependent on HRD1. Thus for mammalian ER quality control, it is not only the location of the misfolded lesion, but also the membrane association of the dislocation substrate that determines which E3 is involved. Certain substrates have been shown to be processed by multiple E3s. Some substrates show promiscuity for E3s, including TCRα, CD3δ, and INSIG-1, while other substrates have only been shown to use one E3. Thus it may be that some substrates can be ubiquitylated by one of several different E3s, while other substrates must be processed by one specific E3. There is also evidence that in some cases, one substrate requires two different E3s acting in concert or sequentially. Such is the case with CFTRΔF508 which is ubiquitylated co-translationally

by RMA1, post-translationally by cytosolic CHIP, and the ubiquitin chain is extended by gp78[82-83]. A list of many of the known substrates and E2s of each E3 involved in ER protein quality control is given in Table 1.1.

The two best-characterized mammalian E3s are gp78 and HRD1. Both ligases are orthologs of yeast Hrd1p with five transmembrane domains and a cytosolic RING finger domain. Gp78 differs from HRD1 in its cytosolic region. Gp78 (but not HRD1) encodes cytosolic CUE, G2 binding region (G2BR), and p97-interacting domains in addition to the RING domain. The p97-interacting domain can be deleted without affecting gp78's activity. In contrast, the G2BR is functionally necessary to recruit UBE2G2[84]. The G2BR enhances the affinity of UBE2G2 for RING-finger domains which in turn increases ubiquitylation activity of the complex[85]. The CUE domain binds ubiquitin and may be involved in mediating chain elongation of ubiquitylated proteins in an E4-like fashion. It has also been suggested that the CUE domain is involved in the assembly of ubiquitin chains that have been observed on UBE2G2. Gp78 is responsible for the sterol-regulated degradation of Insig-1 and HMGCoA Reductase. Gp78 is itself targeted for ubiquitylation by HRD1[86-87]. In this way, reduced expression of HRD1 leads to increased gp78 levels and thus more rapid turnover of gp78 substrates. This regulatory arrangement may be important for the adjustment of the different dislocation complexes.

HRD1, also known as Synoviolin, is another major RING finger E3 associated with ER protein quality control. While HRD1 lacks the CUE domain and G2BR of gp78, it associates with AUP1 which contains both of these missing domains. AUP1 may provide the functional activities with regards to UBE2G2 and ubiquitin in *trans*. HRD1 is able to catalyze the transfer of ubiquitin from at least two different E2s: UBE2G2 and

Table 1.1 Mammalian E3s: their cognate E2(s) and substrates

E3	E2	Substrates	Reference
HRD1	UBE2G2 UBC6e	TCRα CD3δ Pael-R SGK1 p53 NHK gp78 NS1 κ LC Bile salt export pump ΔGly	89 89 95 88,96 175 13 86-87 116 176
gp78	UBE2G2	HMGCoA reductase Insig-1 CD3δ ApoB-100 z variant α-1 anti-trypsin SOD1 ataxin-3 CFTRΔF508 (acting as E4 with RMA1) CYP3A4	177 178 179 180 181 182 182 83 97
TEB4 (MARCH VI)	UBE2G2	TEB4 type 2 iodothyronine deiodinase Bile salt export pump G238V	90,183 184 176
TRC8	?	Insig-1 MHC class I HC (US2)	91 22
RMA1	UBC6e UBC13	CFTRΔF508 (co-translationally) Bile salt export pump G238V TCRα	82-83 176
Kf-1	?	?	93
RFP2	UBCH5	CD3δ RFP2 L-type channels	92 92 185
Parkin CHIP	UBE2G2 UBCH5 UBC13	Pael-R CFTRΔF508 (post-translationally) NMDA Receptor SGK1 CYP3A4	95 82 12 96 97
FBX2	?	pre-integrinB1 SHPS-1 NMDA Receptor	98 186 12
FBS-2	?	TCRα	99

UBC6[88-89]. Although HRD1 is named for yeast Hrd1p (which is itself named for HMGCoA Reductase Degradation), HRD1 mediates basal, but not sterol-mediated, ubiquitylation of HMGCoA Reductase[89].

Several other ER resident E3s are beginning to emerge as part of the ER quality control system. TEB4 (MARCH VI) is the mammalian homologue of yeast Doa10p. It has thirteen transmembrane domains and it is able to ubiquitylate itself[90]. TRC8 encodes a sterol-sensing domain which is relevant for its role in the ubiquitylation of INSIG-1, a protein involved in regulating cholesterol biosysthesis [91]. TRC8 is also implicated in the US2-mediated removal of MHC class I HC from the ER[22]. Little else is known about the complex co-opted by US2 except that it includes Signal Peptide Peptidase[21]. Other ER membrane E3s include RMA1 that coordinates the ubiquitylation of CFTRΔF508 as it is being translated[82], RFP2[92], and Kf-1 that may be related to anxiety disorders[93-94].

Three cytosolic RING-finger containing E3s are also involved in the ubiquitylation of ER quality control substrates. Ubiquitylation of Parkin-associated endothelin receptor-like receptor (Pael-R) is mediated by cytosolic E3 Parkin as well as membrane-anchored HRD1[95]. CHIP, an Hsc70- and Hsp90-interacting E3 also ubiquitylates dislocated substrates, but usually in conjunction with an ER-bound E3: CFTRΔF508 with RMA1[82], SGK1 with HRD1[96], and CYP3A4 with gp78[97]. Two Skp1-Cullin1-F-box protein E3s, FBX2 and FBS2, recognize glycans on their substrates[12,98-99].

Membrane Extraction

How are misfolded ER proteins extracted from the membrane prior to proteasomal degradation? It was found that p97, an AAA+ ATPase with several diverse cellular functions, is important for this step of dislocation. p97 has long been identified as

a segregase, separating ubiquitylated proteins from other binding partners, as well as being involved in spindle disassembly and membrane fusion. p97 associates with several different co-factors that determines its function. Association with the co-factors Ufd1 and Npl4 directs p97 to ERQC activities[100]. p97 is recruited to the site of dislocation by the proteins VIMP, UBXD8, and Erasin (UBXD2)[62,69,101-102]. UBXD8 and Erasin interact with p97 via their UBX domains which structurally resemble ubiquitin. The E3s HRD1 and gp78 also have p97-interacting domains, but their importance has not been established[103-104]. p97 facilitates the degradation of substrates from many of the E3 complexes and, as such, is thought to be the point of convergence in the various dislocation pathways. The contribution of p97 can vary from substrate to substrate, and the dependence is thought to correspond to the stability of the membrane segment[105]: more hydrophobic transmembrane domains are more reliant on p97 for dislocation.

Deubiquitylating enzymes in extraction

How does p97 extract proteins from the ER? Studies in permeabilized cells showed that an ATP-dependent step is required for the dislocation of misfolded polypeptides[106]. p97 is composed of two consecutive ATPase domains and assembles into a homohexamer. The subunits are arranged in a ring formation with a hollow center. ATP hydrolysis rotates the outer ring, producing mechanical energy[107-108]. Thus the conformational change may be the ATP-dependent step required for extraction to proceed. The same study hypothesized that the poly-ubiquitin chains on the dislocation substrate serve as handles for p97 to pull it out of the membrane[106]. A recent paper reports that the YOD1 deubiquitylating enzyme is important for membrane extraction[109]. The authors hypothesize that some of the ubiquitin chains must be removed from the

polypeptides emerging from the ER in order to allow it to pass through the axial channel of the p97 ring. Introduction of a hyperactive deubiquitylating enzyme derived from Epstein-Barr virus results in the accumulation of cytosolic dislocated protein that is not degraded by the proteasome[110]. Taken together, this implies that there are two rounds of ubiquitylation involved in dislocation: once prior to extraction which is removed by YOD1 and then again after p97-mediated extraction for targeting to the proteasome (Fig. 1.6).

Shuttling to the proteasome

Another DUB involved in dislocation is Ataxin-3. Ataxin-3 competes with Ufd1 for binding to p97[111]. In contrast to YOD1, Ataxin-3 is thought to shorten the ubiquitin chains after p97 has extracted the substrate[112]. Ataxin-3 also binds the yeast Rad23p ortholog (HHR23A/B), a protein that binds and shuttles substrates to the proteasome. The thought is that the substrate is transferred from Ataxin-3 to HHR23A/B with shortened ubiquitin chains that are still long enough to be recognized by the proteasome machinery[112]. HHR23A/B also forms a complex with another p97 co-factor, peptide: *N*-glycanase (PNGase)[113]. PNGase removes the bulky glycans from the substrate after dislocation, prior to insertion into the proteasome[114], although glycan removal is not necessary for degradation and may occur downstream of the proteasome[115].

A protein called HERP may be involved in shuttling non-glycosylated dislocation substrates from the dislocon to the proteasome. This hypothesis is based on the fact that HERP associates with HRD1, Derlin-1, and the proteasome[116]. HERP interacts with several non-glycosylated substrates, but not with any of the glycosylated substrates that

Figure 1.6
Model of Membrane Extraction

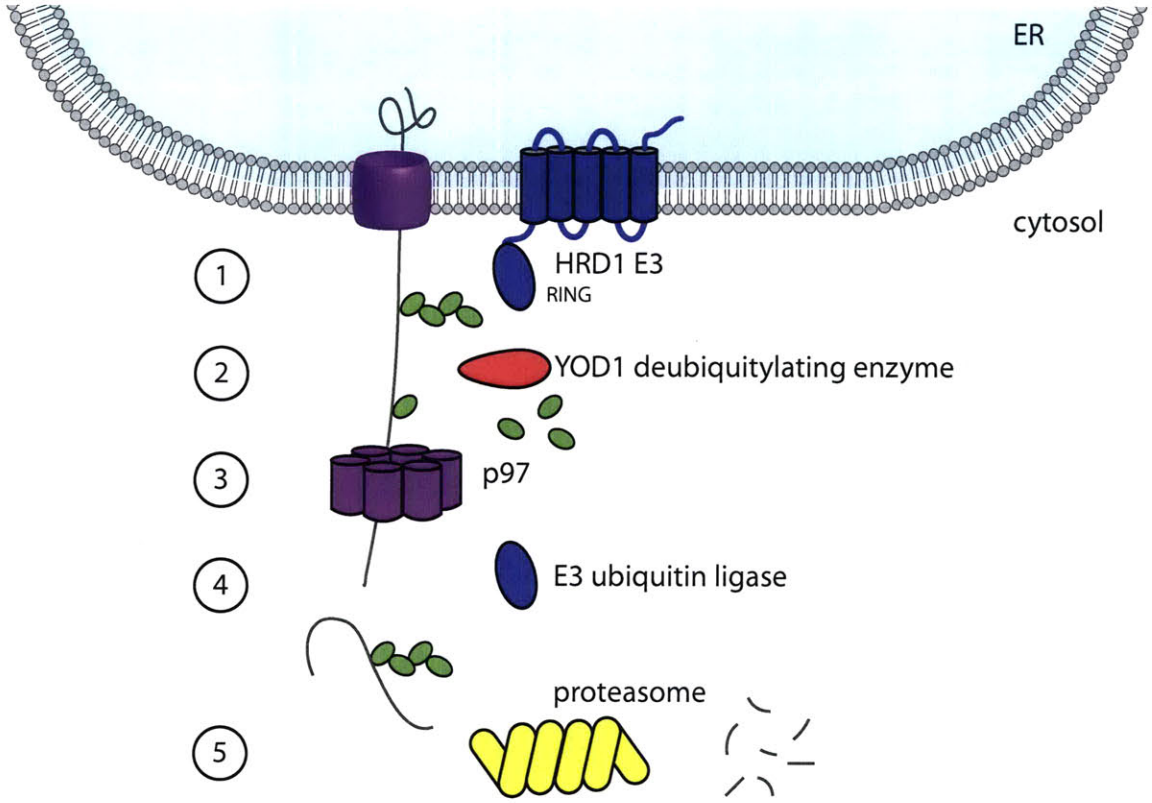

1 Dislocation substrate is first ubiquitylated by an ER membrane E3 ubiquitin ligase (HRD1 here)
2 Ubiquitin is removed by YOD1 deubiquitylating enzyme
3 Polypeptides with trimmed ubiquitin chains enter into core of p97 complex. ATP hydrolysis causes conformational change to p97, thus pulling misfolded protein out of membrane through dislocon
4 Dislocation substrate is re-ubiquitylated by a cytosolic E3 ubiquitin ligase
5 Proteasomal degradation

were tested[116]. How non-glycosylated misfolded ER proteins are initially directed to the dislocation machinery is unclear since they bypass the calnexin/ calreticulin cycle, but BiP is important for their degradation[117].

Proteasomal Degradation

The final step of ER quality control is proteasomal degradation. The proteasome is composed of a 19S regulatory cap and 20S core particle[118]. Several proteins in the regulatory cap prepare the substrate to be threaded into the core particle. RPN10 and RPN13 act as ubiquitin receptors to recognize the substrates[119-120]. A set of DUBs remove the ubiquitin chains in order to salvage the proteins for reuse. Several ATPases unfold the substrate. In the interior of the core particle, the proteolytic subunits degrade the polypeptide into short peptides that are released into the cytoplasm.

The unfolded protein response

When the amount of misfolded proteins exceeds the folding capacity of the ER, the Unfolded Protein Response (UPR) is triggered. The mammalian UPR is comprised of three branches that each possess a sensor protein that recognizes ER stress conditions and initiates a signaling pathway to alleviate the problem. The three sensor proteins are inositol-requiring enzyme-1 (IRE1), protein kinase RNA-like endoplasmic reticulum kinase (PERK), and activating transcription factor 6 (ATF6). The UPR exerts transcriptional and translational changes on the cell with the final result of increasing the folding capacity of the ER, decreasing the folding demands on the ER, clearing misfolded proteins from the ER, and expanding the volume of the ER[121-122]. Genes that are up-regulated during the UPR include those encoding ER chaperones, proteins involved in ER quality control machinery, and phospholipid biosynthetic enzymes. The expression of

secretory proteins is down-regulated, protein translation is inhibited and a specific subset of mRNAs localized to the ER is degraded.

How do each of the UPR branches contribute to these effects? Activation of IRE1's RNase domain results in splicing of mRNA encoding the X-box binding protein-1 (XBP1) transcription factor. Splicing of mammalian *XBP1* results in a frameshift that produces the mRNA encoding the functionally active transcription factor[123]. IRE1 activation also lessens the influx of proteins into the ER by cleaving a subset of mRNAs located near the ER[124-125]. Activation of PERK results in the phosphorylation of eukaryotic translation initiation factor 2α (eIF2α). Phosphorylated eIF2a is unable to efficiently form the ribosomal pre-initiation complex, thus leading to a general decrease in translation. Some transcripts are able to circumvent this block in translation, including the mRNA encoding ATF4, a UPR transcription factor[126]. Activation of ATF6 results in the release of the cytoplasmic transcription factor domain of ATF6 which travels to the nucleus and upregulates genes with ER stress response elements[127].

LIPID DROPLETS

There is accumulating evidence that ER protein quality control and lipid droplets (LDs) may be functionally connected. Lipid droplets (LDs) are a cytoplasmic organelle found in all cells from bacteria to plants to mammals. Although LDs can vary in size and composition based on the organism and tissue type, the fact that they are ubiquitous in living cells indicates their importance as lipid storage organelles. Despite initial microscopic observations over a century ago, LDs were largely unstudied until the past few decades.

Lipid droplet structure

The interior core of the LD is hydrophobic due to the abundance of neutral lipids (Fig. 1.7). The major core components in most mammalian LDs are triacylglycerols (TAGs) and cholesterol esters. Some cells also contain up to 20% of ether lipid monoalk(en)yl diacylglycerol. The ratio of TAG to sterol esters varies according to cell type[128]. Recent advances in mass spectrometry techniques have permitted the analysis of single plant-derived LDs by direct organelle mass spectrometry and reveal that the types of neutral lipids may vary on an individual LD basis[129]. Immunogold EM has also suggested that several different proteins and membranous structures are present in the interior of the LD[130-132], perhaps as ER membrane fragments. How this occurs is not known and will be discussed later.

In contrast to all other known organelles which are delimited by lipid bilayers, LDs are bounded by a phospholipid monolayer. The monolayer was observed by cryoelectron microscopy where it appears as a single electron-dense line[133], as opposed to liposomes or microsomes that are surrounded by double lines indicative of a bilayer. The phospholipid components of isolated LDs have been determined by mass spectrometry. The major polar lipids found in LDs are phosphatidylcholine (PC) and phosphatidylethanolamine (PE)[128,133], as is the case for the ER. In contrast to ER-derived rough microsomes, LDs have a greater abundance of PC with two mono-unsaturated acyl chains[133]. LDs also have an increased amount of lysophospholipids and contain less sphingomyelin and phosphatidylserine compared to total membranes[128]. Since LDs are thought to be derived from the ER, the different lipid mixtures may indicate that the types

Figure 1.7
Lipid droplet structure (cross-section)

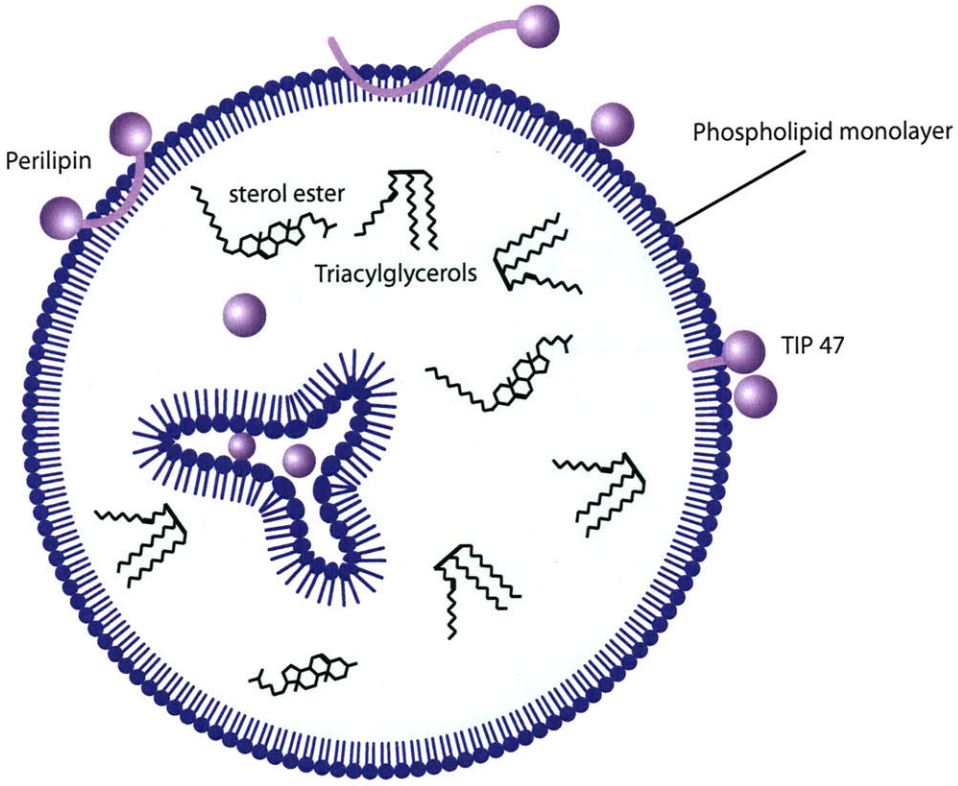

Lipid droplets are cytoplasmic organelles specialized for neutral lipid storage and involved in several other cellular functions. The exterior of the lipid droplet is composed of a phospholipid monolayer. Proteins can be found on the surface of the lipid droplet. These proteins have special membrane domains that dip or insert into the monolayer. The interior core of lipid droplets conatin mainly sterol esters and triacylglycerols. ER membranes and some proteins have also been observed inside lipid droplets.

of lipids incorporated into LDs are regulated or that LDs bud off at specialized microdomains of the ER such as lipid rafts.

Lipid droplet protein components

Many proteins have been identified that are embedded in the lipid monolayer of LDs. The canonical LD proteins belong to the PAT family (named for the founding members of the family: Perilipin, Adipophilin/ADRP, and TIP47) and share structural similarity[134]. These proteins are thought to be structurally important and involved in shielding the LD from lipolysis. Perilipin is only found in adipocytes, whereas ADRP and TIP47 are found in a wider range of cell types[135]. There is some evidence that these proteins are interchangeable. ADRP and Perilipin are found exclusively on the LD. TIP47 is cytosolic until recruited to LDs, at which time its four-helix bundle changes conformation to insert into the phospholipid monolayer[136-137].

Several groups have recently performed proteomic studies on LDs from different cells types[138-143]. LDs were typically isolated by centrifugation through a sucrose gradient. The results included many expected proteins, as well as many unexpected proteins that have proved helpful in understanding the many roles and activities of LDs. The results have been carefully summarized by Hodges and Wu[144]. The proteins identified include the PAT family proteins, enzymes involved in lipid metabolism, ER proteins, chaperones, mitochondrial proteins, and Rab proteins.

Models of lipid droplet formation

Where do LDs come from? LDs are often found very close to the ER, often in an egg-in-eggcup conformation observed by freeze-fracture EM[145]. The enzymes that catalyze the final steps of neutral lipid synthesis are found in the ER. This includes the

enzyme responsible for transferring the third acyl chain onto diacylglycerol to form TAG, acyl CoA:Diacylglycerol acyltransferase (DGAT), which is found in high abundance in ER regions proximal to LDs[146]. Given these observations, it is thought that LDs originate in the ER.

Intramembrane bulges in the ER bilayer have been detected by 1H-NMR *in vitro*[147]. Computer modeling simulations support the spontaneous formation of stable "blisters" containing neutral lipids that are mobile and disordered[148]. These "blisters" of neutral lipids accumulating between the leaflets of the ER membrane may represent the first step of lipid droplet formation.

There are three current models for LD formation (Fig. 1.8). The first model to be proposed is the budding model. In this model, the accumulation of neutral lipids between the ER bilayer continues until it reaches the maximum amount the bilayer can tolerate. At that time, the cytoplasmic leaflet of the ER is expanded as additional neutral lipids are added so that the distension continues asymmetrically, with the resulting bulge protruding out into the cytoplasm. This continues until an LD is formed with a neutral lipid core and a phospholipid monolayer derived from the cytoplasmic layer of the ER membrane[149]. The LD completely detaches from the ER as the connecting lipid stem is resolved.

A second model also begins with the accumulation of neutral lipid between the ER bilayer. As the bulge grows, both leaflets expand such that the nascent LD extends halfway into the ER and halfway into the cytoplasm. For the LD to detach from the ER in this model, bicelle formation is favored at the highly curved sites surrounding the bulge and the LD pops out of the ER[71]. This model would produce an LD whose phospholipid monolayer is derived from equal parts of the luminal and cytoplasmic ER bilayer leaflets.

Figure 1.8
Models of lipid droplet formation and growth

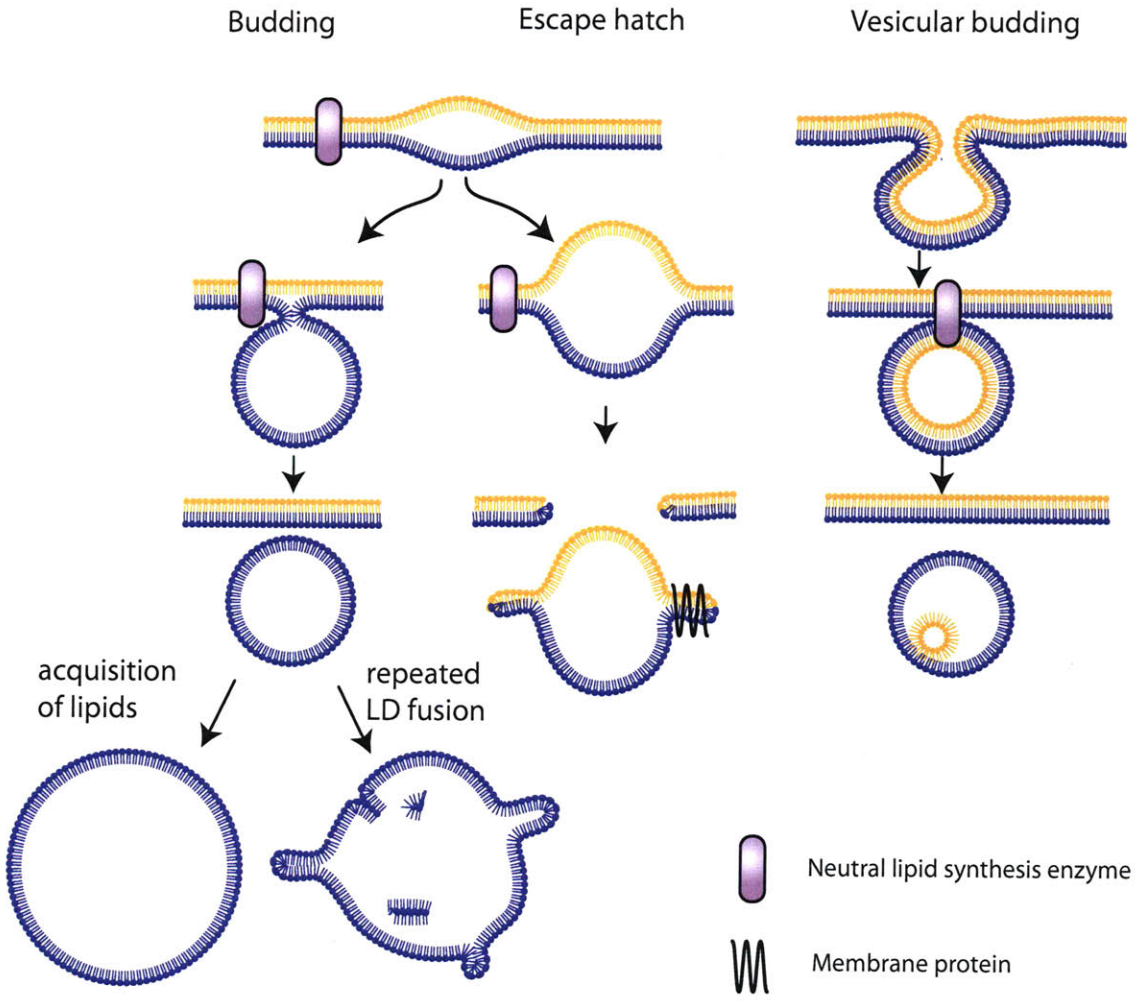

Lipid droplets emerge from the ER. In the budding model of lipid droplet formation, neutral lipids accumulate between the leaflets of the ER phospholipid bilayer until a droplet buds off of the cytoplasmic face, surrounded by a phospholipid monolayer derived of the cytoplasmic leaflet of the ER bilayer. The lipid droplets may grow from aquisition of lipids or from repeated fusion with other lipid droplets. Lipid droplet fusion would result in an excess of phospholipids because of the decrease in surface-to-volume ratio. The extra phospholipids could form "wrinkles" or "tabs" on the exterior of the lipid droplet.
In the escape hatch model, neutral lipids accumulate between the bilayer and the droplet pops out of the ER membrane. A transient hole is formed in the ER membrane and the phospholipid monolayer is derived from both the luminal and cytoplasmic leaflets of the ER membrane. Wrinkles on the curface of the lipid droplet could accomodate membrane-anchored proteins.
In the vesicular budding model, a vesicle is formed and then neutral lipids accumulate between the bilayer of the vesicle. The outer phospholipid leaflet of the vesicle expands and the inner leaflet remains small and on the interior of the lipid droplet.

The surface could retain wrinkles of bilayers that would accommodate proteins with transmembrane domains. A transient hole is formed in the ER in the process, but estimates regarding the disruption of the Ca^{2+} ion gradient predict no significant harmful effects. How the LD is directed into the cytoplasm and not the ER lumen in this model is unknown. This model is called the 'escape hatch' model because it could facilitate the simultaneous exit of two other items from the ER: misfolded proteins and the fully-formed virus particles. The search for a protein-channel based system that can accommodate both misfolded proteins and large virus particles has not been conclusive.

The third model begins with the formation of a vesicle instead of a neutral lipid blister. The vesicle remains associated with the ER via an unidentified protein (perhaps DGAT) that transfers neutral lipids in between the lipid bilayer leaflets of the vesicle. More phospholipids are added to the outer leaflet of the vesicle and the original inner leaflet remains small and in the interior of the LD. The resulting LD has a phospholipid monolayer derived from the outer vesicular leaflet (originally the cytoplasmic leaflet of the ER membrane) and a small portion of the cytoplasm[150]. This is called the 'vesicular budding' model and provides a mechanical explanation for the observation of soluble proteins in the LD core by EM.

Models of lipid droplet growth

Although mature LDs are readily characterized by EM, none of the nascent LD formations predicted by these models have been observed. This may be due to the fact that they are below the size detection limit of EM. Fujimoto and colleagues suggest that very small LDs could be made in the ER according to one of the above models and then these small droplets fuse to form the full-sized droplets observed by microscopy[149].

Fusion of LDs has been observed[151]. This model would result in an extremely large excess of phospholipids as the surface-to-volume ratio decreases in the large droplets. The question is what happens to the surplus phospholipids. Options include destruction by Phospholipase D, rearrangement of the surface into bicellar wrinkles (similar to those predicted by the "escape hatch" model), or internalization of the phospholipids into the core (which localization is known to exist).

Lipid droplets are lipid storage organelles

The most obvious function of LDs pertains to lipid storage. Adipocytes, the mammalian cell type specialized to store large amounts of lipids, are marked by the presence of LDs. This may take the form of a single extremely large (100μm diameter) LD or many smaller droplets. LDs provide a safe storage location for lipids at high cellular concentrations that would otherwise cause lipotoxicity. The cell is able to retrieve the lipid stores as required for cellular energy or for lipid molecules during membrane expansion and cell division. Lipolysis in adipocytes is highly regulated: activated protein kinase A (PKA) phosphorylates perilipin and hormone sensitive lipase (HSL)[152]. This in turn causes perilipin to release CGI-58 and allow Adipocyte Triglyceride Lipase (ATGL) and HSL to bind to the surface of the LD[153-154]. Somehow ATGL and then HSL access the TAGs in the interior of the LD. The acyl chains of TAG are removed one by one; first by ATGL, then HSL, and finally monoacylglycerol lipase, producing three acyl chains and glycerol[155]. These molecules can then be used as substrates for β-oxidation. Alternatively, the TAG could only be partially catabolized into diacylglycerol which could be used as a building block for making phospholipids.

The lipids found in LDs can be transferred to and from other organelles. LDs have been shown to interact with peroxisomes[156], the organelle in which β-oxidation occurs, presumably to transfer fatty-acids from LDs for β-oxidation. In support of this hypothesis, mutant *C. elegans* defective in β-oxidation exhibit enlarged LDs[157]. LDs are also closely associated with early endosomes[158-159] and mitochondria[160] and thus may also exchange lipids with these organelles. Plasma membrane caveolae and caveolins localize to the LDs and are thought to contribute TAGs[161] and phospholipids[162] to growing LDs. LDs have recently been shown to associate with autophagosomes during starvation conditions and autophagosomes may be involved in harvesting of lipids for energy from LDs during nutrient deprivation[163].

Lipid droplets are protein repositories

LDs are now recognized to be involved in several other functions not connected to their lipid storing capacity. LDs appear to act as a storage depot to prevent the aggregation of over-abundant proteins in the cytoplasm[164]. In this model, proteins are directed to LDs in order to regulate their activity and to prevent the formation of toxic aggregates. The proteins that find themselves on the LDs are called "refugee proteins", reflecting the fact that they are normally found in other locations of the cell. A number of proteins have been shown to localize to LDs when expressed at elevated levels. Such is the case for histones during *Drosophila* embryogenesis wherein large amounts of certain histones are stockpiled in the oocyte to sustain subsequent rapid cell divisions[165]. The cell's answer to the problem of how to store such high levels of a protein was apparently to target them to the LD. The histones later leave the LD as needed during the cell cycle and enter the nucleus where they are incorporated into chromatin. Keeping histones on

LDs prevents their aggregation in the cytoplasm while retaining them in a functionally competent conformation. Other proteins that find themselves on LDs when they are artificially overexpressed include stomatin, α-synuclein, and the Hepatitis C core protein[142,166-168].

ENDOPLASMIC RETICULUM QUALITY CONTROL AND LIPID DROPLETS

ER quality control machinery is found on LDs

The first piece of evidence to support the connection between LDs and the process of dislocation is the physical localization of many of the proteins involved in ER protein quality control on LDs[144]. BiP, the major ER Hsp70 chaperone, is found with LDs, as are both lectin chaperones (calnexin and calreticulin). Several subunits of the oligosaccharyl transferase complex (OST48, Ribophorin I, Ribophorin II, and Asparagine-linked glycosylation protein 5/ Alg5) are found on LDs. LDs also contain protein disulfide isomerases (PDIA4/ERp72, PDIA6, P4HB) and peptidyl-prolyl *cis-trans* isomerase B, enzymes responsible for forming, rearranging, and isomerizing disulfide bonds. An E2 ubiquitin conjugating enzyme known to be involved in ER protein quality control (UBE2G2), the protein responsible for its recruitment and regulation (AUP1), and one of its cognate E3 ubiquitin ligases (gp78) are also found associated with LDs. LDs also harbor UBXD8, a UBX domain-containing protein, and the protein it recruits to the site of dislocation, p97. Components of the proteasome (α6 and GC3α) are also found on LDs.

Increases in misfolded proteins results in increase in LDs

Several studies have shown that genetic and pharmacological perturbations of ER quality control and homeostasis result in increased LD formation. Cells treated *in vitro* with the proteasome inhibitor MG-132 contain many more LDs than untreated cells[16]. Under these conditions, the cell would contain high levels of polyubiquitylated protein tagged for degradation, including cytoplasmic proteins and dislocated, terminally misfolded ER proteins. This may be a direct effect of stabilization of some of the PAT proteins that are normally degraded by the proteasome. Studies in yeast and CHO-K1 cells showed a slight increase of LDs upon tunicamycin treatment[169-170]. Tunicamycin inhibits glycosylation and thus causes massive misfolding of proteins in the ER. Yeast strains deficient in glycosylation and ER protein quality control also show a modest increase in LDs[169].

The effect on LD formation of increasing the misfolded ER protein load is exacerbated in cells with an impaired Unfolded Protein Response (UPR). Two separate groups showed that increasing the amount of misfolded ER proteins in mice that have impaired UPR leads to lethal accumulation of LDs in the liver[171-172]. They performed *in vivo* experiments in mice deficient in ATF6α, the protein that triggers one of the three mammalian UPR signaling pathways. Mice deficient in ATF6α grow normally, but are not able to survive intraperitoneal injections of tunicamycin, unlike their wildtype counterparts. Taken together, lipid droplet formation may be another one of the cell's mechanisms to deal with accumulation of misfolded ER proteins along with the UPR and ER associated degradation. When the UPR or proteasome is defective, the cell keeps making more lipid droplets.

Dislocated proteins are found on lipid droplets

LDs have been shown to harbor proteins that are removed from the ER by the dislocation machinery. When cellular sterol levels are high, HMG CoA reductase, a transmembrane protein found in the ER that catalyzes the rate-limiting step of sterol synthesis, is targeted to the ER dislocation complex and ultimately degraded by the proteasome in the cytosol. Hartman and colleagues fractionated cell lysates and found that HMG CoA reductase associates with buoyant LD fraction when the proteasome is inhibited under conditions that promote degradation[173]. Furthermore, pharmacological inhibition of LD formation stabilized HMGCoA reductase under high sterol conditions. Another study presented data that supports the idea that localization of proteins destined for proteasomal destruction to LDs is a general phenomenon. Upon proteasome inhibitor treatment, ubiquitylated proteins were present in the LD fraction[174]. These ubiquitylated proteins could likely include dislocated ER proteins.

This thesis presents data identifying components of the HRD1/SEL1L dislocation complex. The roles of these newly-identified proteins were characterized and ranged from directing glycoproteins to the dislocation complex, to recruitment of p97, to regulation of ubiquitylation. We also expanded the known connections between LD formation and ER protein quality control by identifying a protein that is important for both processes and showing that pharmacological inhibition of LD formation stabilizes a wide range of dislocation substrates.

1. Vembar, S.S. & Brodsky, J.L. One step at a time: endoplasmic reticulum-associated degradation. *Nature reviews* **9**, 944-957 (2008).
2. Hebert, D.N., Bernasconi, R. & Molinari, M. ERAD substrates: which way out? *Seminars in cell & developmental biology* **21**, 526-532 (2009).
3. Lippincott-Schwartz, J., Bonifacino, J.S., Yuan, L.C. & Klausner, R.D. Degradation from the endoplasmic reticulum: disposing of newly synthesized proteins. *Cell* **54**, 209-220 (1988).
4. Klausner, R.D. & Sitia, R. Protein degradation in the endoplasmic reticulum. *Cell* **62**, 611-614 (1990).
5. Sommer, T. & Jentsch, S. A protein translocation defect linked to ubiquitin conjugation at the endoplasmic reticulum. *Nature* **365**, 176-179 (1993).
6. Wiertz, E.J., *et al.* The human cytomegalovirus US11 gene product dislocates MHC class I heavy chains from the endoplasmic reticulum to the cytosol. *Cell* **84**, 769-779 (1996).
7. Sifers, R.N., Brashears-Macatee, S., Kidd, V.J., Muensch, H. & Woo, S.L. A frameshift mutation results in a truncated alpha 1-antitrypsin that is retained within the rough endoplasmic reticulum. *The Journal of biological chemistry* **263**, 7330-7335 (1988).
8. Belcher, C.N. & Vij, N. Protein processing and inflammatory signaling in Cystic Fibrosis: challenges and therapeutic strategies. *Current molecular medicine* **10**, 82-94 (2010).
9. de Virgilio, M., Weninger, H. & Ivessa, N.E. Ubiquitination is required for the retro-translocation of a short-lived luminal endoplasmic reticulum glycoprotein to the cytosol for degradation by the proteasome. *The Journal of biological chemistry* **273**, 9734-9743 (1998).
10. Schubert, U., *et al.* Rapid degradation of a large fraction of newly synthesized proteins by proteasomes. *Nature* **404**, 770-774 (2000).
11. Cattaneo, M., *et al.* SEL1L and HRD1 are involved in the degradation of unassembled secretory Ig-mu chains. *Journal of cellular physiology* **215**, 794-802 (2008).
12. Nelson, R.F., Glenn, K.A., Miller, V.M., Wen, H. & Paulson, H.L. A novel route for F-box protein-mediated ubiquitination links CHIP to glycoprotein quality control. *The Journal of biological chemistry* **281**, 20242-20251 (2006).
13. Bernasconi, R., Galli, C., Calanca, V., Nakajima, T. & Molinari, M. Stringent requirement for HRD1, SEL1L, and OS-9/XTP3-B for disposal of ERAD-LS substrates. *The Journal of cell biology* **188**, 223-235 (2010).
14. Ishikura, S., Weissman, A.M. & Bonifacino, J.S. Serine residues in the cytosolic tail of the T-cell antigen receptor alpha-chain mediate ubiquitination and endoplasmic reticulum-associated degradation of the unassembled protein. *The Journal of biological chemistry* **285**, 23916-23924 (2010).
15. Brodsky, J.L. & Fisher, E.A. The many intersecting pathways underlying apolipoprotein B secretion and degradation. *Trends in endocrinology and metabolism: TEM* **19**, 254-259 (2008).
16. DeBose-Boyd, R.A. Feedback regulation of cholesterol synthesis: sterol-accelerated ubiquitination and degradation of HMG CoA reductase. *Cell research* **18**, 609-621 (2008).

17. Pearce, M.M., Wang, Y., Kelley, G.G. & Wojcikiewicz, R.J. SPFH2 mediates the endoplasmic reticulum-associated degradation of inositol 1,4,5-trisphosphate receptors and other substrates in mammalian cells. *The Journal of biological chemistry* **282**, 20104-20115 (2007).
18. Jones, T.R., *et al.* Multiple independent loci within the human cytomegalovirus unique short region down-regulate expression of major histocompatibility complex class I heavy chains. *Journal of virology* **69**, 4830-4841 (1995).
19. Beersma, M.F., Bijlmakers, M.J. & Ploegh, H.L. Human cytomegalovirus down-regulates HLA class I expression by reducing the stability of class I H chains. *J Immunol* **151**, 4455-4464 (1993).
20. Lilley, B.N. & Ploegh, H.L. A membrane protein required for dislocation of misfolded proteins from the ER. *Nature* **429**, 834-840 (2004).
21. Loureiro, J., *et al.* Signal peptide peptidase is required for dislocation from the endoplasmic reticulum. *Nature* **441**, 894-897 (2006).
22. Stagg, H.R., *et al.* The TRC8 E3 ligase ubiquitinates MHC class I molecules before dislocation from the ER. *The Journal of cell biology* **186**, 685-692 (2009).
23. Mueller, B., Lilley, B.N. & Ploegh, H.L. SEL1L, the homologue of yeast Hrd3p, is involved in protein dislocation from the mammalian ER. *The Journal of cell biology* **175**, 261-270 (2006).
24. Park, B., Spooner, E., Houser, B.L., Strominger, J.L. & Ploegh, H.L. The HCMV membrane glycoprotein US10 selectively targets HLA-G for degradation. *The Journal of experimental medicine* **207**, 2033-2041 (2010).
25. Meacock, S.L., Greenfield, J.J. & High, S. Protein targeting and translocation at the endoplasmic reticulum membrane--through the eye of a needle? *Essays in biochemistry* **36**, 1-13 (2000).
26. von Heijne, G. The signal peptide. *The Journal of membrane biology* **115**, 195-201 (1990).
27. Blobel, G. & Dobberstein, B. Transfer of proteins across membranes. II. Reconstitution of functional rough microsomes from heterologous components. *The Journal of cell biology* **67**, 852-862 (1975).
28. Stroud, R.M. & Walter, P. Signal sequence recognition and protein targeting. *Current opinion in structural biology* **9**, 754-759 (1999).
29. Schuldiner, M., *et al.* The GET complex mediates insertion of tail-anchored proteins into the ER membrane. *Cell* **134**, 634-645 (2008).
30. Haas, I.G. & Wabl, M. Immunoglobulin heavy chain binding protein. *Nature* **306**, 387-389 (1983).
31. Blond-Elguindi, S., *et al.* Affinity panning of a library of peptides displayed on bacteriophages reveals the binding specificity of BiP. *Cell* **75**, 717-728 (1993).
32. Jin, Y., Awad, W., Petrova, K. & Hendershot, L.M. Regulated release of ERdj3 from unfolded proteins by BiP. *The EMBO journal* **27**, 2873-2882 (2008).
33. Jin, Y., Zhuang, M. & Hendershot, L.M. ERdj3, a luminal ER DnaJ homologue, binds directly to unfolded proteins in the mammalian ER: identification of critical residues. *Biochemistry* **48**, 41-49 (2009).
34. Chung, K.T., Shen, Y. & Hendershot, L.M. BAP, a mammalian BiP-associated protein, is a nucleotide exchange factor that regulates the ATPase activity of BiP. *The Journal of biological chemistry* **277**, 47557-47563 (2002).

35. Weitzmann, A., Volkmer, J. & Zimmermann, R. The nucleotide exchange factor activity of Grp170 may explain the non-lethal phenotype of loss of Sil1 function in man and mouse. *FEBS letters* **580**, 5237-5240 (2006).
36. Meunier, L., Usherwood, Y.K., Chung, K.T. & Hendershot, L.M. A subset of chaperones and folding enzymes form multiprotein complexes in endoplasmic reticulum to bind nascent proteins. *Molecular biology of the cell* **13**, 4456-4469 (2002).
37. Matlack, K.E., Misselwitz, B., Plath, K. & Rapoport, T.A. BiP acts as a molecular ratchet during posttranslational transport of prepro-alpha factor across the ER membrane. *Cell* **97**, 553-564 (1999).
38. Molinari, M. & Helenius, A. Chaperone selection during glycoprotein translocation into the endoplasmic reticulum. *Science (New York, N.Y* **288**, 331-333 (2000).
39. Mitra, N., Sinha, S., Ramya, T.N. & Surolia, A. N-linked oligosaccharides as outfitters for glycoprotein folding, form and function. *Trends in biochemical sciences* **31**, 156-163 (2006).
40. Kelleher, D.J. & Gilmore, R. An evolving view of the eukaryotic oligosaccharyltransferase. *Glycobiology* **16**, 47R-62R (2006).
41. Burda, P. & Aebi, M. The dolichol pathway of N-linked glycosylation. *Biochimica et biophysica acta* **1426**, 239-257 (1999).
42. Ruiz-Canada, C., Kelleher, D.J. & Gilmore, R. Cotranslational and posttranslational N-glycosylation of polypeptides by distinct mammalian OST isoforms. *Cell* **136**, 272-283 (2009).
43. Runge, K.W. & Robbins, P.W. A new yeast mutation in the glucosylation steps of the asparagine-linked glycosylation pathway. Formation of a novel asparagine-linked oligosaccharide containing two glucose residues. *The Journal of biological chemistry* **261**, 15582-15590 (1986).
44. Esmon, B., Esmon, P.C. & Schekman, R. Early steps in processing of yeast glycoproteins. *The Journal of biological chemistry* **259**, 10322-10327 (1984).
45. Kapoor, M., *et al.* Interactions of substrate with calreticulin, an endoplasmic reticulum chaperone. *The Journal of biological chemistry* **278**, 6194-6200 (2003).
46. Zapun, A., *et al.* Enhanced catalysis of ribonuclease B folding by the interaction of calnexin or calreticulin with ERp57. *The Journal of biological chemistry* **273**, 6009-6012 (1998).
47. Hebert, D.N., Garman, S.C. & Molinari, M. The glycan code of the endoplasmic reticulum: asparagine-linked carbohydrates as protein maturation and quality-control tags. *Trends in cell biology* **15**, 364-370 (2005).
48. Parodi, A.J. Protein glucosylation and its role in protein folding. *Annual review of biochemistry* **69**, 69-93 (2000).
49. Parodi, A.J., Mendelzon, D.H. & Lederkremer, G.Z. Transient glucosylation of protein-bound Man9GlcNAc2, Man8GlcNAc2, and Man7GlcNAc2 in calf thyroid cells. A possible recognition signal in the processing of glycoproteins. *The Journal of biological chemistry* **258**, 8260-8265 (1983).
50. Hirao, K., *et al.* EDEM3, a soluble EDEM homolog, enhances glycoprotein endoplasmic reticulum-associated degradation and mannose trimming. *The Journal of biological chemistry* **281**, 9650-9658 (2006).

51. Hosokawa, N., *et al.* EDEM1 accelerates the trimming of alpha1,2-linked mannose on the C branch of N-glycans. *Glycobiology* **20**, 567-575 (2010).
52. Tremblay, L.O. & Herscovics, A. Cloning and expression of a specific human alpha 1,2-mannosidase that trims Man9GlcNAc2 to Man8GlcNAc2 isomer B during N-glycan biosynthesis. *Glycobiology* **9**, 1073-1078 (1999).
53. Herscovics, A., Romero, P.A. & Tremblay, L.O. The specificity of the yeast and human class I ER alpha 1,2-mannosidases involved in ER quality control is not as strict previously reported. *Glycobiology* **12**, 14G-15G (2002).
54. Frenkel, Z., Gregory, W., Kornfeld, S. & Lederkremer, G.Z. Endoplasmic reticulum-associated degradation of mammalian glycoproteins involves sugar chain trimming to Man6-5GlcNAc2. *The Journal of biological chemistry* **278**, 34119-34124 (2003).
55. Reggiori, F., *et al.* Coronaviruses Hijack the LC3-I-positive EDEMosomes, ER-derived vesicles exporting short-lived ERAD regulators, for replication. *Cell host & microbe* **7**, 500-508.
56. Cali, T., Galli, C., Olivari, S. & Molinari, M. Segregation and rapid turnover of EDEM1 by an autophagy-like mechanism modulates standard ERAD and folding activities. *Biochemical and biophysical research communications* **371**, 405-410 (2008).
57. Olivari, S., Galli, C., Alanen, H., Ruddock, L. & Molinari, M. A novel stress-induced EDEM variant regulating endoplasmic reticulum-associated glycoprotein degradation. *The Journal of biological chemistry* **280**, 2424-2428 (2005).
58. Yoshida, H., *et al.* A time-dependent phase shift in the mammalian unfolded protein response. *Developmental cell* **4**, 265-271 (2003).
59. Bernasconi, R. & Molinari, M. ERAD and ERAD tuning: disposal of cargo and of ERAD regulators from the mammalian ER. *Current opinion in cell biology* (2010).
60. Groisman, B., Shenkman, M., Ron, E. & Lederkremer, G.Z. Mannose trimming is required for delivery of a glycoprotein from EDEM1 to XTP3-B and to late ER-associated degradation steps. *The Journal of biological chemistry.*
61. Hosokawa, N., Kamiya, Y., Kamiya, D., Kato, K. & Nagata, K. Human OS-9, a lectin required for glycoprotein endoplasmic reticulum-associated degradation, recognizes mannose-trimmed N-glycans. *The Journal of biological chemistry* **284**, 17061-17068 (2009).
62. Mueller, B., Klemm, E.J., Spooner, E., Claessen, J.H. & Ploegh, H.L. SEL1L nucleates a protein complex required for dislocation of misfolded glycoproteins. *Proceedings of the National Academy of Sciences of the United States of America* **105**, 12325-12330 (2008).
63. Christianson, J.C., Shaler, T.A., Tyler, R.E. & Kopito, R.R. OS-9 and GRP94 deliver mutant alpha1-antitrypsin to the Hrd1-SEL1L ubiquitin ligase complex for ERAD. *Nature cell biology* **10**, 272-282 (2008).
64. Cormier, J.H., Tamura, T., Sunryd, J.C. & Hebert, D.N. EDEM1 recognition and delivery of misfolded proteins to the SEL1L-containing ERAD complex. *Molecular cell* **34**, 627-633 (2009).
65. Ushioda, R., *et al.* ERdj5 is required as a disulfide reductase for degradation of misfolded proteins in the ER. *Science (New York, N.Y* **321**, 569-572 (2008).

66. Tirosh, B., Furman, M.H., Tortorella, D. & Ploegh, H.L. Protein unfolding is not a prerequisite for endoplasmic reticulum-to-cytosol dislocation. *The Journal of biological chemistry* **278**, 6664-6672 (2003).
67. Wiertz, E.J., *et al.* Sec61-mediated transfer of a membrane protein from the endoplasmic reticulum to the proteasome for destruction. *Nature* **384**, 432-438 (1996).
68. Van den Berg, B., *et al.* X-ray structure of a protein-conducting channel. *Nature* **427**, 36-44 (2004).
69. Ye, Y., Shibata, Y., Yun, C., Ron, D. & Rapoport, T.A. A membrane protein complex mediates retro-translocation from the ER lumen into the cytosol. *Nature* **429**, 841-847 (2004).
70. Carvalho, P., Stanley, A.M. & Rapoport, T.A. Retrotranslocation of a Misfolded Luminal ER Protein by the Ubiquitin-Ligase Hrd1p. *Cell* **143**, 579-591 (2010).
71. Ploegh, H.L. A lipid-based model for the creation of an escape hatch from the endoplasmic reticulum. *Nature* **448**, 435-438 (2007).
72. Shimizu, Y., Okuda-Shimizu, Y. & Hendershot, L.M. Ubiquitylation of an ERAD Substrate Occurs on Multiple Types of Amino Acids. *Molecular cell* **40**, 917-926.
73. Jin, J., Li, X., Gygi, S.P. & Harper, J.W. Dual E1 activation systems for ubiquitin differentially regulate E2 enzyme charging. *Nature* **447**, 1135-1138 (2007).
74. Li, W., *et al.* Genome-wide and functional annotation of human E3 ubiquitin ligases identifies MULAN, a mitochondrial E3 that regulates the organelle's dynamics and signaling. *PloS one* **3**, e1487 (2008).
75. Lester, D., Farquharson, C., Russell, G. & Houston, B. Identification of a family of noncanonical ubiquitin-conjugating enzymes structurally related to yeast UBC6. *Biochemical and biophysical research communications* **269**, 474-480 (2000).
76. Li, W., Tu, D., Brunger, A.T. & Ye, Y. A ubiquitin ligase transfers preformed polyubiquitin chains from a conjugating enzyme to a substrate. *Nature* **446**, 333-337 (2007).
77. Li, W., *et al.* Mechanistic insights into active site-associated polyubiquitination by the ubiquitin-conjugating enzyme Ube2g2. *Proceedings of the National Academy of Sciences of the United States of America* **106**, 3722-3727 (2009).
78. Bocik, W.E., Sircar, A., Gray, J.J. & Tolman, J.R. Mechanism of polyubiquitin chain recognition by the human ubiquitin conjugating enzyme Ube2g2. *The Journal of biological chemistry*.
79. Flierman, D., Coleman, C.S., Pickart, C.M., Rapoport, T.A. & Chau, V. E2-25K mediates US11-triggered retro-translocation of MHC class I heavy chains in a permeabilized cell system. *Proceedings of the National Academy of Sciences of the United States of America* **103**, 11589-11594 (2006).
80. Carvalho, P., Goder, V. & Rapoport, T.A. Distinct ubiquitin-ligase complexes define convergent pathways for the degradation of ER proteins. *Cell* **126**, 361-373 (2006).
81. Denic, V., Quan, E.M. & Weissman, J.S. A luminal surveillance complex that selects misfolded glycoproteins for ER-associated degradation. *Cell* **126**, 349-359 (2006).

82. Younger, J.M., *et al.* Sequential quality-control checkpoints triage misfolded cystic fibrosis transmembrane conductance regulator. *Cell* **126**, 571-582 (2006).
83. Morito, D., *et al.* Gp78 cooperates with RMA1 in endoplasmic reticulum-associated degradation of CFTRDeltaF508. *Molecular biology of the cell* **19**, 1328-1336 (2008).
84. Chen, B., *et al.* The activity of a human endoplasmic reticulum-associated degradation E3, gp78, requires its Cue domain, RING finger, and an E2-binding site. *Proceedings of the National Academy of Sciences of the United States of America* **103**, 341-346 (2006).
85. Das, R., *et al.* Allosteric activation of E2-RING finger-mediated ubiquitylation by a structurally defined specific E2-binding region of gp78. *Molecular cell* **34**, 674-685 (2009).
86. Ballar, P., Ors, A.U., Yang, H. & Fang, S. Differential regulation of CFTRDeltaF508 degradation by ubiquitin ligases gp78 and Hrd1. *The international journal of biochemistry & cell biology* **42**, 167-173 (2010).
87. Shmueli, A., Tsai, Y.C., Yang, M., Braun, M.A. & Weissman, A.M. Targeting of gp78 for ubiquitin-mediated proteasomal degradation by Hrd1: cross-talk between E3s in the endoplasmic reticulum. *Biochemical and biophysical research communications* **390**, 758-762 (2009).
88. Arteaga, M.F., Wang, L., Ravid, T., Hochstrasser, M. & Canessa, C.M. An amphipathic helix targets serum and glucocorticoid-induced kinase 1 to the endoplasmic reticulum-associated ubiquitin-conjugation machinery. *Proceedings of the National Academy of Sciences of the United States of America* **103**, 11178-11183 (2006).
89. Kikkert, M., *et al.* Human HRD1 is an E3 ubiquitin ligase involved in degradation of proteins from the endoplasmic reticulum. *The Journal of biological chemistry* **279**, 3525-3534 (2004).
90. Hassink, G., *et al.* TEB4 is a C4HC3 RING finger-containing ubiquitin ligase of the endoplasmic reticulum. *The Biochemical journal* **388**, 647-655 (2005).
91. Lee, J.P., *et al.* The TRC8 ubiquitin ligase is sterol regulated and interacts with lipid and protein biosynthetic pathways. *Mol Cancer Res* **8**, 93-106 (2010).
92. Lerner, M., *et al.* The RBCC gene RFP2 (Leu5) encodes a novel transmembrane E3 ubiquitin ligase involved in ERAD. *Molecular biology of the cell* **18**, 1670-1682 (2007).
93. Maruyama, Y., Yamada, M., Takahashi, K. & Yamada, M. Ubiquitin ligase Kf-1 is involved in the endoplasmic reticulum-associated degradation pathway. *Biochemical and biophysical research communications* **374**, 737-741 (2008).
94. Hashimoto-Gotoh, T., Iwabe, N., Tsujimura, A., Takao, K. & Miyakawa, T. KF-1 Ubiquitin Ligase: An Anxiety Suppressor. *Frontiers in neuroscience* **3**, 15-24 (2009).
95. Omura, T., *et al.* A ubiquitin ligase HRD1 promotes the degradation of Pael receptor, a substrate of Parkin. *Journal of neurochemistry* **99**, 1456-1469 (2006).
96. Soundararajan, R., Wang, J., Melters, D. & Pearce, D. Glucocorticoid-induced Leucine zipper 1 stimulates the epithelial sodium channel by regulating serum- and glucocorticoid-induced kinase 1 stability and subcellular localization. *The Journal of biological chemistry* **285**, 39905-39913.

97. Kim, S.M., Acharya, P., Engel, J.C. & Correia, M.A. Liver cytochrome P450 3A ubiquitination in vivo by gp78/autocrine motility factor receptor and C terminus of Hsp70-interacting protein (CHIP) E3 ubiquitin ligases: physiological and pharmacological relevance. *The Journal of biological chemistry* **285**, 35866-35877 (2010).
98. Yoshida, Y., *et al.* E3 ubiquitin ligase that recognizes sugar chains. *Nature* **418**, 438-442 (2002).
99. Yoshida, Y., *et al.* Fbs2 is a new member of the E3 ubiquitin ligase family that recognizes sugar chains. *The Journal of biological chemistry* **278**, 43877-43884 (2003).
100. Jentsch, S. & Rumpf, S. Cdc48 (p97): a "molecular gearbox" in the ubiquitin pathway? *Trends in biochemical sciences* **32**, 6-11 (2007).
101. Liang, J., *et al.* Characterization of erasin (UBXD2): a new ER protein that promotes ER-associated protein degradation. *Journal of cell science* **119**, 4011-4024 (2006).
102. Lilley, B.N. & Ploegh, H.L. Multiprotein complexes that link dislocation, ubiquitination, and extraction of misfolded proteins from the endoplasmic reticulum membrane. *Proceedings of the National Academy of Sciences of the United States of America* **102**, 14296-14301 (2005).
103. Morreale, G., Conforti, L., Coadwell, J., Wilbrey, A.L. & Coleman, M.P. Evolutionary divergence of valosin-containing protein/cell division cycle protein 48 binding interactions among endoplasmic reticulum-associated degradation proteins. *The FEBS journal* **276**, 1208-1220 (2009).
104. Ballar, P., Shen, Y., Yang, H. & Fang, S. The role of a novel p97/valosin-containing protein-interacting motif of gp78 in endoplasmic reticulum-associated degradation. *The Journal of biological chemistry* **281**, 35359-35368 (2006).
105. Carlson, E.J., Pitonzo, D. & Skach, W.R. p97 functions as an auxiliary factor to facilitate TM domain extraction during CFTR ER-associated degradation. *The EMBO journal* **25**, 4557-4566 (2006).
106. Flierman, D., Ye, Y., Dai, M., Chau, V. & Rapoport, T.A. Polyubiquitin serves as a recognition signal, rather than a ratcheting molecule, during retrotranslocation of proteins across the endoplasmic reticulum membrane. *The Journal of biological chemistry* **278**, 34774-34782 (2003).
107. Rouiller, I., *et al.* Conformational changes of the multifunction p97 AAA ATPase during its ATPase cycle. *Nature structural biology* **9**, 950-957 (2002).
108. Zhang, X., *et al.* Structure of the AAA ATPase p97. *Molecular cell* **6**, 1473-1484 (2000).
109. Ernst, R., Mueller, B., Ploegh, H.L. & Schlieker, C. The otubain YOD1 is a deubiquitinating enzyme that associates with p97 to facilitate protein dislocation from the ER. *Molecular cell* **36**, 28-38 (2009).
110. Ernst, R., Claessen, J., Mueller, B., Sanyal, S., Spooner, E., van der Veen, A.G., Kirak, O., Schlieker, C., Weihofen, W., Ploegh, H.L. . Enzymatic Blockade of the Ubiquitin-Proteasome Pathway. *PLoS biology* (2011).
111. Zhong, X. & Pittman, R.N. Ataxin-3 binds VCP/p97 and regulates retrotranslocation of ERAD substrates. *Human molecular genetics* **15**, 2409-2420 (2006).

112. Wang, Q., Li, L. & Ye, Y. Regulation of retrotranslocation by p97-associated deubiquitinating enzyme ataxin-3. *The Journal of cell biology* **174**, 963-971 (2006).
113. Li, G., Zhou, X., Zhao, G., Schindelin, H. & Lennarz, W.J. Multiple modes of interaction of the deglycosylation enzyme, mouse peptide N-glycanase, with the proteasome. *Proceedings of the National Academy of Sciences of the United States of America* **102**, 15809-15814 (2005).
114. Blom, D., Hirsch, C., Stern, P., Tortorella, D. & Ploegh, H.L. A glycosylated type I membrane protein becomes cytosolic when peptide: N-glycanase is compromised. *The EMBO journal* **23**, 650-658 (2004).
115. Kario, E., Tirosh, B., Ploegh, H.L. & Navon, A. N-linked glycosylation does not impair proteasomal degradation but affects class I major histocompatibility complex presentation. *The Journal of biological chemistry* **283**, 244-254 (2008).
116. Okuda-Shimizu, Y. & Hendershot, L.M. Characterization of an ERAD pathway for nonglycosylated BiP substrates, which require Herp. *Molecular cell* **28**, 544-554 (2007).
117. Skowronek, M.H., Hendershot, L.M. & Haas, I.G. The variable domain of nonassembled Ig light chains determines both their half-life and binding to the chaperone BiP. *Proceedings of the National Academy of Sciences of the United States of America* **95**, 1574-1578 (1998).
118. Voges, D., Zwickl, P. & Baumeister, W. The 26S proteasome: a molecular machine designed for controlled proteolysis. *Annual review of biochemistry* **68**, 1015-1068 (1999).
119. Husnjak, K., *et al.* Proteasome subunit Rpn13 is a novel ubiquitin receptor. *Nature* **453**, 481-488 (2008).
120. Deveraux, Q., Ustrell, V., Pickart, C. & Rechsteiner, M. A 26 S protease subunit that binds ubiquitin conjugates. *The Journal of biological chemistry* **269**, 7059-7061 (1994).
121. Schroder, M. & Kaufman, R.J. The mammalian unfolded protein response. *Annual review of biochemistry* **74**, 739-789 (2005).
122. Bernales, S., Papa, F.R. & Walter, P. Intracellular signaling by the unfolded protein response. *Annual review of cell and developmental biology* **22**, 487-508 (2006).
123. Yoshida, H., Matsui, T., Yamamoto, A., Okada, T. & Mori, K. XBP1 mRNA is induced by ATF6 and spliced by IRE1 in response to ER stress to produce a highly active transcription factor. *Cell* **107**, 881-891 (2001).
124. Hollien, J., *et al.* Regulated Ire1-dependent decay of messenger RNAs in mammalian cells. *The Journal of cell biology* **186**, 323-331 (2009).
125. Hollien, J. & Weissman, J.S. Decay of endoplasmic reticulum-localized mRNAs during the unfolded protein response. *Science (New York, N.Y* **313**, 104-107 (2006).
126. Harding, H.P., *et al.* Regulated translation initiation controls stress-induced gene expression in mammalian cells. *Molecular cell* **6**, 1099-1108 (2000).
127. Yoshida, H., Haze, K., Yanagi, H., Yura, T. & Mori, K. Identification of the cis-acting endoplasmic reticulum stress response element responsible for transcriptional induction of mammalian glucose-regulated proteins. Involvement

of basic leucine zipper transcription factors. *The Journal of biological chemistry* **273**, 33741-33749 (1998).
128. Bartz, R., *et al.* Lipidomics reveals that adiposomes store ether lipids and mediate phospholipid traffic. *Journal of lipid research* **48**, 837-847 (2007).
129. Horn, P.J., *et al.* Visualization of lipid droplet composition by direct organelle mass spectrometry. *The Journal of biological chemistry* (2010).
130. Robenek, H., Robenek, M.J. & Troyer, D. PAT family proteins pervade lipid droplet cores. *Journal of lipid research* **46**, 1331-1338 (2005).
131. Robenek, M.J., *et al.* Lipids partition caveolin-1 from ER membranes into lipid droplets: updating the model of lipid droplet biogenesis. *Faseb J* **18**, 866-868 (2004).
132. Wan, H.C., Melo, R.C., Jin, Z., Dvorak, A.M. & Weller, P.F. Roles and origins of leukocyte lipid bodies: proteomic and ultrastructural studies. *Faseb J* **21**, 167-178 (2007).
133. Tauchi-Sato, K., Ozeki, S., Houjou, T., Taguchi, R. & Fujimoto, T. The surface of lipid droplets is a phospholipid monolayer with a unique Fatty Acid composition. *The Journal of biological chemistry* **277**, 44507-44512 (2002).
134. Bickel, P.E., Tansey, J.T. & Welte, M.A. PAT proteins, an ancient family of lipid droplet proteins that regulate cellular lipid stores. *Biochimica et biophysica acta* **1791**, 419-440 (2009).
135. Martin, S. & Parton, R.G. Lipid droplets: a unified view of a dynamic organelle. *Nature reviews* **7**, 373-378 (2006).
136. Ohsaki, Y., Maeda, T., Maeda, M., Tauchi-Sato, K. & Fujimoto, T. Recruitment of TIP47 to lipid droplets is controlled by the putative hydrophobic cleft. *Biochemical and biophysical research communications* **347**, 279-287 (2006).
137. Hickenbottom, S.J., Kimmel, A.R., Londos, C. & Hurley, J.H. Structure of a lipid droplet protein; the PAT family member TIP47. *Structure* **12**, 1199-1207 (2004).
138. Brasaemle, D.L., Dolios, G., Shapiro, L. & Wang, R. Proteomic analysis of proteins associated with lipid droplets of basal and lipolytically stimulated 3T3-L1 adipocytes. *The Journal of biological chemistry* **279**, 46835-46842 (2004).
139. Wu, C.C., Howell, K.E., Neville, M.C., Yates, J.R., 3rd & McManaman, J.L. Proteomics reveal a link between the endoplasmic reticulum and lipid secretory mechanisms in mammary epithelial cells. *Electrophoresis* **21**, 3470-3482 (2000).
140. Liu, P., *et al.* Chinese hamster ovary K2 cell lipid droplets appear to be metabolic organelles involved in membrane traffic. *The Journal of biological chemistry* **279**, 3787-3792 (2004).
141. Bartz, R., *et al.* Dynamic activity of lipid droplets: protein phosphorylation and GTP-mediated protein translocation. *Journal of proteome research* **6**, 3256-3265 (2007).
142. Umlauf, E., *et al.* Association of stomatin with lipid bodies. *The Journal of biological chemistry* **279**, 23699-23709 (2004).
143. Fujimoto, Y., *et al.* Identification of major proteins in the lipid droplet-enriched fraction isolated from the human hepatocyte cell line HuH7. *Biochimica et biophysica acta* **1644**, 47-59 (2004).
144. Hodges, B.D. & Wu, C.C. Proteomic insights into an expanded cellular role for cytoplasmic lipid droplets. *Journal of lipid research* **51**, 262-273 (2010).

145. Robenek, H., *et al.* Adipophilin-enriched domains in the ER membrane are sites of lipid droplet biogenesis. *Journal of cell science* **119**, 4215-4224 (2006).
146. Kuerschner, L., Moessinger, C. & Thiele, C. Imaging of lipid biosynthesis: how a neutral lipid enters lipid droplets. *Traffic (Copenhagen, Denmark)* **9**, 338-352 (2008).
147. Ferretti, A., *et al.* Biophysical and structural characterization of 1H-NMR-detectable mobile lipid domains in NIH-3T3 fibroblasts. *Biochimica et biophysica acta* **1438**, 329-348 (1999).
148. Khandelia, H., Duelund, L., Pakkanen, K.I. & Ipsen, J.H. Triglyceride blisters in lipid bilayers: implications for lipid droplet biogenesis and the mobile lipid signal in cancer cell membranes. *PloS one* **5**, e12811 (2010).
149. Ohsaki, Y., *et al.* Biogenesis of cytoplasmic lipid droplets: from the lipid ester globule in the membrane to the visible structure. *Biochimica et biophysica acta* **1791**, 399-407 (2009).
150. Walther, T.C. & Farese, R.V., Jr. The life of lipid droplets. *Biochimica et biophysica acta* **1791**, 459-466 (2009).
151. Bostrom, P., *et al.* Cytosolic lipid droplets increase in size by microtubule-dependent complex formation. *Arteriosclerosis, thrombosis, and vascular biology* **25**, 1945-1951 (2005).
152. Miyoshi, H., *et al.* Perilipin promotes hormone-sensitive lipase-mediated adipocyte lipolysis via phosphorylation-dependent and -independent mechanisms. *The Journal of biological chemistry* **281**, 15837-15844 (2006).
153. Subramanian, V., *et al.* Perilipin A mediates the reversible binding of CGI-58 to lipid droplets in 3T3-L1 adipocytes. *The Journal of biological chemistry* **279**, 42062-42071 (2004).
154. Miyoshi, H., Perfield, J.W., 2nd, Obin, M.S. & Greenberg, A.S. Adipose triglyceride lipase regulates basal lipolysis and lipid droplet size in adipocytes. *Journal of cellular biochemistry* **105**, 1430-1436 (2008).
155. Zimmermann, R., Lass, A., Haemmerle, G. & Zechner, R. Fate of fat: the role of adipose triglyceride lipase in lipolysis. *Biochimica et biophysica acta* **1791**, 494-500 (2009).
156. Binns, D., *et al.* An intimate collaboration between peroxisomes and lipid bodies. *The Journal of cell biology* **173**, 719-731 (2006).
157. Zhang, S.O., *et al.* Genetic and dietary regulation of lipid droplet expansion in Caenorhabditis elegans. *Proceedings of the National Academy of Sciences of the United States of America* **107**, 4640-4645.
158. Liu, P., *et al.* Rab-regulated interaction of early endosomes with lipid droplets. *Biochimica et biophysica acta* **1773**, 784-793 (2007).
159. Martin, S., Driessen, K., Nixon, S.J., Zerial, M. & Parton, R.G. Regulated localization of Rab18 to lipid droplets: effects of lipolytic stimulation and inhibition of lipid droplet catabolism. *The Journal of biological chemistry* **280**, 42325-42335 (2005).
160. Cohen, A.W., *et al.* Role of caveolin-1 in the modulation of lipolysis and lipid droplet formation. *Diabetes* **53**, 1261-1270 (2004).

161. Ost, A., Ortegren, U., Gustavsson, J., Nystrom, F.H. & Stralfors, P. Triacylglycerol is synthesized in a specific subclass of caveolae in primary adipocytes. *The Journal of biological chemistry* **280**, 5-8 (2005).
162. Blouin, C.M., *et al.* Lipid droplet analysis in caveolin-deficient adipocytes: alterations in surface phospholipid composition and maturation defects. *Journal of lipid research* **51**, 945-956.
163. Singh, R., *et al.* Autophagy regulates lipid metabolism. *Nature* **458**, 1131-1135 (2009).
164. Welte, M.A. Proteins under new management: lipid droplets deliver. *Trends in cell biology* **17**, 363-369 (2007).
165. Cermelli, S., Guo, Y., Gross, S.P. & Welte, M.A. The lipid-droplet proteome reveals that droplets are a protein-storage depot. *Curr Biol* **16**, 1783-1795 (2006).
166. Cole, N.B., *et al.* Lipid droplet binding and oligomerization properties of the Parkinson's disease protein alpha-synuclein. *The Journal of biological chemistry* **277**, 6344-6352 (2002).
167. Outeiro, T.F. & Lindquist, S. Yeast cells provide insight into alpha-synuclein biology and pathobiology. *Science (New York, N.Y* **302**, 1772-1775 (2003).
168. Shi, S.T., *et al.* Hepatitis C virus NS5A colocalizes with the core protein on lipid droplets and interacts with apolipoproteins. *Virology* **292**, 198-210 (2002).
169. Fei, W., Wang, H., Fu, X., Bielby, C. & Yang, H. Conditions of endoplasmic reticulum stress stimulate lipid droplet formation in Saccharomyces cerevisiae. *The Biochemical journal* **424**, 61-67 (2009).
170. Gubern, A., *et al.* Lipid droplet biogenesis induced by stress involves triacylglycerol synthesis that depends on group VIA phospholipase A2. *The Journal of biological chemistry* **284**, 5697-5708 (2009).
171. Rutkowski, D.T., *et al.* UPR pathways combine to prevent hepatic steatosis caused by ER stress-mediated suppression of transcriptional master regulators. *Developmental cell* **15**, 829-840 (2008).
172. Yamamoto, K., *et al.* Induction of liver steatosis and lipid droplet formation in ATF6alpha-knockout mice burdened with pharmacological endoplasmic reticulum stress. *Molecular biology of the cell* **21**, 2975-2986 (2010).
173. Hartman, I.Z., *et al.* Sterol-induced dislocation of 3-hydroxy-3-methylglutaryl coenzyme A reductase from endoplasmic reticulum membranes into the cytosol through a subcellular compartment resembling lipid droplets. *The Journal of biological chemistry* **285**, 19288-19298 (2010).
174. Ohsaki, Y., Cheng, J., Fujita, A., Tokumoto, T. & Fujimoto, T. Cytoplasmic lipid droplets are sites of convergence of proteasomal and autophagic degradation of apolipoprotein B. *Molecular biology of the cell* **17**, 2674-2683 (2006).
175. Yamasaki, S., *et al.* Cytoplasmic destruction of p53 by the endoplasmic reticulum-resident ubiquitin ligase 'Synoviolin'. *The EMBO journal* **26**, 113-122 (2007).
176. Wang, L., *et al.* Degradation of the bile salt export pump at endoplasmic reticulum in progressive familial intrahepatic cholestasis type II. *Hepatology (Baltimore, Md* **48**, 1558-1569 (2008).
177. Song, B.L., Sever, N. & DeBose-Boyd, R.A. Gp78, a membrane-anchored ubiquitin ligase, associates with Insig-1 and couples sterol-regulated

ubiquitination to degradation of HMG CoA reductase. *Molecular cell* **19**, 829-840 (2005).

178. Lee, J.N., Song, B., DeBose-Boyd, R.A. & Ye, J. Sterol-regulated degradation of Insig-1 mediated by the membrane-bound ubiquitin ligase gp78. *The Journal of biological chemistry* **281**, 39308-39315 (2006).
179. Fang, S., *et al.* The tumor autocrine motility factor receptor, gp78, is a ubiquitin protein ligase implicated in degradation from the endoplasmic reticulum. *Proceedings of the National Academy of Sciences of the United States of America* **98**, 14422-14427 (2001).
180. Liang, J.S., *et al.* Overexpression of the tumor autocrine motility factor receptor Gp78, a ubiquitin protein ligase, results in increased ubiquitinylation and decreased secretion of apolipoprotein B100 in HepG2 cells. *The Journal of biological chemistry* **278**, 23984-23988 (2003).
181. Shen, Y., Ballar, P. & Fang, S. Ubiquitin ligase gp78 increases solubility and facilitates degradation of the Z variant of alpha-1-antitrypsin. *Biochemical and biophysical research communications* **349**, 1285-1293 (2006).
182. Ying, Z., *et al.* Gp78, an ER associated E3, promotes SOD1 and ataxin-3 degradation. *Human molecular genetics* **18**, 4268-4281 (2009).
183. Kreft, S.G., Wang, L. & Hochstrasser, M. Membrane topology of the yeast endoplasmic reticulum-localized ubiquitin ligase Doa10 and comparison with its human ortholog TEB4 (MARCH-VI). *The Journal of biological chemistry* **281**, 4646-4653 (2006).
184. Zavacki, A.M., *et al.* The E3 ubiquitin ligase TEB4 mediates degradation of type 2 iodothyronine deiodinase. *Molecular and cellular biology* **29**, 5339-5347 (2009).
185. Altier, C., *et al.* The Cavbeta subunit prevents RFP2-mediated ubiquitination and proteasomal degradation of L-type channels. *Nature neuroscience*.
186. Murai-Takebe, R., *et al.* Ubiquitination-mediated regulation of biosynthesis of the adhesion receptor SHPS-1 in response to endoplasmic reticulum stress. *The Journal of biological chemistry* **279**, 11616-11625 (2004).

Chapter 2

SEL1L nucleates a protein complex required for dislocation of misfolded glycoproteins

Britta Mueller*, Elizabeth J. Klemm*, Eric Spooner, Jasper H. Claessen, and

Hidde L. Ploegh

This work has been published in:

Proc Natl Acad Sci U S A. 2008 Aug 26;105(34):12325-30.

*B.M. and E.J.K. contributed equally to this work.

B.M. performed the immunoprecipitation to identify SEl1L-interacting proteins, characterized the contribution of UBC6e to US11-mediated dislocation, and showed that UBXD8 interacts with p97 (Figs. 2.1, 2.5, 2.6F and 2.7A).

E.J.K. characterized OS-9, UBXD8, and AUP1 and their contributions to dislocation (Figs. 2.2, 2.3, 2.4, 2.6, 2.7B).

E.S. performed the mass spectrometry analysis.

Abstract

Membrane and secretory proteins that fail to pass quality control in the endoplasmic reticulum (ER) are discharged into the cytosol and degraded by the proteasome. Many of the mammalian components involved in this process remain to be identified. We performed a biochemical search for proteins that interact with SEL1L, a protein that is part of the mammalian HRD1 ligase complex and involved in substrate recognition. SEL1L is crucial for dislocation of Class I Major Histocompatibility Complex heavy chains by the human cytomegalovirus US11 protein. We identified AUP1, UBXD8, UBC6e, and OS9 as functionally important components of this degradation complex in mammalian cells, as confirmed by mutagenesis and dominant negative versions of these proteins.

Introduction

Terminally misfolded membrane or secretory proteins that have entered the endoplasmic reticulum (ER) are typically transported back across the ER membrane into the cytosol, a process referred to as dislocation or retrotranslocation. Once in the cytosol, the proteasome degrades these misfolded proteins in a ubiquitin-dependent manner [1].

Although some components show some sequence similarities to yeast proteins, their contribution to dislocation is not always clear. The presence of several mammalian orthologues for each yeast component of the dislocation machinery precludes a functional identification of the relevant mammalian components by homology.

Analysis of two viral proteins encoded by human cytomegalovirus (HCMV), US2 and US11, has helped define the composition of the protein complexes involved in dislocation [2] and emphasizes the complexity of mammalian dislocation compared to simpler eukaryotes. Both US2 and US11 facilitate dislocation of newly synthesized Class I MHC heavy chains (HCs), presumably to evade recognition by cytotoxic T cells at the appropriate stages of the virus' lifecycle [3]. US2 and US11 are ER-resident type I transmembrane proteins that interact with Class I MHC HC in the ER lumen and from there initiate their destruction [4, 5]. US2 and US11 achieve this by recruiting different sets of proteins: US2 uses signal peptide peptidase (SPP) [6] and other proteins that remain to be identified, whereas US11 engages a pathway that includes Derlin-1 [7]. Derlin-1 itself associates with the ubiquitin ligase HRD1 and gp78, both of which share sequence similarities with yeast Hrd1p [8, 9]. Whether HRD1 and gp78 are involved in the ubiquitination of Class I MHC HC is an open question [10], although the human homologue of yeast Hrd3p, SEL1L, is involved in Class I MHC HC dislocation [11]. Derlin-1, HRD1

and the transmembrane protein VIMP form a complex with p97 and its cofactors UFD1/NPL4, and might be involved in their recruitment to the ER [7-9, 12].

How a luminal protein can cross the lipid bilayer is not known, and the existence of a proteinacous pore, consisting of Hrd1p and/or Der1p has been suggested [7-9, 12-14], but alternative modes of extraction might exist [15]. US11 hijacks a pathway that contributes to the degradation of aberrantly folded proteins independently of viral accessories, as shown by examination of the mammalian dislocation substrates α1-antitrypsin null Hong Kong (NHK), truncated ribophorin RI_{332} and misfolded cystic fibrosis transmembrane conductance regulator (CFTR) ΔF508 [11, 16, 17]. Here we identified new components of the mammalian dislocation machinery that are essential for degradation, including the E2 ligase that cooperates with HRD1/SEL1L, and two ER transmembrane proteins that act downstream of the substrate selection process, and verified a recently reported SEl1L-interacting ER luminal protein important for substrate recognition, OS9 [18].

Results

Isolation and identification of proteins that interact with SEL1L.

We conducted a large-scale immunopurification of SEL1L using HA-TEV-tagged SEL1L transduced into HeLa cells (Fig. 2.1). The HA-TEV tag was fused to the N-terminus of SEL1L, for which we replaced its signal sequence with that of the murine Class I MHC molecule H2-K^b. HA-TEV-SEL1L was isolated by immunoprecipitation with anti-HA antibody-coated beads from digitonin extracts. Materials eluted with TEV protease were subjected to SDS-PAGE, and SEL1L-interacting polypeptides were identified by tandem mass-spectrometry (LC/MS/MS, Fig. 2.1). We recovered several proteins already known to be SEL1L interactors: HRD1, a ubiquitin E3-ligase involved in ER dislocation [9, 10], Derlin-2, a multispanning transmembrane protein required for exit of polyomavirus from the ER [19], the ATPase p97 and several other proteins involved in protein folding, such as PDI, BiP, and calnexin (Fig. 2.1B). The latter bind to many different proteins in the ER, and their contribution, if any, to dislocation is not always clear.

We identified two additional proteins not previously known to be part of the mammalian dislocation machinery: ancient ubiquitous protein 1 (AUP1) and UBXD8 (Fig. 2.1). In addition, we identified UBC6e, an enzyme that serves as a ubiquitin conjugating enzyme (E2), [20], and OS9, a protein involved in the degradation of mutant alpha-1 antitrypsin [18]. Because of its physical association, we propose that UBC6e is the E2-type activity that acts in concert with the ubiquitin ligase HRD1.

OS9 was identified as a protein amplified in osteosarcoma. OS9 is ubiquitously expressed and has alternative splice versions [21]. The C-terminus of OS9 interacts with

HIF1α, a subunit of the protein hypoxia inducible factor (HIF) 1. HIF1α is ubiquitinated and degraded, depending on oxygen levels in the cell. OS9 regulates HIF1α levels by increasing the rate of prolyl hydroxylation in HIF1α, thereby initiating ubiquitination [22].

The presence of an N-terminal signal sequence suggests that OS9 is targeted to the ER lumen. OS9 has a glucosidase type II (Mannose-6 phosphate receptor homology, MRH) domain involved in binding to misfolded proteins. OS9, an ER-resident glycosylated protein, is part of the mammalian dislocation machinery through its interactions with SEL1L [Fig. 2.1B, and [18]]. OS9 has been previously located to the cytosol [22, 23]. It remains unclear whether there is a pool of OS-9 that is active in the cytosol or whether OS9 could regulate HIF1α indirectly from within the ER. The yeast homolog Yos9p is a luminal ER protein that binds to the luminal domain of Hrd3p, the homolog of SEL1L. Yeast Yos9p targets terminally misfolded ER proteins to the dislocation machinery, which includes Hrd3p and Der1p [13, 24, 25].

AUP1 is proposed to interact with integrins [26], but its function is obscure. AUP1 has a CUE domain, involved in ubiquitin binding or in recruitment of ubiquitin conjugating enzymes to the site of dislocation [27]. AUP1 has a transmembrane anchor at its N-terminus, with the bulk of the protein predicted to be in the cytosol [26]. AUP1 has not previously been implicated in any aspect of (glyco) protein quality control, and is without an obvious homolog in yeast.

UBXD8 (ETEA) was initially identified among proteins highly upregulated in T-cells obtained from patients with atopic dermatitis [28]. UBXD8 has a UBX domain, a UBA domain, a UAS domain, and a transmembrane domain according to prediction programs (Fig. 2.1B). The UBA domain is found in many proteins of otherwise divergent structure

and function, and mediates binding to ubiquitin. The UBX domain is structurally similar to ubiquitin despite the lack of a high degree of sequence homology. UBX domains may serve as adaptors for the multi-functional AAA ATPase p97 [29]. The UAS domain is a domain of >100 amino acids of unknown function, which assumes a thioredoxin-type fold (InterPro database). The closest relative of UBXD8 in yeast cannot immediately be inferred, because of the limited extent of overall sequence identity and lack of functional data.

UBC6e (UBE2J1) is an ortholog of yeast Ubc6p, a transmembrane ER-bound ubiquitin conjugating enzyme (E2). In yeast, Ubc6p can function together with the ubiquitin ligase Doa10p and the cytosolic E2 Ubc7p [30, 31]. There are two Ubc6p orthologs in mammalian cells, UBE2J1 and UBE2J2 [20]. UBE2J1 was termed UBC6e, and UBE2J2 is called UBC6 [20]. For simplicity we shall refer to UBE2J1 as UBC6e. UBC6e and UBC6 are both involved in the degradation of TCRα and CFTRΔF508 [16, 20]. UBC6e forms a complex with Derlin-1 for CFTRΔF508 disposal [16]. UBC6e displays less sequence identity (25%) to the yeast protein than does UBC6 (40%, [20]. Unlike yeast Ubc6p, human UBC6e is a stable protein [32].

Figure 2.1

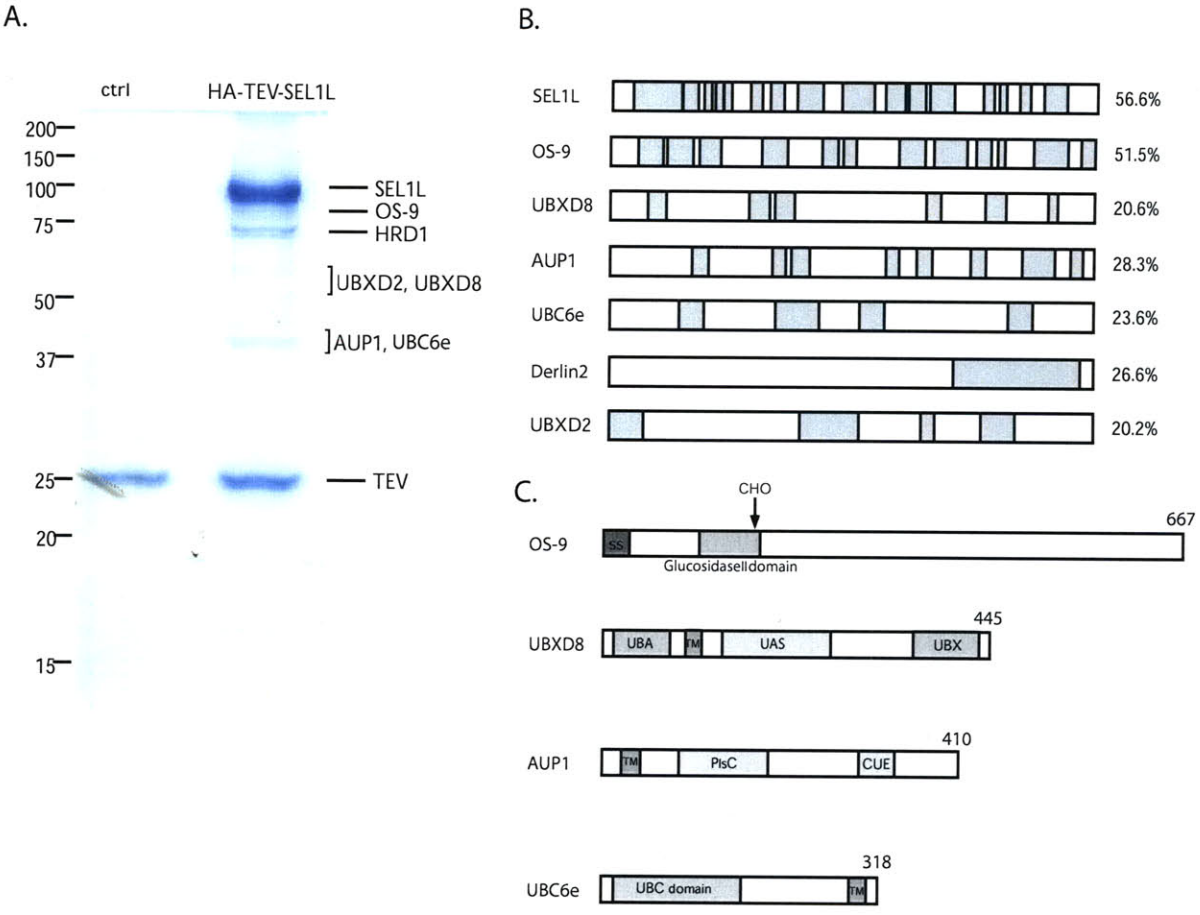

Isolation of SEL1L associated proteins.

A. Immunoprecipitation of HA-TEV-tagged SEL1L. HeLa cells (ctrl) and HA-TEV-SEL1L expressing HeLa cells were lysed in 2% digitonin, and the lysate was subjected to immunoprecipitation with anti-HA antibody beads. Bound material was eluted from the beads with TEV protease and separated on SDS PAGE (10% acrylamide). Polypeptides were visualized by Coomassie Blue staining.

B. Proteins that interact with SEL1L, the peptides identified by LC/MS/Ms are shown in grey together with the sequence coverage (in %, number on the right).

C. Proposed domain structure of the isolated SEL1L-interacting partners. CHO = N-linked glycan, ss = signal sequence, TM = transmembrane domain, UBA = ubiquitin associated, UAS = thioredoxin fold, UBX = ubiquitin fold, PlsC = phosphate acyltransferase domain, UBC = ubiquitin conjugating domain. CUE = domain involved in ubiquitin binding. Numbers on the right represent length in amino acids.

ER localization of the SEL1L-interacting proteins.

We performed immunofluorescence microscopy with affinity purified anti-AUP1 and anti-UBXD8 antibodies in HeLa cells. Immunofluorescence shows the diagnostic reticular ER staining pattern for AUP1 and UBXD8 and co-localization with the ER marker PDI (Fig. 2.2A). Endogenous AUP1 and UBXD8 proteins thus reside in the ER, where dislocation occurs. UBXD8, AUP1, and UBC6e all readily cosediment with the microsomes in the absence of detergent and are largely resistant to extraction with alkaline sodium carbonate and urea (Fig. 2.2B). OS9, consistent with its predicted characterization as a soluble ER luminal protein, is readily extracted from the microsomes by alkaline sodium carbonate. For OS9, we observe the presence of two splice variants [21], both of which are sensitive to digestion with endoglycosidase H (EndoH, Fig. 2.2C), consistent with ER residency and the presence of the single predicted N-linked glycan. We verified the interaction of endogenous OS9, UBC6e, and AUP1 with SEL1L by immunoprecipitation followed by immunoblotting (data not shown).

Figure 2.2

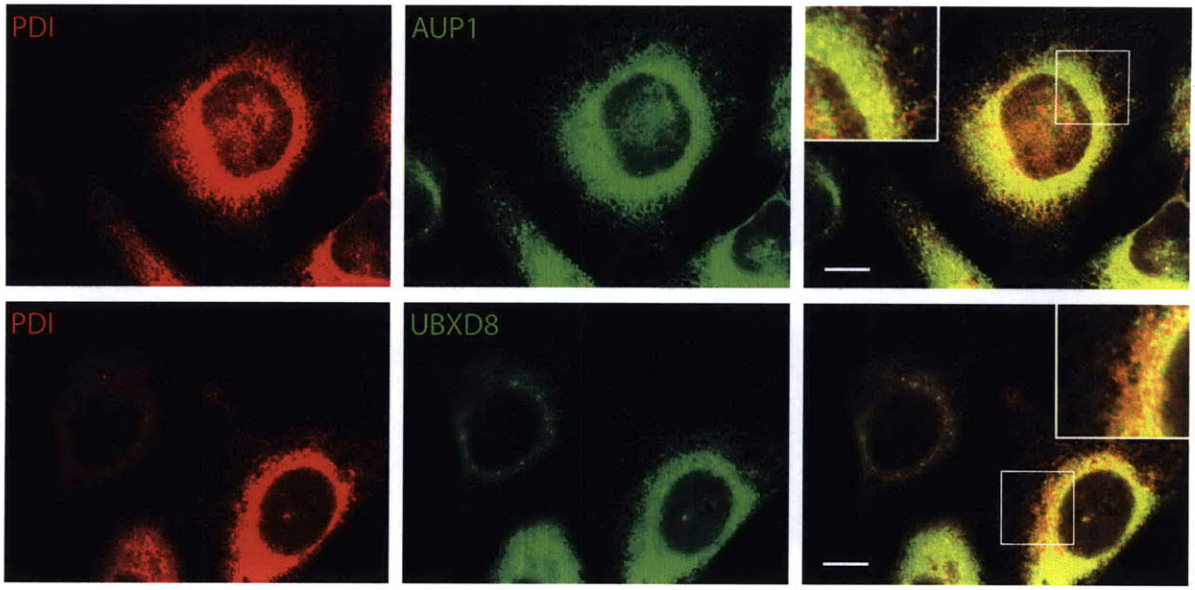

A) HeLa cells were fixed and incubated with anti-PDI antibody and affinity-purified antibodies against AUP1 (upper panels) or UBXD8 (lower panels) for immunofluorescence analysis. Right panels show the merged images. Scale bars= 10μm.
B) Microsomes from U373 cells were incubated with homogenization buffer, 3M Urea, sodium carbonate pH11.6, or 1% SDS, pelleted and immunoblotted as indicated. T=total, P=pellet, S=supernatant. Proteins were separated by 10% (UBC6e and OS9) or 15% (PDI, Calnexin, AUP1, and UBXD8) SDS-PAGE. #= cross-reactive bands.
C) US11 cells were pulse-labeled for 10min with 35S and chased for indicated time points. The cells were lysed in 1% SDS and the lysate was subjected to immunoprecipitation with anti-OS9-antibodies. The bound material was eluted and incubated with or without EndoH for 1hour at 37C. The eluates were separated on SDS-PAGE (8% acrylamide) and visualized on film.

OS9 overexpression perturbs dislocation of RI_{332} but not of Class I MHC via US11

To examine a possible role for OS9 in dislocation, we designed an N-terminal GFP-tagged version and two mutant versions (R188A; E212D) of OS9. These point mutations are predicted to disrupt the MRH (glucosidase II) domain implicated in OS9 substrate interaction [33, 34]. Mutant or tagged versions of OS9 in US11-expressing cells only marginally disrupt Class I MHC HC dislocation (Fig. 2.4 and Fig. 2.6A, lanes 10-12), especially when compared to the effect seen with overexpression of UBC6e, AUP1-GFP or UBXD8-GFP (Fig. 2.5 and 2.6). To explain the comparative dispensability of OS9 in US11-expressing cells, US11 might be directly responsible for substrate recognition instead of OS9 and target Class I MHC HC directly to the dislocation machinery.

Does OS9 play a role in dislocation independent of viral proteins? We generated HeLa cells that stably overexpress wild-type OS9, GFP-OS9, or the mutant versions OS9 R188A, and OS9 E212D. We then transiently transfected these cell lines with a truncated version of ribophorin, RI_{332} [35], a protein dislocated in a SEL1L-dependent manner [11]. For all constructs examined, we observe a delay in RI_{332} degradation (Figure 2.3). Endogenous Ribophorin I is stable and electrophoretically distinct, and it serves as a control for recovery. We conclude that OS9 is involved in the dislocation of the soluble glycoprotein RI_{332}. Overexpression of wild-type OS9 inhibits dislocation of RI_{332}, presumably because OS9 overexpression interferes with the stoichiometry of the dislocation complex. We sought to verify our results with knockdown constructs against OS9, but none of the constructs yielded a level of reduction adequate to achieve inhibition of dislocation.

Figure 2.3

A.

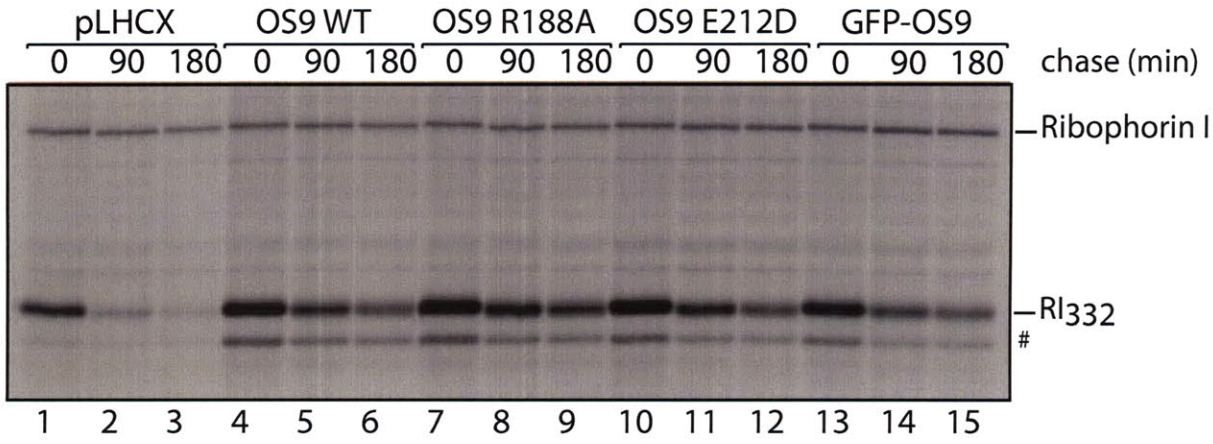

B.

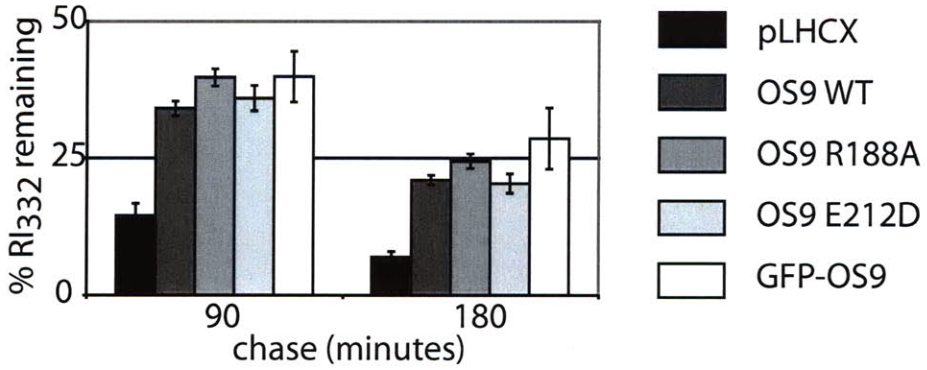

OS9 is crucial for dislocation of the terminally misfolded glycoprotein, RI_{332}

A) HeLa cells were transduced with either empty vector (pLHCX), wild type OS9, OS9 R188A, OS9 E212D, or GFP-OS9, using the same virus preparation as in Fig. 2.4. The five cell lines were then transfected with a construct that specifies truncated Ribophorin I, RI_{332}, pulse-labeled 36 hrs post transfection for 15min with ^{35}S, chased for indicated time points, then lysed in 1% SDS and immunoprecipitated with antibody raised against the luminal portion of ribophorin. The eluates were separated on 10% SDS-PAGE and visualized by autoradiography. The # indicates non-glycosylated RI_{332}.

B) Quantitation of the amount of RI_{332} remaining at the indicated time points.

Figure 2.4

A.

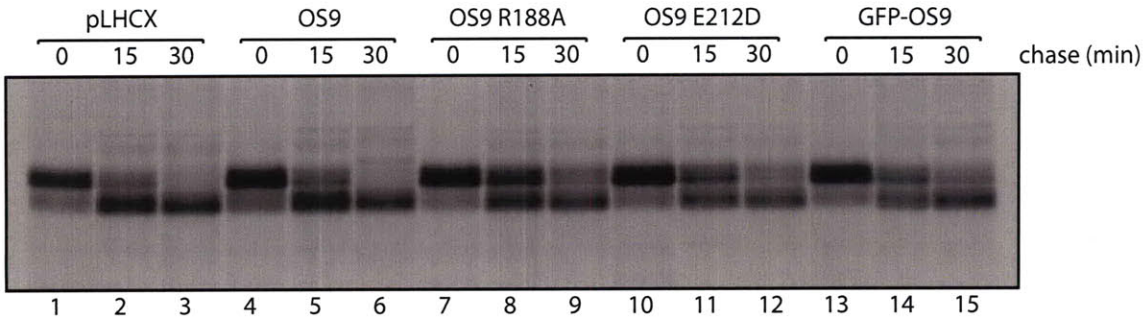

B.

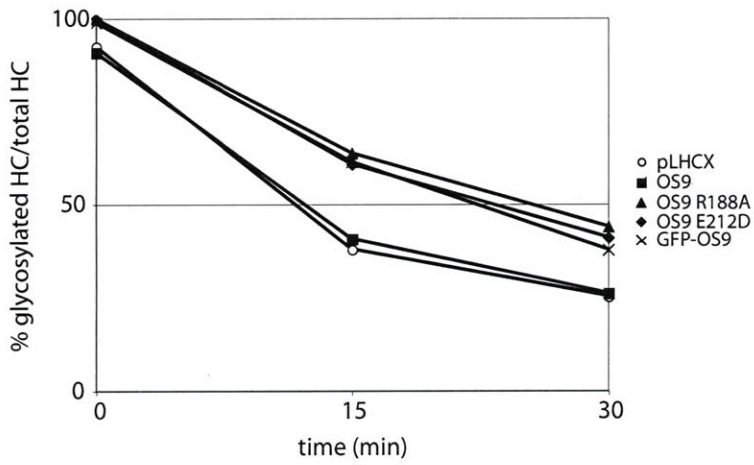

OS9 is not involved in US11-mediated dislocation

A) US11-expressing cells were transduced with the following virus preparations: empty vector (pLHCX), wild type OS9, OS9 R188A, OS9 E212D, or GFP-OS9. The cell lines were treated with ZL_3VS and pulse-labeled for 10min with ^{35}S and chased for indicated time points. The cells were then lysed in 1% SDS and immunoprecipitated with anti-HC antibody. The eluates were separated on SDS-PAGE (12% acrylamide) and visualized on film.

B) Quantitation of the amount of glycosylated Class I MHC HC to total HC counts.

Verification of involvement in dislocation for the SEL1L-interacting proteins UBXD8, AUP1 and UBC6e.

Because US11 and US2 both target Class I MHC molecules, but apparently do so by initially recruiting different proteins, we used US2-mediated dislocation as a control for proper ER function [6, 7, 11]. Manipulations that perturb ER function non-specifically should affect dislocation via both the US2 and the US11 pathways. Our criterion is thus to score as specific those manipulations that interfere with US11-mediated dislocation only.

Among the set of SEL1L-interacting proteins, UBC6e was the only protein known to act as an enzyme and whose catalytic center could be ascertained [20]. We thus destroyed the catalytic activity of UBC6e by replacement of cysteine 91 with serine [32].

We installed a GFP tag onto the C-terminus of AUP1 and UBXD8 and onto the N-terminus of OS9. We reasoned that the GFP domain may interfere with, but not completely abolish, the function or recruitment capabilities of flanking domains and thus yield inhibitory effects for the corresponding GFP fusion proteins [7]. Because UBXD8 has a UBX domain that might recruit p97 to the site of dislocation, the attachment of a globular GFP-sized domain in close proximity to the C-terminal UBX domain might interfere with this interaction. Similarly, the GFP-tagged version of Derlin-1 inhibits Class I MHC HC degradation in US11-dependent fashion [7].

We observe strong inhibition of class I MHC HC degradation in US11 cells that overexpress UBC6e C91S, AUP1-GFP, and UBXD8-GFP, (Figs. 2.5 and 2.6). In pLHCX vector control cells, most Class I MHC HCs have lost their N-linked glycan at the 30 min chase point, due to the activity of the cytoplasmically disposed PNGase [36]. In the

presence of proteasome inhibitor (ZL_3VS), the diagnostic deglycosylated dislocation intermediate accumulates and is recognized by its distinct mobility on SDS PAGE [4]. The overexpression of catalytically inactive UBC6e (C91S) or wild-type UBC6e strongly delays in the degradation of Class I MHC HC: >75% of HC remains in the ER (Fig. 2.5A-1, lanes 4-9). All three cell types express comparable levels of US11, and displays the typical delayed cleavage of its signal peptide [37] (Fig. 2.5A-3, lanes 1-9).

In US2 cells transduced with the same constructs, degradation continues unperturbed: Class I MHC HCs are dislocated at rates similar to those observed in control cells (pLHCX), compared to cells that overexpress UBC6e or UBC6e C91S (Fig. 2.5C-1, lanes 1-9). All three cell lines express similar levels of US2, with its usual mobility on SDS-PAGE: in addition to ER-membrane inserted glycosylated US2, we detect a faster migrating US2 lacking its N-linked glycan, as US2 is inefficiently translocated into the ER [38]. Both the US2 and the US11 cell lines were obtained by viral transduction of UBC6e C91S and WT UBC6e and show equivalent levels of expression of UBC6e (Fig. 2.5A-2, lanes 4-9 and Fig. 2.5C-2, lanes 4-9). The ubiquitin-activating enzyme UBC6e is thus involved in Class I MHC HC dislocation in US11 cells, but not in US2 cells. Because US2 cells remain capable of proper dislocation, ER function as such is not compromised.

We then examined the fate of Class I MHC HC when expressing the GFP-tagged versions of the three identified proteins AUP1, UBXD8 and OS9 (Fig. 2.6). Cells that express AUP1-GFP showed inhibition of dislocation: 50% of Class I MHC HC remains in the ER after 30min of chase (Fig. 2.6A, lanes 4-6, and Fig. 2.6B). The effect is even more pronounced when using cells that express UBXD8-GFP: more than 75% of HCs

fail to reach the cytosol (Fig. 2.6A, lanes 7-9, and Fig. 2.6B). As mentioned above, GFP-OS9 did not significantly inhibit dislocation of Class I MHC HC. Again, US2 cells served as a control. US2-dependent dislocation proceeded unperturbed in AUP1-GFP, UBXD8-GFP, and OS9-GFP cells (Figure 2.6C and D). Equal amounts of the GFP-tagged constructs were expressing in the US2- and US11-expressing cells (Fig. 2.6E).

We compared the ability of UBXD8 and UBXD8-GFP to recruit p97 into the dislocation complex. To this end, we overexpressed UBXD8 and UBXD8-GFP to the same levels in 293T cells and performed an immunoprecipitation with anti-UBXD8 antibodies from digitonin lysates. The recovered material was then analyzed by immunoblotting with anti-p97 antibodies (Fig. 2.6F). The amount of p97 recovered in immunoprecipitates from cells expressing UBXD8-GFP is much reduced compared to cells expressing wild-type UBXD8. We conclude that the GFP tag hinders recruitment of p97 to the ER membrane, and therefore impedes dislocation. The residual p97 recovered is attributable to the endogenous UBXD8 present in the cells.

Figure 2.5

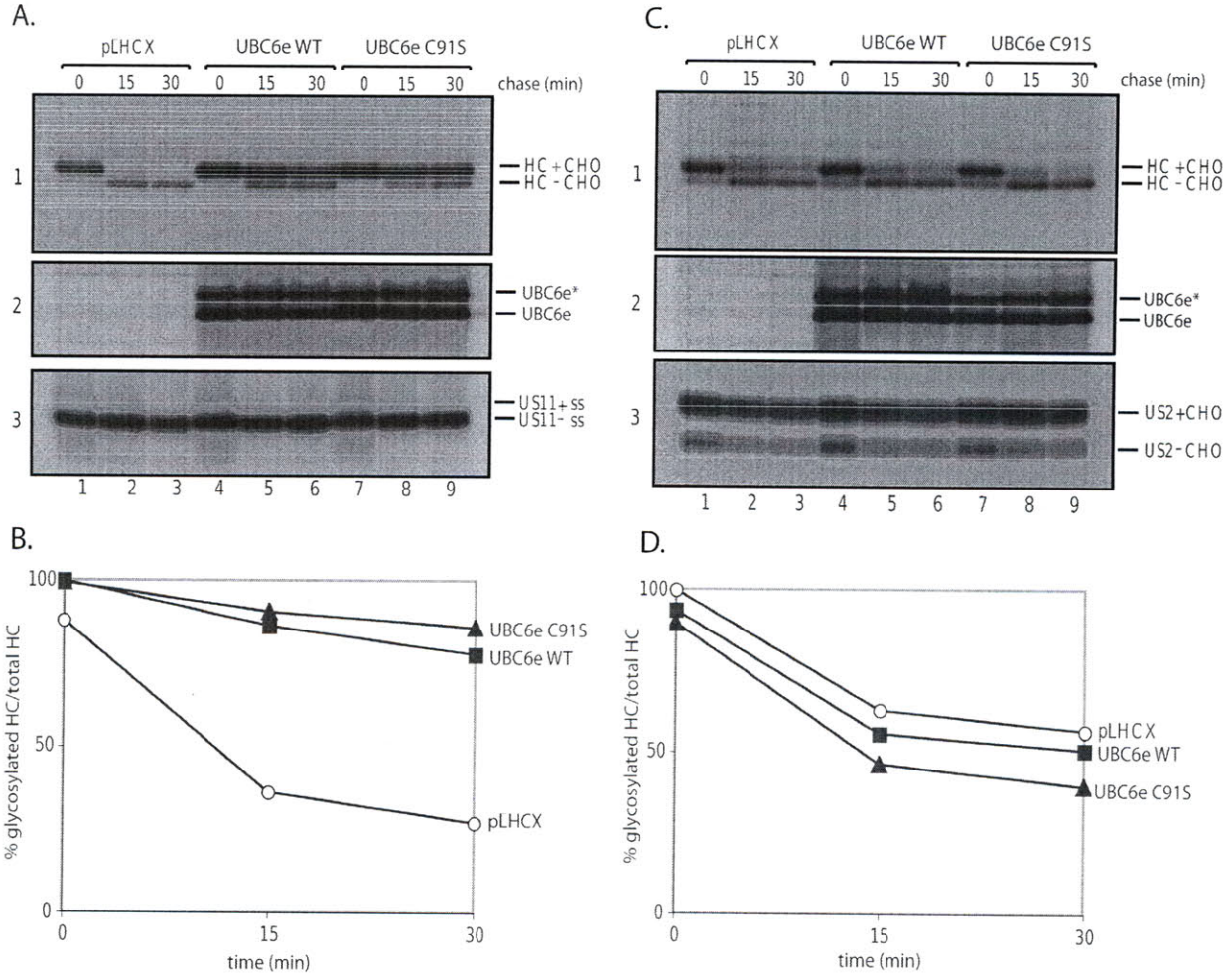

UBC6e is crucial for US11 mediated dislocation.

A) US11-expressing cells were transduced with either empty vector (pLHCX), UBC6e WT, or UBC6e C91S mutant. The three cell lines were treated with ZL_3VS, pulse-labeled for 10min with ^{35}S, chased for indicated time points, and then lysed in 1% SDS and the lysate was immunoprecipitated with anti-HC [1], anti-UBC6e [2], and anti-US11 [3] antibodies sequentially. The eluates were separated on 12% SDS-PAGE and visualized on film. The asterix represents a slower migrating band that occurs upon overexpression of UBC6e and is likely a phosphorylated version of UBC6e (Oh et al., 2006).

B) Quantitation of the amount of glycosylated HC to total HC counts.

C) US2-expressing cells were transduced with the same virus preparation used in (a). The experiment was performed as in (a).

D) Quantitation of the amount of glycosylated Class I MHC HC to total HC counts.

Figure 2.6

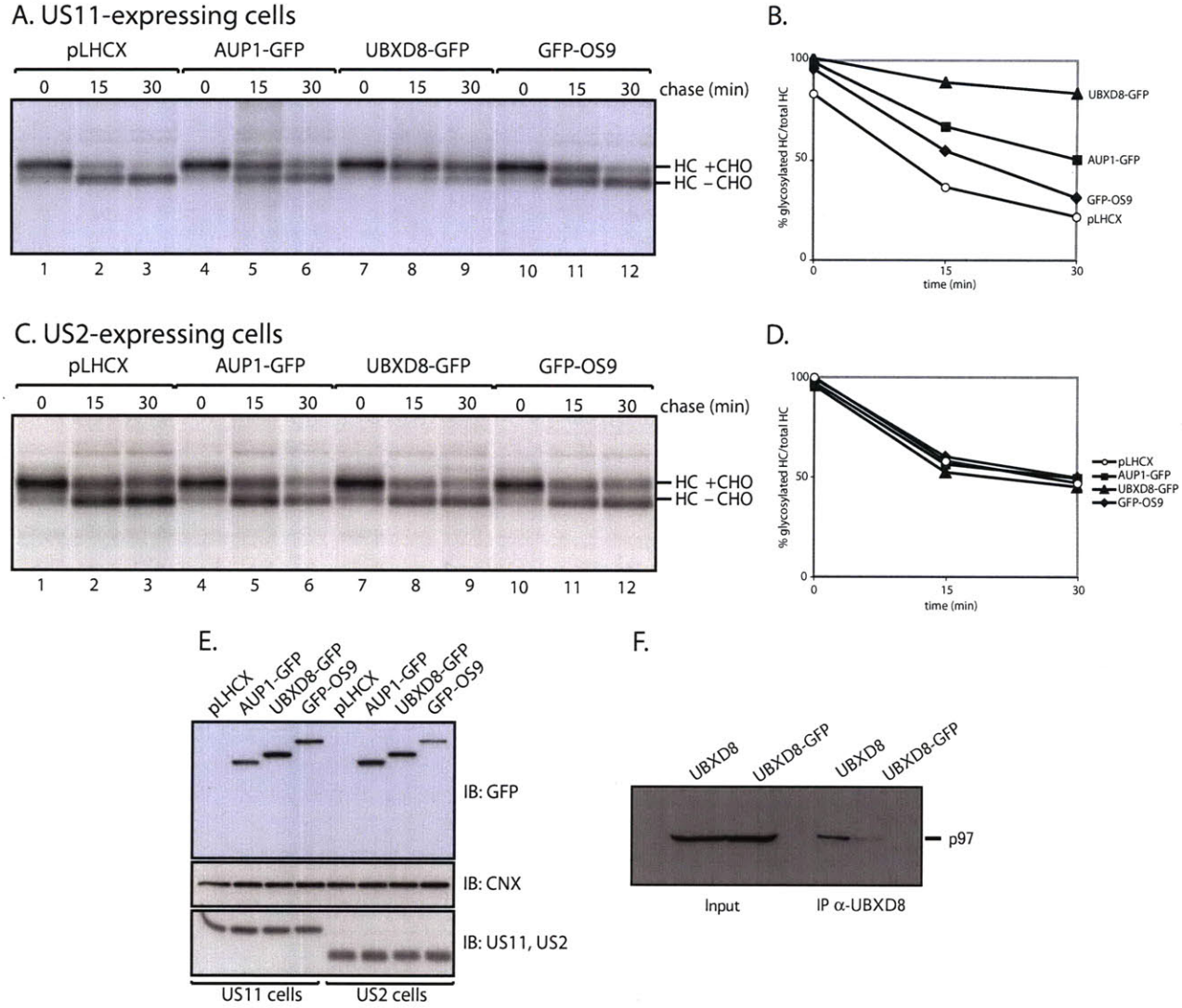

AUP1 and UBXD8 are crucial for US11-mediated dislocation

A) US11-expressing cells were transduced with either empty vector (pLHCX), AUP1-GFP, UBXD8-GFP, or GFP-OS9. The experiment was performed as in Figure 2.5.

B) Quantitation of the amount of glycosylated Class I MHC HC to total HC counts.

C) US2-expressing cells were transduced with the same virus preparation used in (A) and a pulse-chase experiment was performed as for (A).

D) Quantitation of the amount of glycosylated Class I MHC HC to total HC counts.

E) The cell lines used in (A) and (B) were lysed in 1% SDS, separated by SDS-PAGE, and transferred to a PVDF membrane. The membrane was immunoblotted for GFP, calnexin (cnx, loading control), US11, and US2.

F)The GFP-tag on UBXD8 hinders recruitment of p97. UBXD8 WT and UBXD8-GFP were expressed in 293T cells and immunoprecipitated with anti-UBXD8 antibodies from digitonin extracts. The eluates were separated on a 10% SDS-PAGE and immunoblotted with anti-p97 antibodies.

The dominant negative constructs of UBC6e, AUP1 and UBXD8 retain Class I MHC HC in the ER

We used the monoclonal antibody W6/32, which recognizes only correctly assembled Class I MHC molecules in their fully native conformation [39], to explore whether inhibition of dislocation is accompanied by an increase in the amount of correctly folded Class I MHC molecules. We indeed found this to be the case (Fig. 2.7, cell lines used were those from Figure 2.5 and 2.6) and conclude that the intermediates that accumulate when dislocation is inhibited retain their typical orientation within the ER. In pulse chase experiments, the W6/32-reactive Class I MHC molecules do not undergo conversion of their high mannose to the complex type glycans, as inferred by a lack of a shift in mobility assessed by SDS-PAGE. This observation is consistent with the ability of US11 to retain Class I MHC molecules in the ER, also when dislocation is blocked, as observed for the single point mutant in the transmembrane segment of US11 [40]. This experiment also demonstrates that UBC6e C91S, UBC6e WT, AUP1-GFP, and UBXD8-GFP do not disrupt dislocation merely by preventing the association of US11 with Class I MHC HC: as with the empty vector control, US11 co-immunoprecipitates with W6/32-reactive Class I MHC HC in all of the cell lines constructed (Fig. 2.7).

Figure 2.7

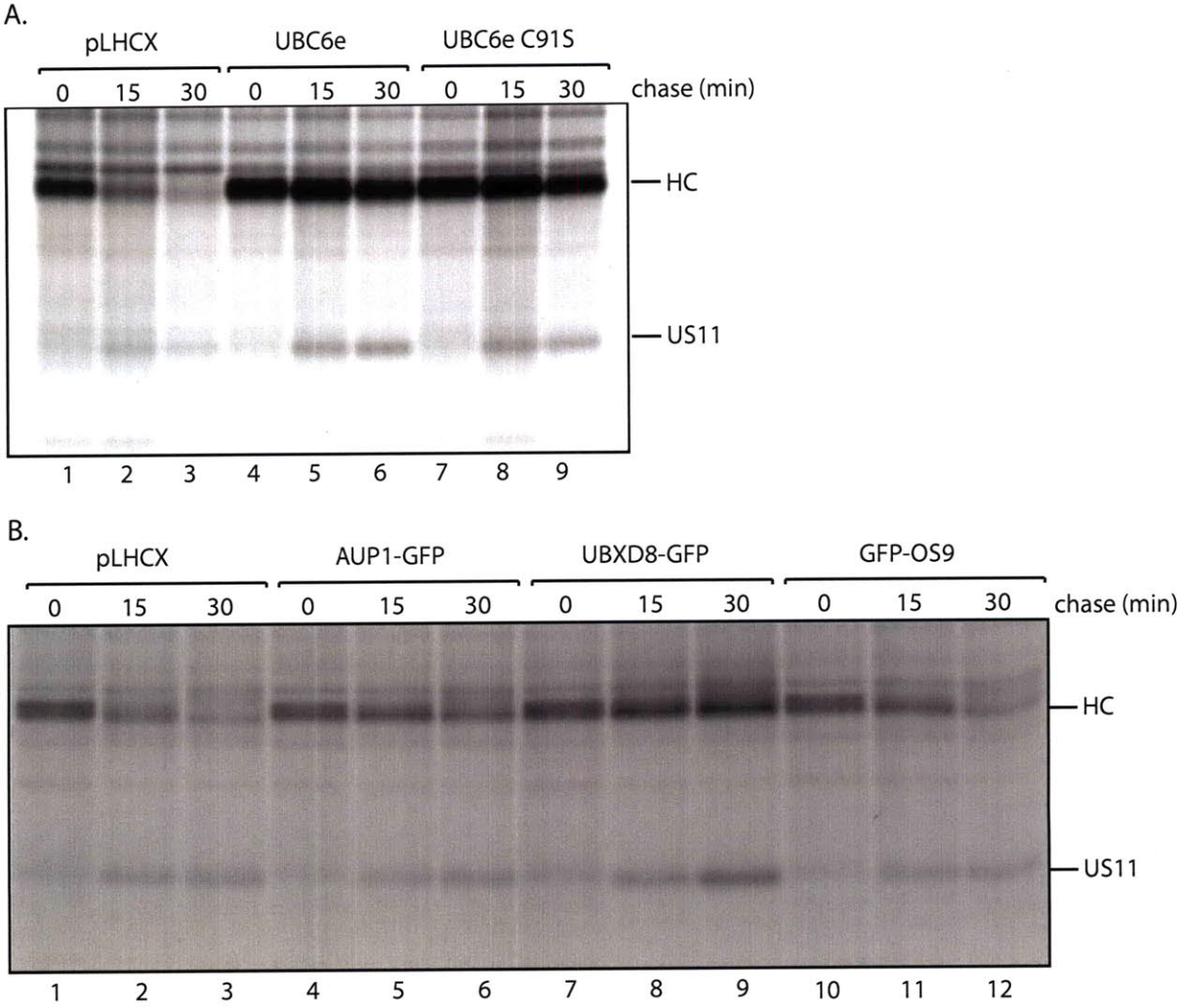

Dominant negative versions of UBC6e, AUP1, and UBXD8 retain Class I MHC HC in the ER
A) Cell lines from Figure 2.5A were pulse labeled for 10 minutes with ^{35}S and chased for the indicated time points. The cells were then lysed in 0.5% NP-40 and properly folded Class I MHC HC was immunoprecipitated with the W6/32 antibody. Eluates were separated on SDS-PAGE (12%) and visualized on film.
B) Cell lines from Figure 2.6A were treated as in (A).

Discussion

We have identified three new components of the mammalian dislocation machinery. We used as the point of departure the isolation of SEL1L-interacting partners. We reasoned that via SEL1L, we should recover additional proteins involved in ER dislocation: both ER luminal components that may be involved in substrate recognition, and, through its binding partner HRD1, additional cytosolic components that act downstream.

We chose a cell line that did not express US11 to isolate the SEL1L complex to avoid possible bias that might derive from remodeling of the dislocation machinery by US11 itself. The significance of the isolated proteins was verified by returning to our model dislocation cell lines, those expressing US11 or US2. US11 uses a pathway that is superficially similar to the Hrd1p/Hrd3p pathway in yeast [7, 9, 11].

From our analysis of the US11 pathway, the role of OS9 in dislocation is not immediately apparent. We thus turned to an examination of the fate of the ribophorin fragment RI_{332} to assess a possible contribution of OS9 to dislocation, because RI_{332} is removed from the ER and destroyed in a SEL1L-dependent manner. When interpreting these results, it is imperative to keep in mind the timescale of dislocation of each of the substrates. Since US11-mediated dislocation proceeds at a rapid pace (Class I MHC HC half-life is only 2-5 minutes), it may well be more sensitive to minor perturbations than the dislocation of other, longer-lived, substrates such as RI_{332}. This sensitivity is valuable for identification of members of the dislocation complex, but requires a more stringent threshold when discussing significance. Thus the same magnitude of stabilization of RI_{332} may well be more significant than for Class I MHC HC. Since the effect of the OS9

mutants and GFP-OS9 on US11-mediated dislocation is much lower than AUP1-GFP and UBXD8-GFP, we consider the role of OS9 to be comparatively minor (Fig. 2.6). In contradistinction, the moderate effect of manipulating OS9 level on RI_{332} degradation is sufficient to implicate OS9 in the quality control mechanism of RI_{332}, as is the case in SEL1L-dependent degradation [11].

Since overexpression of wild-type OS9 inhibits dislocation of RI_{332}, excess OS9 likely disrupts the architecture of the complex by titrating away components and rendering the dislocon incapable of efficiently processing substrates. Interestingly, we do not see such a difference in US11 cells that overexpress OS9 to similar levels. Why does a disruptive level of OS9 not affect the performance of the dislocon in US11-expressing cells? We attribute this discrepancy to the fact that US11 itself may stabilize the complex in a way that is insensitive to excess OS9 levels. Perhaps the rapidity of US11-mediated dislocation in itself also points to a stabilized dislocon and more efficient recognition, inherent in the unique and specific interaction of US11 with its substrate.

Combined, these results are consistent with a model in which US11 serves the specific function of delivering Class I MHC HC to the HRD1/SEL1L complex and accelerates their removal from the ER and degradation (Fig. 2.8). In HeLa cells, OS9 is an integral part of this complex, and contributes to substrate recognition. For neither mammalian OS9 nor for its yeast homolog, Yos9, is it clear what (sets of) endogenous substrates each of them recognize. The example of US11 shows that other proteins can assume a substrate recognition function in the context of the larger HRD1/SEL1L complex and deliver substrates to the ligase complex. OS9 is in fact essential for the degradation of mutant α-1 antitrypsin [18].

We show that UBC6e is involved in the degradation of Class I MHC HCs in US11 cells. The identification of the ubiquitin-conjugating enzyme (E2) that mediates this process has been an important goal, and one possible E2, the E2-25K protein, was uncovered using a permeabilized cell system [41] to assay for its activity. However, this assay does not allow exchange or removal of membrane-bound molecules, and so it is not surprising that UBC6e, an E2-type enzyme equipped with a C-terminal membrane anchor, escaped detection. From the *in vivo* data in intact cells presented here, we believe that UBC6e is the primary E2 enzyme that catalyzes the ubiquitination of Class I MHC HCs in US11 cells. Other E2s, especially if present in excess, might nonetheless be capable of performing the same reaction.

We also identified two UBX domain-containing proteins, UBXD2 and UBXD8, both of which associate with SEL1L. UBXD2 (Erasin), the first mammalian UBX-containing protein linked to dislocation, participates in the degradation of CD3δ [42], but does so through unknown mechanisms. Could UBXD8 be the possible homolog of Ubx2p, a protein that spans the ER membrane twice and is involved in recruiting p97 to the ER membrane [43, 44]? We see strong inhibition of US11-mediated HC dislocation when overexpressing UBXD8-GFP. However, UBXD8 shares only 17% sequence identity with Ubx2p. Curiously, UBXD8 shares the same level of homology with Ubx3p (another cdc48p cofactor of unknown function). Ubx3p was not reported to be part of the dislocation complex in yeast [24, 25]. UBXD8 and Ubx3p share similar organization, reflected by the order of the distinct domains that are present: both are predicted to have a UAS and a UBX domain C-terminal to a single transmembrane domain. In contrast, Ubx2p has two transmembrane domains and lacks the UAS domain, but does have a

UBA domain at its N-terminus. If UBXD8 were to be inserted as a type I or type II ER transmembrane protein, either the UBA or the UBX domain would reside within the ER lumen. Domains that specify involvement in the ubiquitination pathway are not usually found inside the ER. We see clear ER–localization of UBXD8 in immunofluorescence and by sedimentation analysis of microsomes (Fig. 2.1), so we propose a similar mechanism of ER insertion as has been shown for Erasin or UBXD2. UBXD8 might be inserted in the ER membrane by dipping into the outer leaflet of the lipid bilayer (Figure 2.8) with both tails exposed to the cytosol [42]. UBXD8 and UBXD2 might both be involved in recruitment of p97 to the site of dislocation, together or separately, depending on the topology of the substrate. The GFP tag installed on UBXD8 hinders recruitment of p97 which might account for the slowed dislocation (Figure 2.6F). We do not know how AUP1 acts as a dominant negative, but it is plausible that the GFP tag here also hinders the recruitment of a downstream, possibly unknown, component of the dislocation machinery.

It is now clear that UBC6e, AUP1, and UBXD8 are required for the exit of a type I ER-membrane protein from the ER (Figs. 2.5 and 2.6). UBC6e and AUP1 each have one transmembrane segment and UBXD8 may dip into the cytosolic face of the ER membrane, all of which may contribute to the formation of a proteinaceous channel. Each of these three proteins also contain conserved functional domains with cytoplasmic exposure. A schematic representation of the putative organization and composition of this complex is shown in figure 2.6. The initial step of the dislocation pathway involves recognition of the substrate. In the case of Class I MHC HC, this is primarily done by US11, but for RI_{332}, a glycosylated misfolded protein, OS9 is involved in the process.

The other three proteins described here, AUP1, UBXD8 and UBC6e, also act prior to cytoplasmic disposition of the dislocation substrate (Figs. 2.3 and 2.7). UBC6e acts as an E2 ubiquitin ligase and UBXD8 appears to play a role in the recruitment of the AAA+ ATPase p97. The role of AUP1 remains elusive, but its CUE domain may be involved in recruitment of another ubiquitin conjugating enzyme. The identification of additional proteins that participate in these reactions, as reported here, is an important step towards a better understanding of the essential cellular process of dislocation.

Figure 2.8

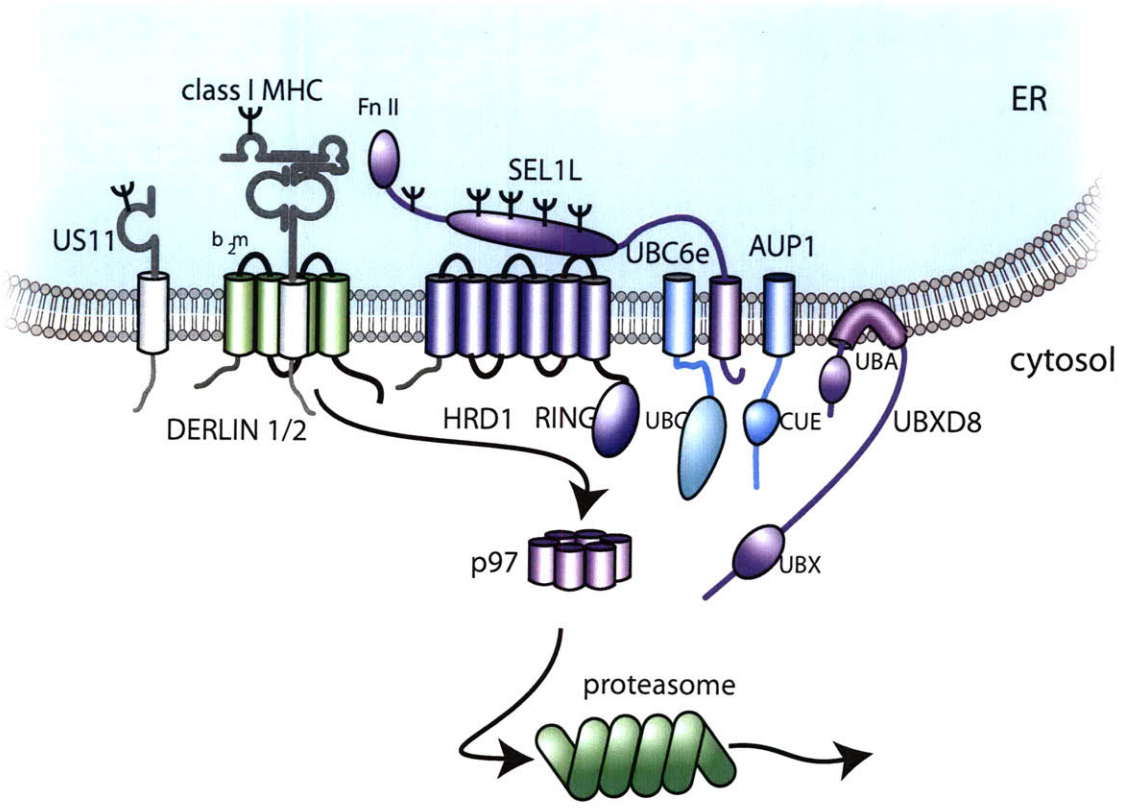

Schematic of US11- mediated dislocation
Depicted is the complex that US11 uses to dislocate class I MHC HCs.
Fn II = fibronectin type II domain, Glc II = glucosidase II domain.

Methods

Antibodies, cell lines, constructs

Antibodies:

The cytosolic parts of the three proteins AUP1 (aa 62-411), UBC6e (aa 1-232), and UBXD8 (aa 361-445) were expressed as N-terminal His-tagged fusions in *E. coli BL21 (DE3) Rosetta* cells and purified. The recombinant His-tagged fusion proteins were sent to Covance Research Products to generate rabbit polyclonal antibodies. Antibodies against AUP1, UBC6e, and UBXD8 were affinity purified as described [7]. Antibodies to Class I MHC HC, US2, US11 have been described [38, 40]. The anti-GFP, anti-PDI, and anti-OS9 antibodies were purchased from Abcam. Alexa 488-conjugated goat anti-mouse and alexa 568-conjugated goat anti-rabbit were from Molecular Probes. Anti-Ribophorin antibody and the RI_{332} cDNA were a generous gift from N. Erwin Ivessa.

Cell lines:

U373, US2, US11 cell lines have been described [11]. HeLa and 293T cells were purchased from ATCC. Cells transduced with pLHCX based vectors were selected and maintained in 125ug/ml hygromycin B (Roche).

Protein Constructs:

The murine H2-K^b signal sequence was fused to the N-terminal HA-TEV tag of SEL1L to ensure proper ER localization. SEL1L was cloned from cDNA using standard methods. The SEL1L sequence is unstable in bacteria and several mutations occured that were removed by single point mutagenesis (Strategene). cDNA clones for UBXD8, OS9, UBC6e, and AUP1 were obtained from Open Biosystems and the open reading frame was cloned into pcDNA3.1(+), pLHCX (clontech), and pEGFP-N1 (clontech). GFP-OS9

was cloned with the OS9 signal sequence replaced by the murine H2-K^b signal sequence followed by GFP.

Anti-HA-affinity purification and MS/MS analysis

$5*10^8$ HeLa cells were lysed for 30 min in 24 ml of ice-cold lysis buffer (2% digitonin, 25mM Tris-HCl pH 7.4, 150mM NaCl, 5mM $MgCl_2$, complete protease inhibitor tablets (Roche), 2.5mM N-ethylmaleimide). The nuclei and cell debris were pelleted at 16000g for 15min, and the cleared lysate was incubated with 250ul anti-HA-agarose beads (clone 3F10, Roche) for 3hours at 4C with gentle agitation. The beads were washed with 50ml wash buffer (0.1%digitonin, 25mM Tris-HCl pH 7.4, 150mM NaCl, 5mM $MgCl_2$) and eluted with 100 units of tobacco etch virus (TEV) protease (Invitrogen, AcTEV) in 250ul wash buffer at 4C overnight. The eluted material was collected, and the beads were washed with 500 ul wash buffer. The washes and eluted materials were pooled and exchanged into 20 mM NH_4CO_3 pH 8.0, 0.1% SDS by using MicroSpin G-25 Columns (Amersham Biosciences). The eluate was concentrated in a speed-vac and separated by SDS-PAGE (10% acrylamide). Polypeptides were revealed by Coomassie Blue staining, excised, and trypsinized as described (Lilley and Ploegh, 2004). Peptides were sequenced by LC/MS/MS.

Pulse-chase experiments, immunoblotting, SDS-PAGE

Methods for pulse-labeling, cell lysis, immunoprecipitation, pulse-chase regarding Class I MHC HCs in US11 and US2 cells, viral transduction of cells, transfection of cells with RI_{332}, SDS-PAGE, and fluorography have been described [11]. All quantitation was performed on a phosphoimager.

Immunofluorescence and microsomal preparation

Cells were seeded onto glass coverslips and allowed to attach overnight. Fixation was achieved with 4% paraformaldehyde for 20 minutes at room temperature. Cells were permeabilized with 0.1% Triton X-100 for 10 minutes at room temperature and incubated with the affinity purified antibody as described [7]. Imaging was performed on a spinning disk confocal microscope at 100x magnification. Microsomes were prepared from U373 cells as previously described [45]. Microsomes were incubated in the indicated buffer conditions for 30 minutes and centrifuged at 20,000xg for 20 minutes. The pellet was resuspended directly in reducing sample buffer and the supernatant was first TCA precipitated.

References

1. Ellgaard, L. & Helenius, A. Quality control in the endoplasmic reticulum. *Nat Rev Mol Cell Biol* **4**, 181-191 (2003).
2. Ahn, K. *et al.* Human cytomegalovirus inhibits antigen presentation by a sequential multistep process. *Proc Natl Acad Sci U S A* **93**, 10990-10995 (1996).
3. Tortorella, D., Gewurz, B., Schust, D., Furman, M. & Ploegh, H. Down-regulation of MHC class I antigen presentation by HCMV; lessons for tumor immunology. *Immunol Invest* **29**, 97-100. (2000).
4. Wiertz, E.J. *et al.* The human cytomegalovirus US11 gene product dislocates MHC class I heavy chains from the endoplasmic reticulum to the cytosol. *Cell* **84**, 769-779. (1996).
5. Wiertz, E.J. *et al.* Sec61-mediated transfer of a membrane protein from the endoplasmic reticulum to the proteasome for destruction. *Nature* **384**, 432-438. (1996).
6. Loureiro, J. *et al.* Signal peptide peptidase is required for dislocation from the endoplasmic reticulum. *Nature* **441**, 894-897 (2006).
7. Lilley, B.N. & Ploegh, H.L. A membrane protein required for dislocation of misfolded proteins from the ER. *Nature* **429**, 834-840 (2004).
8. Ye, Y. *et al.* Inaugural Article: Recruitment of the p97 ATPase and ubiquitin ligases to the site of retrotranslocation at the endoplasmic reticulum membrane. *Proc Natl Acad Sci U S A* **102**, 14132-14138 (2005).
9. Lilley, B.N. & Ploegh, H.L. Multiprotein complexes that link dislocation, ubiquitination, and extraction of misfolded proteins from the endoplasmic reticulum membrane. *Proc Natl Acad Sci U S A* **102**, 14296-14301 (2005).
10. Kikkert, M. *et al.* Human HRD1 is an E3 ubiquitin ligase involved in degradation of proteins from the endoplasmic reticulum. *J Biol Chem* **279**, 3525-3534 (2004).
11. Mueller, B., Lilley, B.N. & Ploegh, H.L. SEL1L, the homologue of yeast Hrd3p, is involved in protein dislocation from the mammalian ER. *J Cell Biol* **175**, 261-270 (2006).
12. Ye, Y., Shibata, Y., Yun, C., Ron, D. & Rapoport, T.A. A membrane protein complex mediates retro-translocation from the ER lumen into the cytosol. *Nature* **429**, 841-847 (2004).
13. Gauss, R., Jarosch, E., Sommer, T. & Hirsch, C. A complex of Yos9p and the HRD ligase integrates endoplasmic reticulum quality control into the degradation machinery. *Nat Cell Biol* **8**, 849-854 (2006).
14. Gauss, R., Sommer, T. & Jarosch, E. The Hrd1p ligase complex forms a linchpin between ER-lumenal substrate selection and Cdc48p recruitment. *Embo J* **25**, 1827-1835 (2006).
15. Ploegh, H.L. A lipid-based model for the creation of an escape hatch from the endoplasmic reticulum. *Nature* **448**, 435-438 (2007).
16. Younger, J.M. *et al.* Sequential quality-control checkpoints triage misfolded cystic fibrosis transmembrane conductance regulator. *Cell* **126**, 571-582 (2006).
17. Oda, Y. *et al.* Derlin-2 and Derlin-3 are regulated by the mammalian unfolded protein response and are required for ER-associated degradation. *J Cell Biol* **172**, 383-393 (2006).

18. Christianson, J.C., Shaler, T.A., Tyler, R.E. & Kopito, R.R. OS-9 and GRP94 deliver mutant alpha1-antitrypsin to the Hrd1?SEL1L ubiquitin ligase complex for ERAD. *Nat Cell Biol* **10**, 272-282 (2008).
19. Lilley, B.N., Gilbert, J.M., Ploegh, H.L. & Benjamin, T.L. Murine polyomavirus requires the endoplasmic reticulum protein Derlin-2 to initiate infection. *J Virol* **80**, 8739-8744 (2006).
20. Lenk, U. *et al.* A role for mammalian Ubc6 homologues in ER-associated protein degradation. *J Cell Sci* **115**, 3007-3014 (2002).
21. Kimura, Y., Nakazawa, M. & Yamada, M. Cloning and characterization of three isoforms of OS-9 cDNA and expression of the OS-9 gene in various human tumor cell lines. *J Biochem (Tokyo)* **123**, 876-882 (1998).
22. Baek, J.H. *et al.* OS-9 interacts with hypoxia-inducible factor 1alpha and prolyl hydroxylases to promote oxygen-dependent degradation of HIF-1alpha. *Mol Cell* **17**, 503-512 (2005).
23. Litovchick, L., Friedmann, E. & Shaltiel, S. A selective interaction between OS-9 and the carboxyl-terminal tail of meprin beta. *J Biol Chem* **277**, 34413-34423 (2002).
24. Carvalho, P., Goder, V. & Rapoport, T.A. Distinct Ubiquitin-Ligase Complexes Define Convergent Pathways for the Degradation of ER Proteins. *Cell* **126**, 361-373 (2006).
25. Denic, V., Quan, E.M. & Weissman, J.S. A Luminal Surveillance Complex that Selects Misfolded Glycoproteins for ER-Associated Degradation. *Cell* **126**, 349-359 (2006).
26. Kato, A. *et al.* Ancient ubiquitous protein 1 binds to the conserved membrane-proximal sequence of the cytoplasmic tail of the integrin alpha subunits that plays a crucial role in the inside-out signaling of alpha IIbbeta 3. *J Biol Chem* **277**, 28934-28941 (2002).
27. Hurley, J.H., Lee, S. & Prag, G. Ubiquitin-binding domains. *Biochem J* **399**, 361-372 (2006).
28. Imai, Y. *et al.* Cloning and characterization of the highly expressed ETEA gene from blood cells of atopic dermatitis patients. *Biochem Biophys Res Commun* **297**, 1282-1290 (2002).
29. Buchberger, A. From UBA to UBX: new words in the ubiquitin vocabulary. *Trends Cell Biol* **12**, 216-221 (2002).
30. Swanson, R., Locher, M. & Hochstrasser, M. A conserved ubiquitin ligase of the nuclear envelope/endoplasmic reticulum that functions in both ER-associated and Matalpha2 repressor degradation. *Genes Dev* **15**, 2660-2674 (2001).
31. Chen, P., Johnson, P., Sommer, T., Jentsch, S. & Hochstrasser, M. Multiple ubiquitin-conjugating enzymes participate in the in vivo degradation of the yeast MAT alpha 2 repressor. *Cell* **74**, 357-369 (1993).
32. Oh, R.S., Bai, X. & Rommens, J.M. Human homologs of Ubc6p ubiquitin-conjugating enzyme and phosphorylation of HsUbc6e in response to endoplasmic reticulum stress. *J Biol Chem* **281**, 21480-21490 (2006).
33. Hancock, M.K., Haskins, D.J., Sun, G. & Dahms, N.M. Identification of residues essential for carbohydrate recognition by the insulin-like growth factor II/mannose 6-phosphate receptor. *J Biol Chem* **277**, 11255-11264 (2002).

34. Bhamidipati, A., Denic, V., Quan, E.M. & Weissman, J.S. Exploration of the topological requirements of ERAD identifies Yos9p as a lectin sensor of misfolded glycoproteins in the ER lumen. *Mol Cell* **19**, 741-751 (2005).
35. Kitzmuller, C. *et al.* Processing of N-linked glycans during endoplasmic-reticulum-associated degradation of a short-lived variant of ribophorin I. *Biochem J* **376**, 687-696 (2003).
36. Hirsch, C., Blom, D. & Ploegh, H.L. A role for N-glycanase in the cytosolic turnover of glycoproteins. *Embo J* **22**, 1036-1046 (2003).
37. Rehm, A., Stern, P., Ploegh, H.L. & Tortorella, D. Signal peptide cleavage of a type I membrane protein, HCMV US11, is dependent on its membrane anchor. *Embo J* **20**, 1573-1582 (2001).
38. Gewurz, B.E., Ploegh, H.L. & Tortorella, D. US2, a human cytomegalovirus-encoded type I membrane protein, contains a non-cleavable amino-terminal signal peptide. *J Biol Chem* **277**, 11306-11313 (2002).
39. Barnstable, C.J. *et al.* Production of monoclonal antibodies to group A erythrocytes, HLA and other human cell surface antigens-new tools for genetic analysis. *Cell* **14**, 9-20 (1978).
40. Lilley, B.N., Tortorella, D. & Ploegh, H.L. Dislocation of a type I membrane protein requires interactions between membrane-spanning segments within the lipid bilayer. *Mol Biol Cell* **14**, 3690-3698 (2003).
41. Flierman, D., Coleman, C.S., Pickart, C.M., Rapoport, T.A. & Chau, V. E2-25K mediates US11-triggered retro-translocation of MHC class I heavy chains in a permeabilized cell system. *Proc Natl Acad Sci U S A* **103**, 11589-11594 (2006).
42. Liang, J. *et al.* Characterization of erasin (UBXD2): a new ER protein that promotes ER-associated protein degradation. *J Cell Sci* **119**, 4011-4024 (2006).
43. Schuberth, C. & Buchberger, A. Membrane-bound Ubx2 recruits Cdc48 to ubiquitin ligases and their substrates to ensure efficient ER-associated protein degradation. *Nat Cell Biol* **7**, 999-1006 (2005).
44. Neuber, O., Jarosch, E., Volkwein, C., Walter, J. & Sommer, T. Ubx2 links the Cdc48 complex to ER-associated protein degradation. *Nat Cell Biol* **7**, 993-998 (2005).
45. Furman, M.H., Ploegh, H.L. & Tortorella, D. Membrane-specific, host-derived factors are required for US2- and US11-mediated degradation of major histocompatibility complex class I molecules. *J Biol Chem* **277**, 3258-3267 (2002).

Chapter 3

The dual role of AUP1 in lipid droplet formation and ER protein quality control

Abstract

Quality control of endoplasmic reticulum proteins involves the identification and engagement of misfolded proteins, dislocation of the misfolded protein across the ER membrane, and ubiquitin-mediated targeting to the proteasome for degradation. Ancient ubiquitous protein 1 (AUP1) physically associates with the mammalian HRD1/SEl1L complex and AUP1-depletion impairs degradation of misfolded ER proteins. One of the functions of AUP1 in ER quality control is to recruit the soluble E2-ubiquitin conjugating enzyme UBE2G2. We further show that the CUE domain of AUP1 regulates poly-ubiquitylation and determines AUP1's interaction with the HRD1 complex and dislocation substrates. AUP1 localizes both to the ER and to lipid droplets. AUP1 expression is necessary for the efficient formation of lipid droplets and as such represents the first protein with lipid droplet regulatory activity to be linked to ER quality control. These findings indicate a possible connection between ER protein quality control and lipid droplets.

Introduction

Eukaryotic cells possess an efficient system to detect and remove misfolded proteins from the endoplasmic reticulum (ER)[1]. The HRD1 complex specializes in the removal of ER proteins with defects in their lumenal domains[2-4]. Once a lumenal ER protein has exhausted its folding options, it is directed to the quality control machinery by a set of proteins that includes OS9, XTP3-B, and SEL1L[5-7]. The misfolded protein is then dislocated from the ER. Transportation across the ER lipid bilayer is generally believed to proceed through a proteinaceous channel, such as the complexes nucleated by Sec61[8], Derlin1[9, 10] or the E3 ligase Hrd1p[11]. Energy for this movement is provided by the cytoplasmic AAA-ATPase p97[12], a protein involved in many different cellular functions. The dislocated protein is ubiquitylated and deglycosylated prior to its degradation by the proteasome in the cytoplasm. Ubiquitylation is a three step process. E1 activates ubiquitin in an ATP-dependent reaction, followed by formation of a thio-ester linked ubiquitin-E2 complex. An E3 ubiquitin ligase then catalyzes transfer of ubiquitin onto the intended substrate. In the case of the HRD1/SEL1L complex, UBE2G2 (also known as UBC7) serves as the E2 and HRD1 as the E3[13]. UBE2G2 also acts as the E2 conjugating enzyme for gp78, another E3 ubiquitin ligase that specializes in the ubiquitylation of dislocated ER proteins[14]. We have also identified Ubc6e as an E2 conjugating enzyme of the HRD1/SEL1L complex[15], suggesting the possibility that protein complexes of overlapping yet distinct composition are involved in ER quality control.

We previously identified ancient ubiquitous protein 1 (AUP1) as a component of the HRD1/SEL1L ER quality control complex and showed that AUP1 is necessary for US11-mediated dislocation of Class I MHC heavy chains[15]. US11 is a protein encoded by Human Cytomegalovirus (HCMV) that targets Class I MHC heavy chains for destruction as part of its

immunoevasive strategy[16]. AUP1 has also been proposed to be involved in integrin signaling[17, 18]. AUP1 contains a hydrophobic region close to the N-terminus that inserts into the membrane such that both termini are found in the cytoplasm[19]. AUP1 contains two conserved cytoplasmic domains according to the Ensembl database: an acyltransferase domain and a CUE domain. Acyltransferase domains transfer fatty acids onto phospholipids using a conserved active site histidine and aspartic acid, separated by four amino acids (HX4D)[20]. Acyltransferase domains differ in the fatty acid and acceptor lipids they use. CUE domains are UBA-like domains, which bind ubiquitin. Residues on the first and third alpha-helices of the CUE domain bind to a hydrophobic surface patch of ubiquitin[21, 22]. We here identify a third region of AUP1 not previously annotated in the domain bioinformatics databases that is necessary for recruitment of UBE2G2. This UBE2G2 binding domain (G2BR) was originally found on the E3 gp78[23]. During the preparation of the manuscript, this G2BR was also identified by another group[19].

At first glance, it is reasonable to hypothesize that in mammalian cells AUP1 merely serves a role similar to that of Cue1p, a component of the yeast Hrd1/Der3p ER protein quality control complex. Both AUP1 and yeast Cue1p are membrane-anchored, contain a CUE domain and a region that binds its cognate E2 ubiquitin ligase. The CUE domain of yeast Cue1p is dispensable for ER quality control. Yeast Cue1p recruits[24] and enhances[25] the activity of Ubc7p, the yeast UBE2G2 homolog, via a U7 binding region at its C-terminus[26]. Aside from these similarities, AUP1 and Cue1p are not homologs, and there is no ortholog of AUP1 in yeast. AUP1's architecture of a membrane anchor, followed by an acyltransferase domain and then a CUE domain, is conserved in organisms with bilateral symmetry. Unlike AUP1, however, yeast Cue1p does not encode a putative acyltransferase domain. Given this difference, AUP1 may perform additional functions beyond those of yeast Cue1p.

We show that AUP1 is found in both the ER and in lipid droplets. Lipid droplets are cytoplasmic organelles that serve as storage depots for cholesteryl esters and triacylglycerols, to be released for membrane biogenesis or as a source of cellular energy via beta-oxidation of fatty acids. Lipid droplets are derived from the ER and are composed of a phospholipid monolayer that surrounds the neutral lipid core[27, 28]. The role of lipid droplets also includes a variety of less obvious functions, such as sequestration of histones in embryogenesis[29], involvement in Hepatitis C[30] and Chlamydia[31] infection, and proteasomal degradation[32, 33].

Here we examine the role of AUP1 in ER protein quality control and in lipid droplet formation. We expand the role of AUP1 to include general ER quality control of soluble misfolded ER proteins. We find that AUP1 binds UBE2G2 at its C-terminus. AUP1-interacting proteins, identified by mass spectrometry, fall into three main categories: ER protein quality control proteins, lipid-modifying enzymes, and subunits of the oligosaccharide transferase complex, further underscoring the connections with the ER. The interaction of AUP1 with the ER protein quality control complex, terminally misfolded proteins, and ubiquitylated proteins is mediated by its CUE domain. The CUE domain and G2BR regulate ubiquitylation and polyubiquitylation. Finally, we show that AUP1 localizes to lipid droplets and contributes to their formation. These unexpected results suggest that lipid droplets might be important for ER protein quality control. This hypothesis is supported by the observation that dislocation substrates are stabilized in the presence of an inhibitor of lipid-modifying enzymes required for lipid droplet formation.

Results

AUP1 is necessary for dislocation of misfolded proteins from the ER

AUP1 has been implicated in the US11-mediated disposal of Class I Major Histocompatibility Complex heavy chains (HC) based on the observation that GFP-tagged versions of AUP1 act in dominant-interfering fashion and impair the US11 mediated disposal pathway[15]. We confirmed this result using shRNA-mediated reduction of AUP1 levels. US11-expressing cells were transduced with a control shRNA specific for luciferase or one of two different shRNAs that target AUP1. These cells were then subjected to pulse chase analysis and immunoprecipitation of Class I heavy chains. The addition of the proteasome inhibitor ZL_3VS allowed recovery of both glycosylated (HC+CHO) and deglycosylated, cytoplasmically disposed, heavy chains (HC-CHO). Cells with decreased levels of AUP1 (as determined by western blot), exhibited slower kinetics of heavy chain removal from the ER (Fig. 3.1A).

Two soluble misfolded proteins, Ribophorin I fragment (RI_{332}) and the Null Hong Kong variant of alpha-1 anti-trypsin (NHK), are known to also use the HRD1 complex for their removal from the ER. NHK and RI_{332} are ER lumenal proteins harboring mutations that prevent them from folding correctly and thus serve as dislocation substrates[34]. Both RI_{332}-HA and NHK are stabilized in AUP1 depleted cells, showing that AUP1 contributes to their dislocation. The magnitude of the effect on dislocation is comparable to those observed for other interventions in ER quality control, such as depletion of members of the Derlin family[35],OS9[5] and AUP1-GFP dominant negatives. The two AUP1 shRNAs have different efficiencies in HeLa cells- construct A shows ~50% reduction of AUP1 levels and construct B shows ~90% reduction. Furthermore, the level of impairment of dislocation negatively correlated with the level of AUP1: greater reduction of AUP1 levels leads to slower dislocation rates (Fig. 3.1B and 3.1C).

Figure 3.1

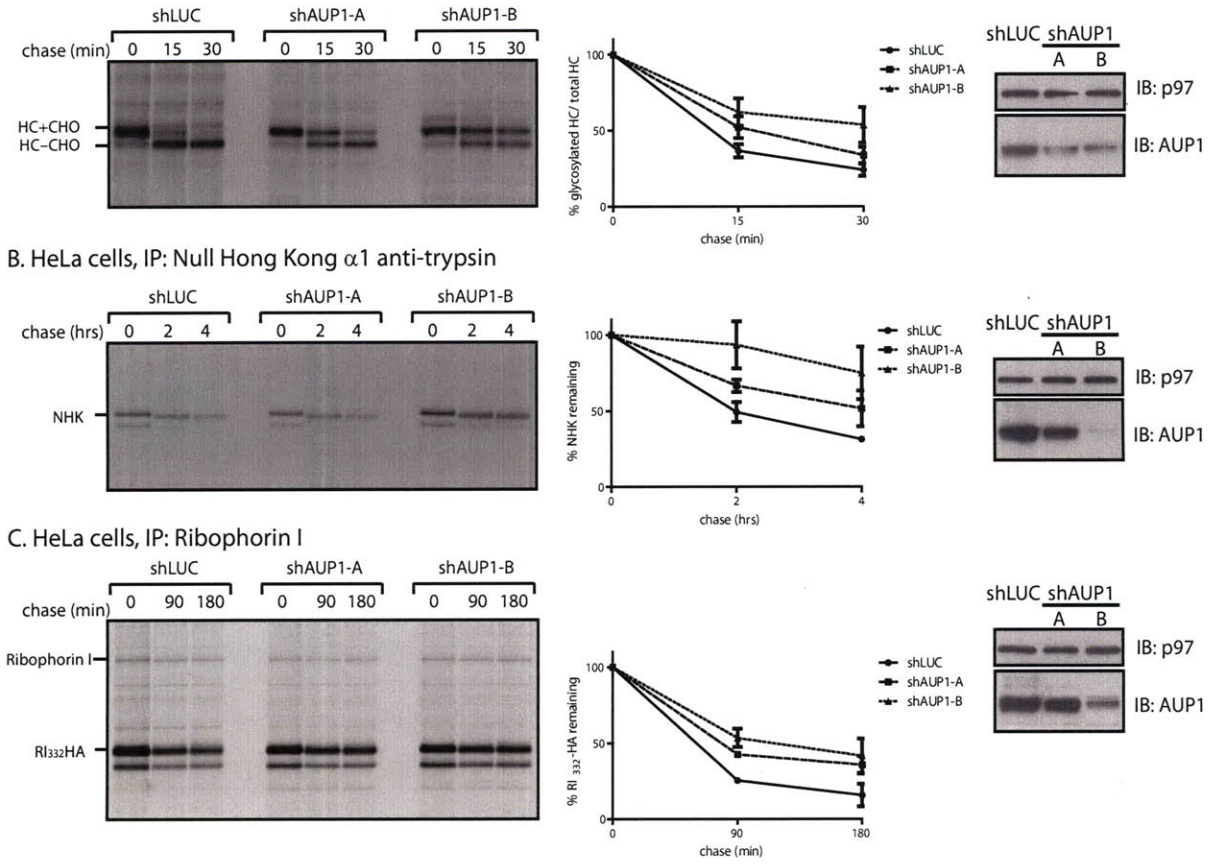

AUP1 is necessary for ER quality control. A) US11-expressing astrocytoma cells were transduced with shRNA specific against luciferase (shLUC), as a control, or one of two different constructs targeting AUP1 (A or B). Four days post-transduction, cells were treated with ZL_3VS proteasome inhibitor and pulse-labeled with ^{35}S-labelled cysteine and methionine. Samples were taken at the indicated chase times and Class I MHC heavy chain was recovered from the lysates. Immunoprecipitates were separated by SDS-PAGE and imaged by autoradiography. Amount of recovered protein was quantified by phophorimagery and is shown as a percentage of glycosylated heavy chain compared to total heavy chain. Error bars represent standard deviation of three individual experiments. The level of AUP1 depletion was determined by immunoblotting with p97 as a loading control. The same experiment as described for (A) was performed using shRNA-transduced HeLa cells transfected with NHK (B) or RI_{332}-HA (C) without the addition of ZL_3VS. NHK was immunoprecipitated using an anti-α1 anti-trypsin antibody. RI_{332}-HA was immunoprecipitated using an anti-Ribophorin I antibody that recovers both the full-length and the misfolded fragment of Ribophorin I. Quantification in (B) and (C) shows the percentage of protein remaining compared to the amount recovered at the zero minutes chase time.

AUP1 binds proteins involved in ER protein quality control, lipid modification, and glycosylation

We identified proteins that interact with AUP1 by mass spectrometry. HA-tagged AUP1 was transfected into HeLa cells and recovered from digitonin lysates with anti-HA antibody and resolved by SDS-PAGE (Fig. 3.2). We identified the co-precipitating proteins by LC/MS-MS (Table 3.1). Many of the known components of the HRD1 dislocation complex were recovered: HRD1, SEL1L, OS9, UBXD8, p97, and UBE2G2. We also recovered several components of the oligosaccharyl transferase complex: Ribophorin I and II (OST1 and OST2), and OST48. In addition, we identified several proteins involved in lipid modification: Long-chain fatty acyl-CoA ligase 3 (ACSL3), serine palmitoyltransferase subunit 1, and lysophosphatidylcholine acyltransferase 1 (LPCAT1). In those cases where the necessary antibodies were available, we could confirm by immunoprecipitation and immunoblot the interactions established by mass spectrometry (Fig. 3.4A).

Figure 3.2

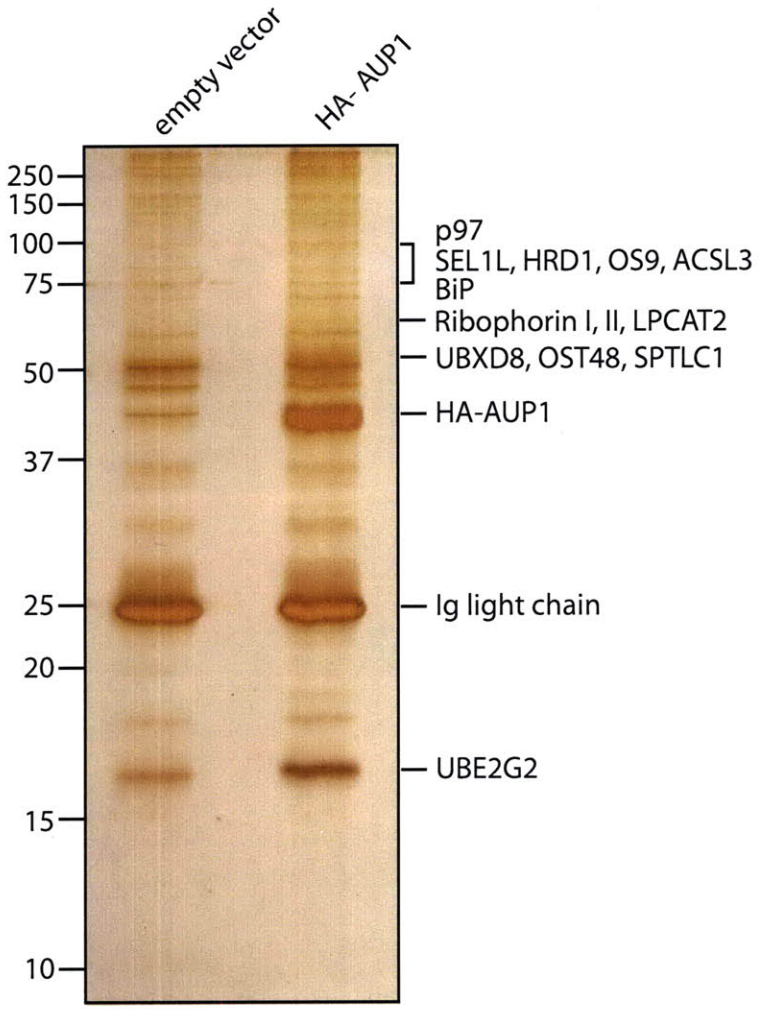

AUP1-interacting proteins. Cells were transfected with empty vector (control) or HA-AUP1. Anti-HA immoprecipitates were separated by SDS-PAGE and visualized by silver staining. Associated proteins were identified by LC/MS-MS and reported in Table 3.1.

Table 3.1

	Protein **Accession Number**	Molecular Weight (Da)	Unique Peptides	Sequence Coverage (%)
ER Quality Control				
AUP1	gi|31712030	45,758	13	45
p97	gi|6005942	89,266	13	20
UBE2G2	gi|33359701	15,603	5	59
SEL1L	gi|19923669	88,699	10	19
OS9	gi|63252870	73,775	6	13
UBXD8	gi|24797106	52,591	6	20
HRD1	gi|27436927	67,641	3	5
Oligosaccharide Transferase Complex				
Ribophorin I	gi|4506675	68,527	16	33
Ribophorin II	gi|209413738	67,682	10	27
Oligosaccharide Transferase 48	gi|20070197	50,670	5	13
Lipid Metabolism				
Acyl-CoA Synthetase 3	gi|42794754	80,368	5	9
Serine palmitoyltransferase subunit 1	gi|5454084	52,711	4	8
Lysophosphatidylcholine acyltransferase 1	gi|33946291	59,114	3	8

AUP1-interacting proteins. A partial list of proteins recovered from the HA-AUP1 immoprecipitates and identified by LC/MS-MS is given. Unique peptides indicates the total number of different peptides recovered from the immunoprecipitate. GenBank GI numbers and calculated molecular weight (Da) are also given. Data analysis was performed by MSRAT.

AUP1 binds the E2 Ubiquitin ligase UBE2G2 via a C-terminal G2 binding region

A striking AUP1-interacting protein that we recovered is UBE2G2. This association was also identified in a large scale protein-protein interaction study[36]. Five peptides of this 15.6 kDa protein were identified by mass spectrometry, accounting for 59% of its sequence (Table 3.1). UBE2G2 is a cytosolic E2 ubiquitin ligase, the mammalian homolog of yeast Ubc7p. The mammalian E3 ubiquitin ligase gp78 binds UBE2G2 via a stretch of 27 amino acids found at its C-terminus (termed the G2 Binding Region, G2BR)[23]. An amino acid sequence alignment between the gp78 G2BR and AUP1 identifies a region of high similarity at the C-terminus of AUP1 (Fig. 3.3A). We made constructs of AUP1 lacking its putative G2BR-containing C-terminus as well as constructs with mutations in the other two domains of AUP1 described above (Fig. 3.3B). Full-length AUP1 and AUP1 with mutations in the acyltransferase or CUE domains interact with UBE2G2, whereas AUP1ΔG2BR does not, as determined by immunoprecipitation for myc-UBE2G2, followed by immunoblotting for HA-AUP1 (Fig. 3.3C). We thus conclude that AUP1 binds UBE2G2, and that this interaction is dependent on the C-terminus of AUP1 that constitutes a G2BR domain.

Figure 3.3

A.

AUP1_HUMAN	378	**S**SWA**RQ**ES**L**Q**E****RK**QA**L**YEY**AR**R**RF**TER 404
gp78 _HUMAN	574	**S**ADE**RQ**RM**L**V**Q****RK**DE**LL**QQ**AR**K**RF**LNK 600
Cue1p_YEAST	170	DLDIEE-----**RK**RL**L**VWQ**AR**KNLETK 191

B.

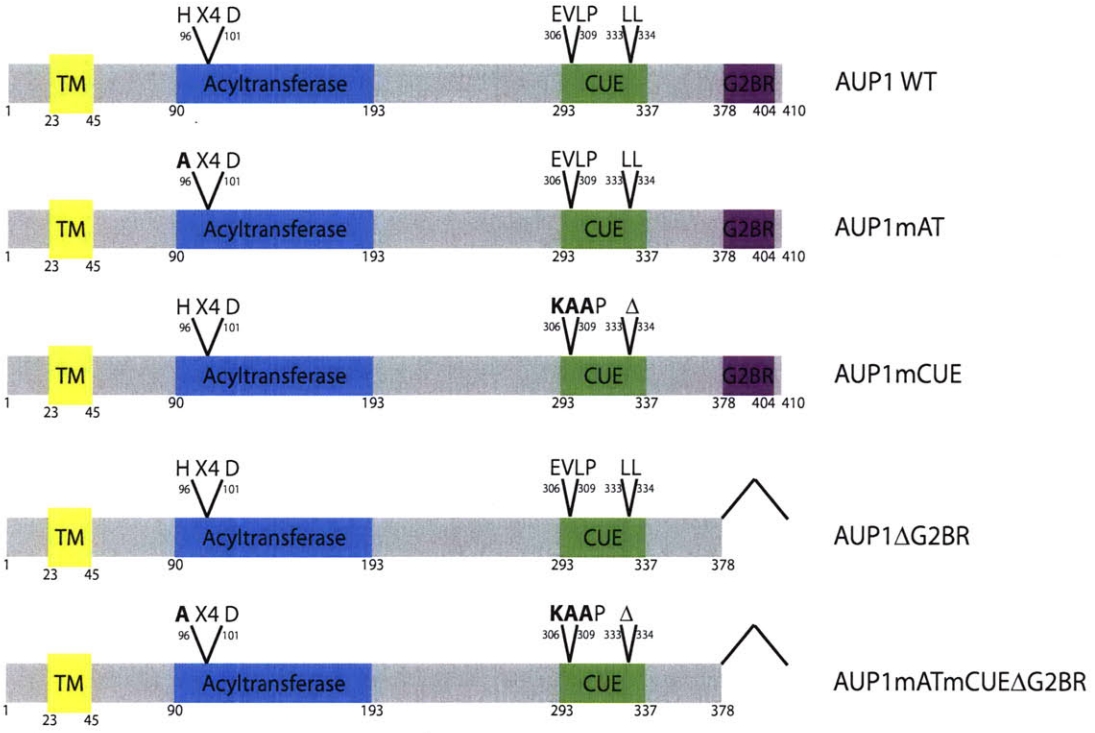

C.

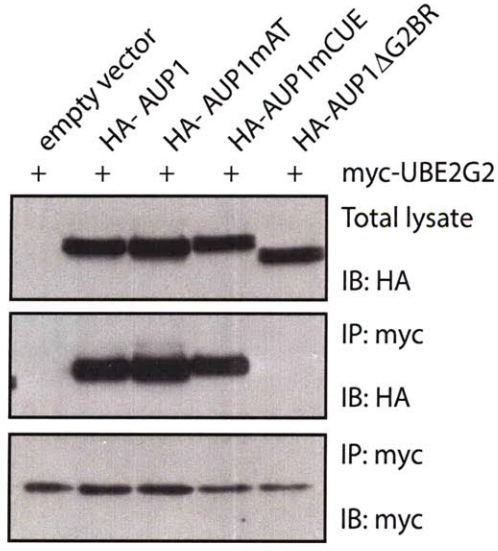

AUP1 interacts with UBE2G2 via a binding region at its C-terminus. A) A protein alignment of the G2 binding regions of AUP1 and gp78 shows strong sequence similarity. The U7 region of Cue1p shows weaker similarity. B) AUP1 and the mutant constructs used in this study are represented here. AUP1mAT has a H96A point mutation. AUP1mCUE has residues from 306-308 mutated from EVL to KAA and Δ333-334. AUP1ΔG2BR has residues 378-410 deleted. AUP1mATmCUEΔG2BR has H96A, E306K, V307A, L308A, Δ333-334, Δ378-410 C) HeLa cells were transfected with myc-UBE2G2 and one of the HA-AUP1 WT or mutant constructs. myc-UBE2G2 was recovered from NP-40 lysates. Immunoblotting for HA detected associated HA-AUP1.

The CUE domain of AUP1 mediates its binding to ER quality control machinery and dislocation substrates

CUE domains possess conserved sequences on their first and third alpha-helices that bind to hydrophobic patches on the surface of ubiquitin. For AUP1, these areas correspond to a valine-leucine-proline and di-leucine sequence[21]. We mutated these regions to compromise the binding of AUP1 to ubiquitin. These mutations affected the association of AUP1 with many components of the ER quality control machinery. HeLa cells were transfected with HA-AUP1 constructs (wildtype, mutant acyltransferase domain, mutant CUE domain, or G2BR deletion) or empty vector plasmid as a negative control and HA-AUP1 was recovered by immunoprecipitation from digitonin lysates. We then immunoblotted for several of the AUP1-interacting proteins identified by mass spectrometry (Table 3.1). AUP1 with the mutant CUE domain (AUP1mCUE) was less efficient at interacting with most of the proteins involved in dislocation (p97, SEL1L, UBXD8, OS9, UBC6e and HRD1). Components of the oligosaccharide transferase complex (Ribophorin I, OST48 and STT3B) were recruited equally well for all forms of HA-AUP1 (Fig. 3.4A).

Given the role of AUP1 and the ER quality control complex in processing of misfolded ER proteins, we examined whether AUP1 associates with dislocation substrates. HeLa cells were transfected with AUP1 constructs and one of two terminally misfolded proteins, NHK or RI_{332}-HA. NHK or RI_{332}-HA immunoprecipitates were analyzed for AUP1 content by immunoblotting. AUP1 with CUE domain mutations associated less well with both of the dislocation substrates than did wildtype AUP1 (Fig. 3.4B and 3.4C).

Figure 3.4

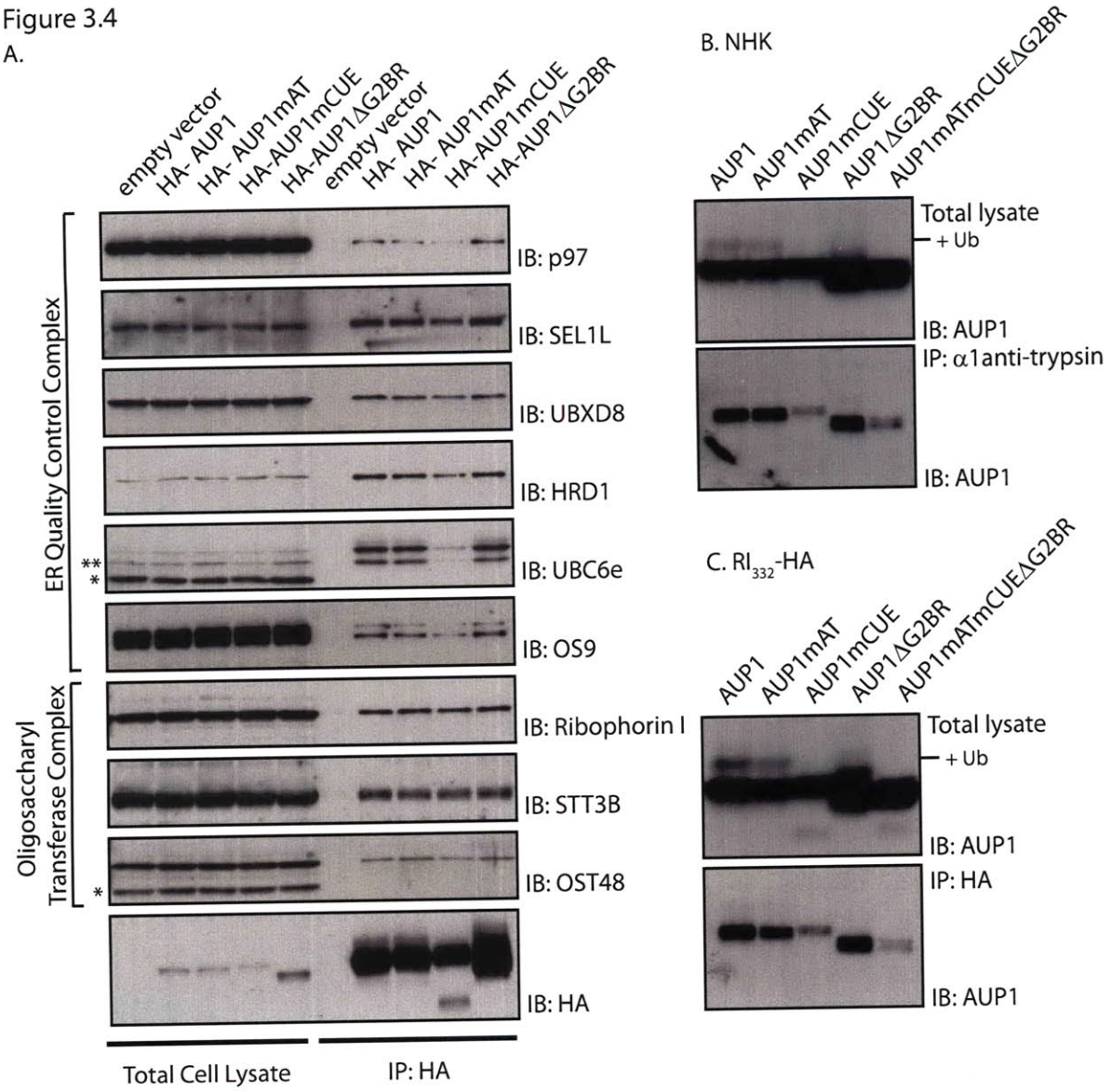

The CUE domain of AUP1 mediates interaction with ER quality control proteins and terminally misfolded proteins. A) HeLa cells were transfected with empty vector or one of the HA-AUP1 WT or mutant constructs. HA-AUP1 was recovered with 3F10 (anti-HA) antibody from digitonin lysates. Immunoblotting with antibodies for the indicated proteins showed the presence of endogenous proteins in the total cell lysates and immunoprecipitates. * indicates cross-reactive proteins and ** indicates degradation product of UBC6e. B) HeLa cells were transfected with NHK variant of alpha-1 anti-trypsin and one of the AUP1 WT or mutant constructs as indicated. These cells were incubated with 5 μM ZL3VS overnight. NHK was recovered from NP-40 lysates and the content of AUP1 in total cell lysates and immunoprecipitates was determined by immunoblotting with an anti-AUP1 antibody. Both endogenous and transiently-introduced AUP1 is present in the immunoblots. C) The same experiment as in (B) was repeated with RI_{332}-HA instead of NHK.

AUP1 is modified by ubiquitin and binds ubiquitylated proteins

AUP1 is itself modified by ubiquitin. Cells transfected with HA-ubiquitin and GFP-AUP1 were solubilized in mild detergent (digitonin). HA-Ub and HA-Ub-modified proteins were immunoprecipitated from the lysates, followed by immunoblotting for AUP1. Anti-AUP1-reactive material was detected at ~8kDa and ~16kDa above the expected molecular weight of GFP-AUP1, consistent with mono- and di-ubiquitylation of AUP1 (Fig. 3.5A). A polypeptide corresponding to the size of unmodified GFP-AUP1 is also detected, suggesting that GFP-AUP1 self-oligomerizes with both ubiquitylated and nonubiquitylated GFP-AUP1 in a digitonin-resistant manner. Very little GFP-AUP1mCUE was recovered, indicating that the CUE domain is essential for interaction with HA-Ub, and GFP-AUP1mCUE is minimally ubiquitylated *in vivo*. Endogenous AUP1 is also present in the immunoprecipitates, but less is recovered in the presence of GFP-AUP1 constructs containing the G2BR, suggesting that the G2BR, and perhaps the associated UBE2G2, competes with endogenous AUP1 for binding with HA-Ub.

The same experiment was also performed in reverse order: GFP-AUP1 was natively immunoprecipitated from the lysates followed by immunoblotting for HA-Ub. The amount of HA-reactive material recovered by GFP-AUP1mCUE in digitonin lysates was less than for GFP-AUP1 wildtype (Fig. 3.5B), most likely because the CUE domain of AUP1 mediates the interaction between AUP1 and ubiquitylated proteins. We recovered relatively more HA-reactive material from GFP-AUP1ΔG2BR digitonin lysates than for GFP-AUP1 wildtype, consistent with the possiblility that the G2BR domain of AUP1 acts as a negative regulator of ubiquitylation or disrupts AUP1's association with ubiquitylated proteins.

Given that AUP1 recruits both E2 and E3 enzymes, UBE2G2 and HRD1, respectively, we wondered if the material recovered by immunoprecipitation of HA-AUP1 is sufficient to sustain ubiquitylation *in vitro*. E1 ubiquitin ligase and FLAG-ubiquitin were added to the HA-AUP1 immunoprecipitates. All HA-AUP1 constructs could be poly-ubiquitylated *in vitro*, producing the typical ubiquitin "ladder" in anti-FLAG immunoblots (Fig. 3.6). There is very little mono-ubiquitylated HA-AUP1mCUE compared to the other constructs, indicating that the CUE domain of AUP1 may negatively regulate poly-ubiquitylation.

Figure 3.5

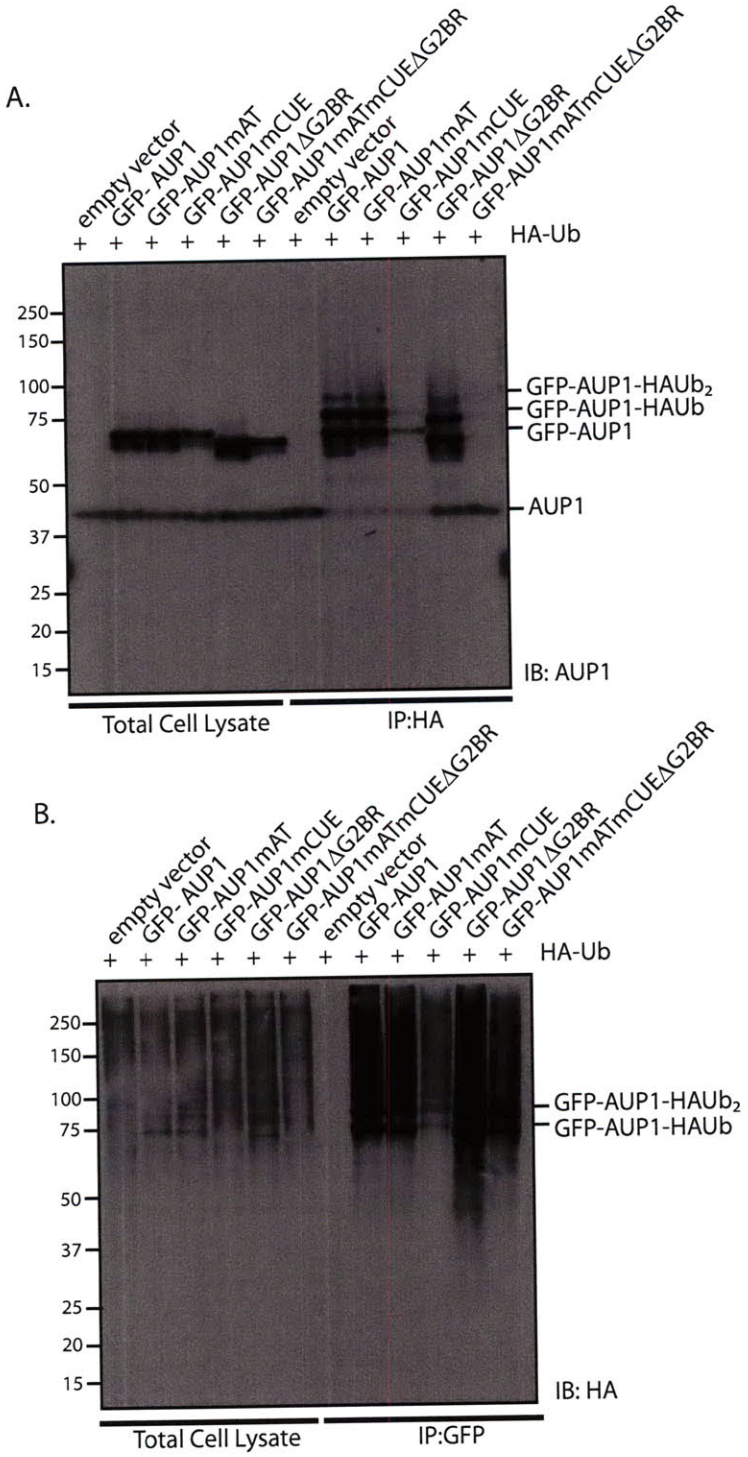

AUP1 is both ubiquitylated and binds ubiquitin-modified proteins A) HeLa cells were transfected with HA-Ubiquitin and empty vector or one of the GFP-AUP1 contructs (WT or mutants, as indicated). HA-Ub was recovered with 3F10 (HA-specific) antibody from digitonin lysates supplemented with 2.5mM N-ethylmaleimide (NEM). GFP-AUP1 content in total cell lysates and immunoprecipitates was determined by immunoblotting with an anti-AUP1 antibody. B) GFP-AUP1 was recovered with anti-GFP antibody from lysates described in (A). HA-Ub content in total cell lysates and immunoprecipitates was determined by immunoblotting with an anti-HA antibody.

Figure 3.6

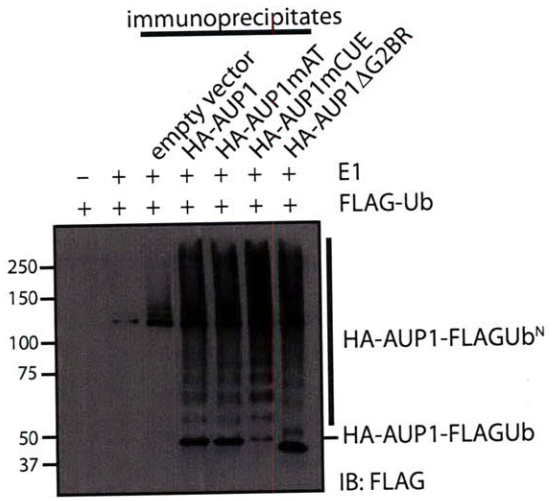

anti-AUP1 immunoprecipitates are able to perform ubiquitin transfer in vitro. HeLa cells were tranfected with empty vector or one of the HA-AUP1 constructs (WT or mutant, as indicated). HA-AUP1 was immunoprecipitated from digitonin lysates. E1 (100 nM), FLAG-Ubiquitin (60 μM), and an ATP-regenerating buffer was added to the immunoprecipitates and kept at 37° C for 60 minutes. Separate samples containing only FLAG-Ubiquitin and buffer or E1, FLAG-Ubiquitin and buffer served as controls. Samples were run on an 8% tris-tricine SDS-PAGE gel, and were immunoblotted with a FLAG-specific antibody.

AUP1 localizes to the ER and lipid droplets and is involved in the formation of lipid droplets

Recent proteomic studies have identified AUP1 as a component of lipid droplets[37-39]. We confirmed this result for endogenous AUP1 in HeLa cells by microscopy. We performed anti-AUP1 immunofluorescence microscopy of HeLa cells fed oleic acid to induce lipid droplet formation. Lipid droplets were stained with the lipophilic dye BODIPY 493/503. AUP1 clearly localizes to the periphery of lipid droplets as well as to the ER (Fig. 3.7). Similar results were found in A431, Huh7, MDCK and COS7 cells[19].

To see if AUP1 plays a role in lipid droplet formation, we looked at the ability of AUP1 knockdown cells to form lipid droplets. HeLa cells were transduced with the AUP1-targeting shRNA constructs and then either incubated with oleic acid for 16 hours or left untreated. Lipid droplets were stained with BODIPY 493/503 and fluorescence intensity levels were determined by flow cytometry. The AUP1-depleted cells accumulated only ~60% as much lipid droplet staining upon oleic acid treatment as did control cells (Fig. 3.8A). This effect matches those observed for TIP47-depleted cells[40], a lipid droplet component. Thus AUP1 contributes directly or indirectly to the formation of lipid droplets.

Overexpression of several other known protein components of lipid droplets, such as ADRP, induces the formation of lipid droplets[41]. Similarly, cells stably expressing AUP1-GFP under the strong CMV promoter exhibit increased numbers of lipid droplets[42]. This is readily apparent in bright field images (Fig. 3.8B) as well as confocal microscopy with BODIPY 493/503 co-stain for lipid droplets (Fig. 3.8D). Electron

microscopy of these cells produced images of dark electron-dense filled structures characteristic of lipid droplets (Fig. 3.8C).

Figure 3.7

AUP1 localizes to lipid droplets. HeLa cells were incubated with 250μM oleic acid for 16 hours. AUP1 was stained with purified anti-AUP1 antibody and lipid droplets were stained with BODIPY 493/503. Cells were visualized by spinning disk confocal microscopy. Scale bar= 10μm.

Figure 3.8

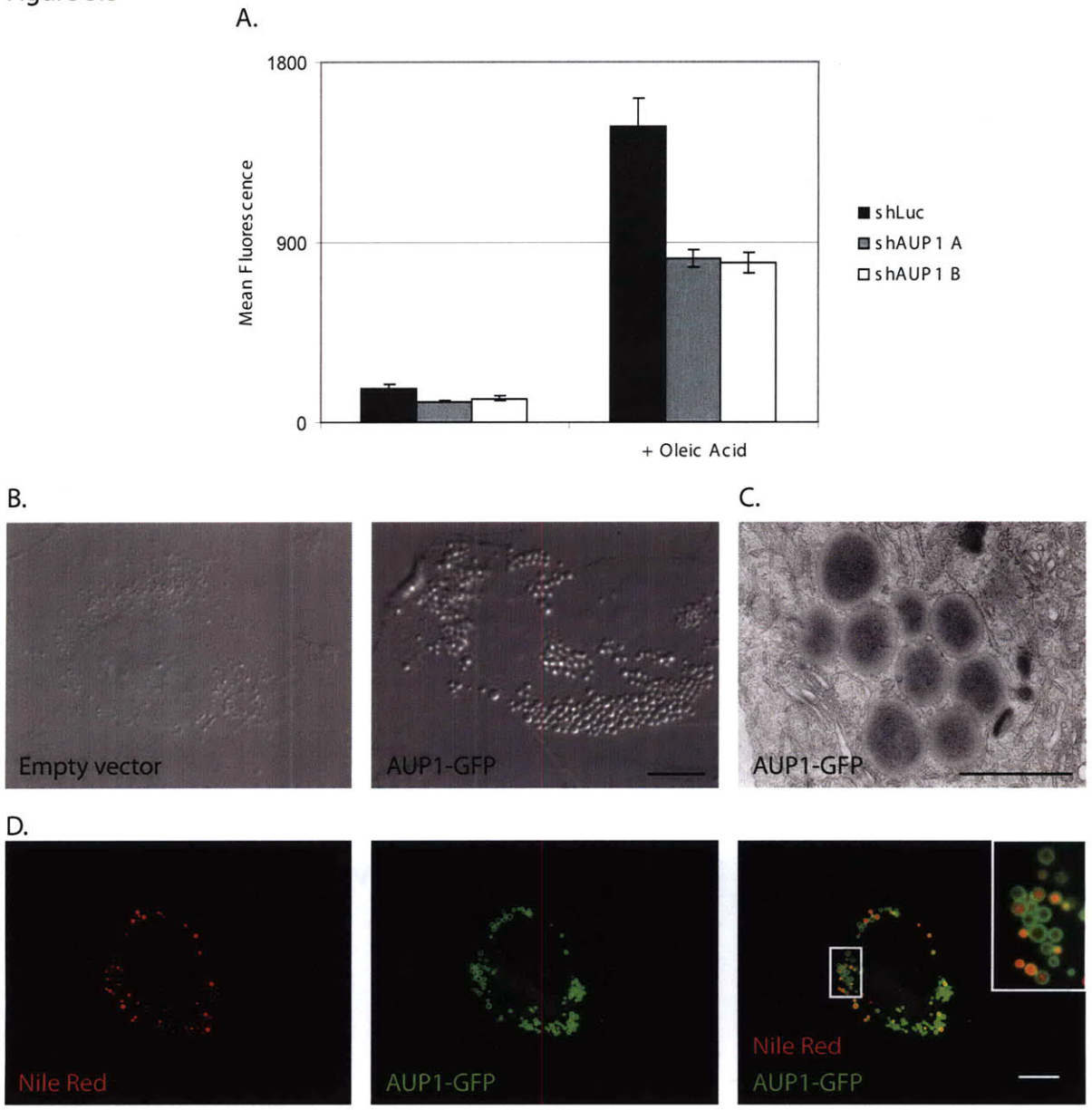

AUP1 is involved in the formation of lipid droplets. A) HeLa cells were transduced with the shRNA constructs used in Figure 3.1. Three days post-transduction, cells were left untreated or incubated with 0.4mM oleic acid for 16 hours. Lipid droplets were stained with BODIPY 493/503 and the amount of cellular fluorescence was determined by flow cytometry. Error bars represent standard deviation from three independent experiments. B) HeLa cells were stably transduced with empty vector or AUP1-GFP as indicated and imaged by Nomarski imaging. Scale bar= 10μm. C) US11-expressing astrocytoma cells transduced with AUP1-GFP were imaged by electron microscopy. Scale bar= 1μm. D) HeLa cells stably transduced with AUP1-GFP were visualized by spinning disk confocal microscopy. Lipid droplets were stained with Nile Red dye. Scale bar= 10μm.

Pharmacological inhibition of lipid droplets formation perturbs dislocation

Upon finding that AUP1 plays a role in both lipid droplet formation and ER protein quality control, we wondered whether the two processes were functionally related. Inhibition of a subset of Long-chain Acyl-CoA Synthetases (ACSL1, 3, and 4) by Triacsin C impairs lipid droplet formation[43, 44]. In cells treated with this inhibitor, dislocation of MHC class I heavy chain in US11-expressing cells was slowed, as was the degradation of two soluble dislocation substrates, NHK and RI332-HA (Fig. 3.9A-C). Triacsin C treatment does not disrupt the folding capacity of the ER since XBP-1 splicing, a read-out of Unfolded Protein Response (UPR) activation, was only slightly triggered after longer incubation times (Fig. 3.9D). The minor induction of the UPR may be a result of impaired dislocation. As a comparison, tunicamycin, an inhibitor of N-linked glycosylation, causes significant XBP-1 splicing at much earlier time-points.

Figure 3.9

A. US11-expressing U373 astrocytoma cells, IP: Heavy Chain

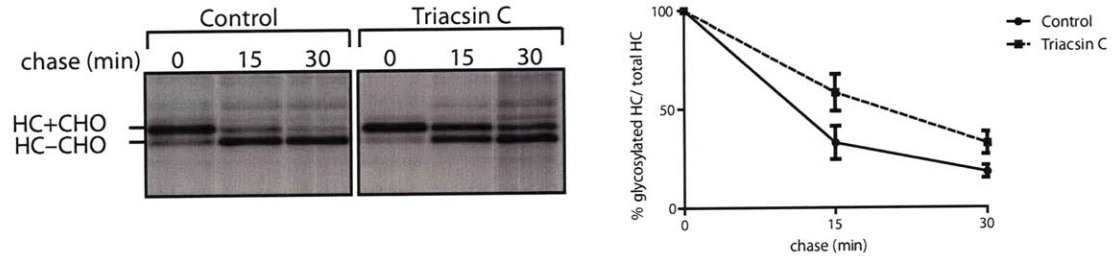

B. HeLa cells, IP: Null Hong Kong α1 anti-trypsin

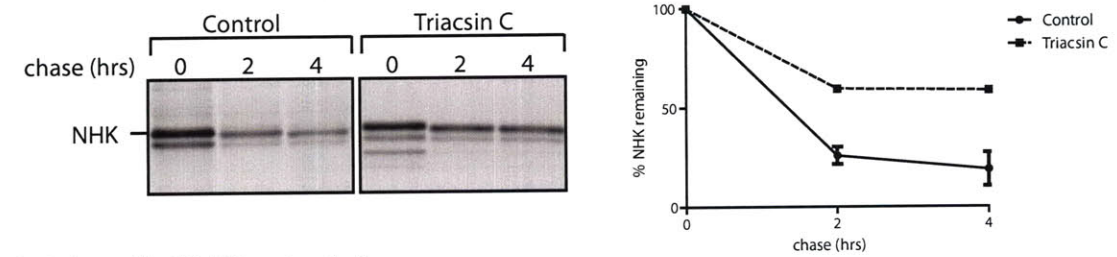

C. HeLa cells, IP: Ribophorin I

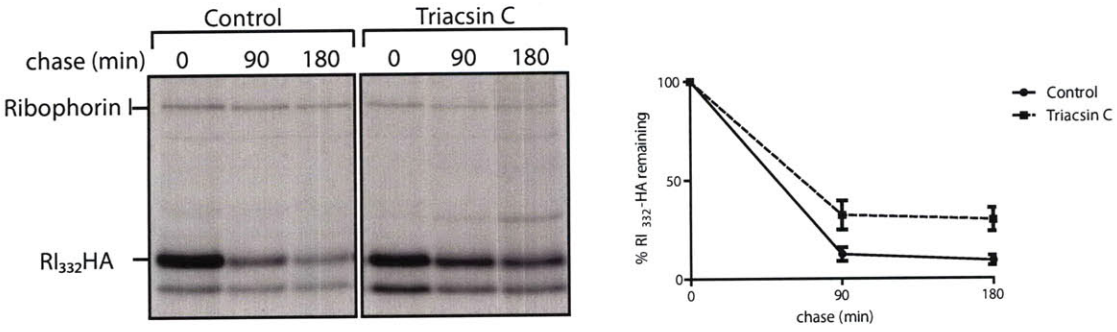

D.

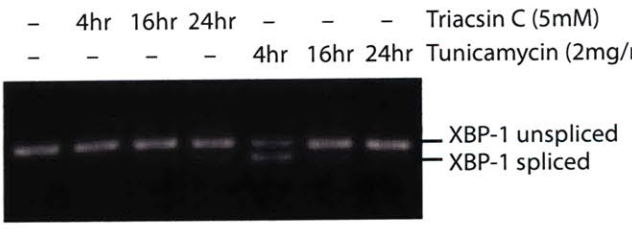

Pharmacological inhibition of lipid droplet formation affects dislocation
A) US11-expressing astrocytoma cells were treated with 5mM Triacsin C for 24 hours. Cells were pulse-labeled with ^{35}S-labelled cysteine and methionine. Samples were taken at the indicated chase times and Class I MHC heavy chain was recovered from the lysates. Immunoprecipitates were separated by SDS-PAGE and imaged by autoradiography. Amount of recovered protein was quantified by phophorimagery and is shown as a percentage of glycosylated heavy chain compared to total heavy chain. Error bars represent standard deviation of three individual experiments. B) HeLa cells were transfected with NHK and the same experiment as in (A) was performed, using anti-α1 anti-trypsin antibody for immunoprecipitation. C) HeLa cells were transfected with RI_{332}-HA and the same experiment as in (A) was performed, using anti-Ribophorin I antibody for immunoprecipitation. Quantification in (B) and (C) shows the percentage of protein remaining compared to the amount recovered at the zero minutes chase time. D) HeLa cells were treated with 5μM Triacsin or 2μg/mL Tunicamycin for the indicated times. RNA was purified and reverse transcribed. XBP-1 cDNA was amplified by PCR, run on a 2% agarose gel, and visualized by UV.

Discussion

AUP1 contributes to the degradation of misfolded ER proteins and plays a key role in lipid droplet formation. AUP1 localizes to both the ER and to the surface of lipid droplets. Reduced levels of AUP1 impair the cell's ability to efficiently degrade the soluble terminally misfolded proteins RI_{332}-HA and NHK. Cells that lack AUP1 form fewer lipid droplets, and overexpression of AUP1-GFP induces the formation of lipid droplets. AUP1 associates with most of the components of the HRD1 dislocation complex, as well as lipid modifying proteins and the oligosaccharide transferase complex. The role of AUP1 in ER protein quality control appears to be conceptually similar to that of the yeast protein Cue1p, because both have a CUE domain and a domain for recruitment of an E2 ubiquitin ligase, although there are important differences between the two proteins.

Lipid droplet connection

A key difference between AUP1 and yeast Cue1p is the contribution of AUP1 to lipid droplet formation, while no such role is apparent for Cue1p, which is not known to localize to lipid droplets. Furthermore, AUP1 interacts with lipid-modifying proteins and encodes a putative acyltransferase domain, which is absent from Cue1p. This putative acyltransferase activity of AUP1 may be directly involved in lipid droplet formation, or AUP1 may contribute to lipid droplet formation by recruiting other lipid modifying proteins -such as those we identified by mass spectrometry- to the site of lipid droplet formation. The dual roles of AUP1 may indicate a deeper connection between ER protein quality control and lipid droplet formation. This idea is supported by the fact pharmacological inhibition of lipid droplet formation affects dislocation. AUP1 may

serve as the fulcrum responsible for linking and coordinating these two processes. This connection may be specific for mammalian cells and absent from yeast, as manifest by the differences between AUP1 and Cue1p with regards to lipid droplets.

How could lipid droplets be involved in ER protein quality control? In one model, the lipid rearrangements required to form lipid droplets may facilitate the movement of misfolded proteins from the ER to the cytoplasm[45]. Alternatively, AUP1 may shuttle the cytoplasmic dislocated proteins from the ER membrane to lipid droplets *en route* to their proteasomal destruction. The lipid droplet could then serve as an appropriate reservoir for aggregation-prone misfolded proteins with exposed hydrophobic residues. Similarly, previous studies have shown that lipid droplets can store highly charged histones during Drosophila embryogenesis. These authors hypothesize that proteins could be stored on the droplet in a partially-unfolded state, with their unfolding and refolding aided by chaperones that are present on the lipid droplets[29]. By analogy, misfolded ER proteins could temporarily be parked on lipid droplets when the load of dislocated proteins exceeds the capacity or local availability of proteasomes. In times of low misfolded protein load, substrates would go directly to the proteasome.

Several connections between lipid droplets and ER protein quality control have been suggested in other studies. Components of the proteasome have been identified in lipid droplet preparations by mass spectrometry. The proteasome is responsible for the degradation of two major protein components of lipid droplets, ADRP[46, 47] and perilipin[48]. Cells treated with proteasome inhibitor resulted in the accumulation of ubiquitylated proteins in the lipid droplet-containing fraction[32]. These lipid droplet-localized ubiquitylated proteins could include dislocated ER proteins. Such is the case for

a mammalian ER quality control substrate, HMGCoA reductase, that is also found associated with lipid droplets post-dislocation[49]. These data are consistent with the idea that proteins destined for proteasomal degradation may be stored on lipid droplets.

CUE domain

The CUE domain of AUP1 facilitates several important protein-protein interactions. This is in contrast with yeast Cue1p, whose CUE domain appears to be dispensable in ER protein quality control. The CUE domain of AUP1 is necessary for the assembly of AUP1 with the dislocation complex, for the interaction of AUP1 with dislocation substrates, for the ubiquitylation of AUP1, for the interaction of AUP1 with ubiquitylated proteins, and as a possible negative regulator of poly-ubiquitylation: mutation of this domain in the context of AUP1 yields ubiquitin adducts of greater average size than those seen for wild type AUP1. The lack of association between AUP1mCUE and terminally misfolded ER proteins may be due to the fact that AUP1mCUE is not efficiently incorporated into the HRD1 complex. Alternatively, AUP1 may interact directly with the dislocation substrates, possibly via the ubiquitin modifications that are attached during dislocation, which would account for the effect of the CUE domain mutations on AUP1's interaction with RI_{332}-HA and NHK. CUE domain mutations show reduced levels of mono-ubiquitylated AUP1 and an increase in more extensively ubiquitylated AUP1 *in vitro,* possibly because the CUE domain restricts access to the Lysine-48 of ubiquitin, the residue on which poly-ubiquitylation occurs[50]. The CUE domain of yeast CUE2 CUE domain bound to ubiquitin, as solved by NMR, shows that the K48 of ubiquitin is largely blocked[22], although CUE domain binding of poly-ubiquitin is possible and has been observed *in vitro*[51]. Thus AUP1 CUE

domain-mediated binding of ubiquitin may also serve a regulatory function to control poly-ubiquitin chain formation on the dislocated ER protein.

G2BR domain

The G2BR domain we identify in AUP1 is similar to the U7 domain of Cue1p, and both are essential for recruitment of their cognate E2 (UBE2G2 for AUP1 and Ubc7p for Cue1p). The U7 domain of Cue1p enhances the activity of Ubc7p *in vitro*. Our analysis of the G2BR and *in vitro* ubiquitylation experiments indicate that AUP1 binding of E2 may actually negatively regulate the ubiquitylation of AUP1 and dislocated substrates, because ubiquitylation proceeds more efficiently when the G2BR is deleted.

Model

A working model for the role of AUP1 places it in the HRD1/SEL1L complex (Fig. 3.10). AUP1 may need to either bind ubiquitylated proteins or be ubiquitylated itself before it can be incorporated into the dislocation complex. Both of these functions are dependent on an intact CUE domain. Once the entire complex is assembled, it can proceed to process misfolded ER proteins. Ubiquitin is transferred from E1 to UBE2G2, an E2. UBE2G2 is recruited to the site of dislocation by the G2BR of AUP1. HRD1, an E3, then catalyzes the transfer of ubiquitin from UBE2G2 to misfolded ER proteins. The G2BR limits the transfer of ubiquitin and thus the interaction of AUP1 with ubiquitylated proteins. This negative regulation may serve as a feedback mechanism to exert control over degradation rates or to serve as an additional checkpoint in quality control. AUP1 then binds the dislocated ER proteins via interactions between its CUE domain and the ubiquitin moiety covalently attached to dislocated ER proteins. This CUE domain-ubiquitin interaction also regulates poly-ubiquitin chain extension. Finally, the dislocated

substrates are delivered to the proteasome where they are degraded, but may first be stored on lipid droplets under certain conditions. Thus AUP1 is involved in several steps of ER protein quality control that include ubiquitylation and processing.

Figure 3.10

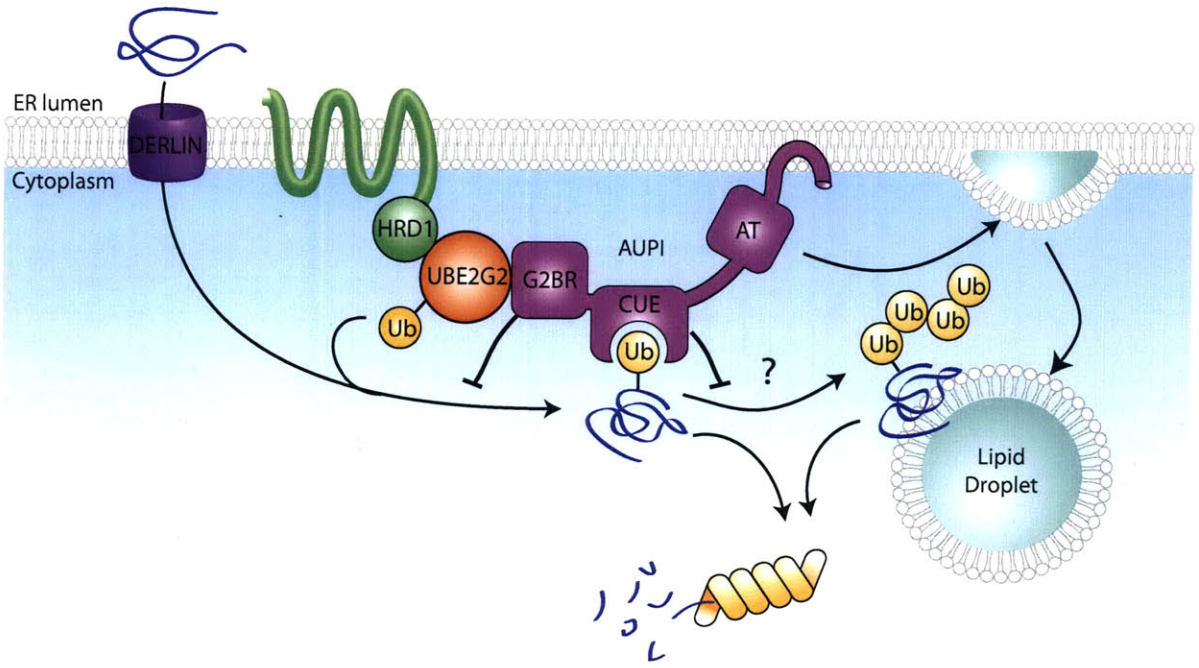

A possible model for the role of AUP1 in processing of misfolded ER proteins . AUP1 recruits UBE2G2, the E2 that works with HRD1 to ubiquitylate dislocated ER proteins. AUP1 binds the misfolded ER protein and regulates the ubiquitylation and poly-ubiquitylation of dislocation substrates via its G2BR and CUE domain, respectively. AUP1 is also involved in the formation of lipid droplets, a cytoplasmic organelle that may serve as a temporary storage location for misfolded ER proteins. Further explanation can be found in the discussion.

Materials and Methods

Antibodies

The following antibodies have been described: anti-AUP1, anti-UBXD8, and anti-Ubc6e[15]; anti-SEL1L[52]; anti-Class I MHC HC (HC-70)[9]. Other antibodies were purchased: anti-GFP, anti-PDI, anti-GAPDH, and anti-Calnexin (Abcam); anti-FLAG and anti-HA-HRP 3F10 (Sigma); immobilized anti-HA 3F10 (Roche); anti-OS9 and anti-α1 anti-trypsin (Novus); anti-HRD1 (Abgent); anti-p97 (Fitzgerald Industries International); and anti-myc M2 (Cell Signaling). Anti-Ribophorin I antibody was a generous gift of N. Erwin Ivessa (Vienna Biocenter, Vienna, Austria). Anti-STT3B and anti-OST48 antibodies were a generous gift of Reid Gilmore (University of Massachusetts Medical School, Worcester, Massachusetts).

Cell culture, oleic acid treatment, Triacsin C, transfection

HeLa cells (ATCC) were cultured in DMEM. For lipid droplet loading, cells were incubated with oleic acid adsorbed to BSA[53], for the concentrations and times indicated. Triacsin C was purchased from Biomol. FuGene6 (Roche) was used for transfections.

shRNA

shRNA constructs targeting AUP1 were obtained from The RNAi Consortium. shLUC corresponds to clone SHC007, mature sense sequence CGCTGAGTACTTCGAAATGTC, shAUP1-construct A corresponds to clone TRCN0000004269, mature sense sequence TCAGCCAACAGCCCTAACATT and shAUP1-B corresponds to clone TRCN0000004272, mature sense sequence ACACCTTTCGACCACAACATA. Lentivirus was made and HeLa cells were infected

as described[52]. Cells were grown in DMEM supplemented with 1μg/ml Puromycin and experiments were performed 4 days post-infection.

DNA constructs

mAT and mCUE mutations were made to AUP1 using site-directed mutagenesis with the following primers (forward primers are given); for mAT (H96A): GGTCCTCATTTCCAACgcTGTGACACCTTTCGACC; for mCUE (E306K, V307A, L308A) : GCTCAGAGAGTCAAGaaggcagcaCCCCATGTGCCATTG, and (Δ333-334): CTTGACTATCACTAATGAGGGGGCCGTAGCTTTC. For the ΔG2BR construct, the following reverse primer was used in PCR: CGTGAATTCTCA CTTGGCAAATGTTAGGGCTG. Constructs were cloned into pcDNA3.1+ (Clontech) (untagged and N-terminal HA) or pEGFP-C1/N1 (Clontech). GFP-AUP1 constructs also contain silent mutations rendering them resistant to shAUP1-B. UBE2G2 was obtained from open biosystems and cloned into pcDNA3.1+ with an N-teminal myc epitope tag. HA-Ubiquitin was also cloned into pcDNA3.1+.

Immunoprecipitation and immunoblotting

Cells were lysed on ice in buffer containing 25mM Tris pH7.4, 5mM $MgCl_2$, 150mM NaCl, and the detergent indicated: 0.5% Nonidet-P40 or 1% digitonin. Protein concentration of the cytoplasmic fraction was determined and equalized across the samples. Samples were incubated for 3 hours at 4°C with the antibody and Protein A agarose beads or immobilized anti-HA as indicated. The immunoprecipitates were washed, boiled in reducing sample buffer, and run on SDS-PAGE. Proteins were transferred to PVDF membrane, membranes were blocked in PBS-Tween-milk,

incubated with primary and secondary antibodies, washed, and developed with Western Lighting Chemiluminescence Reagent Plus (PerkinElmer Life Sciences).

Pulse chase metabolic labeling

HeLa cells were starved for 45 minutes in DMEM lacking cysteine and methionine. 250μCi ^{35}S-labeled cysteine and methionine (PerkinElmer) was added to each sample during the pulse (10min for US11 and 15min for RI_{332} and NHK). Media containing cold cysteine and methionine was added and equal numbers of cells were removed at the indicated chase times. Cells were lysed by agitation in a small volume of 1% SDS in PBS and then diluted in NP-40 lysis buffer. Incoproration of radioactivity was measured by TCA precipiation and liquid scintillation spectrometry to equalize, for each sample, the amount of input radioactivity to that at the zero chase timepoint. ^{35}S labeled proteins were visualized on X-ray film and quantified by phosphorimaging.

Mass Spectrometry

Approximately 90 million HeLa cells were transfected with HA-AUP1 or empty vector (pcDNA3.1+) plasmid and 3F10 beads were used for immunoprecipitation. Proteins were visualized in the SDS-PAGE gel by silver staining. The entire lane was excised from the gel in 4 x 10 mm strips and each individual gelslice was subjected to trypsinolysis. Disulfide bonds were reduced and alkylated prior to trypsinolysis. Recovered peptides were analyzed by reversed-phase liquid chromatography electrospray ionization mass spectrometry using a Waters NanoAcquity pump coupled to a ThermoFisher LTQ linear in nano flow configuration. The mass spectrometer was operated in a dependant data acquisition mode where the five most abundant peptides detected in full scan mode were subjected to daughter ion fragmentation. Peptides were

identified from the MS data using SEQUEST algorithms that searched a human specific database generated from the NCBI database. SEQUEST filters used for indication of positive peptide identification were: XCorr vs Charge State = 1.5, 2.00, 2.50; Sp – Preliminary Score = 500. Data interpretation from all bands was aided by the MSRAT program (Protein Forest).

In vitro ubiquitylation

Following digitonin lysis and immunoprecipitation, 100nM E1 (Boston Biochem), and 60μM FLAG-Ubiquitin (Boston Biochem), was added in an ATP-regenerating buffer (50mM Tris pH7.6, 5mM $MgCl_2$, 5mM ATP, 10mM creatine phosphate, 3.5U/mL creatine kinase) and kept at 37° C for one hour with gentle shaking.

Immunofluorescence

Cells were grown on glass coverslips, fixed in 4% paraformaldehyde, and permeabilized in 0.1% Triton X-100. Permeabilized cells were incubated with primary and secondary (Alexa Fluor 568 labeled) antibodies and washed with PBS before being mounted on a slide with Fluoromount-G (southern Biotech). Imaging was performed at 37°C on an inverted spinning disk confocal microscope (Nikon TE2000-U) using a Nikon x100 magnification, 1.4 numerical aperture, differential interference contrast oil lens and Hamamatsu ORCA camera using Metamorph Imaging software as described [54].

Electron microscopy

Cells were fixed in 2.5% glutaraldehyde, 3% paraformaldehyde, with 5% sucrose in 0.1 M sodium cacodylate buffer (pH 7.4). Cells were then postfixed in 1% OsO_4 in veronal-acetate buffer. The cells were stained in block overnight with 0.5% uranyl acetate in veronal-acetate buffer (pH 6.0), dehydrated, and embedded in Spurr's resin. Sections

were cut on a Reichert Ultracut E microtome with a Diatome diamond knife at a thickness setting of 50 nm, and stained with 2% uranyl acetate, followed by 0.1% lead citrate. Samples were examined using an FEI Tecnai Spirit TEM at 80 KV and imaged with an AMT camera.

Flow cytometry

HeLa cells were transduced with shRNA. Three days post-infection, 0.4mM oleic acid was added to half of the samples for 16 hours. Lipid droplets were stained with 10 μg/mL BODIPY 493/503 for 2 hours as described[40]. Median BODIPY 493/503 intensity was measured on a FACSCalibur (Becton, Dickinson) using forward scatter measurements to exclude dead cells. Data was analysed using FlowJo software.

XBP-1 splicing assay

Total cellular RNA was isolated from cells using the Qiagen RNeasy kit. cDNA was made using the Superscript II reverse transcriptase from Invitrogen. XBP-1 was amplified using the following primers: TCCTTCTGGGTAGACCTCTGGGAG (forward) and CAAGGGGAATGAAGTGAGGCCAG (reverse) which flank the splice site.

References

1. Hebert, D.N., Bernasconi, R. & Molinari, M. ERAD substrates: which way out? *Seminars in cell & developmental biology* **21**, 526-532.
2. Carvalho, P., Goder, V. & Rapoport, T.A. Distinct ubiquitin-ligase complexes define convergent pathways for the degradation of ER proteins. *Cell* **126**, 361-373 (2006).
3. Denic, V., Quan, E.M. & Weissman, J.S. A luminal surveillance complex that selects misfolded glycoproteins for ER-associated degradation. *Cell* **126**, 349-359 (2006).
4. Bernasconi, R., Galli, C., Calanca, V., Nakajima, T. & Molinari, M. Stringent requirement for HRD1, SEL1L, and OS-9/XTP3-B for disposal of ERAD-LS substrates. *The Journal of cell biology* **188**, 223-235.
5. Christianson, J.C., Shaler, T.A., Tyler, R.E. & Kopito, R.R. OS-9 and GRP94 deliver mutant alpha1-antitrypsin to the Hrd1-SEL1L ubiquitin ligase complex for ERAD. *Nature cell biology* **10**, 272-282 (2008).
6. Mueller, B., Lilley, B.N. & Ploegh, H.L. SEL1L, the homologue of yeast Hrd3p, is involved in protein dislocation from the mammalian ER. *The Journal of cell biology* **175**, 261-270 (2006).
7. Bernasconi, R., Pertel, T., Luban, J. & Molinari, M. A dual task for the Xbp1-responsive OS-9 variants in the mammalian endoplasmic reticulum: inhibiting secretion of misfolded protein conformers and enhancing their disposal. *The Journal of biological chemistry* **283**, 16446-16454 (2008).
8. Scott, D.C. & Schekman, R. Role of Sec61p in the ER-associated degradation of short-lived transmembrane proteins. *The Journal of cell biology* **181**, 1095-1105 (2008).
9. Lilley, B.N. & Ploegh, H.L. A membrane protein required for dislocation of misfolded proteins from the ER. *Nature* **429**, 834-840 (2004).
10. Ye, Y., Shibata, Y., Yun, C., Ron, D. & Rapoport, T.A. A membrane protein complex mediates retro-translocation from the ER lumen into the cytosol. *Nature* **429**, 841-847 (2004).
11. Carvalho, P., Stanley, A.M. & Rapoport, T.A. Retrotranslocation of a Misfolded Luminal ER Protein by the Ubiquitin-Ligase Hrd1p. *Cell* **143**, 579-591.
12. Rabinovich, E., Kerem, A., Frohlich, K.U., Diamant, N. & Bar-Nun, S. AAA-ATPase p97/Cdc48p, a cytosolic chaperone required for endoplasmic reticulum-associated protein degradation. *Molecular and cellular biology* **22**, 626-634 (2002).
13. Kikkert, M. *et al.* Human HRD1 is an E3 ubiquitin ligase involved in degradation of proteins from the endoplasmic reticulum. *The Journal of biological chemistry* **279**, 3525-3534 (2004).
14. Fang, S. *et al.* The tumor autocrine motility factor receptor, gp78, is a ubiquitin protein ligase implicated in degradation from the endoplasmic reticulum. *Proceedings of the National Academy of Sciences of the United States of America* **98**, 14422-14427 (2001).
15. Mueller, B., Klemm, E.J., Spooner, E., Claessen, J.H. & Ploegh, H.L. SEL1L nucleates a protein complex required for dislocation of misfolded glycoproteins.

Proceedings of the National Academy of Sciences of the United States of America **105**, 12325-12330 (2008).

16. Wiertz, E.J. *et al.* The human cytomegalovirus US11 gene product dislocates MHC class I heavy chains from the endoplasmic reticulum to the cytosol. *Cell* **84**, 769-779 (1996).
17. Kato, A. & Oshimi, K. Ancient ubiquitous protein 1 and Syk link cytoplasmic tails of the integrin alpha(IIb)beta(3). *Platelets* **20**, 105-110 (2009).
18. Kato, A. *et al.* Ancient ubiquitous protein 1 binds to the conserved membrane-proximal sequence of the cytoplasmic tail of the integrin alpha subunits that plays a crucial role in the inside-out signaling of alpha IIbbeta 3. *The Journal of biological chemistry* **277**, 28934-28941 (2002).
19. Spandl, J., Lohmann, D., Kuerschner, L., Moessinger, C. & Thiele, C. Ancient ubiquitous protein 1 (AUP1) localizes to lipid droplets and binds the E2 ubiquitin conjugase G2 (UBE2G2) via its G2 binding region. *The Journal of biological chemistry*.
20. Heath, R.J. & Rock, C.O. A conserved histidine is essential for glycerolipid acyltransferase catalysis. *Journal of bacteriology* **180**, 1425-1430 (1998).
21. Prag, G. *et al.* Mechanism of ubiquitin recognition by the CUE domain of Vps9p. *Cell* **113**, 609-620 (2003).
22. Kang, R.S. *et al.* Solution structure of a CUE-ubiquitin complex reveals a conserved mode of ubiquitin binding. *Cell* **113**, 621-630 (2003).
23. Chen, B. *et al.* The activity of a human endoplasmic reticulum-associated degradation E3, gp78, requires its Cue domain, RING finger, and an E2-binding site. *Proceedings of the National Academy of Sciences of the United States of America* **103**, 341-346 (2006).
24. Biederer, T., Volkwein, C. & Sommer, T. Role of Cue1p in ubiquitination and degradation at the ER surface. *Science (New York, N.Y* **278**, 1806-1809 (1997).
25. Bazirgan, O.A. & Hampton, R.Y. Cue1p is an activator of Ubc7p E2 activity in vitro and in vivo. *The Journal of biological chemistry* **283**, 12797-12810 (2008).
26. Kostova, Z., Mariano, J., Scholz, S., Koenig, C. & Weissman, A.M. A Ubc7p-binding domain in Cue1p activates ER-associated protein degradation. *Journal of cell science* **122**, 1374-1381 (2009).
27. Farese, R.V., Jr. & Walther, T.C. Lipid droplets finally get a little R-E-S-P-E-C-T. *Cell* **139**, 855-860 (2009).
28. Martin, S. & Parton, R.G. Lipid droplets: a unified view of a dynamic organelle. *Nat Rev Mol Cell Biol* **7**, 373-378 (2006).
29. Cermelli, S., Guo, Y., Gross, S.P. & Welte, M.A. The lipid-droplet proteome reveals that droplets are a protein-storage depot. *Curr Biol* **16**, 1783-1795 (2006).
30. Miyanari, Y. *et al.* The lipid droplet is an important organelle for hepatitis C virus production. *Nature cell biology* **9**, 1089-1097 (2007).
31. Cocchiaro, J.L., Kumar, Y., Fischer, E.R., Hackstadt, T. & Valdivia, R.H. Cytoplasmic lipid droplets are translocated into the lumen of the Chlamydia trachomatis parasitophorous vacuole. *Proceedings of the National Academy of Sciences of the United States of America* **105**, 9379-9384 (2008).

32. Ohsaki, Y., Cheng, J., Fujita, A., Tokumoto, T. & Fujimoto, T. Cytoplasmic lipid droplets are sites of convergence of proteasomal and autophagic degradation of apolipoprotein B. *Molecular biology of the cell* **17**, 2674-2683 (2006).
33. Guo, Y. *et al.* Functional genomic screen reveals genes involved in lipid-droplet formation and utilization. *Nature* **453**, 657-661 (2008).
34. Tsao, Y.S., Ivessa, N.E., Adesnik, M., Sabatini, D.D. & Kreibich, G. Carboxy terminally truncated forms of ribophorin I are degraded in pre-Golgi compartments by a calcium-dependent process. *The Journal of cell biology* **116**, 57-67 (1992).
35. Oda, Y. *et al.* Derlin-2 and Derlin-3 are regulated by the mammalian unfolded protein response and are required for ER-associated degradation. *The Journal of cell biology* **172**, 383-393 (2006).
36. Ewing, R.M. *et al.* Large-scale mapping of human protein-protein interactions by mass spectrometry. *Molecular systems biology* **3**, 89 (2007).
37. Sato, S. *et al.* Proteomic profiling of lipid droplet proteins in hepatoma cell lines expressing hepatitis C virus core protein. *Journal of biochemistry* **139**, 921-930 (2006).
38. Wan, H.C., Melo, R.C., Jin, Z., Dvorak, A.M. & Weller, P.F. Roles and origins of leukocyte lipid bodies: proteomic and ultrastructural studies. *Faseb J* **21**, 167-178 (2007).
39. Brasaemle, D.L., Dolios, G., Shapiro, L. & Wang, R. Proteomic analysis of proteins associated with lipid droplets of basal and lipolytically stimulated 3T3-L1 adipocytes. *The Journal of biological chemistry* **279**, 46835-46842 (2004).
40. Bulankina, A.V. *et al.* TIP47 functions in the biogenesis of lipid droplets. *The Journal of cell biology* **185**, 641-655 (2009).
41. Imamura, M. *et al.* ADRP stimulates lipid accumulation and lipid droplet formation in murine fibroblasts. *American journal of physiology* **283**, E775-783 (2002).
42. Spandl, J., White, D.J., Peychl, J. & Thiele, C. Live cell multicolor imaging of lipid droplets with a new dye, LD540. *Traffic (Copenhagen, Denmark)* **10**, 1579-1584 (2009).
43. Fujimoto, Y. *et al.* Involvement of ACSL in local synthesis of neutral lipids in cytoplasmic lipid droplets in human hepatocyte HuH7. *Journal of lipid research* **48**, 1280-1292 (2007).
44. Igal, R.A., Wang, P. & Coleman, R.A. Triacsin C blocks de novo synthesis of glycerolipids and cholesterol esters but not recycling of fatty acid into phospholipid: evidence for functionally separate pools of acyl-CoA. *The Biochemical journal* **324 (Pt 2)**, 529-534 (1997).
45. Ploegh, H.L. A lipid-based model for the creation of an escape hatch from the endoplasmic reticulum. *Nature* **448**, 435-438 (2007).
46. Masuda, Y. *et al.* ADRP/adipophilin is degraded through the proteasome-dependent pathway during regression of lipid-storing cells. *Journal of lipid research* **47**, 87-98 (2006).
47. Xu, G. *et al.* Post-translational regulation of adipose differentiation-related protein by the ubiquitin/proteasome pathway. *The Journal of biological chemistry* **280**, 42841-42847 (2005).

48. Xu, G., Sztalryd, C. & Londos, C. Degradation of perilipin is mediated through ubiquitination-proteasome pathway. *Biochimica et biophysica acta* **1761**, 83-90 (2006).
49. Hartman, I.Z. *et al.* Sterol-induced dislocation of 3-hydroxy-3-methylglutaryl coenzyme A reductase from endoplasmic reticulum membranes into the cytosol through a subcellular compartment resembling lipid droplets. *The Journal of biological chemistry* **285**, 19288-19298.
50. Hochstrasser, M. Origin and function of ubiquitin-like proteins. *Nature* **458**, 422-429 (2009).
51. Shih, S.C. *et al.* A ubiquitin-binding motif required for intramolecular monoubiquitylation, the CUE domain. *The EMBO journal* **22**, 1273-1281 (2003).
52. Lilley, B.N. & Ploegh, H.L. Multiprotein complexes that link dislocation, ubiquitination, and extraction of misfolded proteins from the endoplasmic reticulum membrane. *Proceedings of the National Academy of Sciences of the United States of America* **102**, 14296-14301 (2005).
53. Brasaemle, D.L. & Wolins, N.E. Isolation of lipid droplets from cells by density gradient centrifugation. *Current protocols in cell biology / editorial board, Juan S. Bonifacino ... [et al* **Chapter 3**, Unit 3 15 (2006).
54. Vyas, J.M. *et al.* Tubulation of class II MHC compartments is microtubule dependent and involves multiple endolysosomal membrane proteins in primary dendritic cells. *J Immunol* **178**, 7199-7210 (2007).

Chapter 4

Summary and Future Directions

ER quality control in mammalian cells is an important process that prevents the harmful accumulation of misfolded proteins. The HCMV US11 immunovasin co-opts this process and has been used as a tool to study dislocation. A general picture of the US11-associated complex has been reconstructed using serial immunopurification experiments. For each experiment, a component of the US11 complex was used as bait and the associated proteins were identified using mass spectrometry. US11 was immunoprecipitated from cells and Derlin1 was identified as a member of the complex[1]. Immunoprecipitation of Derlin1 identified SEL1L and HRD1[2]. Using SEL1L as the bait yielded AUP1, UBXD8, OS9 and UBC6e (Figure 2.1)[3]. AUP1-associated proteins include components of the oligosaccharide transferase complex and lipid modifying enzymes (Figure 3.2 and Table 3.1).

We verified the role of each of the newly-identified proteins in ER quality control. GFP-tagged versions of UBXD8 and AUP1 and catalytically dead UBC6e act in dominant negative fashion to disrupt US11-mediated dislocation of MHC class I heavy chain. UBXD8 serves to recruit p97, the protein responsible for membrane extraction of dislocation substrates. Installation of the GFP at the C-terminus of UBXD8 prevents p97 recruitment. OS9 does not perturb US11-mediated dislocation, but does delay the degradation of a soluble misfolded protein, RI_{332}. The explanation for the differential involvement of OS9 in dislocation is that OS9 specializes in directing soluble dislocation

substrates to the ER quality control machinery[4]. MHC class I is a type I membrane protein that is directed to the dislocon by US11, not OS9.

AUP1 is important for the dislocation of both soluble membrane proteins with misfolded luminal domains as well as membrane proteins (Fig. 3.1). AUP1 plays a role in the ubiquitylation of dislocation substrates. The soluble cytoplasmic E2 UBE2G2 is recruited to the dislocation machinery by AUP1 (Fig. 3.1C). AUP1 is ubiquitylated and binds ubiquitylated proteins, including misfolded ER proteins (Figs. 3.5 and 3.4B). AUP1 also negatively regulates mono- and poly-ubiquitylation (Figs. 3.5 and 3.6). Unexpectedly, we also found that AUP1 is involved in lipid droplet formation. AUP1 localizes to lipid droplets and overexpression results in the accumulation of lipid droplets (Fig. 3.7). Depletion of AUP1 impairs lipid droplet formation (Fig. 3.8). Lipid droplets have never been shown to be mechanistically involved in ER protein quality control, but several studies have reported a link between the two processes (discussed in Chapter 1). We found that inhibition of lipid droplet formation (by AUP1 depletion and pharmacological inhibition of lipid biosynthetic enzymes) stabilized dislocation substrates (Figs. 3.1 and 3.9). This data prompt many further questions about how AUP1 contributes to ER quality control, lipid droplet formation and other cellular processes and how these processes are co-regulated.

In order to better understand the role of AUP1 in dislocation, several open questions should be answered. First, how does AUP1-mediated ubiquitylation regulation impact dislocation? This question could be addressed by comparing the dislocation efficiency of cells expressing AUP1 with mutant CUE or G2BR domains compared to cells expressing wildtype AUP1. This experiment would have to be performed on cells

that have been transduced with the AUP1-specific shRNA to eliminate endogenous AUP1 activity. It is possible that mutation of AUP1's G2BR could slow dislocation since UBE2G2 would not be recruited. The fact that mutation of AUP1's CUE domain results in increased substrate poly-ubiquitylation may mean that the degradation of dislocated proteins could proceed more quickly in cells expressing AUP1 with mutant CUE domain compared to wildtype. Second, we would like to identify the ubiquitylated proteins that associate with AUP1. Presumably they are misfolded ER proteins, but do these proteins share common characteristics? Immunoprecipitation of AUP1 followed by the subsequent re-immunoprecipitation of ubiquitin will isolate the AUP1-associated ubiquitylated proteins that can then be identified by mass spectrometry. This experiment can be done either at steady-state in cells transfected with epitope-tagged AUP1 and ubiquitin or in an *in vitro* ubiquitylation assay. For the latter case, cells would be permeabilized using the pore-forming toxin PFO. PFO creates large pores in the plasma membrane through which the cytoplasm is removed during centrifugation and replaced by a mixture of biotin-labeled ubiquitin, purified E1 and ATP. After incubation and lysis, AUP1 would be immunoprecipitated, the associated material would be dissociated with SDS, the biotin-ubiquitin would be captured with streptavidin beads and then released. Known dislocation substrates including RI_{332} and NHK can be used as positive controls. Finally, from the AUP1 immunoprecipitation experiment, we know that the AUP1 complex includes two E2 ubiquitin conjugating enzymes: UBC6e and UBE2G2. Are multiple E2s involved in the ubiquitylation of the same substrate? Or if only one E2 is used for each substrate, does it matter which one is used? If UBC6e and UBE2G2 act interchangeably, you would expect depletion of both UBC6e and UBE2G2 to severely

block HRD1-mediated ubiquitylation. But if they are not interchangeable or a substrate requires both E2s, then depletion of just one of the E2s will be as problematic as the double depletion. This could be tested by *in vitro* ubiquitylation assays.

The functional role of lipid droplets in ER protein quality control remains unclear, but we hypothesize that AUP1 provides the link between the two systems. It is not known whether all of the dislocation machinery localizes to lipid droplets along with AUP1 or if AUP1 interacts with different proteins in the different cellular locations. Are any of the other components of the dislocation machinery found on lipid droplets? UBXD8 is a second protein that localizes to both the ER and lipid droplets and plays a role in dislocation[3,5]. Initial experiments indicate that overexpression of GFP-OS9 may also induce lipid droplet formation (data not shown). In contrast to AUP1 and UBXD8, the GFP fluorescence is found at the core of lipid-droplet like structures. This may be because OS9 is a soluble ER protein, whereas both AUP1 and UBXD8 have membrane-anchor domains that dip into the outer leaflet of the bilayer. It would be interesting to determine whether these GFP-OS9-containing structures are in fact lipid droplets in as much as they contain lipids. This could be determined by thin layer chromatography of the isolated structures. If the ER quality control machinery is present on lipid droplets, does ubiquitylation occur there? Isolated lipid droplets could be used in *in vitro* ubiquitylation assays to see if exogenous epitope-tagged ubiquitin is attached to proteins on the lipid droplet.

One possible model for the involvement of lipid droplet formation in dislocation is that LDs form according to the "escape hatch" model and dislocation substrates "piggy back" on the LD to exit the ER. In this model, dislocated proteins would be associated

with lipids. For single-pass transmembrane proteins, this could be just enough lipids to form a coat to shield the hydrophobic membrane anchor. In US11-expressing cells, lipids associated with the cytoplasmic MHC class I could be detected by thin layer chromatography.

An alternative model is that misfolded proteins exit through a proteinaceous channel, but then are harbored on the LD surface in order to prevent their aggregation. This idea is an extension of the "refugee model"[6-7]. One way to distinguish between these two models would be to see whether dislocation proceeds normally under lipolytically stimulating conditions. Lipolytically stimulating conditions are triggered by treatment with the phosphodiesterase inhibitor IBMX and the β-adrenergic receptor agonist isoproterenol[8-9]. If the "escape hatch" model is true, disruption of already-formed lipid droplets will not affect dislocation. If the "refugee model" is true, these treatments will perturb the degradation of misfolded proteins by decreasing the storage sites for dislocated proteins.

Misfolded ER proteins may move from the ER to lipid droplets before they are degraded by the proteasome. Are dislocated proteins found on lipid droplets? HMGCoA reductase, a lipid regulatory dislocation substrate, has been observed associated with lipid droplets[10]. Is this a general observation for all dislocation substrates or only for those involved in the regulation of lipid biosynthesis? It remains to be seen whether other dislocation substrates that are not related to lipid biosynthesis, including RI_{332} and NHK, are found in the buoyant lipid droplet layer after fractionation. If they are, is AUP1 required for these dislocation substrates to localize to lipid droplets? To answer these questions, wildtype and AUP1-depleted cells could be fractionated and immunoblotted

for the dislocation substrate. If misfolded ER proteins localize to the lipid droplets and AUP1 acts as a shuttle to deposit them onto the lipid droplet, then we would expect to see the dislocation substrate in the lipid droplet fraction of wildtype, but not AUP1-depleted cells.

What are the possible ways that AUP1 could link ER protein quality control with lipid droplets? As mentioned above, AUP1 could act as a shuttle to transport misfolded proteins from the ER to the lipid droplet. AUP1 may also regulate the amount of lipid droplet formation in response to the burden of unfolded proteins on ER protein quality control. Current data suggests two possible ways that AUP1 may contribute to lipid droplet formation: directly via its putative acyltransferase domain or indirectly through the recruitment of lipid modifying enzymes including. Is AUP1 with a point mutation in the active site of the acyltransferase domain able to induce lipid droplet formation? The size and number or lipid droplets in AUP1mAT cells can be assessed by microscopy and flow cytometry. If AUP1 is an active acyltransferase, the AUP1-depleted cells may not be able to make certain types of lipids, which could account for the observation that these cells are less able to form lipid droplets upon oleic acid treatment. The lipid profiles of wildtype and AUP1-depleted cells can be determined by mass spectrometry. Differences in the abundance of specific lipids might indicate the lipid substrate specificity of AUP1's acyltransferase domain which could then be confirmed *in vitro.*

AUP1 in found in association with several enzymes involved in lipid droplets formation. It could be that these lipid-modifying enzymes play a role in dislocation. We know that pharmacological inhibition of ACSL3 and other long-chain acyl coA

synthetases affects dislocation. Does shRNA-mediated depletion of ACSL3 and the other lipid biosynthetic enzymes likewise stabilize dislocation substrates?

Do increases in lipid droplets enable cells to better tolerate ER stress? If lipid droplets do serve as storage depots for misfolded proteins, increasing their numbers would allow the cell to survive higher concentrations of misfolded proteins. ER stress can be induced with tunicamycin or dithiothreitol, and these treatments will result in apoptotic cell death over time. Cells with more lipid droplets due to AUP1 overexpression or oleic acid treatment may be able to survive the ER stress for extended periods of time.

Because AUP1 is important for lipid droplet formation, it may also be required for the several pathogens that use lipid droplets for replication. If this were the case, AUP1-GFP and AUP1 depleted cells would be good tools for studying the lifecycles and localization of these pathogens. Pathogens that use lipid droplets include Hepatitis C Virus, rotaviruses, Dengue, and Chlamydia. AUP1 may interact with proteins of the different pathogens and these associations could be identified by immunoprecipitation of AUP1 followed mass spectrometry.

AUP1 reportedly interacts with the autophagy-associated ubiquitin-like modifier, APG12[11]. This interaction was found in a mass spectrometry study using ATG12L as the bait. Although ATG12 was not found when AUP1 was used as the bait (Fig. 3.2), this may be because ATG12 was probably expressed at low levels in these cells since they were not engaged in autophagy. Autophagy and lipid droplets have been previously linked[12], as have autophagy and ER turn-over[13]. AUP1 may be involved in all three of these processes. A first step to test whether AUP1 is involved in autophagy would be to

confirm the interaction between AUP1 and ATG12 with epitope-tagged proteins as well as in autophagic cells. Could AUP1 be necessary for autophagy? Experiments in AUP1-depleted cells under autophagy-inducing conditions would answer this question. Fluorescent microscopy experiments would show whether AUP1 localizes to autophagosomes.

The initial identification of AUP1 as a SEL1L-interacting led to a better understanding of how HRD1-mediated ubiquitylation proceeds and also brought about the exciting hypothesis that ER quality control is related to lipid droplets. This connection must be further validated and understood. As the questions mentioned above are answered, we will move toward a better understanding of how and why lipid droplets contribute to ER protein quality control. There are also indications that AUP1 may be involved in other cellular processes which may also present interesting future directions.

1. Lilley, B.N. & Ploegh, H.L. A membrane protein required for dislocation of misfolded proteins from the ER. *Nature* **429**, 834-840 (2004).
2. Lilley, B.N. & Ploegh, H.L. Multiprotein complexes that link dislocation, ubiquitination, and extraction of misfolded proteins from the endoplasmic reticulum membrane. *Proceedings of the National Academy of Sciences of the United States of America* **102**, 14296-14301 (2005).
3. Mueller, B., Klemm, E.J., Spooner, E., Claessen, J.H. & Ploegh, H.L. SEL1L nucleates a protein complex required for dislocation of misfolded glycoproteins. *Proceedings of the National Academy of Sciences of the United States of America* **105**, 12325-12330 (2008).
4. Bernasconi, R., Galli, C., Calanca, V., Nakajima, T. & Molinari, M. Stringent requirement for HRD1, SEL1L, and OS-9/XTP3-B for disposal of ERAD-LS substrates. *The Journal of cell biology* **188**, 223-235 (2010).
5. Zehmer, J.K., *et al.* Targeting sequences of UBXD8 and AAM-B reveal that the ER has a direct role in the emergence and regression of lipid droplets. *Journal of cell science* **122**, 3694-3702 (2009).
6. Cermelli, S., Guo, Y., Gross, S.P. & Welte, M.A. The lipid-droplet proteome reveals that droplets are a protein-storage depot. *Curr Biol* **16**, 1783-1795 (2006).
7. Welte, M.A. Proteins under new management: lipid droplets deliver. *Trends in cell biology* **17**, 363-369 (2007).
8. Brasaemle, D.L., Dolios, G., Shapiro, L. & Wang, R. Proteomic analysis of proteins associated with lipid droplets of basal and lipolytically stimulated 3T3-L1 adipocytes. *The Journal of biological chemistry* **279**, 46835-46842 (2004).
9. Cheung, W., *et al.* Rotaviruses associate with cellular lipid droplet components to replicate in viroplasms, and compounds disrupting or blocking lipid droplets inhibit viroplasm formation and viral replication. *Journal of virology* **84**, 6782-6798.
10. Hartman, I.Z., *et al.* Sterol-induced dislocation of 3-hydroxy-3-methylglutaryl coenzyme A reductase from endoplasmic reticulum membranes into the cytosol through a subcellular compartment resembling lipid droplets. *The Journal of biological chemistry* **285**, 19288-19298 (2010).
11. Ewing, R.M., *et al.* Large-scale mapping of human protein-protein interactions by mass spectrometry. *Molecular systems biology* **3**, 89 (2007).
12. Singh, R., *et al.* Autophagy regulates lipid metabolism. *Nature* **458**, 1131-1135 (2009).
13. Bernales, S., Schuck, S. & Walter, P. ER-phagy: selective autophagy of the endoplasmic reticulum. *Autophagy* **3**, 285-287 (2007).

Appendix

Viral Interference with B7-1 Costimulation: A New Role for Murine Cytomegalovirus Fc Receptor-1[1]

Justine D. Mintern,* Elizabeth J. Klemm,* Markus Wagner,* Marie Eve Paquet,* Melanie D. Napier,* You Me Kim,* Ulrich H. Koszinowski,† and Hidde L. Ploegh[2]*

Murine CMV (MCMV), a β-herpesvirus, infects dendritic cells (DC) and impairs their function. The underlying events are poorly described. In this study, we identify MCMV *m138* as the viral gene responsible for promoting the rapid disappearance of the costimulatory molecule B7-1 (CD80) from the cell surface of DC. This was unexpected, as *m138* was previously identified as *fcr-1*, a putative virus-encoded FcR. m138 impaired the ability of DC to activate $CD8^+$ T cells. Biochemical analysis and immunocytochemistry showed that m138 targets B7-1 in the secretory pathway and reroutes it to lysosomal associated membrane glycoprotein-1^+ compartments. These results show a novel function for m138 in MCMV infection and identify the first viral protein to target B7-1. *The Journal of Immunology*, **2006, 177: 8422–8431.**

Herpesviruses are large DNA viruses that establish latent infection in the host by actively limiting the immune response (reviewed in Ref. 1). To disable host cell immune strategies, murine CMV (MCMV)[3] possesses a dsDNA genome of ~230 kb that potentially encodes 170 predicted genes (2). The central core of the genome is conserved among all β-herpesviruses and contains genes essential for virus assembly and replication (3). In contrast, the genome termini contain >100 predicted genes that are dispensable for viral replication in vitro (4), but are considered critical for infection and immune modulation in vivo (5). Although for a small number of these genes, immune modulatory activities have been described, the majority possess unknown potential for novel immune evasion strategies.

$CD8^+$ CTLs serve as the major immune effectors that control CMV infection in both humans (6, 7) and mice (8, 9). CMV-infected cells are targeted by TCR recognition of host cell MHC class I molecules displaying virus-derived peptide(s). Given the critical nature of the TCR:MHC class I-peptide interaction, it is attacked by CMV at multiple levels. Immune evasion proteins impair the MHC class I molecule by promoting its retention (10, 11) or degradation (12–14), by blocking the peptide-loading complex (15), or by preventing TCR recognition at the cell surface (16). Disruption of MHC class I Ag presentation has mostly been studied in non-APC, thereby mimicking the effector stage of recognition, in which an infected cell in the tissue must avoid an already primed host cell immune response. For the virus, it is equally important to target the initiation of events. This occurs in the secondary lymphoid organs in which circulating naive T cells are primed by dendritic cells (DC) expressing virus-derived peptide in the context of MHC class I. In addition to MHC class I-peptide complexes, DC display multiple costimulatory molecules that enhance TCR-mediated signaling and enable optimal T cell activation (17). Costimulatory molecule-deficient mice display impaired viral clearance in a number of viral infection models, illustrating the critical role for costimulation in eliciting antiviral immunity (reviewed in Ref. 18).

The B7 family of costimulatory molecules is the best described to date (reviewed in Ref. 19) and currently includes seven known members: B7-1 (CD80), B7-2 (CD86), inducible costimulatory molecule ligand (ICOSL), programmed death ligand (PD-L)1, PD-L2, B7H3, and B7H4, all of which are expressed by APC. Through interactions with their receptors on T cells, the B7 family members modulate TCR signaling. Impaired expression of B7 costimulatory molecules occurs upon infection with numerous viruses, including Kaposi's sarcoma-associated herpesvirus (KSHV) (20), lymphocytic choriomeningitis virus (21), varicella-zoster virus (22), vaccinia (23), and HIV type 1 (HIV-1) (24). In most cases, neither the viral genes responsible, nor the mechanism of modulation, are known. Two exceptions are the targeting of B7-2 by K5, an E3 ubiquitin ligase expressed by KSHV (20), and modB7-2 encoded by MCMV (25). Consequently, the removal of specific costimulatory molecules from the DC surface affords a particularly potent strategy of viral-mediated immune evasion. In this study, we investigated the ability of MCMV to modulate B7 costimulatory molecule expression in DC. We have identified the first virus protein to target B7-1 and have identified a novel function for the previously described MCMV *fcr-1* gene, *m138*.

Materials and Methods

Cells

The DC line D2SC/1 (provided by P. Ricciardi-Castagnoli (University of Milano-Bicocca, Italy) and referred to as DC2 throughout this work) (26), DC2.4 (27, 28), M210B4 (29), Chinese hamster ovary (CHO) cells (American Type Culture Collection), CHO-B7-1 (provided by A. Sharpe,

*Department of Pathology, Harvard Medical School, Boston, MA 02115; and †Max von Pettenkofer Institut, Ludwig-Maximilians-Universität München, Munich, Germany

Received for publication April 28, 2006. Accepted for publication September 18, 2006.

The costs of publication of this article were defrayed in part by the payment of page charges. This article must therefore be hereby marked *advertisement* in accordance with 18 U.S.C. Section 1734 solely to indicate this fact.

[1] J.D.M. was supported by a CJ Martin Fellowship. M.W. was supported by a Long-term Fellowship from the Human Frontiers Science Organization. Y.M.K. was supported by a Leukemia & Lymphoma Society Fellowship. M.E.P. was funded by Fonds de la Recherche en Sante du Quebec.

[2] Address correspondence and reprint requests to Dr. Hidde L. Ploegh, Whitehead Institute for Biomedical Research, 9 Cambridge Center, Cambridge, MA 02142-1479. E-mail address: ploegh@wi.mit.edu

[3] Abbreviations used in this paper: MCMV, murine CMV; DC, dendritic cell; BMDC, bone marrow-derived DC; CHO, Chinese hamster ovary; DC2, D2SC/1 DC; EEA-1, early endosomal Ag-1; Endo H, endoglycosidase H; ER, endoplasmic reticulum; HA, hemagglutinin; ICOSL, inducible costimulatory molecule ligand; KSHV, Kaposi's sarcoma-associated herpesvirus; LAMP-1, lysosomal-associated membrane glycoprotein-1; MOI, multiplicity of infection; PD-L, programmed death ligand; PDI, protein disulfide isomerase; Tfn, transferrin.

Harvard University, Boston, MA) (30), NIH 3T3 (American Type Culture Collection), B3Z (provided by N. Shastri, University of California, Berkeley, CA) (31), and BALB/c murine embryonic fibroblasts were grown, as previously described. Primary bone marrow-derived DC (BMDC) were generated from bone marrow harvested from C57BL/6 mice (The Jackson Laboratory). Mice were maintained at the Whitehead Institute for Biomedical Research Animal Facility, according to institutional guidelines. Bone marrow was cultured in the presence of 200 μg/ml GM-CSF (PeproTech) and 20 μg/ml IL-4 (PeproTech) for 4–5 days.

DNA constructs

The N-terminal hemagglutinin (HA) construct (provided by B. Lilley, Harvard University, Boston, MA) contained the H-2K^b signal sequence, followed by the HA tag in the pcDNA 3.1 expression vector (Invitrogen Life Technologies). The *m138* gene was introduced into the *Eco*RI/*Not*I site using the following primer sequences: 5′-CGCAATTGCATCAATTAC CTGCGTGC-3′ and 5′-AAGAAGCGGCCGCTTAGGCGTAGTCGGG GAC-3′. GFP-tagged B7-1 was generated using B7-1 cDNA (provided by G. Freeman). The *B7-1* gene was cloned into the *Xho*I/*Sal*I site of the pEGFP-N1 expression vector (BD Clontech) by PCR. The primer sequences used were as follows: 5′-CCGCTCGAGACCACCATGGCTTG CAATTGTCAG-3′ and 5′-CGCGTCGACGCAAGGAAGACGGTCT GTTC-3′. m138 truncation proteins were generated by the following primer combinations: *tailm138*, 5′-ACGGCCTTCCGCGCTGACGCG-3′; *CD4TMtailm138*, 5′-CCAATGGCCCTGATTGTGCTG-3′ and 5′-CTG GCGGCCGCTCAAATGGGGCTACATGTC-3′. The human CD4 transmembrane and tail domain (aa 396–458) was generated by PCR using the primers 5′-CCAATGGCCCTGATTGTGCTG-3′ and 5′-CTGGCGGC CGCTCAAATGGGGCTACATGTC-3′. Cells were transiently transfected using Fugene-6 (Roche).

Viruses

MCMV were propagated in M210B4 cells. MCMV infections were performed by centrifugation at 2000 rpm for 30 min at 25°C. Supernatant was harvested from DC2 infected with wild-type MCMV 16 h postinfection and filtered through a 0.45-μm syringe filter (Corning Glass). The pMIG retrovirus, containing an internal ribosomal entry site followed by GFP, was used to generate stable cell lines. The *m138* gene was cloned into the *Bgl*II/*Eco*RI site by PCR using the primer sequences 5′-GAGGATCCAC CACCATGGCGCCTTCGACGCTG-3′ and 5′-CCCGCAATTGTTACGT GTGACGTACGC-3′.

Mutagenesis of MCMV genome

Mutagenesis was performed by homologous recombination between a linear DNA PCR fragment and the MCMV-BAC pSM3fr in *Escherichia coli*, as previously described (4). To delete MCMV genes, linear DNA fragments containing the *kanamycin resistance* gene flanked by regions of homology to the MCMV genome were generated. The specific primers used to generate *Δm138MCMV* were as follows: 5′-GGGTCAGTCATT AGTAAGTGTTAGTAGTCGATGACTTGAGCGTCGTGGAATGCCTT CGAATTC-3′ and 5′-CTCAAGTCGCCATCATCTCTCGGTCGGCA GAGCCGAGGCGACAAGGACGACGACGACAAGTAAG-3′. The loss of *m138* was confirmed by restriction enzyme pattern analysis of the rMCMV genome with *Hin*dIII and by immunoblotting for m138 protein in infected cell lysates.

Flow cytometry

Cells were harvested and stained with the following Abs: anti-B7-1 PE (16-10A1; BD Biosciences), anti-B7-2 PE (GL1; BD Biosciences), anti-ICOSL PE (HK5.3; eBioscience), anti-PD-L1 (MIH5; eBioscience), anti-PD-L2 (TY25; eBioscience), anti-CD11c (HL3; BD Biosciences), and anti-mouse IgG2,κ-PE (BD Biosciences). When DC were analyzed, cells were incubated with purified anti-mouse CD16/CD32 (BD Pharmingen) before cell surface staining. To detect MCMV infection, cells were fixed with 0.5% paraformaldehyde (EM grade; Electron Microscopy Sciences) and permeabilized with 0.5% saponin (Sigma-Aldrich). Cells were stained with mouse anti-pp89 (provided by S. Jonjic, University of Rijeka, Croatia), followed by goat anti-mouse IgG (H + L)-Alexa 660 (Molecular Probes). Detection of Ig binding at the cell surface was undertaken by incubation of virus-infected cells with mouse IgG (Sigma-Aldrich) for 30 min, followed by staining with anti-mouse IgG2,κ-PE (BD Biosciences). Flow cytometry analysis was performed using a FACSCalibur flow cytometer (BD Biosciences) and analyzed with CellQuest software (BD Biosciences).

Immunoblotting

Cells were harvested and lysed in 1% SDS. Protein quantity was determined by a bicinchonic acid protein assay (Pierce). Immunoblotting was performed by standard techniques. Anti-m138 rabbit polyclonal serum was generated by immunization with a mixture of three peptides (amino acid residues 115–127, 213–225, and 499–513) (Cocalico). Proteins were detected using rabbit anti-B7-1 (Abcam), mouse anti-β-actin (Sigma-Aldrich), anti-mouse IgG-HRP (Southern Biotechnology Associates), and anti-rabbit IgG-HRP (Southern Biotechnology Associates).

Radio or biotin labeling and immunoprecipitation

For radiolabeling, cells were starved in complete medium lacking cysteine and methionine, supplemented with 0.5 μCi/ml [^{35}S]methionine/cysteine. Chase periods were performed with medium containing 2.5 mM methionine and 0.5 mM cysteine. For surface biotin labeling, cells were washed with PBS and labeled with 0.2 mg/ml sulfo-NHS- LC-biotin (Pierce) in PBS. Following labeling, cells were washed with PBS/10 mM glycine. Labeled cells were lysed in 1% detergent (Nonidet P-40 or digitonin). Proteins were immunoprecipitated with specific Abs and protein A-agarose (RepliGen). Immunoprecipitations were performed from equivalent amounts of radioactive protein following the pulse label and preclearing of cell lysates. Radioactive counts were determined by trichloroacetic acid precipitation of 10 μl of total lysate. Endoglycosidase H (Endo H; New England Biolabs) digestion was performed by incubation at 37°C for 1 h. Anti-GFP rabbit polyclonal serum (Abcam), anti-HA rabbit polyclonal serum (12CA5), and mouse Ig (Sigma-Aldrich) were used for immunoprecipitation. Radioactive polypeptides were visualized by fluorography and exposure to Kodak X-OMAT films.

Immunostaining and fluorescent confocal microscopy

Cells were grown on coverslips and fixed with 4% paraformaldehyde (EM grade; Electron Microscopy Sciences) in PBS. Cells were permeabilized with 1% Triton X-100. The following Abs were used: anti-HA (3F10; Roche), anti-B7-1 (16-10A1; BD Biosciences), anti-lysosomal-associated membrane glycoprotein-1 (LAMP-1) (Abcam), anti-early endosomal Ag-1 (EEA-1) (Abcam), anti-protein disulfide isomerase (PDI; Abcam), anti-hamster IgG-Cy3 (Jackson ImmunoResearch Laboratories), and anti-rabbit Ig-Alexa 488, 647 (Molecular Probes). To label transferrin (Tfn)-containing compartments, cells were serum starved and incubated with Tfn-Alexa 594 (Molecular Probes). Cells were imaged with a spinning disk confocal microscope.

RT-PCR

RNA extraction was performed (Qiagen) and cDNA generated (Invitrogen Life Technologies). RT-PCR was performed using B7-1 primers (32).

Ag presentation assay

DC2.4 were pulsed with 1.1-μm-diameter latex beads (Sigma-Aldrich) or 0.89-μm diameter flash red fluorescent beads (Bangs Laboratories) previously adsorbed with OVA (10 mg/ml) for 6 h. Cells were fixed with 0.5% paraformaldehyde (EM grade; Electron Microscopy Sciences) and washed with PBS. Indicated cultures were incubated with 25 μg/ml anti-B7-1 (BD Pharmingen). A total of 1×10^6 B3Z T cells was added to each culture and harvested 24 h later. B3Z T cells are CD8$^-$ OVA-specific T cells that express the *lacZ* gene under the transcriptional control of NF-AT (31). Expression of lacZ was assessed by the chromogenic β-galactosidase enzyme assay (Promega).

Results

MCMV modulates cell surface expression of B7 costimulatory molecules

To study MCMV infection of DC, we used D2SC/1 (DC2) (26), a DC line that can readily be infected with MCMV. The impact of MCMV infection on the cell surface expression of B7 costimulatory molecules was examined by flow cytometry (Fig. 1*A*). Uninfected DC2 expressed high levels of B7-1 and B7-2 and low levels of PD-L1, PD-L2, and ICOSL (data not shown). The extent of MCMV infection of DC2 was determined by intracellular staining for pp89, an immediate early MCMV protein. In all cases, MCMV infection at a multiplicity of infection (MOI) = 10 resulted in >50% of DC2 expressing the pp89 protein (data not shown). Upon MCMV infection, the expression of both PD-L1 and PD-L2 was

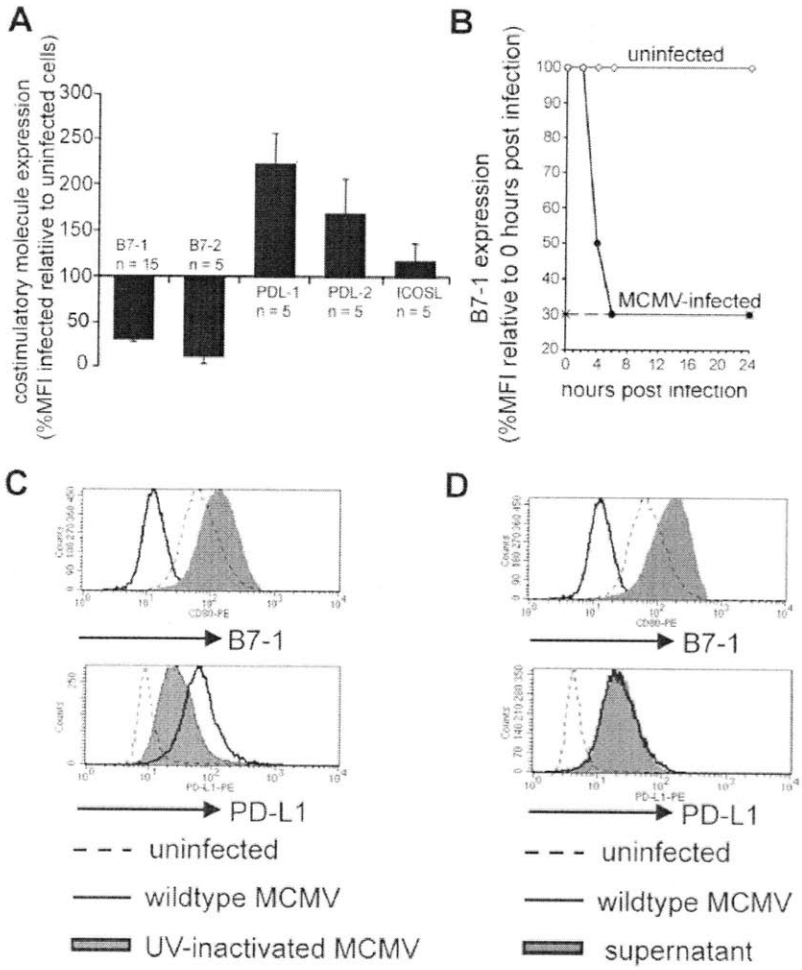

FIGURE 1. MCMV modulates cell surface expression of B7 costimulatory molecules. *A*, DC2 were infected with MCMV (MOI = 10) or left uninfected and examined 16 h postinfection. The graph displays the mean percentage of the mean fluorescence intensity (MFI) of infected ($pp89^+$) cells relative to uninfected cells ± SEM. *B*, DC2 were infected with MCMV (MOI = 10). The graph displays the mean percentage MFI of B7-1 expressed by $pp89^+$ MCMV-infected cells or uninfected cells relative to that at 0 h postinfection. Background fluorescence in the absence of Ab (dashed line). *C*, DC2 were infected with wild-type MCMV (MOI = 10), UV-inactivated MCMV, or left uninfected and examined 16 h postinfection. For wild-type MCMV-infected cells, the histograms are gated on $pp89^+$ DC2. *D*, DC2 were infected with wild-type MCMV (MOI = 10), treated with supernatant harvested from MCMV-infected DC2, or left uninfected and examined 16 h postinfection. For wild-type MCMV-infected cells, the histograms are gated on $pp89^+$ DC2.

up-regulated in MCMV-infected DC2, most notably PD-L1, which was expressed at 2-fold higher levels compared with uninfected cells. The low expression of ICOSL remained unaltered in MCMV-infected DC2. The most striking effect of MCMV infection was the specific targeting of the B7-1 and B7-2 molecules, which could no longer be detected at the cell surface 16 h following infection. We focused on MCMV interference with B7-1, given that there are no known viral proteins that interfere with its expression. Examination of uninfected cells and MCMV-infected DC2 at various time points following infection showed that cell surface expression of B7-1 is rapidly lost. B7-1 was completely absent from the cell surface as early as 6 h following infection (Fig. 1*B*).

Because viral infection can alter the cell surface expression of proteins via secondary effects, we determined whether a specific MCMV gene was responsible for B7-1 down-modulation. DC2 were exposed to either UV-inactivated MCMV or supernatant harvested from live MCMV-infected DC2. In both cases, the exclusion of active virus was confirmed by the complete absence of pp89-expressing cells (data not shown). Although up-regulation of PD-L1 was promoted by exposure to both UV-inactivated MCMV and MCMV-infected DC2 supernatant, the loss of B7-1 from the cell surface required direct infection with live MCMV (Fig. 1, *C* and *D*). Therefore, the up-regulation of PD-L1 promoted by MCMV does not require live virus and might be attributable to cytokines produced by DC2 in response to MCMV exposure. In contrast, active virus-mediated mechanisms are responsible for down-modulation of B7-1.

MCMV m138 is responsible for down-modulation of B7-1

To determine the identity of the MCMV gene responsible for modulation of B7-1, we used six MCMV deletion mutants (Δ*m01–22*MCMV, Δ*m32–36*MCMV, Δ*m37–43*MCMV, Δ*m128-133*MCMV, Δ*m128–139*MCMV, and Δ*m01–17* + *m144–158* + *m159–170*MCMV) that target regions that are nonessential for viral replication in vitro (4). In total, a combined 73 individual MCMV genes were examined for their ability to manipulate B7-1 expression (data not shown). Using MCMV deletion mutants spanning progressively smaller genomic regions (Δ*m134–136*MCMV, Δ*m137–139*MCMV, Δ*m137*MCMV, Δ*m138*MCMV, Δ*m139*MCMV) and by overexpression of the individual genes (data not shown), the open reading frame responsible for B7-1 modulation was identified as *m138* or *fcr-1*, a previously characterized MCMV-encoded FcR (33). Introduction of the full-length *m138* gene into DC2, in the absence of any other MCMV gene, caused the down-modulation of B7-1 from the cell surface, but not that of B7-2 (Fig. 2*A*). Expression of *m138* promoted loss of B7-1 from the cell surface in all cell lines examined. To demonstrate that m138 specifically down-regulated B7-1 during MCMV infection, a Δ*m138* MCMV deletion mutant virus was generated. Immunoblotting with m138 antiserum confirmed the absence of the m138 protein in Δ*m138* MCMV-infected cell lysates (Fig. 2*B*). Infection of DC2 with Δ*m138* MCMV at MOI = 10 generated an equivalent number of pp89-expressing cells, as did wild-type MCMV (data not shown). In contrast to wild-type

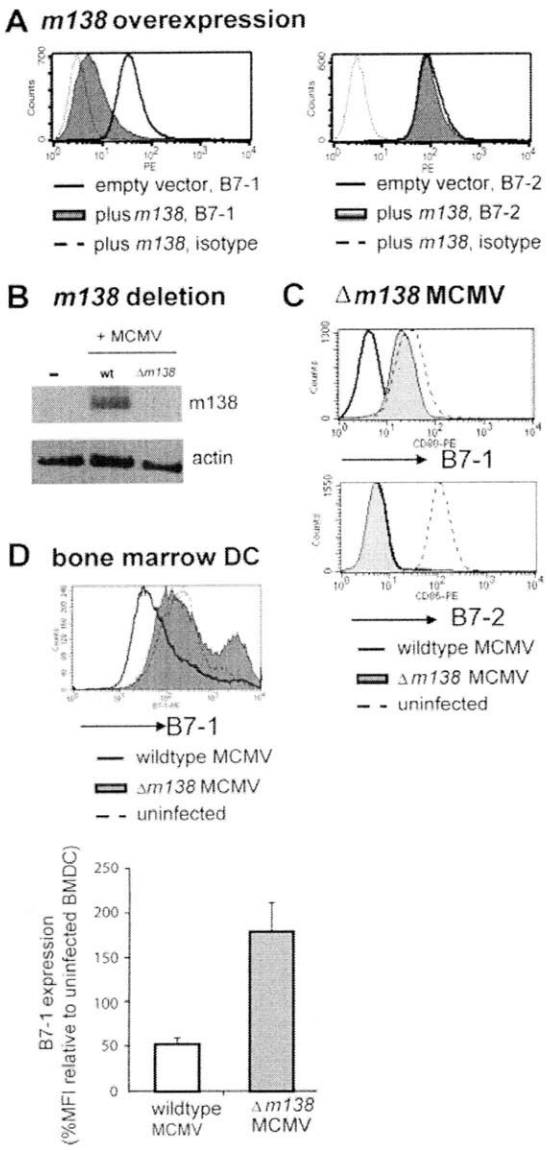

FIGURE 2. MCMV *m138* is responsible for down-modulation of B7-1. *A*, DC2 were transduced with empty vector-pMIG retrovirus or pMIG retrovirus-expressing *m138* and stained with anti-B7-1, anti-B7-2, or an isotype control (IgG2, κ) Ab. The histograms are gated for GFP^+ cells representing cells transduced with the pMIG retrovirus. The data are representative of five independent experiments. *B*, 3T3 fibroblasts were infected with wild-type MCMV (MOI = 1), *Δm138* MCMV (MOI = 1), or left uninfected. A total of 10 μg of 1% SDS lysates was examined by immunoblotting for m138 or β-actin protein using anti-m138 or β-actin antiserum. *C*, DC2 were infected with wild-type MCMV (MOI = 10) or *Δm138* MCMV (MOI = 10) or left uninfected. Sixteen hours postinfection, B7-1 or B7-2 cell surface expression was examined by flow cytometry. The histograms are gated on $pp89^+$, MCMV-infected DC2. The data are representative of three independent experiments. *D*, Primary BMDC (day 4) were infected with wild-type MCMV (MOI = 10) or *Δm138* MCMV (MOI = 10) or left uninfected and examined 16 h postinfection. The histogram is gated on $CD11c^+$ cells (for uninfected cells) or $pp89^+$, MCMV-infected $CD11c^+$ cells (for wild-type and *Δm138* MCMV-infected cells). The graph summarizes the percentage of mean fluorescence intensity (MFI) of B7-1 expression relative to uninfected BMDC (mean ± SEM). The data are representative of three individual experiments.

virus, *Δm138* MCMV was incapable of down-regulating B7-1 from the cell surface, whereas B7-2 expression was abrogated similar to infection with wild-type virus (Fig. 2*C*).

To examine the impact of m138 on the expression of B7-1 in primary DC, BMDC were infected with wild-type MCMV (MOI = 10) or *Δm138* MCMV (MOI = 10) (Fig. 2*D*). MCMV infection of BMDC at day 4 did not alter the number of $CD11c^+$ cells generated, and equivalent levels of infection, as assessed by staining for pp89, were observed with both viruses (data not shown). Infection with wild-type MCMV caused down-regulation of B7-1 in $CD11c^+$, $pp89^+$ cells to an extent similar to that observed for the cell lines examined. Infection with *Δm138* MCMV did not attenuate B7-1 expression, confirming that *m138* is the MCMV gene responsible for B7-1 modulation. *Δm138* MCMV promoted the generation of a $B7\text{-}1^{high}$ population, as the BMDC were activated in response to virus exposure. Therefore, *m138* was identified as the MCMV gene that specifically and independently interferes with the cell surface expression of B7-1 and does so in primary BMDC.

MCMV m138 impairs the ability of DC to activate T cells

The costimulatory signal provided by B7-1 engagement of CD28 is required for optimal T cell responses (34). Therefore, the impact of *m138* expression on the ability of DC to stimulate T cell responses was examined. To do so, an assay was designed in which *m138* could be examined in the absence of the numerous immune evasion genes present in the MCMV genome. This excluded the direct infection of DC with virus. Instead, *m138* was introduced into the DC line DC2.4 ($H\text{-}2^b$) using the pMIG retrovirus. Stable cell lines expressing either empty vector or *m138* were pulsed with OVA-coated beads, and their ability to promote stimulation of OVA-specific B3Z $CD8^+$ T cells was examined. This is an in vitro assay of cross-presentation and was determined to be dose dependent, Ag specific, and proteasome dependent (data not shown). Cells loaded with a high dose of the OVA-derived class I peptide, SIINFEKL, served as positive controls for B3Z T cell activation. The expression of *m138* by DC2.4 did not alter the $H\text{-}2K^b$ levels at the cell surface (Fig. 3*A*), the phagocytosis of OVA beads (Fig. 3*B*), or the loading of $H\text{-}2K^b$ with the SIINFEKL peptide, as determined by staining with the anti-$H\text{-}2K^b$-SIINFEKL Ab 25D1.16 (Fig. 3*C*). In the presence of *m138*, the response to SIINFEKL-loaded DC2.4 was not altered due to the strong signal provided by high dose of peptide that overcomes any requirement for B7-1-mediated costimulation. In contrast, *m138* significantly impaired the ability of DC2.4 to promote the activation of B3Z T cells in response to OVA beads (Fig. 3*D*). This response was greater than the suppression observed when the assay was performed in the presence of anti-B7-1 blocking Ab. In this case, B3Z T cell activation was 62 ± 3% (mean ± SEM) of activation observed in the absence of Ab. Therefore, the expression of *m138* and the consequent loss of B7-1 from the cell surface impact the ability of DC to promote optimal T cell activation.

Characterization of MCMV m138 protein

m138 encodes a 569-aa type I glycoprotein (2). To investigate the expression kinetics of m138 protein during MCMV infection, DC2 were infected with wild-type MCMV (MOI = 10) and harvested at various time points. m138, detected by immunoblotting as an 80-kDa polypeptide, was observed as early as 2 h postinfection and persisted throughout the infectious cycle (Fig. 4*A*). To characterize the biosynthesis of m138, an N-terminal HA-tagged m138 protein was generated for pulse-chase analysis of transiently transfected cells. HA-m138 was capable of B7-1 down-modulation similar to untagged and C-terminal HA-tagged m138 protein (data not shown). m138 was immunoprecipitated from radiolabeled CHO lysates and digested with Endo H to determine the maturation of its associated glycans. The m138 protein was expressed as a 75- to

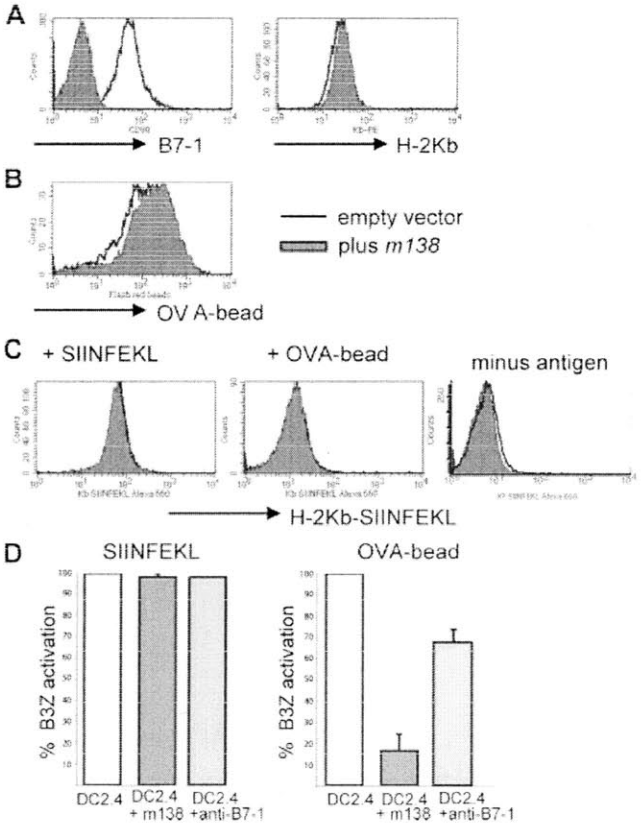

FIGURE 3. MCMV *m138* impairs the ability of DC to activate T cells. DC2.4 transduced with empty vector pMIG (DC2.4) or pMIG-*m138* (DC2.4 + m138) were examined for the following: *A*, cell surface levels of B7-1 or H-2K^b; *B*, uptake of OVA-fluorescent beads; or *C*, cell surface levels of H-2K^b-SIINFEKL in response to loading with 1 μM SIINFEKL, pulsing with OVA beads, or in the absence of Ag. *D*, B3Z activation by Ag-expressing DC2.4 was assessed upon expression of *m138* or in the presence of an anti-B7-1 Ab. Activation was assessed using a chromogenic assay for *lacZ* expression. The data are presented as the percentage of B3Z activation observed in response to Ag presented by DC2.4 transduced with empty vector (mean ± SEM). The graphs summarize four independent experiments.

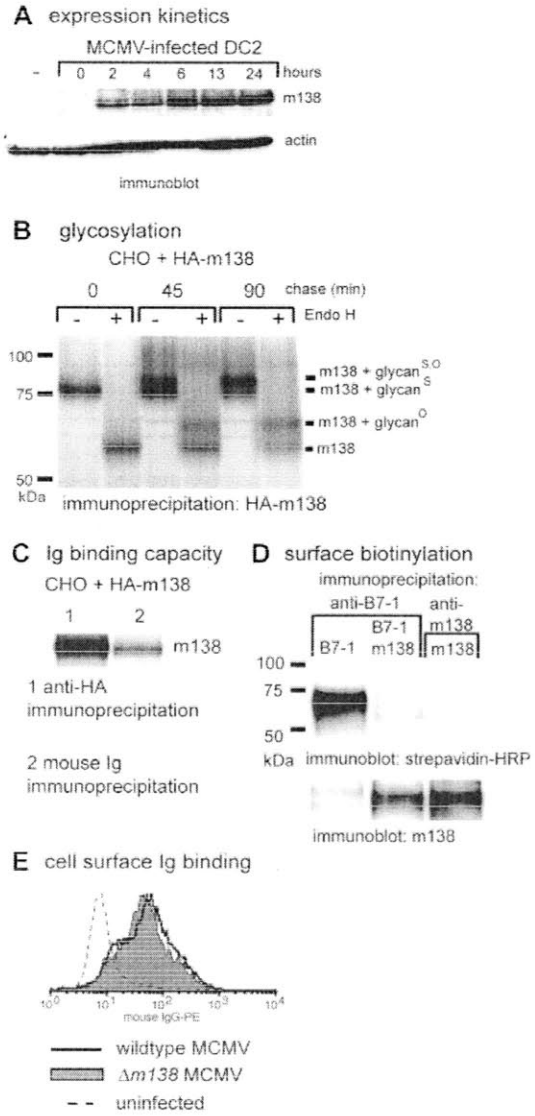

FIGURE 4. Characterization of the MCMV m138 protein. *A*, DC2 were infected with MCMV (MOI = 10), and the expression of m138 in 60 μg of 1% SDS lysates was examined by immunoblotting with anti-m138 antiserum. Detection of β-actin served as a loading control. *B*, CHO-expressing HA-m138 were radiolabeled for 15 min and chased for 45 and 90 min. m138 was recovered from 1% Nonidet P-40 lysates by immunoprecipitation (anti-HA) and digested with Endo H, where indicated. m138-associated glycans are designated Endo H sensitive (S) or *O* linked (O). *C*, CHO-expressing HA-m138 were radiolabeled for 15 min and subject to 1% Nonidet P-40 lysis. m138 was recovered by anti-HA immunoprecipitation or using 10 μg of mouse Ig. *D*, CHO-expressing B7-1-GFP, B7-1-GFP, plus HA-m138 or HA-m138 were surface biotinylated for 30 min. B7-1 and m138 were recovered from 1% Nonidet P-40 lysates by immunoprecipitation with anti-GFP and anti-HA Abs, respectively. Biotinylated proteins were detected by blotting with streptavidin-HRP. The membrane was stripped and reblotted using anti-m138 antiserum. *E*, DC2 cells were not infected or infected with wild-type MCMV (MOI = 10) or Δ*m138* MCMV (MOI = 10) and incubated with mouse Ig. Binding of Ig at the cell surface was detected by anti-mouse Ig Ab. The histograms are gated on pp89$^+$ cells. The data are representative of two independent experiments.

80-kDa polypeptide that matured to a slower migrating polypeptide of ~85 kDa (Fig. 4*B*). The maturation pattern was consistent with m138 possessing *N*-linked glycans that remained Endo H sensitive. Even following up to 4 h of chase, m138 remained Endo H sensitive (data not shown). The increase in m.w., together with the observed heterogeneity, is consistent with *O*-linked glycosylation, predicted to occur in the proline-glutamate-serine-threonine domain of m138.

m138 was previously identified in a screen for MCMV proteins that bind Ig (33). We also examined this function for m138. HA-m138 was recovered from radiolabeled CHO lysates either by anti-HA or mouse Ig immunoprecipitation. Consistent with previous findings, we also observed m138 binding to mouse Ig (Fig. 4*C*). Given this, we examined the putative FcR function of m138, by assessing expression of m138 at the cell surface. In the absence of an anti-m138 Ab for flow cytometry, we investigated this by cell surface biotinylation of transiently transfected CHO cells expressing *m138* alone, or cells expressing *B7-1* or *B7-1* plus *m138* (serving as positive and negative controls for cell surface access). The m138 or B7-1 proteins were recovered by immunoprecipitation, and the presence of the biotin tag, acquired only upon cell surface display, was detected by streptavidin blotting. Surface biotinylation was equivalent in all cases, as observed by immunoblotting of total unfractionated lysate (data not shown). As expected, in the absence of m138, B7-1 readily accessed the cell surface, as inferred by the detection of biotinylated B7-1. This was not the case in the presence of m138, consistent with the flow cytometry data. m138 did not gain access to the cell surface at detectable levels

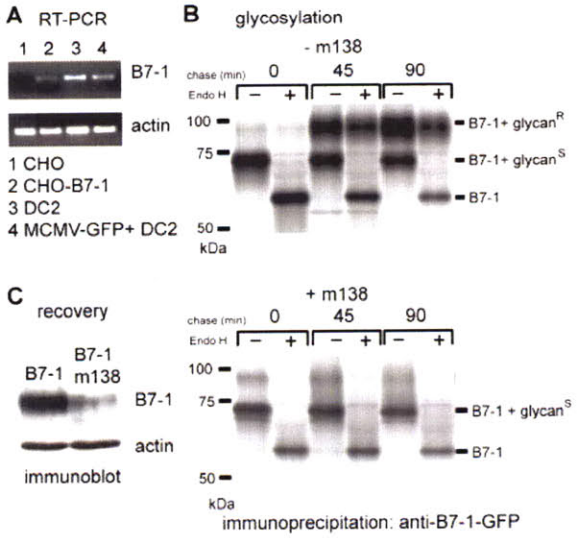

FIGURE 5. The fate of B7-1 in the presence of MCMV m138. *A*, RT-PCR analysis of *B7-1* or *β-actin* transcription in CHO, CHO-B7-1, DC2, and MCMV-infected DC2. *B*, CHO-expressing B7-1-GFP in the presence or absence of m138 were radiolabeled for 15 min and chased for 45 and 90 min. B7-1-GFP was recovered from 1% Nonidet P-40 lysates by immunoprecipitation (anti-GFP) and digested with Endo H, where indicated. The B7-1-associated glycans are designated Endo H sensitive (S) or Endo H resistant (R). *C*, CHO-B7-1 or CHO-B7-1-m138 were subject to 1% SDS lysis, and 10 μg of lysate was examined for the expression of B7-1 or β-actin by immunoblotting.

(Fig. 4*D*). Its expression and recovery were verified by immunoblotting with anti-m138 antiserum. Finally, we assessed the impact of m138 expression upon the binding of Ig at the cell surface of MCMV-infected cells. The capacity of MCMV-infected cells to bind cell surface Ig was not impaired upon infection with Δ*m138* MCMV (Fig. 4*E*).

Fate of B7-1 in the presence of MCMV m138

The fate of B7-1 upon MCMV infection, and specifically the contribution of *m138* to the behavior of B7-1, was investigated. First, we examined whether the failure to detect B7-1 at the cell surface was due to MCMV-mediated inhibition of *B7-1* transcription. DC2 were infected with MCMV-GFP, and GFP-positive cells were isolated by flow cytometry. RT-PCR of RNA extracted from CHO, CHO-B7-1, uninfected DC2, or MCMV-infected DC2 showed the presence of a *B7-1*-specific product amplified from CHO-B7-1, DC2, and MCMV-infected DC2 (Fig. 5*A*). Therefore, MCMV infection does not shut off *B7-1* gene transcription.

To assess where in the course of its biosynthetic maturation m138 targets B7-1, pulse-chase analysis, in conjunction with Endo H digestion, was performed. GFP-tagged B7-1 was used to facilitate immunoprecipitation of B7-1 with anti-GFP serum. The GFP tag did not interfere with m138 down-modulation of B7-1 expression (data not shown). CHO cells were used, rather than DC2, given that the level of B7-1 expression by DC2 was insufficient for the methodology undertaken. Analysis was performed using transiently transfected cells. In the absence of m138, B7-1 acquired Endo H-resistant complex oligosaccharides as the protein matured (Fig. 5*B*, *top panel*). A shift in molecular mass of ~24 kDa was observed, consistent with B7-1 containing eight potential *N*-linked glycans. In contrast, in the presence of m138, B7-1 glycan maturation was not observed (Fig. 5*B*, *bottom panel*). This suggests that m138 targets B7-1 early in the secretory pathway, before complex oligosaccharide acquisition that occurs in the *trans*-Golgi.

The ultimate fate of the B7-1 protein in the presence of m138 was examined by generating a CHO stable cell line that expressed

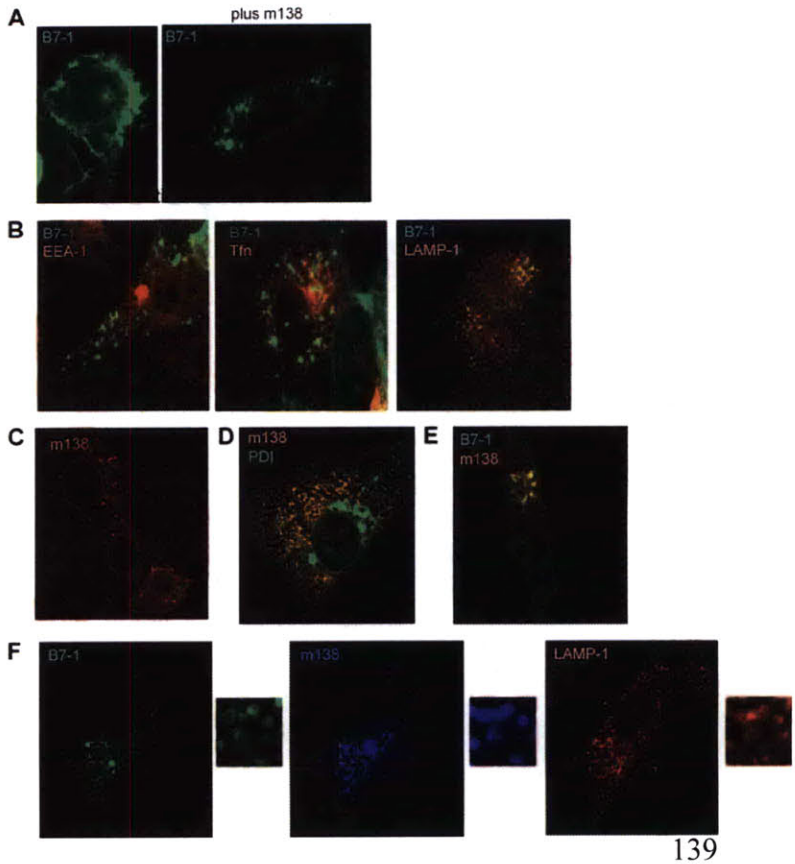

FIGURE 6. MCMV m138 promotes mislocalization of B7-1 to LAMP-1$^+$ compartments. Confocal microscopy analysis of CHO expressing: *A*, B7-1-GFP, in the presence or absence of m138; *B*, B7-1-GFP and HA-m138, stained with anti-EEA-1, LAMP-1 Abs, or pulsed with Tfn-Alexa 594 for 30 min; *C*, HA-m138, stained with anti-HA Ab; *D*, HA-m138, stained with anti-HA and anti-PDI Ab; *E*, B7-1 and HA-m138, stained with anti-HA Ab; *F*, B7-1-GFP and HA-m138, stained with anti-HA and LAMP-1 Ab.

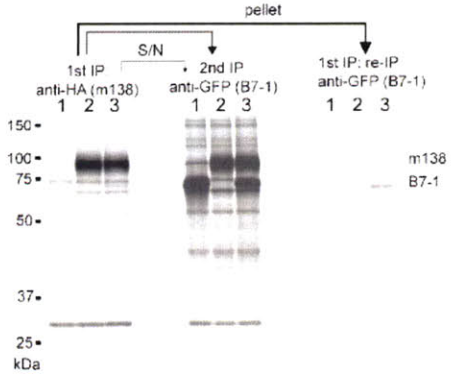

FIGURE 7. m138 and B7-1 interact. CHO expressing B7-1-GFP (1), HA-m138 (2), or B7-1-GFP plus HA-m138 (3) were radiolabeled for 60 min. HA-m138 was immunoprecipitated (IP) from 1% digitonin lysates using anti-HA Ab. Both the recovered immunoprecipitate (pellet) and the supernatant (S/N) were subjected to B7-1 immunoprecipitation (re-IP) using anti-GFP Ab.

both B7-1 and m138. Immunoblotting of cell lysates for B7-1 expression showed significantly reduced detection of B7-1 in the presence of m138 (Fig. 5*C*).

MCMV m138 promotes mislocalization of B7-1 to LAMP-1$^+$ compartments

Confocal microscopy analysis was performed to examine the cellular localization of m138, and B7-1 in the presence of m138. In the absence of m138, B7-1 is localized at the cell surface, as expected. In contrast, m138 promoted B7-1 mislocalization to intracellular vesicles (Fig. 6*A*). To identify the specific cellular compartment to which B7-1 was mislocalized, costaining with markers of the endosomal or lysosomal pathway was performed. The m138-mediated accumulation of B7-1 occurred in organelles that were EEA-1 negative (Fig. 6*B*, *left panel*). In addition, the compartments lacked fluorescently labeled Tfn that was added to intact cells to allow visualization of TfnR-positive early endosomes (Fig. 6*B*, *middle panel*). Therefore, B7-1 is not mislocalized in early, recycling endosomes. In contrast, vesicles containing B7-1 costained with LAMP-1 (Fig. 6*B*, *right panel*).

The cellular localization of m138 was also examined by confocal microscopy. Analysis of the distribution of m138 by immunofluorescence showed its localization in large punctate vesicles (Fig. 6*C*), similar to the images presented by Thale et al. (33). m138 was detected in intracellular compartments together with markers of the ER: PDI (Fig. 6*D*) and calnexin (data not shown), in addition to the lysosomal marker LAMP-1 (Fig. 6*F*). Given the similar localization pattern of m138, and B7-1 in the presence of m138, we examined a possible colocalization of the two proteins by immunofluorescence microscopy. Colocalization of m138 and B7-1 was indeed observed (Fig. 6*E*). Colocalization of m138, B7-1, and LAMP-1 was also detected (Fig. 6*F*).

m138 and B7-1 interact

A potential interaction between the m138 and B7-1 proteins was further investigated. Radiolabeled CHO cells transiently transfected with either *B7-1*, *m138*, or *B7-1* plus *m138* were lysed in 1% digitonin. The mild lysis conditions should favor the preservation of protein coassociation. The m138 protein was recovered by immunoprecipitation (Fig. 7, *left panel*). The supernatant of the m138 immunoprecipitate (proteins not associated with m138), in addition to the pelleted material (m138 and its associated proteins), was subjected to anti-GFP immunoprecipitation to recover B7-1. In the

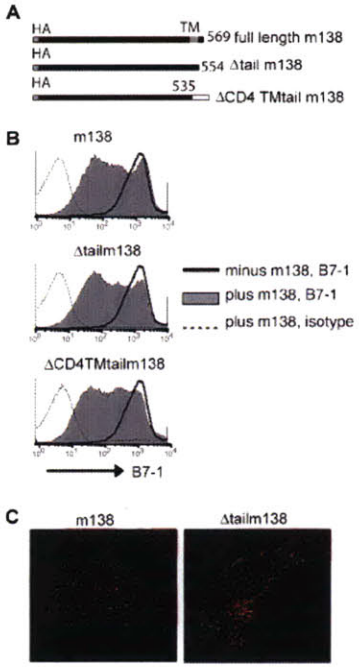

FIGURE 8. The cytoplasmic tail and transmembrane (TM) domain of m138 are not required for modulation of B7-1 expression. *A*, Diagram of m138 truncation mutants. *B*, CHO-B7-1 were cotransfected with full-length *m138*, *Δtailm138*, or *ΔCD4TMtailm138* and GFP. Forty-eight hours following transfection, the cells were stained with anti-B7-1 or an isotype control Ab, and assessed by flow cytometry. The histograms display GFP$^+$ cotransfected cells and represent three independent experiments. *C*, Confocal microscopy analysis of CHO expressing B7-1-GFP, in the presence or absence of full-length m138 or Δtailm138.

supernatant, B7-1 was recovered, showing the protein to be present upon expression in the absence of m138 (Fig. 7, *middle panel*). In the presence of m138, some B7-1 is recovered from the supernatant, demonstrating the presence of a fraction of B7-1 that does not associate with m138. m138 is also detected in the B7-1 immunoprecipitation due to its capacity to bind Ig (in this case, the anti-GFP Ab used to immunoprecipitate B7-1). For the pelleted material, we recovered a protein of the same m.w. as immature B7-1, but only when m138 was present (Fig. 7, *right panel*). The data therefore indicate that the mechanism of m138-mediated down-modulation of B7-1 occurs via an interaction between the m138 and B7-1 proteins.

The cytoplasmic tail and transmembrane domain of MCMV m138 are not required for modulation of B7-1 expression

Many proteins involved in lysosomal trafficking pathways possess consensus-sorting motifs in their cytoplasmic tails (35). Inspection of the amino acid composition of m138 did not reveal any obvious sorting motifs. Therefore, to examine the role of the cytoplasmic tail (aa 555–569) and/or the transmembrane domain (aa 534–554) of m138, we generated N-terminal HA-tagged m138 truncation mutant proteins (Fig. 8*A*): 1) Δtailm138, lacking the 15 most C-terminal amino acids, and 2) ΔCD4TMtailm138, in which the m138 transmembrane region and tail were replaced with human CD4 transmembrane and tail. Expression of the proteins was confirmed by immunoblotting for HA (data not shown). Δtailm138 or ΔCD4TMtailm138 (Fig. 8*B*) promoted the loss of B7-1 from the cell surface of CHO-B7-1 cells, equivalent to full-length m138. The down-modulation was not as extensive as that observed for DC2, presumably due to the high levels of B7-1 protein expressed

by CHO-B7-1. Regardless, the mutant m138 proteins behaved similarly to full-length m138. To further eliminate a role for the cytoplasmic tail in this response, we examined the mislocalization of B7-1 in the presence of Δtailm138 by confocal microscopy. The cytoplasmic tail of m138 was not required to mislocalize B7-1 to intracellular punctate compartments (Fig. 8*C*). Therefore, neither the cytoplasmic tail or the transmembrane domain of m138 was required for modulation of B7-1 expression.

Discussion

CMV actively suppresses the expression of costimulatory molecules in DC. This is an effective immune evasion strategy, given that infection correlates with an inability of CMV-infected DC to promote T cell activation (36–39). At the cellular level, CMV promotes the loss of cell surface expression of CD40, CD54, CD83, B7-1, and B7-2 in various DC subsets (25, 36–40). Consistent with these studies, we also observed the abrogation of both B7-1 and B7-2 expression upon MCMV infection. In all cases of CMV-mediated immune suppression of DC function, the specific viral gene(s) responsible has not been identified. A possible exception is MCMV *m147.5*, which encodes a 23-kDa protein referred to as mod B7-2. Mod B7-2 is responsible for B7-2 loss from the cell surface of RAW 264.7 macrophages (25). Its role in DC, its mechanism of action, or the fate of B7-2 in its presence is unknown. In this study, we describe the specific interference of B7-1 cell surface expression by the MCMV protein m138 in both cell lines and primary DC. To our knowledge, this is the first demonstration of the impact of a viral immune evasion gene in primary DC.

Although MCMV modulates both B7-1 and B7-2 from the cell surface, *m138* and *m147.5* specifically interfere only with B7-1 or B7-2, respectively, and do so independently of each other. Given that B7-1 and B7-2 both bind the same T cell coreceptors, CD28 and CTLA4, this specificity is, at first glance, unexpected. Both B7-1 and B7-2 are type I transmembrane glycoproteins that possess a V-type and C-type Ig superfamily domain (41). Despite their functional overlap, however, they are only 25% identical in amino acid sequence, and consequently possess rather divergent structures (42–45). Although B7-1 forms a homodimer at the cell surface (42, 43), B7-2 does so only upon receptor-induced clustering (45). In addition, B7-2 contains a longer cytoplasmic tail. Thus, the structural features that distinguish B7-1 and B7-2 most likely explain the presence of individual and specific modulators in the MCMV genome.

The MCMV gene responsible for B7-1 down-modulation was identified as *m138*. *m138* was previously reported as the *fcr-1* MCMV gene, encoding a putative FcR. It was postulated that FcR-1 (m138) expression at the MCMV-infected cell surface would prevent the recognition of MCMV-infected cells by circulating anti-MCMV Ab (33). This role was questioned, however, when the attenuated growth observed in vivo for Δ*m138* MCMV was not restored in B cell-deficient mice (46). Hence, the absence of Ab did not alter the course of infection with Δ*m138* MCMV. This prompted a re-evaluation of a role for m138 as an FcR that has remained elusive until now. Our experiments are also inconsistent with FcR function, given that m138 was not definitively shown to be expressed at the cell surface and its absence did not promote loss of Ig binding at the infected cell surface. Therefore, despite its putative role as an FcR, the clear consequences of m138 expression for the cell surface display of B7-1 suggest an attractive alternative for the major role of m138 in the immune evasion activities in MCMV infection. There is emerging evidence to support the notion that a single viral protein can exert several distinct immune evasion functions (47, 48), potentially in a cell type-specific manner. Of interest, while this manuscript was in preparation, a role for m138 in the down-modulation of NKG2D ligands MULT-1 and H60 was described (49). Consequently, the complex immune evasion strategies used by MCMV may explain the divergent functions of m138.

B7-1 is a critical costimulatory signal required for T cell immunity. B7-1-deficient APC display a significant reduction in their ability to promote T cell activation (34). Indeed, the loss of B7-1 at the cell surface, upon m138 expression, inhibited the ability of DC2.4 to promote optimal $CD8^+$ T cell responses in vitro. We would therefore expect m138, in concert with other MCMV-encoded modulators of costimulatory and MHC class I molecule expression, to act together to effectively suppress antiviral $CD8^+$ T cell immunity in vivo. Unexpectedly, attenuation of Δ*m138*MCMV growth in vivo was not restored upon T cell (or NK cell) depletion (46). A direct examination of m138 function in vivo is complicated by its potential role in cell to cell spreading of the virus similar to that of its functional FcR homologues encoded by HSV (50, 51) and pseudorabies virus (52). m138 may also participate in other B7-1-mediated functions. In addition to a role in T cell responses, B7-1 can evoke, independently of CD28 engagement, signaling events in the APC itself (53, 54). For example, triggering of B7-1 blocks B cell proliferation and Ab production (55). Other examples include the induction of B7-1 in kidney podocytes, resulting in an increase in glomerular filtration and transient proteinuria (56) and the induction of B7-1 expression on keratinocytes by inflammatory stimuli (57). Therefore, the function of costimulatory molecules extends beyond their traditional role in T cell signaling and may explain the broader expression pattern of these molecules on cell types other than APC (reviewed in Ref. 19). m138 may consequently interfere with B7-1 function both in the context of an immune response and in potentially undiscovered roles that the virus must manipulate for successful propagation in vivo.

Host proteins suffer different fates in the presence of viral immune evasion proteins. Expression can be suppressed at the level of transcription, or the protein itself can be targeted via retention, inhibition of function, or enhanced degradation. In the case of B7-1, MCMV m138 does not shut off its transcription, but hijacks newly synthesized protein early during biosynthesis. This may occur in the ER given that m138 is localized both in the ER and in a lysosomal compartment. Unlike KSHV K5, which targets B7-2 already present at the cell surface (20), m138 recruits B7-1 early in the secretory pathway. The mechanism most likely requires an association between m138 and B7-1, and presumably involves the recruitment of other proteins. The involvement of accessory proteins such as the adaptor protein complexes or mannose 6-phosphate receptor remains to be investigated. m138 redirects B7-1 to a $LAMP\text{-}1^+$ compartment. Of interest is that neither the m138 or B7-1 proteins acquire complex glycan modifications, despite their lysosomal localization. This is also the case for TLR9, which is recruited from the ER to an endosomal compartment without concomitant conversion of TLR9-associated glycans to Endo H resistance (58).

Mislocalization of host proteins to lysosomes is also promoted by other viral proteins, including MCMV m6/gp48 (14), HIV Nef (59), and HHV-7 U21 (60). For both m6/gp48 (14) and Nef (61, 62), lysosomal mislocalization is mediated by consensus-sorting signals in their cytoplasmic domains. These motifs recruit adaptor protein complexes that form part of the endocytic sorting machinery. In contrast, the mechanism of m138 function did not require the presence of its predicted transmembrane or cytoplasmic domains. Therefore, m138-mediated B7-1 mislocalization is reminiscent of the

action of HHV-7 U21, in which its lumenal domain is sufficient for targeting of MHC class I to a lysosomal compartment (63).

In summary, we have identified the first viral protein that targets and disables the function of B7-1, a critical costimulatory molecule. MCMV m138, although possessing Ig-binding capacity, is the protein responsible for modulation of the cell surface expression of B7-1. Therefore, through the manipulation of B7-1, rather than acting as an FcR, m138 participates in the complex mechanisms of immune evasion activity that is ultimately responsible for the establishment of persistent herpesvirus infection. An understanding of the interference of B7-1 by a viral protein also provides insight into targeting and turning off B7-1 expression in contexts other than viral immunity.

Acknowledgments

We thank Drs. Howard Hang and Rene Maehr for critical reading of the manuscript, and Dr. Brendan Lilley for excellent scientific advice.

Disclosures

The authors have no financial conflict of interest.

References

1. Alcami, A., and U. H. Koszinowski. 2000. Viral mechanisms of immune evasion. *Trends Microbiol.* 8: 410–418.
2. Rawlinson, W. D., H. E. Farrell, and B. G. Barrell. 1996. Analysis of the complete DNA sequence of murine cytomegalovirus. *J. Virol.* 70: 8833–8849.
3. Mocarski, E. S., and C. T. Courcelle. 2001. *Cytomegaloviruses and Their Replication.* Lippincott Williams & Wilkins, Philadelphia.
4. Brune, W., M. Wagner, and M. Messerle. 2005. Manipulating cytomegalovirus genomes by BAC mutagenesis: strategies and applications. In *Cytomegaloviruses: Molecular Biology and Immunology.* M. J. Reddehase, ed. Caister Academic Press, Norwich.
5. Mocarski, E. S., Jr. 2002. Immunomodulation by cytomegaloviruses: manipulative strategies beyond evasion. *Trends Microbiol.* 10: 332–339.
6. Riddell, S. R., K. S. Watanabe, J. M. Goodrich, C. R. Li, M. E. Agha, and P. D. Greenberg. 1992. Restoration of viral immunity in immunodeficient humans by the adoptive transfer of T cell clones. *Science* 257: 238–241.
7. Sacre, K., G. Carcelain, N. Cassoux, A. M. Fillet, D. Costagliola, D. Vittecoq, D. Salmon, Z. Amoura, C. Katlama, and B. Autran. 2005. Repertoire, diversity, and differentiation of specific CD8 T cells are associated with immune protection against human cytomegalovirus disease. *J. Exp. Med.* 201: 1999–2010.
8. Reddehase, M. J., F. Weiland, K. Munch, S. Jonjic, A. Luske, and U. H. Koszinowski. 1985. Interstitial murine cytomegalovirus pneumonia after irradiation: characterization of cells that limit viral replication during established infection of the lungs. *J. Virol.* 55: 264–273.
9. Polic, B., H. Hengel, A. Krmpotic, J. Trgovcich, I. Pavic, P. Luccaronin, S. Jonjic, and U. H. Koszinowski. 1998. Hierarchical and redundant lymphocyte subset control precludes cytomegalovirus replication during latent infection. *J. Exp. Med.* 188: 1047–1054.
10. Jones, T. R., E. J. Wiertz, L. Sun, K. N. Fish, J. A. Nelson, and H. L. Ploegh. 1996. Human cytomegalovirus US3 impairs transport and maturation of major histocompatibility complex class I heavy chains. *Proc. Natl. Acad. Sci. USA* 93: 11327–11333.
11. Ziegler, H., R. Thale, P. Lucin, W. Muranyi, T. Flohr, H. Hengel, H. Farrell, W. Rawlinson, and U. H. Koszinowski. 1997. A mouse cytomegalovirus glycoprotein retains MHC class I complexes in the ERGIC/*cis*-Golgi compartments. *Immunity* 6: 57–66.
12. Wiertz, E. J., T. R. Jones, L. Sun, M. Bogyo, H. J. Geuze, and H. L. Ploegh. 1996. The human cytomegalovirus US11 gene product dislocates MHC class I heavy chains from the endoplasmic reticulum to the cytosol. *Cell* 84: 769–779.
13. Wiertz, E. J., D. Tortorella, M. Bogyo, J. Yu, W. Mothes, T. R. Jones, T. A. Rapoport, and H. L. Ploegh. 1996. Sec61-mediated transfer of a membrane protein from the endoplasmic reticulum to the proteasome for destruction. *Nature* 384: 432–438.
14. Reusch, U., W. Muranyi, P. Lucin, H. G. Burgert, H. Hengel, and U. H. Koszinowski. 1999. A cytomegalovirus glycoprotein re-routes MHC class I complexes to lysosomes for degradation. *EMBO J.* 18: 1081–1091.
15. Hewitt, E. W., S. S. Gupta, and P. J. Lehner. 2001. The human cytomegalovirus gene product US6 inhibits ATP binding by TAP. *EMBO J.* 20: 387–396.
16. Kavanagh, D. G., M. C. Gold, M. Wagner, U. H. Koszinowski, and A. B. Hill. 2001. The multiple immune-evasion genes of murine cytomegalovirus are not redundant: m4 and m152 inhibit antigen presentation in a complementary and cooperative fashion. *J. Exp. Med.* 194: 967–978.
17. Lafferty, K. J., and J. Woolnough. 1977. The origin and mechanism of the allograft reaction. *Immunol. Rev.* 35: 231–262.
18. Bertram, E. M., W. Dawicki, and T. H. Watts. 2004. Role of T cell costimulation in anti-viral immunity. *Semin. Immunol.* 16: 185–196.
19. Greenwald, R. J., G. J. Freeman, and A. H. Sharpe. 2005. The B7 family revisited. *Annu. Rev. Immunol.* 23: 515–548.
20. Coscoy, L., and D. Ganem. 2001. A viral protein that selectively down-regulates ICAM-1 and B7-2 and modulates T cell costimulation. *J. Clin. Invest.* 107: 1599–1606.
21. Sevilla, N., D. B. McGavern, C. Teng, S. Kunz, and M. B. Oldstone. 2004. Viral targeting of hematopoietic progenitors and inhibition of DC maturation as a dual strategy for immune subversion. *J. Clin. Invest.* 113: 737–745.
22. Morrow, G., B. Slobedman, A. L. Cunningham, and A. Abendroth. 2003. Varicella-zoster virus productively infects mature dendritic cells and alters their immune function. *J. Virol.* 77: 4950–4959.
23. Engelmayer, J., M. Larsson, M. Subklewe, A. Chahroudi, W. I. Cox, R. M. Steinman, and N. Bhardwaj. 1999. Vaccinia virus inhibits the maturation of human dendritic cells: a novel mechanism of immune evasion. *J. Immunol.* 163: 6762–6768.
24. Majumder, B., M. L. Janket, E. A. Schafer, K. Schaubert, X. L. Huang, J. Kan-Mitchell, C. R. Rinaldo, Jr., and V. Ayyavoo. 2005. Human immunodeficiency virus type 1 Vpr impairs dendritic cell maturation and T-cell activation: implications for viral immune escape. *J. Virol.* 79: 7990–8003.
25. Loewendorf, A., C. Kruger, E. M. Borst, M. Wagner, U. Just, and M. Messerle. 2004. Identification of a mouse cytomegalovirus gene selectively targeting CD86 expression on antigen-presenting cells. *J. Virol.* 78: 13062–13071.
26. Bachmann, M. F., M. B. Lutz, G. T. Layton, S. J. Harris, T. Fehr, M. Rescigno, and P. Ricciardi-Castagnoli. 1996. Dendritic cells process exogenous viral proteins and virus-like particles for class I presentation to $CD8^+$ cytotoxic T lymphocytes. *Eur. J. Immunol.* 26: 2595–2600.
27. Mutini, C., S. Falzoni, D. Ferrari, P. Chiozzi, A. Morelli, O. R. Baricordi, G. Collo, P. Ricciardi-Castagnoli, and F. Di Virgilio. 1999. Mouse dendritic cells express the P2X7 purinergic receptor: characterization and possible participation in antigen presentation. *J. Immunol.* 163: 1958–1965.
28. Shen, Z., G. Reznikoff, G. Dranoff, and K. L. Rock. 1997. Cloned dendritic cells can present exogenous antigens on both MHC class I and class II molecules. *J. Immunol.* 158: 2723–2730.
29. Lutarewych, M. A., M. R. Quirk, B. A. Kringstad, W. Li, C. M. Verfaillie, and M. C. Jordan. 1997. Propagation and titration of murine cytomegalovirus in a continuous bone marrow-derived stromal cell line (M2-10B4). *J. Virol. Methods* 68: 193–198.
30. Freedman, A. S., G. Freeman, J. C. Horowitz, J. Daley, and L. M. Nadler. 1987. B7, a B-cell-restricted antigen that identifies preactivated B cells. *J. Immunol.* 139: 3260–3267.
31. Karttunen, J., S. Sanderson, and N. Shastri. 1992. Detection of rare antigen-presenting cells by the lacZ T-cell activation assay suggests an expression cloning strategy for T-cell antigens. *Proc. Natl. Acad. Sci. USA* 89: 6020–6024.
32. Wang, Y. Q., A. Wada, S. Ugai, and M. Tagawa. 2003. Expression of the Mig (CXCL9) gene in murine lung carcinoma cells generated angiogenesis-independent antitumor effects. *Oncol. Rep.* 10: 909–913.
33. Thale, R., P. Lucin, K. Schneider, M. Eggers, and U. H. Koszinowski. 1994. Identification and expression of a murine cytomegalovirus early gene coding for an Fc receptor. *J. Virol.* 68: 7757–7765.
34. Freeman, G. J., F. Borriello, R. J. Hodes, H. Reiser, K. S. Hathcock, G. Laszlo, A. J. McKnight, J. Kim, L. Du, D. B. Lombard, et al. 1993. Uncovering of functional alternative CTLA-4 counter-receptor in B7-deficient mice. *Science* 262: 907–909.
35. Bonifacino, J. S., and L. M. Traub. 2003. Signals for sorting of transmembrane proteins to endosomes and lysosomes. *Annu. Rev. Biochem.* 72: 395–447.
36. Andrews, D. M., C. E. Andoniou, F. Granucci, P. Ricciardi-Castagnoli, and M. A. Degli-Esposti. 2001. Infection of dendritic cells by murine cytomegalovirus induces functional paralysis. *Nat. Immunol.* 2: 1077–1084.
37. Moutaftsi, M., A. M. Mehl, L. K. Borysiewicz, and Z. Tabi. 2002. Human cytomegalovirus inhibits maturation and impairs function of monocyte-derived dendritic cells. *Blood* 99: 2913–2921.
38. Senechal, B., A. M. Boruchov, J. L. Reagan, D. N. Hart, and J. W. Young. 2004. Infection of mature monocyte-derived dendritic cells with human cytomegalovirus inhibits stimulation of T-cell proliferation via the release of soluble CD83. *Blood* 103: 4207–4215.
39. Mathys, S., T. Schroeder, J. Ellwart, U. H. Koszinowski, M. Messerle, and U. Just. 2003. Dendritic cells under influence of mouse cytomegalovirus have a physiologic dual role: to initiate and to restrict T cell activation. *J. Infect. Dis.* 187: 988–999.
40. Beck, K., U. Meyer-Konig, M. Weidmann, C. Nern, and F. T. Hufert. 2003. Human cytomegalovirus impairs dendritic cell function: a novel mechanism of human cytomegalovirus immune escape. *Eur. J. Immunol.* 33: 1528–1538.
41. Henry, J., M. M. Miller, and P. Pontarotti. 1999. Structure and evolution of the extended B7 family. *Immunol. Today* 20: 285–288.
42. Stamper, C. C., Y. Zhang, J. F. Tobin, D. V. Erbe, S. Ikemizu, S. J. Davis, M. L. Stahl, J. Seehra, W. S. Somers, and L. Mosyak. 2001. Crystal structure of the B7-1/CTLA-4 complex that inhibits human immune responses. *Nature* 410: 608–611.
43. Ikemizu, S., R. J. Gilbert, J. A. Fennelly, A. V. Collins, K. Harlos, E. Y. Jones, D. I. Stuart, and S. J. Davis. 2000. Structure and dimerization of a soluble form of B7-1. *Immunity* 12: 51–60.
44. Schwartz, J. C., X. Zhang, A. A. Fedorov, S. G. Nathenson, and S. C. Almo. 2001. Structural basis for co-stimulation by the human CTLA-4/B7-2 complex. *Nature* 410: 604–608.
45. Zhang, X., J. C. Schwartz, S. C. Almo, and S. G. Nathenson. 2003. Crystal structure of the receptor-binding domain of human B7-2: insights into organization and signaling. *Proc. Natl. Acad. Sci. USA* 100: 2586–2591.
46. Crnkovic-Mertens, I., M. Messerle, I. Milotic, U. Szepan, N. Kucic, A. Krmpotic, S. Jonjic, and U. H. Koszinowski. 1998. Virus attenuation after deletion of the

cytomegalovirus Fc receptor gene is not due to antibody control. *J. Virol.* 72: 1377–1382.

47. Krmpotic, A., D. H. Busch, I. Bubic, F. Gebhardt, H. Hengel, M. Hasan, A. A. Scalzo, U. H. Koszinowski, and S. Jonjic. 2002. MCMV glycoprotein gp40 confers virus resistance to CD8$^+$ T cells and NK cells in vivo. *Nat. Immunol.* 3: 529–535.
48. Lodoen, M., K. Ogasawara, J. A. Hamerman, H. Arase, J. P. Houchins, E. S. Mocarski, and L. L. Lanier. 2003. NKG2D-mediated natural killer cell protection against cytomegalovirus is impaired by viral gp40 modulation of retinoic acid early inducible 1 gene molecules. *J. Exp. Med.* 197: 1245–1253.
49. Lenac, T., M. Budt, J. Arapovic, M. Hasan, A. Zimmermann, H. Simic, A. Krmpotic, M. Messerle, Z. Ruzsics, U. H. Koszinowski, et al. 2006. The herpesviral Fc receptor *fcr-1* down-regulates the NKG2D ligands MULT-1 and H60. *J. Exp. Med.* 203: 1843–1850.
50. Dingwell, K. S., C. R. Brunetti, R. L. Hendricks, Q. Tang, M. Tang, A. J. Rainbow, and D. C. Johnson. 1994. Herpes simplex virus glycoproteins E and I facilitate cell-to-cell spread in vivo and across junctions of cultured cells. *J. Virol.* 68: 834–845.
51. Dingwell, K. S., and D. C. Johnson. 1998. The herpes simplex virus gE-gI complex facilitates cell-to-cell spread and binds to components of cell junctions. *J. Virol.* 72: 8933–8942.
52. Card, J. P., M. E. Whealy, A. K. Robbins, and L. W. Enquist. 1992. Pseudorabies virus envelope glycoprotein gI influences both neurotropism and virulence during infection of the rat visual system. *J. Virol.* 66: 3032–3041.
53. Doty, R. T., and E. A. Clark. 1996. Subcellular localization of CD80 receptors is dependent on an intact cytoplasmic tail and is required for CD28-dependent T cell costimulation. *J. Immunol.* 157: 3270–3279.
54. Doty, R. T., and E. A. Clark. 1998. Two regions in the CD80 cytoplasmic tail regulate CD80 redistribution and T cell costimulation. *J. Immunol.* 161: 2700–2707.
55. Suvas, S., V. Singh, S. Sahdev, H. Vohra, and J. N. Agrewala. 2002. Distinct role of CD80 and CD86 in the regulation of the activation of B cell and B cell lymphoma. *J. Biol. Chem.* 277: 7766–7775.
56. Reiser, J., G. von Gersdorff, M. Loos, J. Oh, K. Asanuma, L. Giardino, M. P. Rastaldi, N. Calvaresi, H. Watanabe, K. Schwarz, et al. 2004. Induction of B7-1 in podocytes is associated with nephrotic syndrome. *J. Clin. Invest.* 113: 1390–1397.
57. Wakem, P., R. P. Burns, Jr., F. Ramirez, D. Zlotnick, B. Ferbel, C. G. Haidaris, and A. A. Gaspari. 2000. Allergens and irritants transcriptionally up-regulate CD80 gene expression in human keratinocytes. *J. Invest. Dermatol.* 114: 1085–1092.
58. Latz, E., A. Schoenemeyer, A. Visintin, K. A. Fitzgerald, B. G. Monks, C. F. Knetter, E. Lien, N. J. Nilsen, T. Espevik, and D. T. Golenbock. 2004. TLR9 signals after translocating from the ER to CpG DNA in the lysosome. *Nat. Immunol.* 5: 190–198.
59. Schwartz, O., V. Marechal, S. Le Gall, F. Lemonnier, and J. M. Heard. 1996. Endocytosis of major histocompatibility complex class I molecules is induced by the HIV-1 Nef protein. *Nat. Med.* 2: 338–342.
60. Hudson, A. W., P. M. Howley, and H. L. Ploegh. 2001. A human herpesvirus 7 glycoprotein, U21, diverts major histocompatibility complex class I molecules to lysosomes. *J. Virol.* 75: 12347–12358.
61. Piguet, V., F. Gu, M. Foti, N. Demaurex, J. Gruenberg, J. L. Carpentier, and D. Trono. 1999. Nef-induced CD4 degradation: a diacidic-based motif in Nef functions as a lysosomal targeting signal through the binding of β-COP in endosomes. *Cell* 97: 63–73.
62. Mangasarian, A., V. Piguet, J. K. Wang, Y. L. Chen, and D. Trono. 1999. Nef-induced CD4 and major histocompatibility complex class I (MHC-I) down-regulation are governed by distinct determinants: N-terminal α helix and proline repeat of Nef selectively regulate MHC-I trafficking. *J. Virol.* 73: 1964–1973.
63. Hudson, A. W., D. Blom, P. M. Howley, and H. L. Ploegh. 2003. The ER-lumenal domain of the HHV-7 immunoevasin U21 directs class I MHC molecules to lysosomes. *Traffic* 4: 824–837.

XBP-1-Deficient Plasmablasts Show Normal Protein Folding but Altered Glycosylation and Lipid Synthesis[1]

Annette M. McGehee,* Stephanie K. Dougan,* Elizabeth J. Klemm,* Guanghou Shui,† Boyoun Park,* You-Me Kim,* Nicki Watson,* Markus R. Wenk,†‡ Hidde L. Ploegh,[2]* and Chih-Chi Andrew Hu[2]*

The accumulation of misfolded secreted IgM in the endoplasmic reticulum (ER) of X-box binding protein 1 (XBP-1)-deficient B cells has been held responsible for the inability of such cells to yield plasma cells, through the failure to mount a proper unfolded protein response. LPS-stimulated B cells incapable of secreting IgM still activate the XBP-1 axis normally, as follows: XBP-1 is turned on by cues that trigger differentiation and not in response to accumulation of unfolded IgM, but the impact of XBP-1 deficiency on glycoprotein folding and assembly has not been explored. The lack of XBP-1 compromised neither the formation of functional hen egg lysozyme-specific IgM nor the secretion of free κ-chains. Although XBP-1 deficiency affects the synthesis of some ER chaperones, including protein disulfide isomerase, their steady state levels do not drop below the threshold required for proper assembly and maturation of the Igα/Igβ heterodimer and MHC molecules. Intracellular transport and surface display of integral membrane proteins are unaffected by XBP-1 deficiency. Given the fact that we failed to observe any defects in folding of a variety of glycoproteins, we looked for other means to explain the requirement for XBP-1 in plasma cell development. We observed significantly reduced levels of phosphatidylcholine, sphingomyelin, and phosphatidylinositol in total membranes of XBP-1-deficient B cells, and reduced ER content. Terminal *N*-linked glycosylation of IgM and class I MHC was altered in these cells. XBP-1 hence has important roles beyond folding proteins in the ER. *The Journal of Immunology*, **2009, 183: 3690–3699.**

Plasma cells produce large amounts of secreted Igs, which is their primary task in the adaptive immune response. In contrast, naive B cells express the membrane form of IgM (mIgM),[3] but do not secrete IgM until they are activated. B cell differentiation to plasma cells begins when a B cell is activated by an encounter with its cognate Ag or in conjunction with ligands for TLRs. This leads to the expansion of the B cell's endoplasmic reticulum (ER) in preparation for the increase in synthesis of the secreted form of IgM (sIgM) (1). Eventually, such B cells fully differentiate into Ig-secreting plasma cells (2), a process proposed to depend critically on the unfolded protein response (UPR) (3, 4).

X-box binding protein 1 (XBP-1) is a transcription factor that drives this UPR. Its expression is ultimately controlled by the transmembrane kinase/endoribonuclease inositol-requiring enzyme 1 (IRE-1) (3, 5), the activation of which occurs in response to pharmacologically induced ER stress. IRE-1 modulates XBP-1 activity by catalyzing an unusual reaction that generates spliced XBP-1 mRNA, encoding a 54-kDa "spliced" XBP-1 protein (XBP-1s) with transcriptional activity. XBP-1s translocates to the nucleus and regulates the synthesis of chaperones and other proteins believed to contribute to the proper function of the secretory pathway (4, 6, 7).

XBP-1 plays an important role in B cell differentiation, as follows: when XBP-1 is absent from B cells, the number of plasma cells is dramatically reduced (8). It has been argued that the action of XBP-1 in B cell differentiation ensures expression of proteins equipped to deal with an excess of unfolded sIgM; this excess is thought to be an unavoidable byproduct of the increased synthesis of sIgM (3, 4). In this model, the increase in synthesis of sIgM subsequent to B cell activation exceeds the folding capacity of the ER and causes an accumulation of excess unfolded proteins that activate IRE-1, which in turn triggers XBP-1 activation. Activation of XBP-1 by IRE-1 serves to increase the size of the ER and enhances its folding capacity to handle the increased levels of sIgM. This model predicts that, in the absence of XBP-1, differentiating B cells are unable to deal with the increased load of sIgM in the ER, and thus, misfolded sIgM will accumulate in the ER, rather than be secreted. As a correlate, other proteins destined for surface display or secretion may be misfolded, and operation of the secretory pathway in its entirety could be compromised (9). This model would further predict that B cells that do not manufacture

*Whitehead Institute for Biomedical Research, Cambridge, MA 02142; †Department of Biochemistry, Yong Loo Lin School of Medicine, National University of Singapore, Singapore, Singapore; and ‡Department of Biological Sciences, National University of Singapore, Singapore, Singapore

Received for publication March 26, 2009. Accepted for publication July 8, 2009.

The costs of publication of this article were defrayed in part by the payment of page charges. This article must therefore be hereby marked *advertisement* in accordance with 18 U.S.C. Section 1734 solely to indicate this fact.

[1] This work was supported by grants from the National Institutes of Health (to H.L.P.). A.M.M. was supported by a National Science Foundation graduate research fellowship. S.K.D. is supported by a Cancer Research Institute fellowship. E.J.K. was supported by a National Science Foundation East Asia and Pacific Summer Institutes fellowship grant and the Singapore National Research Foundation. National Research Foundation under Competitive Research Programme Award 2007-04, the Academic Research Fund (R-183-000-160-112), the Biomedical Research Council of Singapore (R-183-000-211-305), and the National Medical Research Council (R-183-000-224-213) to M.R.W. are gratefully acknowledged.

[2] Address correspondence and reprint requests to Dr. Chih-Chi Andrew Hu and Dr. Hidde L. Ploegh, Whitehead Institute for Biomedical Research, Nine Cambridge Center, Cambridge, MA 02142. E-mail addresses: chih-chi@wi.mit.edu and ploegh@wi.mit.edu

[3] Abbreviations used in this paper: mIgM, membrane form of IgM; ATF, activating transcription factor; Cer, ceramide; eIF2α, eukaryotic initiation factor 2α; ER, endoplasmic reticulum; HEL, hen egg lysozyme; KO, knockout; NEM, *N*-ethylmaleimide; PC, phosphatidylcholine; PDI, protein disulfide isomerase; PG, phosphatidylglycerol; PI, phosphatidylinositol; PS, phosphatidylserine; PTP-1B, protein-tyrosine phosphatase 1B; sIgM, secreted form of IgM; SM, sphingomyelin; μM, membrane μ; μS, secreted μ; UPR, unfolded protein response; WT, wild type; Endo H, endoglycosidase H; IRE-1, inositol-requiring enzyme 1; PERK, RNA-dependent protein kinase (PKR)-like ER kinase; PNGase F, peptide: *N*-glycosidase F; XBP-1, X-box binding protein 1; XBP-1s, spliced XBP-1 protein.

 0022-1767/09/$2.00

sIgM should fail to activate XBP-1 if misfolded sIgM is the exclusive driver of the UPR.

In earlier experiments, we have produced evidence that activation of XBP-1 occurs even in B cells that do not synthesize massive quantities of sIgM (10). In this study, we set out to examine whether the presence or absence of XBP-1, through its impact on ER homeostasis, affects glycoprotein folding in B cells. To that end, we generated mice in which XBP-1 is conditionally deleted in B cells by crossing the XBP-$1^{flox/flox}$ mouse line (XBP-1^{WT}, where WT represents wild type) (11) to mice in which expression of Cre recombinase is under the control of the B cell-specific CD19 promoter (12), henceforth referred to as XBP-1^{KO} (where KO represents knockout) mice. In addition to the XBP-1^{KO} mice, we used mice unable to synthesize sIgM (XBP-$1^{KO}/\mu S^{-/-}$) (13), and thus expressing only mIgM. Finally, we used transgenic MD4 mice (XBP-1^{WT}/MD4 and XBP-1^{KO}/MD4) in which both the H and L chains of IgM specifically recognize hen egg lysozyme (HEL) (14); this mouse model allowed us to investigate the Ag reactivity of IgM produced in the absence of XBP-1, a rigorous test of successful glycoprotein synthesis, folding, and assembly.

Lipids are not template encoded and cannot be manipulated by genetic mutation as readily as proteins, but they are important in physiology. Enforced expression of XBP-1s in NIH3T3 fibroblasts established the role of XBP-1 in controlling synthesis of phosphatidylcholine (PC) and phosphatidylethanolamine (15, 16). Although a liver-specific KO of XBP-1 leads to hypocholesterolemia and hypotriglyceridemia, a lipomics analysis shows that lipid composition in hepatocytes is not affected by XBP-1 deficiency (17). These results suggested that XBP-1 can regulate expression of a tissue-specific lipid profile in individual organs. The changes in lipid composition have not been systematically examined in the context of B cells with a deficiency in XBP-1. A change in lipid synthesis can alter lipid environments (such as lipid rafts), making B cells respond differently to stimulation with Ag.

In this study, we show that XBP-1-deficient B cells are fully capable of correctly folding both sIgM and mIgM. Our investigation of the biogenesis of a number of essential membrane proteins in XBP-1-deficient B cells revealed no defects in their synthesis, folding, assembly, or intracellular transport. XBP-1-deficient B cells also secrete free κ-chains at rates comparable to those seen in XBP-1-proficient cells. Examination of the lipid contents in total membranes of XBP-1-deficient B cells shows decreased levels of a select group of lipids. XBP-1-deficient B cells expand their ER in response to LPS stimulation, but do so to a lesser extent than WT B cells. A subtly altered pattern of terminal *N*-linked glycosylation was observed for IgM as well as class I MHC products. We conclude that the operation of the secretory pathway shows no obvious abnormalities in XBP-1-deficient B cells, and that XBP-1 is required in differentiating B cells for processes other than the up-regulation of ER-folding capacity.

Materials and Methods

Mice

XBP-$1^{flox/flox}$ mice have been described (11). To obtain B cell-specific deletion, XBP-$1^{flox/flox}$ mice were crossed with CD19-Cre mice (12) obtained from Y. Shi (Harvard Medical School, Boston, MA). Mice with a B cell-specific XBP-1 deletion were additionally crossed to secreted μ knockout ($\mu S^{-/-}$) mice (13) or to MD4 mice (14), which harbor a transgene for HEL-specific IgM.

Abs and reagents

Polyclonal Abs against Igα, Igβ, and protein disulfide isomerase (PDI) were generated in rabbits. Class I MHC was detected using p8 antiserum directed against the cytoplasmic tail, and class II MHC was detected using JV1 antiserum directed against the class II α-chain. Reagents purchased from commercial sources include Abs to actin (Sigma-Aldrich), p97 (Fitzgerald), XBP-1 (Santa Cruz Biotechnology), μ (Southern Biotechnology Associates), and κ (Southern Biotechnology Associates). FACS Abs were purchased from BD Pharmingen, and the following clones were used: CD40 (3/23), CD80 (16-10A1), and CD1d (1B1). Ligands to TLRs were procured from commercial sources, as follows: Pam_3CSK_4 from Alexis Biochemicals; poly(I:C) and LPS (*Escherichia coli* O26:B6) from Sigma-Aldrich; imiquimod from InvivoGen; and CpG DNA from TIB-MOLBIOL.

Cell culture

B lymphocytes were purified from mouse spleens by negative selection using anti-CD43 magnetic beads (Miltenyi Biotec). B cells were cultured in the RPMI 1640 medium (Life Technologies) supplemented with 10% heat-inactivated FBS, 2 mM L-glutamine, 100 U/ml penicillin G sodium, 100 μg/ml streptomycin sulfate, 1 mM sodium pyruvate, 0.1 mM nonessential amino acids, and 0.1 mM 2-ME. For differentiation of B cells into plasmablasts, LPS (20 μg/ml) was added to the culture medium. The NKT cell hybridoma 24.7 (18) was a gift of S. Behar (Brigham and Women's Hospital, Boston, MA). IL-2 and IL-6 concentrations were measured by ELISA (BD Pharmingen).

Protein isolation and immunoblotting

Cells were lysed in Nonidet P-40 lysis buffer (50 mM Tris (pH 7.4), 0.5% Nonidet P-40, 5 mM $MgCl_2$, and 150 mM NaCl) or radioimmunoprecipitation assay buffer (10 mM Tris-HCl (pH 7.4), 150 mM NaCl, 1% Nonidet P-40, 0.5% sodium deoxycholate, 0.1% SDS, and 1 mM EDTA) supplemented with protease inhibitor mixture (Roche). The protein concentrations of the supernatants were determined by bicinchoninic acid assay (Pierce). Samples were boiled in SDS-PAGE sample buffer (62.5 mM Tris-HCl (pH 6.8), 2% SDS, 10% glycerol, and 0.1% bromphenol blue) with 2-ME (or *N*-ethylmaleimide (NEM) where indicated) and separated by SDS-PAGE. Proteins were transferred to nitrocellulose or polyvinylidene difluoride membranes, blocked in 5% (w/v) milk, and immunoblotted with the indicated Abs and appropriate HRP-conjugated secondary Abs. Following three washes in PBS-Tween 20 (0.1%), the blots were developed using Western Lighting Chemiluminescence Reagent (PerkinElmer).

Pulse-chase labeling

Pulse-chase experiments were performed, as described (19). Briefly, plasmablasts were starved in methionine- and cysteine-free medium, then pulse labeled with [^{35}S]methionine/cysteine (PerkinElmer). After labeling, cells were incubated in chase medium containing unlabeled methionine (2.5 mM) and cysteine (0.5 mM). At the end of each chase interval, cells were lysed in radioimmunoprecipitation assay buffer containing protease inhibitors. Lysates were then analyzed by immunoprecipitation, SDS-PAGE, and fluorography. Band intensity was determined using a phosphor imager (Fujifilm BAS 2500), and quantitation was done using the MultiGauge software (Fujifilm).

FACS analysis

Live plasmablasts were stained with the indicated Abs and analyzed by a FACSCalibur flow cytometer (BD Biosciences). Data were analyzed using CellQuest (BD Biosciences).

Triton X-114 phase separation

Triton X-114 phase separation was performed, as described (20). Briefly, cells were lysed in Triton X-114 lysis buffer (10 mM Tris-HCl (pH 7.4), 150 mM NaCl, and 1% Triton X-114) containing protease inhibitors. Lysates were placed onto a sucrose cushion (6% sucrose, 10 mM Tris-HCl (pH 7.4), 150 mM NaCl, and 0.06% Triton X-114), and incubated at 30°C until the lysates turned cloudy. The detergent phase was recovered by centrifugation for 5 min at 300 × *g*. The aqueous supernatant was removed and re-extracted with 0.5% Triton X-114, and overlaid onto the original sucrose cushion. After a subsequent round of separation, both the detergent (sediment) and the soluble (supernatant) fractions were brought to the same buffer and detergent concentrations for further analysis.

Biotinylated HEL affinity purification of HEL-specific Igs

Cells were metabolically labeled and subjected to Triton X-114 phase separation, as described above. Samples were incubated with either anti-μ, biotinylated HEL, or unconjugated biotin. Proteins were then recovered with either protein G-agarose beads or anti-biotin beads (Sigma-Aldrich), washed, eluted with SDS-PAGE sample buffer, and analyzed by SDS-PAGE. For serial depletions using biotinylated HEL, supernatants from the

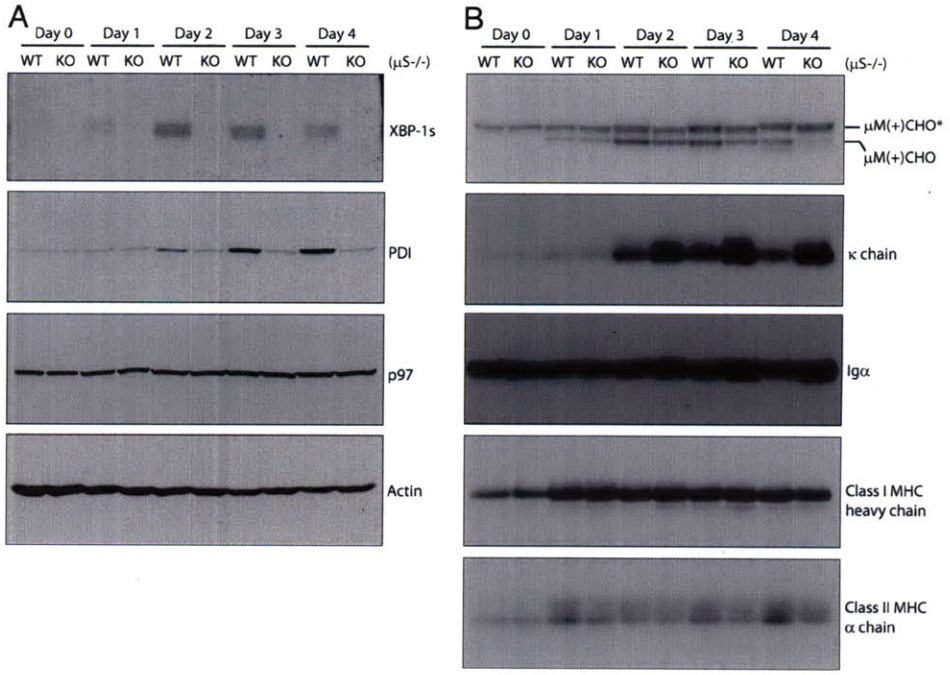

FIGURE 1. *A* and *B*, Naive B cells from XBP-$1^{WT}/\mu S^{-/-}$ and XBP-$1^{KO}/\mu S^{-/-}$ mice were cultured in vitro in the presence of LPS for the indicated times. Cell lysates were prepared and analyzed by SDS-PAGE and immunoblotting for the indicated proteins. Immunoblots shown in both *A* and *B* were performed using the same set of lysates.

initial purification were subjected to five sequential rounds of retrieval by biotinylated HEL, and a final round of immunoprecipitation using the anti-μ Ab.

Enzymatic deglycosylation

Total lysates or immunoprecipitates from lysates were denatured in glycoprotein denaturing buffer (0.5% SDS, 1% 2-ME) at 95°C for 5 min, followed by addition of sodium citrate (pH 5.5) to a final concentration of 50 mM, and incubated with endoglycosidase H (Endo H) (New England Biolabs) at 37°C for 2 h. Alternatively, sodium phosphate (pH 7.5) and Nonidet P-40 were added to the denatured cell lysates to a final concentration of 50 mM and 1%, respectively, and the mixture was incubated with peptide: *N*-glycosidase F (PNGase F) (New England Biolabs) at 37°C for 2 h.

Liquid chromatography-mass spectrometry analysis of lipids

Lipid extract was prepared using a modified version of Bligh and Dyer method (21), with two sequential extraction steps to maximize yield. A total of 0.9 ml of a chloroform:methanol (1:2) mix was added to 10 million cells (in 0.1 ml of PBS), and the mixture was vortexed vigorously for 3 × 1 min with a 5-min interval in between. Next, 0.3 ml of chloroform and 0.3 ml of 1 M KCl were added to the tube, and the mixture was again vortexed. The mixture was then centrifuged for 2 min at 9000 rpm to separate the phases. The lower organic layer was transferred to a clean microfuge tube. Residual aqueous phase and cell remnants were re-extracted with 0.5 ml of chloroform, as described above, and the organic phase was combined with extract 1. The combined extract was dried in a Speedvac. Before analysis, lipids were dissolved in chloroform/methanol (1:1, v/v).

An Agilent HPLC system coupled with an Applied Biosystems Triple Quadrupole/Ion Trap mass spectrometer (4000Qtrap) was used for quantification of individual polar lipids. Based on product ion and precursor ion analyses of head groups, two comprehensive sets of multiple reaction monitoring transitions were set up for quantitative analysis of various lipids, including PC, phosphatidylethanolamine, phosphatidylserine (PS), phosphatidylinositol (PI), phosphatidylglycerol (PG), sphingomyelin (SM), and ceramide (Cer) (22, 23). The signal intensity obtained for each lipid species was calculated by comparing to corresponding internal standards, including di14:0-PC, di14:0-phosphatidylethanolamine, di14:0-PS, di14:0-PG, di8:0-PI, Cer d18:1/17:0, and SM18/14:0.

Electron microscopy

B cells were fixed for electron microscopy either immediately after isolation, or after 3 days in culture in the presence of LPS. The cells were fixed in 2.5% glutaraldehyde, 3% paraformaldehyde, with 5% sucrose in 0.1 M sodium cacodylate buffer (pH 7.4). Cells were then postfixed in 1% OsO_4 in veronal-acetate buffer. The cells were stained in block overnight with 0.5% uranyl acetate in veronal-acetate buffer (pH 6.0), dehydrated, and embedded in Spurr's resin. Sections were cut on a Reichert Ultracut E microtome with a Diatome diamond knife at a thickness setting of 50 nm, and stained with 2% uranyl acetate, followed by 0.1% lead citrate. Samples were examined using an FEI Tecnai Spirit TEM at 80 KV and imaged with an AMT camera.

Results

XBP-1 activation occurs in the absence of sIgM

We set out to test the connection between XBP-1 and glycoprotein quality control during B cell differentiation. B cells were analyzed over the course of a 4-day in vitro differentiation scheme in which naive splenic B cells were cultured in the presence of LPS, to induce differentiation into Ig-secreting plasmablasts (24).

We assessed the expression of XBP-1s in B cells from $\mu S^{-/-}$ mice over 4 days of in vitro LPS-stimulated differentiation. XBP-1s was induced as early as day 1, and its expression persisted for the remainder of the time in culture (Fig. 1*A*) (10). This expression pattern is similar to what is observed in WT mice (10, 25). XBP-$1^{WT}/\mu S^{-/-}$, but not XBP-$1^{KO}/\mu S^{-/-}$ B cells showed up-regulation of PDI following LPS stimulation (Fig. 1*A*), indicating that up-regulation of PDI requires both LPS and XBP-1s.

Because $\mu S^{-/-}$ B cells do not express sIgM, but are readily induced by LPS to express XBP-1, activation of XBP-1 in these B cells cannot be due to an accumulation of unfolded sIgM. We therefore investigated the expression of membrane μ (μM), κ, Igα, and class I and II MHC molecules in $\mu S^{-/-}$ B cells to determine whether there was an aberration in the expression of proteins other than IgM that could result in an accumulation of unfolded proteins and activation of XBP-1. The μM was only modestly up-regulated over the 4-day time course of differentiation in both control and XBP-1-deficient B cells (Fig. 1*B*). This increase is insignificant when compared with the increase of sIgM upon LPS stimulation in normal B cells; in XBP-1-proficient cells, sIgM levels increase by at least 15-fold (25). In both XBP-1-deficient and -proficient B cells, expression of κ-chain increased over the course of LPS stimulation and was increased in XBP-1-deficient B cells (Fig. 1*B*). However, free κ-chains are unlikely to be the trigger for XBP-1 activation, because pulse-chase experiments showed that these κ-chains are secreted normally (see below).

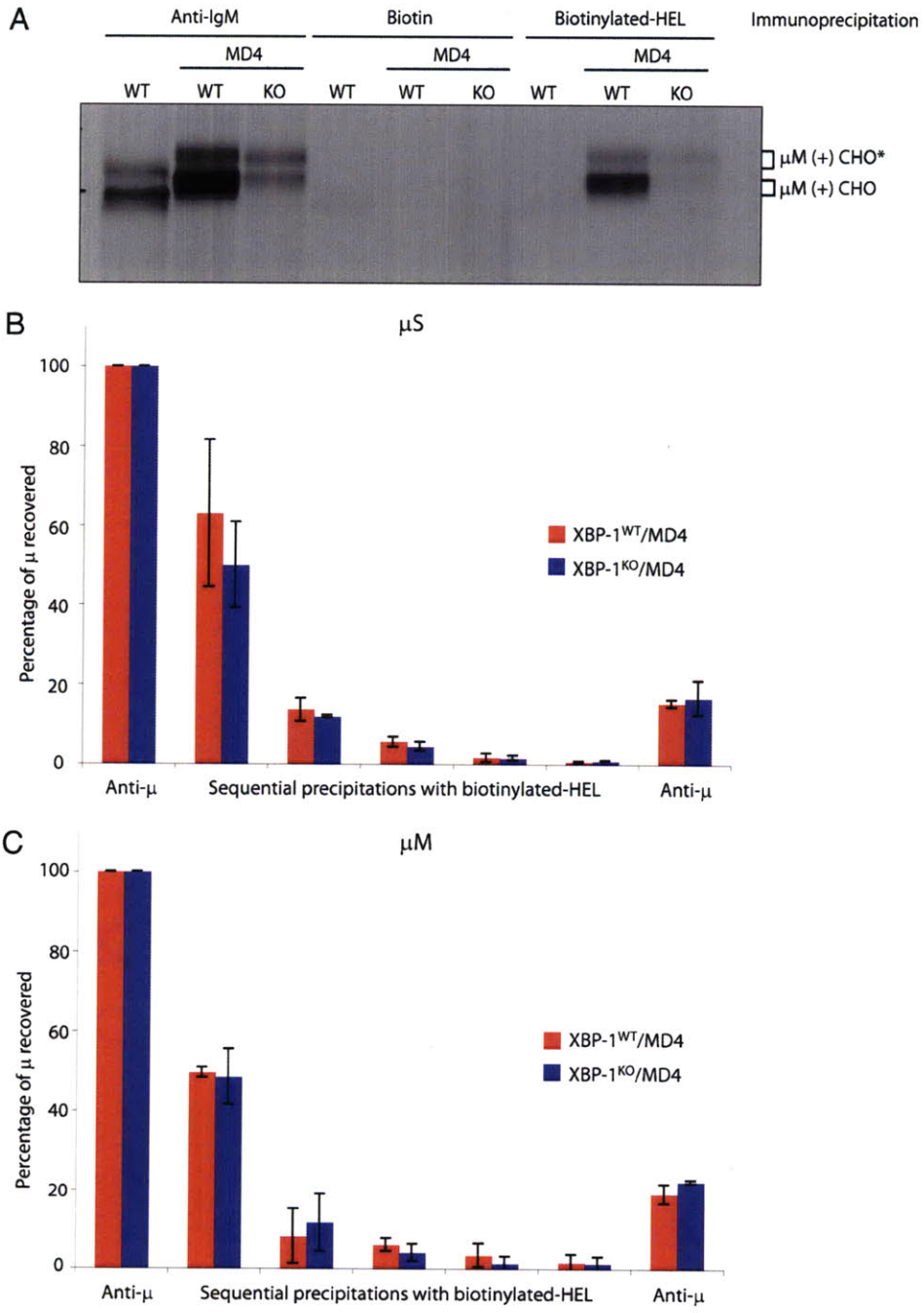

FIGURE 2. *A*, Naive B cells from XBP-1^{WT}, XBP-1^{WT}/MD4, and XBP-1^{KO}/MD4 mice were cultured in the presence of LPS for 4 days and then labeled with [^{35}S]methionine/cysteine for 4 h. Triton X-114 lysis and separation were performed. Both the pellet and soluble fractions were precipitated with an Ab against μ, or with biotin or biotinylated HEL. The pellet fraction containing μM is shown. *B* and *C*, Cell lysates were prepared as in *A*. Lysates were split into two fractions, one of which was immunoprecipitated with an anti-μ Ab, and the other of which was subjected to five sequential rounds of precipitation with biotinylated HEL, followed by a subsequent immunoprecipitation using the anti-μ Ab. For each cell type (XBP-1^{WT}/MD4 and XBP-1^{KO}/MD4), the amount of μ recovered from the first fraction by immunoprecipitation using the anti-μ Ab was designated as the total μ. By comparing with the total μ, the percentage of μ recovered from the second fraction was designated for each of the five sequential biotinylated HEL recovery steps and for the final recovery with the anti-μ Ab. The quantitation of μS (*B*) was performed on fractions taken from the Triton X-114 supernatant, and the μM quantitation (*C*) was performed on the Triton X-114 pellet fractions. The results shown are an average of two separate experiments.

Expression of Igα remained constant over the 4-day course of LPS stimulation, and MHC molecules were slightly up-regulated after LPS stimulation (Fig. 1*B*).

The absence of XBP-1 does not alter the efficiency of IgM folding

The defect attributable to the absence of XBP-1 is expected to yield systemic folding defects in glycoproteins due to dysregulation of chaperone synthesis. Such a defect could manifest itself in several ways, as follows: an increase in misfolded proteins, a defect in protein assembly, or a decrease in trafficking from the ER to the targeted locations.

We performed a stringent test for the presence of misfolded IgM, using MD4 transgenic mice that express IgM specific for HEL. Ag binding represents a robust test of correct folding and assembly of IgM, because Ag-Ab interaction requires both correct folding and assembly of the H and L chains. To isolate correctly folded IgM from MD4 B cells, the Ag HEL was conjugated to biotin, which was then used to recover IgM capable of recognizing HEL by adsorption to anti-biotin agarose beads. We performed these experiments following separation of mIgM and sIgM using the Triton X-114 phase separation method (20). By retrieval of IgM using biotinylated HEL, we found that the majority of IgM recovered from MD4 B cells is indeed specific for HEL, because immobilized biotinylated HEL led to retrieval of IgM only from MD4, but not from WT B cells (Fig. 2*A*). There was no obvious difference in the percentage of HEL-reactive IgM recovered from XBP-1^{WT}/MD4 and XBP-1^{KO}/MD4 B cells (Fig. 2, *B* and *C*). After five rounds of sequential retrieval with immobilized biotinylated HEL, we recovered the remaining unfolded IgM by

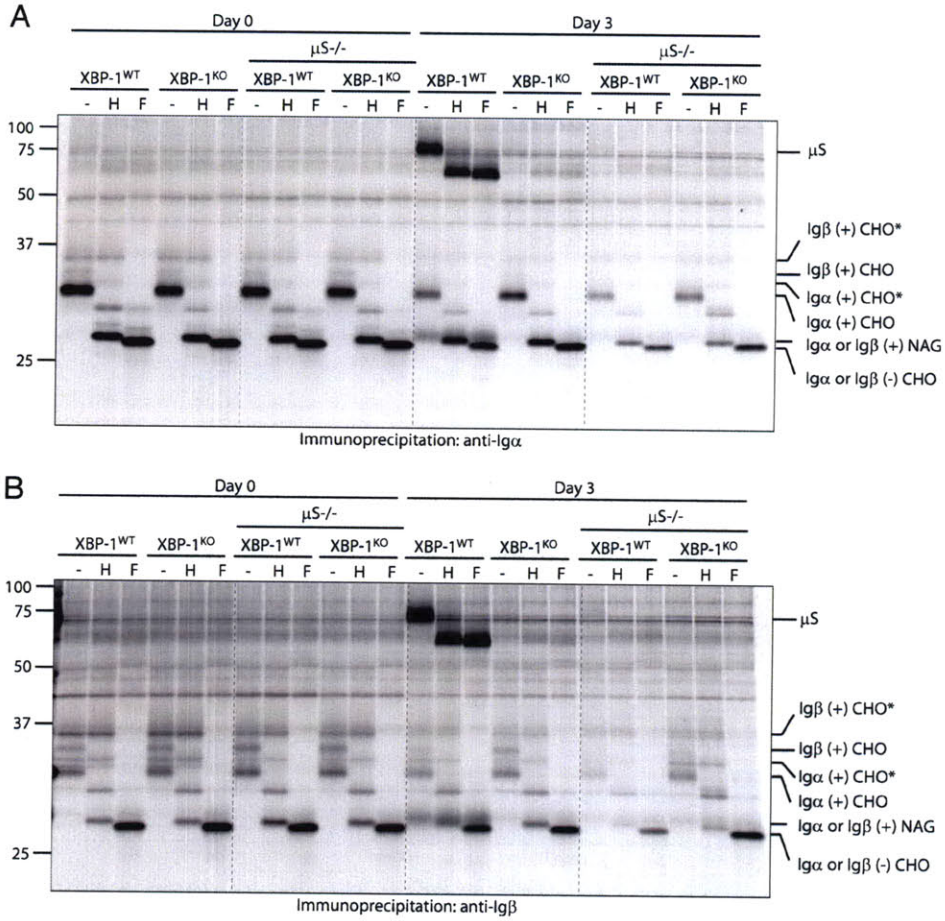

FIGURE 3. Naive B cells or 3-day LPS-stimulated plasmablasts from indicated mice were labeled with [^{35}S]methionine/cysteine for 4 h. Cell lysates were immunoprecipitated using Abs to Igα (*A*) and Igβ (*B*). The immunoprecipitates were treated with either Endo H (H) or PNGase F (F) before analyses by SDS-PAGE and fluorography. CHO, CHO*, and NAG represent high mannose-type glycans, complex-type glycans, and *N*-acetylglucosamines, respectively. Note that the sIgM was precipitated from the 3-day LPS-stimulated XBP-1^{WT} B cell lysates via nonspecific binding of sIgM to protein G-conjugated agarose beads.

immunoprecipitation using an anti-μ Ab. Had the ability of IgM to fold properly been compromised by the XBP-1 deficiency, we should have detected a surplus of free, unbound μ-chains in XBP-1-deficient MD4 B cells, but this was not the case. We observed no significant differences in the percentage of misfolded IgM between XBP-1^{WT}/MD4 and XBP-1^{KO}/MD4 B cells, suggesting a similar ability to correctly fold both sIgM and mIgM (Fig. 2, *B* and *C*).

Igα/Igβ heterodimer formation proceeds normally in XBP-1-deficient B cells

Igα must assemble with Igβ before the heterodimer can leave the ER. To assess the association of Igα with Igβ, we radiolabeled both naive and 3-day LPS-stimulated B cells, and performed immunoprecipitations using Abs against Igα or Igβ, either of which should allow recovery of both Igα and Igβ due to the fact that these proteins remain disulfide linked under nonreducing conditions. In both naive and 3-day LPS-stimulated B cells, there was no detectable difference in the association/stoichiometry of Igα and Igβ as a result of XBP-1 deficiency (Fig. 3). The synthesis of Igα and Igβ was apparently not affected by the absence of XBP-1 because we detected similar amounts of Igα and Igβ in XBP-1^{WT} and XBP-1^{KO} B cells (Fig. 3). Because both Igα and Igβ acquire complex-type glycans in the Golgi apparatus, the exit of Igα and Igβ from the ER is normal in the absence of XBP-1 (Fig. 3). Similar results were found in either XBP-1^{KO} or XBP-1^{KO}/μS$^{-/-}$ B cells (Fig. 3).

Disulfide formation proceeds normally in the absence of XBP-1

XBP-1-deficient B cells did not up-regulate PDI in response to LPS stimulation (Fig. 1*A*), consistent with the known mechanism of transcriptional control of the PDI gene by XBP-1 (6, 7). Several components of the BCR associate through disulfide bonds: Igα and Igβ form a heterodimer held together by a disulfide bond, as do Ig H (μ) and L (κ) chains to yield IgM. Lysates from XBP-1^{WT}/μS$^{-/-}$ and XBP-1^{KO}/μS$^{-/-}$ B cells cultured in the presence of LPS for 2 or 4 days were treated with *N*-ethylmaleimide (NEM) to preserve disulfide bond arrangements and to prevent de novo formation of disulfide bonds. We found no difference in the levels of nonreduced Igα/Igβ heterodimers in XBP-1^{KO}/μS$^{-/-}$ B cells (Fig. 4*A*), suggesting that the disulfide bond between them formed normally. Similarly, μ- and κ-chains assembled correctly into higher-order dimers (μ + κ) and tetramers ($\mu_2\kappa_2$) (Fig. 4*B*). Thus, the prevailingly low levels of PDI in XBP-1-deficient B cells are sufficient to sustain normal disulfide bond formation.

Normal kinetics of synthesis and ER exit are observed for proteins that enter the secretory pathway in XBP-1-deficient B cells

We investigated protein synthesis and trafficking in XBP-1-deficient B cells by pulse-chase analyses on IgM, κ-chains, class I MHC, Igα/Igβ, and class II MHC molecules. We detected no defects in the trafficking of mIgM to the cell surface, because levels of the complex oligosaccharide-bearing μ-chain (indicated by μM(+)CHO*) were not altered in XBP-1-deficient B cells after 120 min of chase (Fig. 5). Although XBP-1-deficient B cells synthesized more κ-chains (Fig. 1) than their WT counterparts, all of the excess κ-chains were effectively secreted (Fig. 5*B*).

We observed a barely detectable delay in the exit of class I MHC from the ER in XBP-1-deficient B cells as compared with XBP-1-proficient B cells, regardless of whether this was measured for XBP-1^{KO}/μS$^{-/-}$ or XBP-1^{KO}/MD4 mice (Fig. 6, *A* and *B*). At

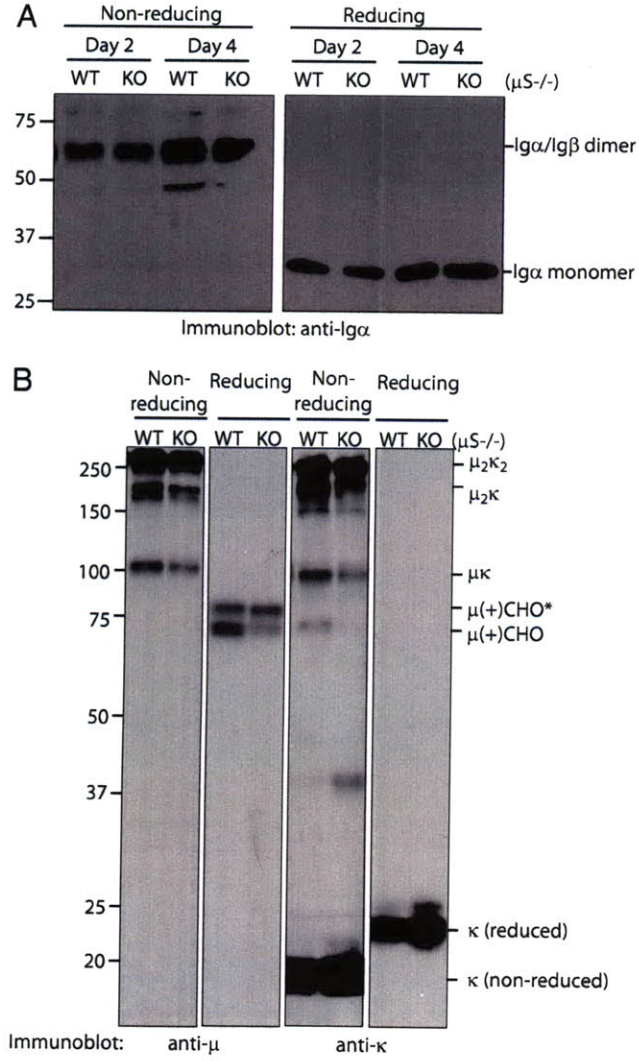

FIGURE 4. *A*, XBP-1^{WT}/$\mu S^{-/-}$ and XBP-1^{KO}/$\mu S^{-/-}$ B cells were cultured in the presence of LPS for 2 or 4 days and lysed in Nonidet P-40, and lysates were treated with either NEM to retain disulfide bonds or DTT to reduce disulfide bonds. Cell lysates were then analyzed by SDS-PAGE and immunoblotting for Igα. *B*, Four-day LPS-stimulated XBP-1^{WT}/$\mu S^{-/-}$ and XBP-1^{KO}/$\mu S^{-/-}$ B cells were lysed in Nonidet P-40, and lysates were treated with either NEM or DTT. Lysates were then immunoblotted using Abs to μ or κ.

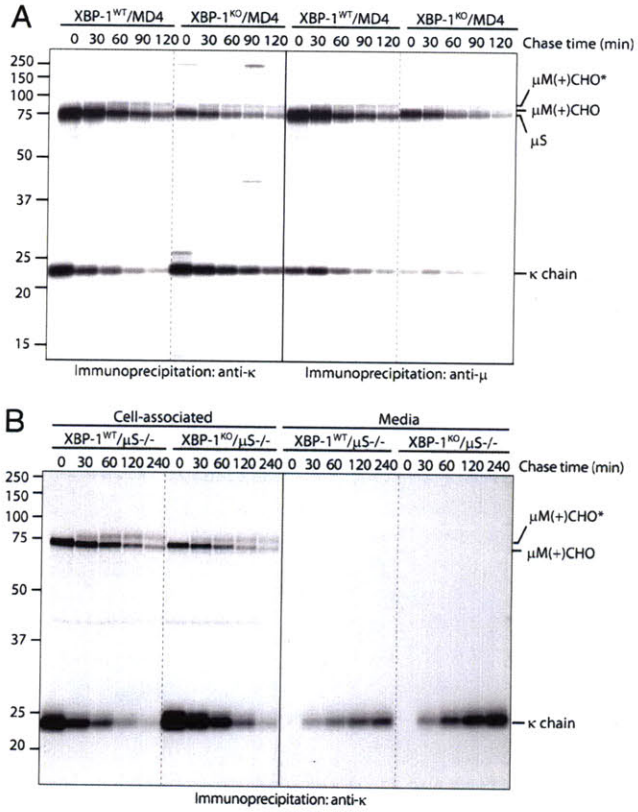

FIGURE 5. *A*, Naive XBP-1^{WT}/MD4 and XBP-1^{KO}/MD4 B cells were cultured in the presence of LPS for 3 days. Cells were then labeled with [^{35}S]methionine/cysteine for 10 min and chased for the indicated times. Immunoprecipitations were performed using Abs against κ or μ, and were analyzed by SDS-PAGE and fluorography. *B*, Three-day LPS-stimulated XBP-1^{WT}/$\mu S^{-/-}$ and XBP-1^{KO}/$\mu S^{-/-}$ B cells were radiolabeled for 10 min and chased for the indicated times. Immunoprecipitations were performed on both cell lysates and the culture medium using an Ab against κ.

later time points, all class I MHC molecules exit the ER. There was no detectable difference in the synthesis or trafficking of Igα and Igβ when comparing XBP-1^{WT}/$\mu S^{-/-}$ and XBP-1^{KO}/$\mu S^{-/-}$ B cells (Fig. 6*C*). We also did not detect any difference in the rate of trafficking of class II MHC molecules as a result of XBP-1 deficiency (Fig. 6*D*).

XBP-1 deficiency does not alter cell surface display of glycoproteins or compromise their functions

No differences were found in the cell surface levels of CD1d, CD80, or CD40 (Fig. 7, *A–C*) as measured by cytofluorimetry. Signaling through various TLRs by distinct TLR ligands was indistinguishable for XBP-1^{WT}/MD4 and XBP-1^{KO}/MD4 B cells, as measured by the secretion of IL-6 in response to stimulation (Fig. 7*D*). Consistently, B cells were found irresponsive to poly(I:C) (26). The ability of CD1d to present lipid Ags to NKT hybridoma cells was also tested, and no apparent defect was detected in XBP-1-deficient B cells (Fig. 7*E*). Thus, all proteins examined function normally in XBP-1-deficient B cells, implying that they do not obviously suffer from a folding or transport defect.

XBP-1-deficient B cells synthesize significantly less PC, SM, and PI

We examined changes in lipid composition of total membranes extracted from both naive and LPS-stimulated XBP-1-deficient B cells using liquid chromatography-mass spectrometry. Data from four independent experiments suggest that the lipid composition in total membranes of the naive XBP-1-deficient B cells is similar to that of the naive XBP-1-proficient B cells. However, significantly lower levels of PC, SM, and PI were found in the membranes of 4-day LPS-stimulated XBP-1-deficient B cells (Fig. 8 and supplemental Fig. S1),[4] suggesting that the presence of XBP-1 is required for production of these lipids in LPS-stimulated plasmablasts.

XBP-1-deficient B cells show a reduced expansion of the ER

We investigated expansion of the ER in XBP-1-deficient B cells in response to LPS stimulation. Naive B cells contained relatively little ER, and no differences between the XBP-1-deficient B cells and their WT counterparts were detectable by electron microscopy (Fig. 9). In both XBP-1-proficient and XBP-1-deficient B cells,

[4] The online version of this article contains supplemental material.

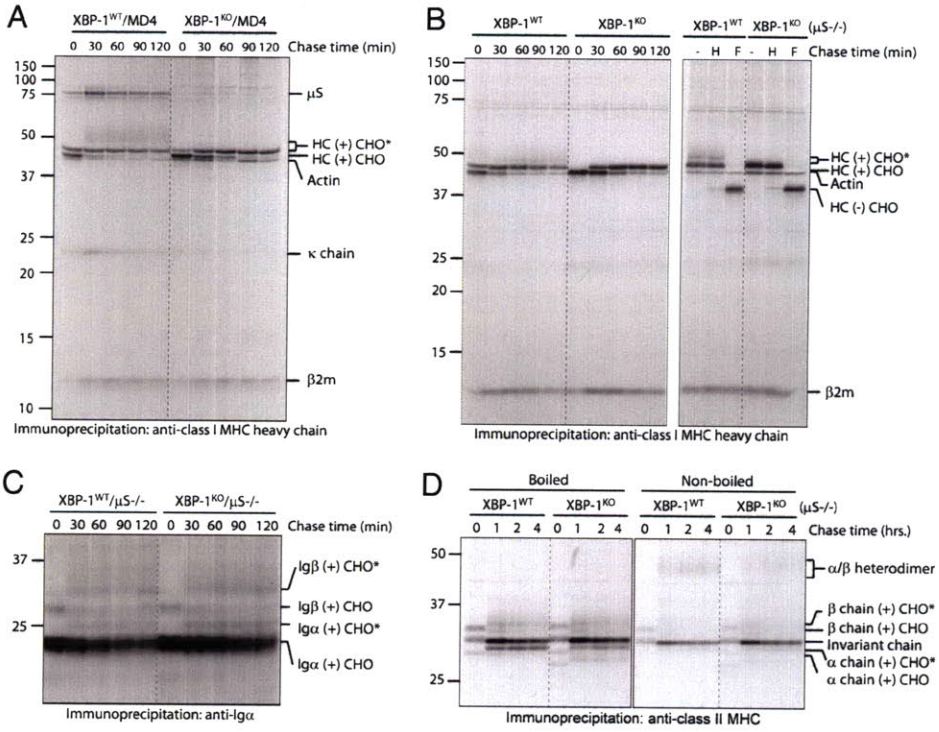

FIGURE 6. Naive B cells from indicated mouse lines were cultured in the presence of LPS for 3 days. Cells were labeled with [^{35}S]methionine/cysteine for 10 min and chased for the indicated times. Immunoprecipitations were performed using Abs to class I MHC H chain (*A* and *B*), Igα (*C*), or class II MHC α-chain (*D*), and were analyzed by SDS-PAGE and fluorography. Additionally, in *B*, lysates from the 90- and 120-min chase points were combined, immunoprecipitated with the Ab to class I MHC H chain, and subsequently treated with either Endo H (H) or PNGaseF (F) before SDS-PAGE analysis.

similar percentages of the cell population respond to LPS stimulation by increasing ER content. The expansion was more pronounced in XBP-1-proficient B cells (Fig. 9).

XBP-1-deficient B cells have subtly altered patterns of terminal glycosylation

We noticed subtle differences in the patterns of glycosylation of IgM and class I MHC when comparing LPS-stimulated XBP-1-proficient and XBP-1-deficient B cells. XBP-1^{WT}/MD4 B cells contained more of the ER form of both mIgM and sIgM than XBP-1^{KO}/MD4 B cells (Fig. 10*A*). By carefully investigating the glycosylation status of mIgM, we observed a difference in the mobility of the Endo H-resistant fraction of mIgM between XBP-1^{WT}/$\mu S^{-/-}$ and XBP-1^{KO}/$\mu S^{-/-}$ B cells (Fig. 10*B*), and an increased heterogeneity in the acquisition of Endo H-resistant complex-type glycans in XBP-1^{KO}/$\mu S^{-/-}$ B cells (Fig. 10*B*, indicated by <). Because each μ-chain has five potential *N*-linked glycosylation sites, heterogeneity can arise from any of these sites due to differences in terminal glycosylation. Similar defects in glycosylation also occurred to class I MHC molecules (Fig. 6, *A* and *B*). The XBP-1-proficient B cells synthesized a population of class I MHC with Endo H-resistant glycan modifications that migrated more slowly in SDS-PAGE, which was absent from XBP-1-deficient B cells (Fig. 6, *A* and *B*).

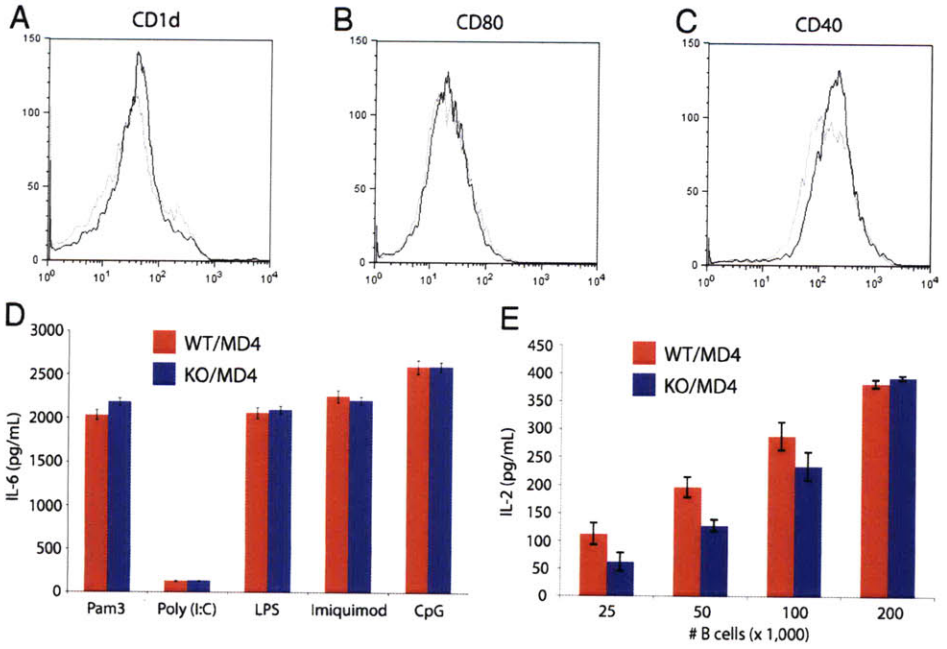

FIGURE 7. *A–C*, XBP-1^{WT}/MD4 and XBP-1^{KO}/MD4 B cells that had been cultured with LPS for 3 days were analyzed for the cell surface display of indicated markers by FACS. The black lines are from XBP-1^{WT}/MD4 cells, and the gray lines are from XBP-1^{KO}/MD4 cells. *D*, XBP-1^{WT}/MD4 and XBP-1^{KO}/MD4 B cells were cultured with Pam_3CSK_4 (100 ng/ml), poly(I:C) (100 μg/ml), LPS (20 μg/ml), imiquimod (25 μM), and CpG DNA (1 μM) for 3 days. Culture supernatants were analyzed for the presence of IL-6 by ELISA. *E*, XBP-1^{WT}/MD4 and XBP-1^{KO}/MD4 B cells were cultured in the presence of LPS for 4 days. Varying numbers of these LPS-stimulated B cells were then incubated with a CD1d-responsive NKT cell line (NKT 24.7) overnight, and the NKT cell activation was assessed by secretion of IL-2, measured by ELISA

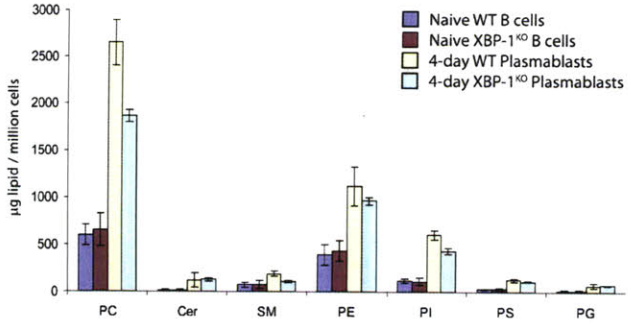

FIGURE 8. XBP-1-deficient plasmablasts synthesize significantly less PC, SM, and PI. Naive B cells purified from the spleens of either XBP-1^{WT} or XBP-1^{KO} mice were cultured with LPS for 4 days. Lipids were extracted from at least 100 million cells. Quantitation of each lipid was conducted using liquid chromatography/mass spectrometry. Lipid abundance was calculated by comparing with internal standards. Experiments were repeated four times using B cells pooled from nine mice of each genotype. Data are presented as mean ± SD. Lipids analyzed include PC, Cer, SM, phosphatidylethanolamide (PE), PI, PS, and PG.

Discussion

The UPR is commonly viewed as a stereotypic set of changes in gene expression, triggered by the accumulation of misfolded proteins. Its regulation involves the activation of IRE-1, which executes a splicing reaction to yield XBP-1s mRNA, the translation of which starts a transcriptional program that targets a variety of genes encoding chaperones and enzymes involved in protein folding and lipid synthesis. The literature frequently equates the activation of XBP-1 with the activation of the UPR, a response commonly evoked experimentally through the application of toxic drugs such as tunicamycin, thapsigargin, or DTT. The extent to which the UPR functions in a more physiological manner is not immediately obvious, and none of the above treatments used to induce the UPR can be considered subtle. Tunicamycin treatment interferes with glycoprotein folding through inhibition of glycosylation, but the extent of folding damage inflicted is difficult to gauge. At the same time, tunicamycin treatment also leads to accumulation of the dolichol precursor and presumably affects the lipid environment in which ER membrane proteins function. Thapsigargin depletes the ER of its calcium stores, compromises the function of calcium-dependent ER-resident chaperones such as calnexin and calreticulin, and is therefore expected to increase the failure rate of protein folding in the ER. Imposition of stress by generating a strongly reducing environment using DTT is also a common method to unleash the UPR. All of these triggers activate XBP-1 (3). More rarely the UPR can be induced by overexpression of genetically engineered misfolded proteins (27, 28), but it is interesting to note that these two examples concern a polytopic (multispanning) ER membrane protein and a surfactant-binding protein, respectively, both of which might act not only through their misfolded state per se, but also through sequestration of lipids and their metabolites at inappropriate locations. Experiments in yeast suggest that massive quantities of a misfolded type I membrane protein are far less effective at induction of the UPR than even mild tunicamycin treatment (29).

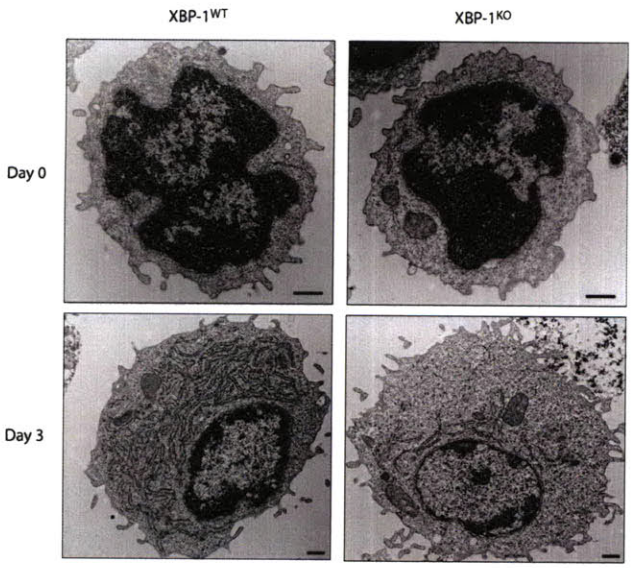

FIGURE 9. Naive (day 0) or 3-day LPS-stimulated XBP-1^{WT} and XBP-1^{KO} B cells were fixed and prepared for analysis by electron microscopy. Approximately one-third of the purified B cells respond to LPS with increased ER content and show the represented morphology. Scale bar = 500 nm.

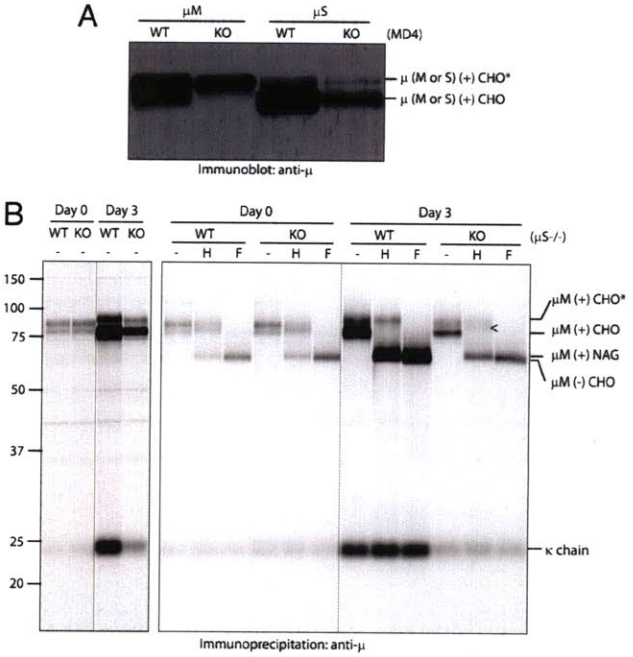

FIGURE 10. *A*, Four-day LPS-stimulated XBP-1^{WT}/MD4 and XBP-1^{KO}/MD4 B cells were lysed in Triton X-114, and sIgM and mIgM were separated, as described. Lysates were then immunoblotted using the anti-μ Ab. *B*, Naive and 3-day LPS-stimulated XBP-1^{WT}/$\mu S^{-/-}$ and XBP-1^{KO}/$\mu S^{-/-}$ B cells were labeled with [^{35}S]methionine/cysteine for 4 h. Immunoprecipitations were performed using an Ab to μ. Immunoprecipitates were subsequently treated with either Endo H (H) or PNGaseF (F), and analyzed by SDS-PAGE and fluorography. The arrowhead (<) indicates the partially Endo H-resistant IgM.

Development of B cells into plasma cells is an example of a physiological process that triggers the UPR, as defined by activation of XBP-1. Although misfolded sIgM has been speculated to provide the impetus for XBP-1 activation in differentiating plasma cells (3, 4), our data provide no support for this suggestion, because XBP-1 activation occurs also in B cells that cannot make sIgM, with kinetics that mimic those in normal B cells (Fig. 1) (10). Because an excess of unfolded sIgM cannot be the cause of XBP-1 activation in these cells, we conclude that there must be an as yet unidentified (differentiation-dependent) trigger that leads to XBP-1 activation through IRE-1. IRE-1 is usually activated by the presence of unfolded proteins in the lumen of the ER, either

through a direct interaction with unfolded proteins (30), or through its dissociation from Ig H chain binding protein (BiP) as a result of competition for unfolded proteins (31, 32). Unfolded ER proteins alone may not be sufficient for full IRE-1 activation. Protein-tyrosine phosphatase 1B (PTP-1B) has been implicated in assisting complete function of IRE-1, because cells that lack PTP-1B are less efficient in turning on downstream effectors of IRE-1 in response to UPR triggers (33), thus linking PTP-1B to IRE-1. Full activation of the IRE-1 pathway can thus be controlled by multiple inputs, and not merely by the presence of unfolded proteins.

LPS-induced differentiation activates XBP-1 (4, 34), leading to up-regulation of chaperones like PDI (Fig. 1*A*). Assuming that the failure to increase PDI levels in XBP-1-deficient plasmablasts would cause misassembly and/or misfolding of proteins, we investigated the fate of IgM H and L chains, as well as the ability of IgM to bind HEL in the absence of XBP-1 (Fig. 2). We saw no difference between XBP-1^{WT}/MD4 and XBP-1^{KO}/MD4 plasmablasts in terms of their ability to correctly assemble sIgM and mIgM capable of HEL binding. Free κ-chains were synthesized at increased levels and were readily secreted by XBP-1-deficient B cells (Figs. 1*B* and 5). XBP-1 deficiency also did not affect synthesis, assembly, and trafficking of Igα and Igβ, or class I and class II MHC molecules (Figs. 3, 4*A*, and 6), with the possible exception of a barely perceptible delay in the exit of class I MHC molecules from the ER in XBP-1-deficient B cells (Fig. 6, *A* and *B*). XBP-1-deficient B cells obtained from chimeric XBP-1$^{-/-}$/RAG2$^{-/-}$ mice showed no obvious delay in class I MHC trafficking, a difference we attribute to the slight difference in the pulse-chase protocols used (25). We hence suggest that glycoproteins fold and function normally in XBP-1-deficient B cells. This conclusion is inconsistent with the proposal that an XBP-1-deficient B cell produces an ER that is defective in protein folding.

CD40, CD80, and CD1d were all present at the cell surface of XBP-1-deficient B cells in normal amounts (Fig. 7, *A–C*), and CD1d was fully functional in the presentation of lipid Ags to NKT cells (Fig. 7*E*). Production of IL-6 triggered by various TLR ligands was not significantly different for XBP-1-proficient and XBP-1-deficient plasmablasts (Fig. 7*D*), suggesting that the examined TLRs function properly in their distinct cellular compartments. Taken together, these results show that the ER of XBP-1-deficient plasmablasts sustains folding and assembly of all proteins we have examined to date. The activation of stress responses triggered by prion replication was not influenced by XBP-1 deficiency (11), further supporting the notion that XBP-1 is not required to handle misfolded proteins, in the form of cytotoxic aggregates.

It is possible that we do not detect a defect in protein folding in XBP-1-deficient B cells due to a compensatory up-regulation of other branches of the UPR. In addition to the responses initiated by the IRE-1/XBP-1 axis, RNA-dependent protein kinase (PKR)-like ER kinase (PERK) and activating transcription factor (ATF)6 contribute as well. The presence of unfolded proteins in the ER stimulates phosphorylation by PERK of eukaryotic initiation factor 2α (eIF2α). This attenuates translation initiation, thus reducing the number of proteins that enter the ER (31). However, there is no indication that initiation of translation is somehow compromised through engagement of the PERK axis in XBP-1-deficient B cells. ATF6 is a membrane-bound transcription factor. In response to ER stress, ATF6 traffics to the Golgi apparatus, where its transmembrane segment is cleaved to release its transcription factor domain, which then translocates to the nucleus to initiate the transcription of ER chaperones that can aid in protein folding (35, 36). The PERK branch of the UPR is not required for B cell differentiation (37), and XBP-1 deficiency does not lead to the up-regulation of eIF2α and phospho-eIF2α, important indictors for PERK activation (10) (data not shown). The ATF6 pathway is induced during plasma cell differentiation (38), but whether it is essential for plasma cell differentiation remains to be established. Finally, XBP-1 deficiency alone is sufficient to cause a block in plasma cell differentiation, with no obvious compensation by either PERK or ATF6 activation.

The exact role of XBP-1 in plasma cell differentiation remains to be defined. PC, SM, and PI decrease in response to XBP-1 deficiency in total membranes of LPS-stimulated plasmablasts cells, but not unstimulated naive B cells (Fig. 8 and supplemental Fig. S1), suggesting that XBP-1 is required for lipid synthesis in support of plasma cell differentiation. PC is most drastically affected by XBP-1 deficiency in plasmablasts because it is the primary phospholipid of the ER membranes. Although no lipid was found altered in hepatocytes lacking XBP-1 (17), PC and phosphatidylethanolamine increase significantly in NIH3T3 fibroblasts overexpressing XBP-1s (15, 16). Unlike in fibroblasts, we do not find phosphatidylethanolamine affected by XBP-1 deficiency in B cells; however, SM and PI decrease significantly in XBP-1-deficient plasmablasts, although the levels of these two lipids are lower than that of PC. To find reduced levels of SM and PI in plasmablasts is interesting, because both lipids play important roles in signal transduction. SM is a crucial lipid in rafts, and PI is an essential intermediate in the PI-3-phosphate signaling pathway. These lipid defects may compromise the recruitment of IgM, Igα/Igβ, and other B cell coreceptors (CD19, CD20, CD21, and CD81) into lipid rafts, and contribute to the observed defective signal transduction in XBP-deficient B cells (10).

Activated XBP-1-deficient plasmablasts had decreased ER content compared with XBP-1-proficient plasmablasts, as visualized by transmission electron microscopy (Fig. 9), whereas unstimulated controls showed no such difference. Although XBP-1 is not required for B cells to increase their ER content in response to differentiation, the extent of the ER expansion does depend on XBP-1. This is consistent with XBP-1's role in setting the levels of PC (Fig. 8 and supplemental Fig. S1A). Thus, it appears that expansion of the ER, but not necessarily the ER-folding capacity per se, is under the control of XBP-1.

We observed minor differences in the pattern of terminal glycosylation of both IgM and class I MHC in XBP-1-deficient cells (Figs. 6, *A* and *B*, and 10). Although these changes are slight and require a more detailed analysis by glycan sequencing, such differences could certainly contribute to the defect in plasma cell differentiation in XBP-1-deficient mice. Whether alterations in glycosyltransferase levels, nucleotide sugars, and their transporters or the environment in which these enzymes function are responsible for the observed glycosylation defects is not known at present. Proper glycosylation is most likely critical to B cell differentiation, given that the blockade of high mannose to complex-type *N*-linked glycans imposed by the ER mannosidase inhibitor 1-deoxymannojirimycin can completely block the formation of Ig-secreting B cell blasts from human peripheral blood B cells (39), although mannosidase inhibition does not inhibit B cell proliferation or Ig secretion per se. Some factors required for B cell differentiation may well be sensitive to changes in terminal glycan modifications.

XBP-1^{WT}/MD4 and XBP-1^{KO}/MD4 B cells differ in signaling through the BCR, and regulation of the transcription factors IFN regulatory factor 4 and Blimp-1 (10). In addition, XBP-1-deficient B cells after Ag stimulation fail to migrate to the bone marrow (10). These, together with altered lipid synthesis and glycosylation in XBP-1-deficient B cells, could account for failure of B cells to fully differentiate into plasma cells, but accumulation of misfolded

proteins does not appear to be a key contributing factor. Altogether, our results suggest that XBP-1 activation in B cells is a differentiation-dependent event unlinked to accumulation of misfolded IgM. Furthermore, protein folding occurs normally in XBP-1-deficient B cells, indicating an essential role for XBP-1 beyond the UPR.

Acknowledgments

We thank J. Antos and M. Brinkmann for critical reading of the manuscript, and members in the Ploegh Laboratory for their support.

Disclosures

The authors have no financial conflict of interest.

References

1. Chen-Bettecken, U., E. Wecker, and A. Schimpl. 1987. Transcriptional control of μ- and κ-gene expression in resting and bacterial lipopolysaccharide-activated normal B cells. *Immunobiology* 174: 162–176.
2. Shapiro-Shelef, M., and K. Calame. 2005. Regulation of plasma-cell development. *Nat. Rev. Immunol.* 5: 230–242.
3. Calfon, M., H. Zeng, F. Urano, J. H. Till, S. R. Hubbard, H. P. Harding, S. G. Clark, and D. Ron. 2002. IRE1 couples endoplasmic reticulum load to secretory capacity by processing the XBP-1 mRNA. *Nature* 415: 92–96.
4. Iwakoshi, N. N., A. H. Lee, and L. H. Glimcher. 2003. The X-box binding protein-1 transcription factor is required for plasma cell differentiation and the unfolded protein response. *Immunol. Rev.* 194: 29–38.
5. Shen, X., R. E. Ellis, K. Lee, C. Y. Liu, K. Yang, A. Solomon, H. Yoshida, R. Morimoto, D. M. Kurnit, K. Mori, and R. J. Kaufman. 2001. Complementary signaling pathways regulate the unfolded protein response and are required for *C. elegans* development. *Cell* 107: 893–903.
6. Shaffer, A. L., M. Shapiro-Shelef, N. N. Iwakoshi, A. H. Lee, S. B. Qian, H. Zhao, X. Yu, L. Yang, B. K. Tan, A. Rosenwald, et al. 2004. XBP1, downstream of Blimp-1, expands the secretory apparatus and other organelles, and increases protein synthesis in plasma cell differentiation. *Immunity* 21: 81–93.
7. Acosta-Alvear, D., Y. Zhou, A. Blais, M. Tsikitis, N. H. Lents, C. Arias, C. J. Lennon, Y. Kluger, and B. D. Dynlacht. 2007. XBP1 controls diverse cell type- and condition-specific transcriptional regulatory networks. *Mol. Cell* 27: 53–66.
8. Reimold, A. M., N. N. Iwakoshi, J. Manis, P. Vallabhajosyula, E. Szomolanyi-Tsuda, E. M. Gravallese, D. Friend, M. J. Grusby, F. Alt, and L. H. Glimcher. 2001. Plasma cell differentiation requires the transcription factor XBP-1. *Nature* 412: 300–307.
9. Lee, A. H., G. C. Chu, N. N. Iwakoshi, and L. H. Glimcher. 2005. XBP-1 is required for biogenesis of cellular secretory machinery of exocrine glands. *EMBO J.* 24: 4368–4380.
10. Hu, C. C., S. K. Dougan, A. M. McGehee, J. C. Love, and H. L. Ploegh. 2009. XBP-1 regulates signal transduction, transcription factors and bone marrow colonization in B cells. *EMBO J.* 28: 1624–1636.
11. Hetz, C., A. H. Lee, D. Gonzalez-Romero, P. Thielen, J. Castilla, C. Soto, and L. H. Glimcher. 2008. Unfolded protein response transcription factor XBP-1 does not influence prion replication or pathogenesis. *Proc. Natl. Acad. Sci. USA* 105: 757–762.
12. Rickert, R. C., J. Roes, and K. Rajewsky. 1997. B lymphocyte-specific, Cre-mediated mutagenesis in mice. *Nucleic Acids Res.* 25: 1317–1318.
13. Boes, M., C. Esau, M. B. Fischer, T. Schmidt, M. Carroll, and J. Chen. 1998. Enhanced B-1 cell development, but impaired IgG antibody responses in mice deficient in secreted IgM. *J. Immunol.* 160: 4776–4787.
14. Goodnow, C. C., J. Crosbie, S. Adelstein, T. B. Lavoie, S. J. Smith-Gill, R. A. Brink, H. Pritchard-Briscoe, J. S. Wotherspoon, R. H. Loblay, K. Raphael, et al. 1988. Altered immunoglobulin expression and functional silencing of self-reactive B lymphocytes in transgenic mice. *Nature* 334: 676–682.
15. Sriburi, R., S. Jackowski, K. Mori, and J. W. Brewer. 2004. XBP1: a link between the unfolded protein response, lipid biosynthesis, and biogenesis of the endoplasmic reticulum. *J. Cell Biol.* 167: 35–41.
16. Sriburi, R., H. Bommiasamy, G. L. Buldak, G. R. Robbins, M. Frank, S. Jackowski, and J. W. Brewer. 2007. Coordinate regulation of phospholipid biosynthesis and secretory pathway gene expression in XBP-1(S)-induced endoplasmic reticulum biogenesis. *J. Biol. Chem.* 282: 7024–7034.
17. Lee, A. H., E. F. Scapa, D. E. Cohen, and L. H. Glimcher. 2008. Regulation of hepatic lipogenesis by the transcription factor XBP1. *Science* 320: 1492–1496.
18. Gumperz, J. E., C. Roy, A. Makowska, D. Lum, M. Sugita, T. Podrebarac, Y. Koezuka, S. A. Porcelli, S. Cardell, M. B. Brenner, and S. M. Behar. 2000. Murine CD1d-restricted T cell recognition of cellular lipids. *Immunity* 12: 211–221.
19. Rehm, A., P. Stern, H. L. Ploegh, and D. Tortorella. 2001. Signal peptide cleavage of a type I membrane protein, HCMV US11, is dependent on its membrane anchor. *EMBO J.* 20: 1573–1582.
20. Bordier, C. 1981. Phase separation of integral membrane proteins in Triton X-114 solution. *J. Biol. Chem.* 256: 1604–1607.
21. Bligh, E. G., and W. J. Dyer. 1959. A rapid method of total lipid extraction and purification. *Can. J. Biochem. Physiol.* 37: 911–917.
22. Fei, W., G. Shui, B. Gaeta, X. Du, L. Kuerschner, P. Li, A. J. Brown, M. R. Wenk, R. G. Parton, and H. Yang. 2008. Fld1p, a functional homologue of human seipin, regulates the size of lipid droplets in yeast. *J. Cell Biol.* 180: 473–482.
23. Chan, R., P. D. Uchil, J. Jin, G. Shui, D. E. Ott, W. Mothes, and M. R. Wenk. 2008. Retroviruses human immunodeficiency virus and murine leukemia virus are enriched in phosphoinositides. *J. Virol.* 82: 11228–11238.
24. Stevens, R. H., B. A. Askonas, and J. L. Welstead. 1975. Immunoglobulin heavy chain mRNA in mitogen-stimulated B cells. *Eur. J. Immunol.* 5: 47–53.
25. Tirosh, B., N. N. Iwakoshi, L. H. Glimcher, and H. L. Ploegh. 2005. XBP-1 specifically promotes IgM synthesis and secretion, but is dispensable for degradation of glycoproteins in primary B cells. *J. Exp. Med.* 202: 505–516.
26. Genestier, L., M. Taillardet, P. Mondiere, H. Gheit, C. Bella, and T. Defrance. 2007. TLR agonists selectively promote terminal plasma cell differentiation of B cell subsets specialized in thymus-independent responses. *J. Immunol.* 178: 7779–7786.
27. Mulugeta, S., J. A. Maguire, J. L. Newitt, S. J. Russo, A. Kotorashvili, and M. F. Beers. 2007. Misfolded BRICHOS SP-C mutant proteins induce apoptosis via caspase-4- and cytochrome *c*-related mechanisms. *Am. J. Physiol.* 293: L720–L729.
28. Dhaunchak, A. S., and K. A. Nave. 2007. A common mechanism of PLP/DM20 misfolding causes cysteine-mediated endoplasmic reticulum retention in oligodendrocytes and Pelizaeus-Merzbacher disease. *Proc. Natl. Acad. Sci. USA* 104: 17813–17818.
29. Casagrande, R., P. Stern, M. Diehn, C. Shamu, M. Osario, M. Zuniga, P. O. Brown, and H. Ploegh. 2000. Degradation of proteins from the ER of *S. cerevisiae* requires an intact unfolded protein response pathway. *Mol. Cell* 5: 729–735.
30. Credle, J. J., J. S. Finer-Moore, F. R. Papa, R. M. Stroud, and P. Walter. 2005. On the mechanism of sensing unfolded protein in the endoplasmic reticulum. *Proc. Natl. Acad. Sci. USA* 102: 18773–18784.
31. Bertolotti, A., Y. Zhang, L. M. Hendershot, H. P. Harding, and D. Ron. 2000. Dynamic interaction of BiP and ER stress transducers in the unfolded-protein response. *Nat. Cell Biol.* 2: 326–332.
32. Okamura, K., Y. Kimata, H. Higashio, A. Tsuru, and K. Kohno. 2000. Dissociation of Kar2p/BiP from an ER sensory molecule, Ire1p, triggers the unfolded protein response in yeast. *Biochem. Biophys. Res. Commun.* 279: 445–450.
33. Gu, F., D. T. Nguyen, M. Stuible, N. Dube, M. L. Tremblay, and E. Chevet. 2004. Protein-tyrosine phosphatase 1B potentiates IRE1 signaling during endoplasmic reticulum stress. *J. Biol. Chem.* 279: 49689–49693.
34. Van Anken, E., E. P. Romijn, C. Maggioni, A. Mezghrani, R. Sitia, I. Braakman, and A. J. Heck. 2003. Sequential waves of functionally related proteins are expressed when B cells prepare for antibody secretion. *Immunity* 18: 243–253.
35. Haze, K., H. Yoshida, H. Yanagi, T. Yura, and K. Mori. 1999. Mammalian transcription factor ATF6 is synthesized as a transmembrane protein and activated by proteolysis in response to endoplasmic reticulum stress. *Mol. Biol. Cell* 10: 3787–3799.
36. Yoshida, H., T. Okada, K. Haze, H. Yanagi, T. Yura, M. Negishi, and K. Mori. 2000. ATF6 activated by proteolysis binds in the presence of NF-Y (CBF) directly to the *cis*-acting element responsible for the mammalian unfolded protein response. *Mol. Cell. Biol.* 20: 6755–6767.
37. Gass, J. N., H. Y. Jiang, R. C. Wek, and J. W. Brewer. 2008. The unfolded protein response of B-lymphocytes: PERK-independent development of antibody-secreting cells. *Mol. Immunol.* 45: 1035–1043.
38. Gass, J. N., N. M. Gifford, and J. W. Brewer. 2002. Activation of an unfolded protein response during differentiation of antibody-secreting B cells. *J. Biol. Chem.* 277: 49047–49054.
39. Tulp, A., M. Barnhoorn, E. Bause, and H. Ploegh. 1986. Inhibition of *N*-linked oligosaccharide trimming mannosidases blocks human B cell development. *EMBO J.* 5: 1783–1790

Supplemental Figure Legend

Figure S1. The levels of the different classes of lipids presented in Fig. 8 are the summation of specific lipid species analyzed by mass spectrometry. The abundance of the specific lipids analyzed is presented here according to class: (A) phosphatidylcholine, (B) ceramide, (C) sphingomyelin, (D) phosphatidylethanolamide, (E) phosphatidylinositol, (F) phosphatidylserine and (G) phosphatidylglycerol. Data were acquired as described for Fig. 8 and are presented as mean±SD.

Figure S1

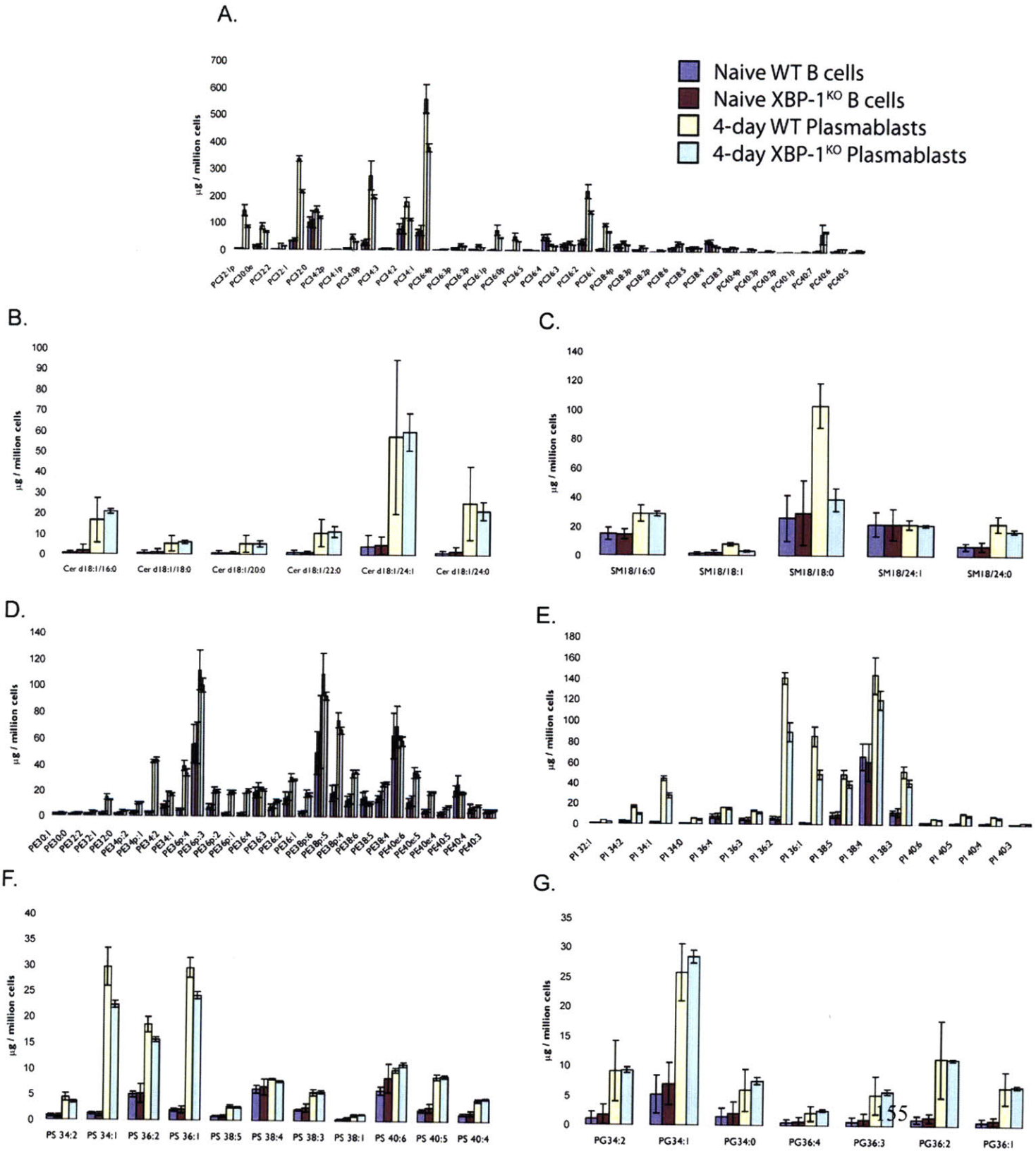
A.
Naive WT B cells
Naive XBP-1KO B cells
4-day WT Plasmablasts
4-day XBP-1KO Plasmablasts
µg / million cells
B.
Cer d18:1/16:0
Cer d18:1/18:0
Cer d18:1/20:0
Cer d18:1/22:0
Cer d18:1/24:1
Cer d18:1/24:0
C.
SM18/16:0
SM18/18:1
SM18/18:0
SM18/24:1
SM18/24:0
D.
E.
PI 32:1
PI 34:2
PI 34:1
PI 34:0
PI 36:4
PI 36:3
PI 36:2
PI 36:1
PI 38:5
PI 38:4
PI 38:3
PI 40:6
PI 40:5
PI 40:4
PI 40:3
F.
PS 34:2
PS 34:1
PS 36:2
PS 36:1
PS 38:5
PS 38:4
PS 38:3
PS 38:1
PS 40:6
PS 40:5
PS 40:4
G.
PG34:2
PG34:1
PG34:0
PG36:4
PG36:3
PG36:2
PG36:1